

A STUDY OF APERIODIC (RANDOM) ARRAYS OF VARIOUS GEOMETRIES

A Thesis

by

KRISTOPHER RYAN BUCHANAN

Submitted to the Office of Graduate Studies of
Texas A&M University
in partial fulfillment of the requirements for the degree of

MASTER OF SCIENCE

May 2011

Major Subject: Electrical Engineering

A Study of Aperiodic (Random) Arrays of Various Geometries

Copyright 2011 Kristopher Ryan Buchanan

A STUDY OF APERIODIC (RANDOM) ARRAYS OF VARIOUS GEOMETRIES

A Thesis

by

KRISTOPHER RYAN BUCHANAN

Submitted to the Office of Graduate Studies of
Texas A&M University
in partial fulfillment of the requirements for the degree of

MASTER OF SCIENCE

Approved by:

Chair of Committee,
Committee Members,

Gregory Huff
Robert Nevels
Helen Reed

Head of Department,

Jean-Francois Chamberland-Tremblay
Costas Georghiadis

May 2011

Major Subject: Electrical Engineering

ABSTRACT

A Study of Aperiodic (Random) Arrays of Various Geometries. (May 2011)

Kristopher Ryan Buchanan, B.S., University of Nevada Las Vegas

Chair of Advisory Committee: Dr. Gregory Huff

The use of wireless communication techniques and network centric topologies for portable communication networks and platforms makes it important to investigate new distributed beamforming techniques. Platforms such as micro air vehicles (MAVs), unattended ground sensors (UGSs), and unpiloted aerial vehicles (UAVs) can all benefit from advances in this area by enabling advantages in stealth, enhanced survivability, and maximum maneuverability. Collaborative beamforming is an example of a new technique to utilize these systems which uses a randomly distributed antenna array with a fitting phase coefficient for the elements. In this example, the radiated signal power of each element is coherently added in the far-field region of a specified target direction with net destructive interference occurring in all other regions to suppress sidelobe behavior.

A wide variety of topologies can be used to confine geometrically these mobile random arrays for analysis. The distribution function for these topologies must be able to generalize the randomness within the geometry. Gaussian and Uniform distributions are investigated in this analysis, since they provide a way to calculate the statistically averaged beampattern for linear, planar (square and circular), and volumetric (cubical,

cylindrical, and spherical) geometries. They are also of practical interest since the impact of array topology on the beampattern can typically be described in closed form. A rigorous analysis is presented first for disc-shaped topologies to motivate the discussion on random array properties and provide several new insights into their behavior. The analyses of volumetric geometries which are of interest to this work are drawn from this planar topology to provide a tractable and coherent discussion on the properties of more complex geometries. This analysis considers Normal and Gaussian distributed array element populations to derive the average beampattern, sidelobe behavior, beamwidth, and directivity. The beampattern is also examined in a similar manor for circular and spherical arrays with a truncated Gaussian distribution. A summary of the random array analysis and its results concludes this thesis.

DEDICATION

This thesis is dedicated to my grandfather, David Hunter.

ACKNOWLEDGEMENTS

I would like to thank my committee chair, Dr. Gregory Huff for his guidance and support during the course of this research. I would also like to thank my committee members, Dr. Chamberland, Dr. Robert Nevels and Dr. Helen Reed for taking the time to survey this work.

Special thanks are credited to Dr. Hidiki Ochiai and Dr. Vorobyov Sergiv for help in understanding mathematical derivations in their work. Additional appreciation is given to Dr. Steven Weiss and the members of the Adelphi Army Research Laboratory for the time provided to derive much of these derivations.

I would also like to thank my friends and colleagues for the fun times we've shared away from the office.

Finally, thanks to my mother for her love and support.

TABLE OF CONTENTS

	Page
ABSTRACT	iii
DEDICATION.....	v
ACKNOWLEDGEMENTS.....	vi
TABLE OF CONTENTS.....	vii
LIST OF FIGURES.....	x
LIST OF TABLES.....	xvi
 CHAPTER	
I INTRODUCTION.....	1
1.1 Advantages of Aperiodic Arrays.....	2
1.2 Disadvantages of Aperiodic Arrays.....	4
1.3 Historical Advancement.....	5
1.4 Application of Classical (adaptive) Beamforming Aperiodic Arrays.....	6
1.5 Application of Distributed Beamforming.....	10
1.6 Closed Loop and Open Loop Beamforming.....	11
1.7 Organization of this Thesis.....	13
II SYSTEM MODEL AND ASSUMPTIONS.....	14
2.1 Initial Conditions.....	14
2.2 Array Factor Open Loop Generalization.....	15
2.3 Array Factor Closed Loop Generalization.....	17
2.4 Radiation Intensity Generalization.....	18
2.5 Average Radiation Intensity Generalization.....	19
2.6 Directivity.....	19
III LINEAR ARRAYS.....	21
3.1 Periodic.....	22
3.2 Aperiodic.....	25

CHAPTER	Page
IV PLANAR ARRAYS.....	31
4.1 Periodic.....	31
4.2 Aperiodic.....	35
V CIRCULAR ARRAYS.....	42
5.1 Periodic.....	42
5.2 Aperiodic.....	47
VI SPHERICAL ARRAYS.....	94
6.1 Periodic.....	94
6.2 Aperiodic.....	109
VII ADDITIONAL VOLUMETRIC ARRAYS.....	137
7.1 Aperiodic.....	137
VIII ONGOING AND FUTURE WORK.....	148
8.1 Flying Antenna's.....	148
8.2 Wideband Antenna's.....	149
IX CONCLUSION.....	154
REFERENCES.....	156
APPENDIX A. INTEGRAL IDENTITIES.....	167
APPENDIX B. SUMMATION IDENTITIES.....	170
APPENDIX C. TRIGONOMETRIC IDENTITIES.....	171
APPENDIX D. SPECIAL FUNCTIONS.....	173
APPENDIX E. VECTOR IDENTITIES.....	175
APPENDIX F. PROOF OF SELECT INTEGRALS.....	176
APPENDIX G. SUMMATION PROOF.....	195

VITA.....198

LIST OF FIGURES

		Page
Fig. 1.	Notional diagram showing a periodic (left) and aperiodic (right) antenna array.....	2
Fig. 2.	Random deployment of sensor nodes from a UAV.....	8
Fig. 3.	F22 with randomly distributed antennas (represented by black dots).....	9
Fig. 4.	Distributed beamforming in the battlefield.....	11
Fig. 5.	Random distribution of elements in a spherical volumetric array.....	15
Fig. 6.	Geometry of an N-element periodic linear array.....	21
Fig. 7.	Radiation intensity of 16 elements periodically spaced along the line (X-Axis) with spacing $dx=.625$	23
Fig. 8.	Radiation intensity of 16 elements periodically spaced along the line (X-Axis).....	24
Fig. 9.	Geometry of an N-element random linear array.....	24
Fig. 10.	Average radiation intensity at the meridian elevation angle of a random linear array (X-axis).....	28
Fig. 11.	Average radiation pattern of 16 and 256 elements randomly spaced along the line (X-Axis) of length $A = 10\lambda$	29
Fig. 12.	Simulated and analytical results for a linear random array along the x-direction with $A = 10$, $N = 16$ and 256	30
Fig. 13.	16 (left) and 256 (right) elements uniformly distributed in a normalized linear aperture along the x-axis.....	31
Fig. 14.	Geometry of an MxN periodic planar array.....	31
Fig. 15.	Radiation pattern of 16 elements periodically spaced within a planar aperture with spacing $dx=dy=.625 \lambda$	34

	Page
Fig. 16. Radiation pattern of 16 elements periodically spaced within a planar aperture with spacing $D_x=D_y=2\lambda$	34
Fig. 17. Geometry of an $M \times N$ random planar array.....	35
Fig. 18. Average radiation intensity at the meridian elevation angle of a random planar array (XY-Plane).....	38
Fig. 19. Average radiation pattern of 16 and 256 elements randomly spaced within a planar aperture of $A = 10\lambda$	39
Fig. 20. Simulated and analytical results for a uniformly distributed planar random array in the XY-Plane with $A = 10$, $N = 16$ and 256.....	40
Fig. 21. 16 (left) and 256 (right) elements uniformly distributed in a normalized planar aperture in the XY-plane.....	41
Fig. 22. Geometry of an N-element periodic circular array.....	42
Fig. 23. Radiation pattern of 16 elements periodically spaced about one circular ring of radius $.625\lambda$	45
Fig. 24. Radiation pattern of 16 elements periodically spaced about one circular ring of radius 2λ	46
Fig. 25. Geometry of an N-element random circular array.....	47
Fig. 26. Average radiation pattern of 16 and 256 elements randomly spaced (Uniformly) within a circular aperture of 10λ	53
Fig. 27. Average radiation pattern of 16 and 256 elements randomly spaced (uniformly) within a circular aperture of 10λ at the meridian angle.....	54
Fig. 28. Graphical solution of the three Db sidelobe.....	57
Fig. 29. 3dB sidelobe region, sidelobe peaks, zeros, and half power beamwidth locations with $A = 8$, $N = 16$	60
Fig. 30. Threshold angle of the three Db beamwidth and three Db sidelobe region with respect to A and N	61

	Page
Fig. 31. Graphical solution for lower-bounding the directivity of a circular random array.....	65
Fig. 32. Average radiation pattern of 16 elements randomly spaced within a circular aperture of 10λ with Gaussian distribution and $\sigma = .5$	81
Fig. 33. Average radiation pattern of 16 and 256 elements randomly spaced within a circular aperture of 10λ with Gaussian distribution and $\sigma = 1$	82
Fig. 34. Average radiation pattern of 16 and 256 elements randomly spaced within a circular aperture of 10λ with Gaussian distribution.....	83
Fig. 35. Simulated and analytical radiation intensity for a circular random array (uniformly distributed) in the XY-plane with $A = 10$, $N = 16$ and 256.....	91
Fig. 36. 16 (left) and 256 (right) elements uniformly distributed in a normalized circular aperture along the XY-plane.....	91
Fig. 37. Simulated and analytical radiation intensity for a circular random array (Gaussian distributed) in the XY-plane with $A = 10$, $N = 16$ and 256.....	92
Fig. 38. 16 (left) and 256 (right) elements Gaussian distributed in a normalized circular aperture along the XY-plane.....	93
Fig. 39. Geometry of an N-element periodic spherical array of circularly polarized elements.....	94
Fig. 40. Geometry of a periodic spherical array referenced to the element.....	95
Fig. 41. Geometry of a periodic spherical array rotated about the element in order to be referenced to the origin.....	96
Fig. 42. Geometry of an icosahedron.....	105
Fig. 43. Average radiation pattern of 177 elements periodically spaced about a spherical radius of $.625\lambda$	108
Fig. 44. Average radiation pattern of 177 elements periodically spaced about a spherical radius of 2λ	108

	Page
Fig. 45. 177 elements periodically spaced in a spherical geometry based upon icosahedron geometry.....	109
Fig. 46. Distribution of aircraft randomly distributed in three dimensional space.....	110
Fig. 47. Geometry of an N-element random spherical array.....	111
Fig. 48. Average radiation pattern of 16 and 256 elements randomly spaced (Uniformly) within a spherical aperture of 10λ	115
Fig. 49. Average radiation pattern of 16 elements randomly spaced (uniformly) within a spherical aperture of 10λ	116
Fig. 50. Average radiation pattern of 16 elements randomly spaced (uniformly) within a circular aperture of 10λ	117
Fig. 51. Average 3dB beamwidth of a spherical random array.....	119
Fig. 52. 3 dB sidelobe region, and null and peak positions of a spherically bound random array.....	121
Fig. 53. Spherical random array threshold angle of the three Db beamwidth and three Db sidelobe region with respect to A and N	122
Fig. 54. Circular random array threshold angle of the three Db beamwidth and three Db sidelobe region with respect to A and N	122
Fig. 55. Comparison of the average directivity of a random circular and spherical array for $N=16$	124
Fig. 56. Average radiation pattern of 16 elements randomly spaced (Gaussian distributed) within a spherical aperture of 10λ and $\sigma=.5$	130
Fig. 57. Average radiation pattern of 16 and 256 elements randomly spaced within a spherical aperture of 10λ with Gaussian distribution and $\sigma=1$	131
Fig. 58. Average radiation pattern of 16 and 256 elements randomly spaced within a spherical aperture of 10λ with Gaussian distribution.....	131

	Page
Fig. 59. Radiation pattern of a random spherical array with 16 and 256 elements uniformly distributed in a spherical radius 10λ	134
Fig. 60. 16 and 256 elements uniformly distributed in a normalized spherical aperture.....	135
Fig. 61. Radiation pattern of a random spherical array with 16 and 256 elements Gaussian distributed in a spherical radius 10λ	135
Fig. 62. 16 and 256 elements Gaussian distributed in a normalized spherical aperture.....	136
Fig. 63. Geometry of an N-element random cubical array.....	137
Fig. 64. Average radiation pattern of 16 and 256 elements randomly spaced (uniformly) within a cubical aperture of 10λ	140
Fig. 65. Average radiation intensity at the meridian elevation angle of a random cubic array.....	141
Fig. 66. Radiation pattern of a random cubical array with 16 and 256 elements uniformly distributed in a radius of 10λ	142
Fig. 67. 16 and 256 elements uniformly distributed in a normalized cubical aperture.....	143
Fig. 68. Geometry of an N-element random cylindrical array.....	144
Fig. 69. Average radiation pattern of 16 elements randomly spaced (uniformly) within a cylindrical aperture of 10λ	146
Fig. 70. Average radiation pattern of 16 and 256 elements randomly spaced (uniformly) within a cylindrical aperture of 10λ at the meridian elevation angle.....	146
Fig. 71. Radiation pattern of a random cylindrical array with 16 and 256 elements uniformly distributed in a radius of 10λ	147
Fig. 72. 16 and 256 elements uniformly distributed in a normalized cylindrical aperture.....	147

	Page
Fig. 73. Box shaped flyer.....	149
Fig. 74. Characteristics of a cavity backed and conical spiral antenna.....	151
Fig. 75. Characteristics of a biconical and biconical w/polarizer antenna.....	153

LIST OF TABLES

	Page
Table 1. Comparison of analytic peaks vs. numerical peaks for a circular random array $\tilde{A} = 5$ and $(N=32,128)$	59
Table 2. Comparison of analytic peaks vs. numerical peaks for a spherical random array $\tilde{A} = 5$ and $(N=32,128)$	59
Table 3. Element placement.....	106

CHAPTER I

INTRODUCTION

Applications today require radiation characteristics which may not be achievable by a single antenna operating on its own behalf. Ultra wide band (UWB) antennas have been used to mitigate some of the bandwidth limitations and provide high-resolution scanning capabilities [1]-[18], but a single broadband antenna will typically not provide a sufficient amount of both bandwidth [19]-[22] *and* directivity. However, it is possible for a collection or distribution of radiating elements arranged in an aggregate geometrical arrangement (called an array) to provide the desired radiation characteristics [23]-[26]. A random and sparse distribution of radiating elements (called an aperiodic array) may achieve more desirable behavior when compared to a well-populated periodic distribution [27]-[34] since they can be designed to limit radiation outside of the desired direction and mitigate spatial constraints due to the array spacing and element size that is typically required to achieve broadband behavior.

The analysis of random arrays was considered initially by numerous researchers from [26], and [34]-[36]. The more widely recognized probabilistic approach for analysis of random arrays in linear and planar topologies contexts was examined in rigor by Lo *et al.* in [28]-[31] and benchmarked experimentally in [37] for planar topology. These works provided a foundation for further studies (e.g., [6]-[14]), which extended the theory into the treatment of other canonical geometries. The goal of this work is to provide a summary of an alternate and potentially more tractable formulation for several

of these works which originates solely on closed form expressions. As such, this thesis compliments the formulation of earlier works and provides an analytical framework from which it is possible to extend the results from [9]-[12].

1.1 Advantages of Aperiodic Arrays

Fig. 1 shows a notional example of periodic and aperiodic arrays. Most arrays have periodic element spacing. This is especially true when the elements have a narrow bandwidth. A half-wavelength spacing is common in these circumstances because it creates an acceptable beam pattern. An array of electrically large antennas can suffer degradation due to mutual coupling and prevent the full utilization of its instantaneous bandwidth [30], and [38]-[39]. A solution to this problem is to remove the periodicity and space the N elements aperiodically into a larger aperture. This allows for greater bandwidth in beamforming across larger distances [26], [27], [35]. It also reduces the need to have elements spaced close to each other.

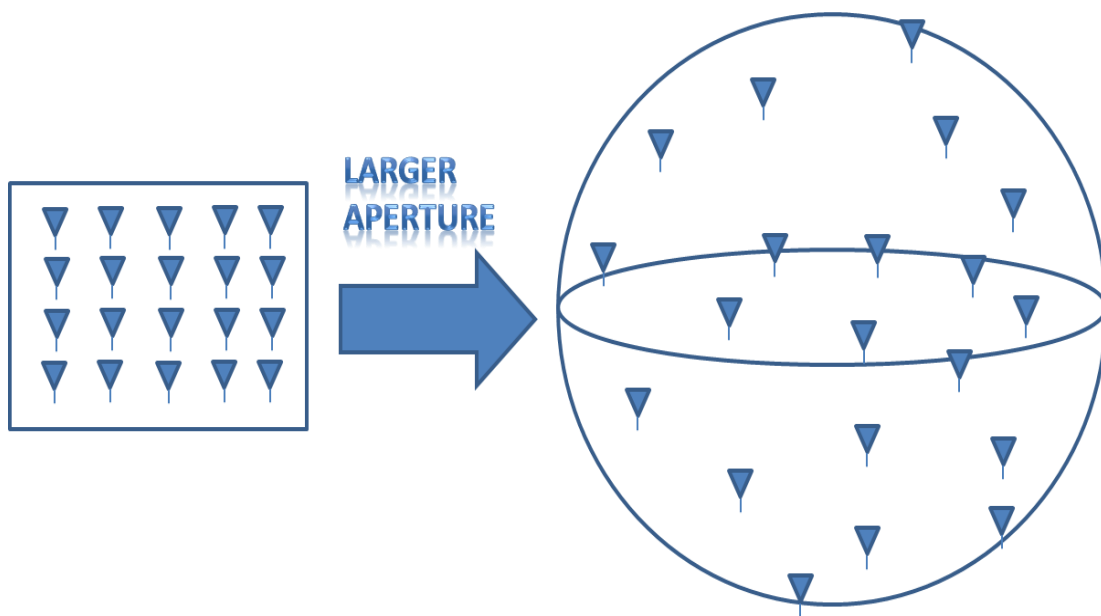


Fig. 1. Notional diagram showing a periodic (left) and aperiodic (right) antenna array.

Randomly distributed arrays have many unique capabilities. With adequate phase control and synchronization these arrays can coherently add signals in the desired direction. This randomizes their phase information in all other regions to the extent that a net destructive interference occurs. The most notable results from this randomization include a reduction in side-lobe levels without amplitude tapering and the mitigation of grating lobes over wide bandwidths [27]-[33]. A narrower beam is typically achieved in these arrays and the directive gain reaches a fundamental limit of order N when the element distribution is sparse. The resolution of this beam depends mainly upon the effective aperture dimension in wavelengths and N , but also on the probability density function to which the elements are placed. Accordingly, the resolution of the aperture can be improved for a fixed number of elements by spreading them over a larger aperture. This can also be used to eliminate high peaking sidelobes [31] that are undesirable.

Sparsely populated arrays [40]-[43] are utilized to relax physical size restrictions on element dimensions and spacing. The use of electrically larger radiators enables broadband or wideband capabilities [44]-[48]. Increased spacing significantly reduces the unintended effects of mutual coupling on scan impedance and this is of course, very different from current sheet arrays (CSAs) and other densely populated or continuous [49]-[53] wideband array designs that exploit the inter-element interactions. The primary difference between beamforming techniques using random arrays and CSAs or other more widely recognized arrangements (planar and volumetric) is the absence of periodicity.

1.2 Disadvantages of Aperiodic Arrays

In general a desired lattice structure for many aperiodic arrangements is difficult to achieve in situations where dynamic and potentially uncoordinated movement is desired from platforms that host radiating elements. Constraints from the host platform require an accurate estimation of position and location information along with adequate synchronization. These operational parameters are assumed ideal in the theoretical framework proposed here, but certainly play a major role in the use (and usefulness) of random array techniques for platforms such as micro air vehicles (MAVs), portable communications networks (PCNs), unattended ground sensors (UGSs) and unpiloted aerial vehicles (UAVs) [54].

In the past random arrays have suffered from limited knowledge of radiative properties. In addition, complexity of analysis, synthesis, and cost to test made them disadvantageous to implement in real time. However, over the past few decades further contributions have been added to the literature of random arrays. In part this is due, because of an increasing interest in ultra wide band antennas structures and technology developments.

The synthesis of random arrays remains an open problem today even though attempts have been made to optimize such systems. For example, an examination from [55] has determined null locations may be prescribed to a pattern when elements are known with a tolerance of approximately one wavelength or better. Alternative synthesis approaches have been investigated from [56] to optimize the aperture with a fixed set of elements to provide better performance characteristics.

Bandwidth is another downfall of a random array since it declines from growth in aperture size relative to wavelength. This occurs, because of greater disparity in phase; i.e. when the aperture size grows relative to the wavelength, phase precision is lost. As a consequence, elements located far away will incur unrealistic requirements in terms of accuracy to reach the destination with collaborative structure. On the other hand, decreasing the effective aperture size allows for greater bandwidth, in exchange for a small growth in sidelobe level.

Loss in effectively scanning the main beam of a random array is experienced from decreasing the total number of elements too low. This induces higher sidelobes in the pattern and predictability in the pattern is lost past the third null of the main beam [57]. For this reason, a large collection of artifacts is collected during scanning. Last of all fewer elements reduces gain such that the periodic structure of the same aperture size, element type and feed structure becomes superior [57].

1.3 Historical Advancement

Periodically spaced phased arrays have been known for decades, and the most popular types are planar. For these arrays, it is known the main beam tends to deteriorate rapidly as it is scanned towards the plane of the array [58]-[62]. This demise makes geometries like circular and spherical topology of greater interest. The difficulty though is these arrays are not expressed in terms of simple polynomials and when the array is random; these types of arrays have a tendency to become very complex. The investigation of randomly spaced circular and spherical arrays was first done by [58] in the late 60's and later in the late 70's [59]-[61]. For the time being it was believed, "no

particular element arrangement on the circle or sphere of a random array could result in mathematical simplicity, thereby leading to a closed form solution except for the special case of very small element spacing's where some approximate solution could be found [58]. Conversely, it is shown a structure of mathematical simplicity does exist and is used to formulate simple closed form solutions. In addition, Panicalli and Lo simulated experiments using the Monte Carlo method to test the validity of their theory. Instead, this thesis will not use the Monte Carlo method since simple closed form solutions are now known to exist.

By the same token, this thesis along with other recent papers [6]-[14] is designed to provide better insight into the characteristics of random arrays. Care has been taken in the derivations such that the topic is traced easily to its origins from [26], [31], and [34]-[36]. In addition, the understanding framework of the theory makes more advanced concepts easier to grasp.

1.4 Application of Classical (adaptive) Beamforming for Aperiodic Arrays

The difference between classical (adaptive) and distributed (opportunistic) beamforming is the former knows position of each antenna *a priori* whereas the latter acquires data dynamically.

Fig. 2 shows an example of classical beamforming. This application entails expending UAVs to quickly deploy sensor nodes to create a wireless sensor network (WSN). In this type of network the initial position of each node is not required. This is due since the array initiates distributed beamforming to start the network. Once an exact position of each node is collected a transition is made towards a more simple form of

classical beamforming. This is under the assumption the network is going to be unattended by humans. Moreover, these nodes (arrays) can be deployed for a variety of attractive applications such as: remote sensing and military applications to include: detection of nuclear biological and chemical weapons, IED (improvised explosive device) detection and reconnaissance operations.

Another possibility within the realm of classical beamforming is to cluster antennas amongst an aircraft randomly such that a cluster has an ability to share information *a priori*. From this standpoint a cluster head will be able to choose a best fit amongst the distribution to synchronously transmit data collaboratively as shown in Fig. 3. The downfall of an intra-cluster of antennas is acquired overhead. However, this overhead is typically small such that the resultant efficiency is greater for transmission to receivers located far away.

Additional applications for classical beamforming include: increased penetration depth of ground-probing radar, improving resolution capability of imaging radar, and enhancing overall performance of medical diagnosis and therapeutic techniques that utilize electromagnetic impulses [63]-[66].

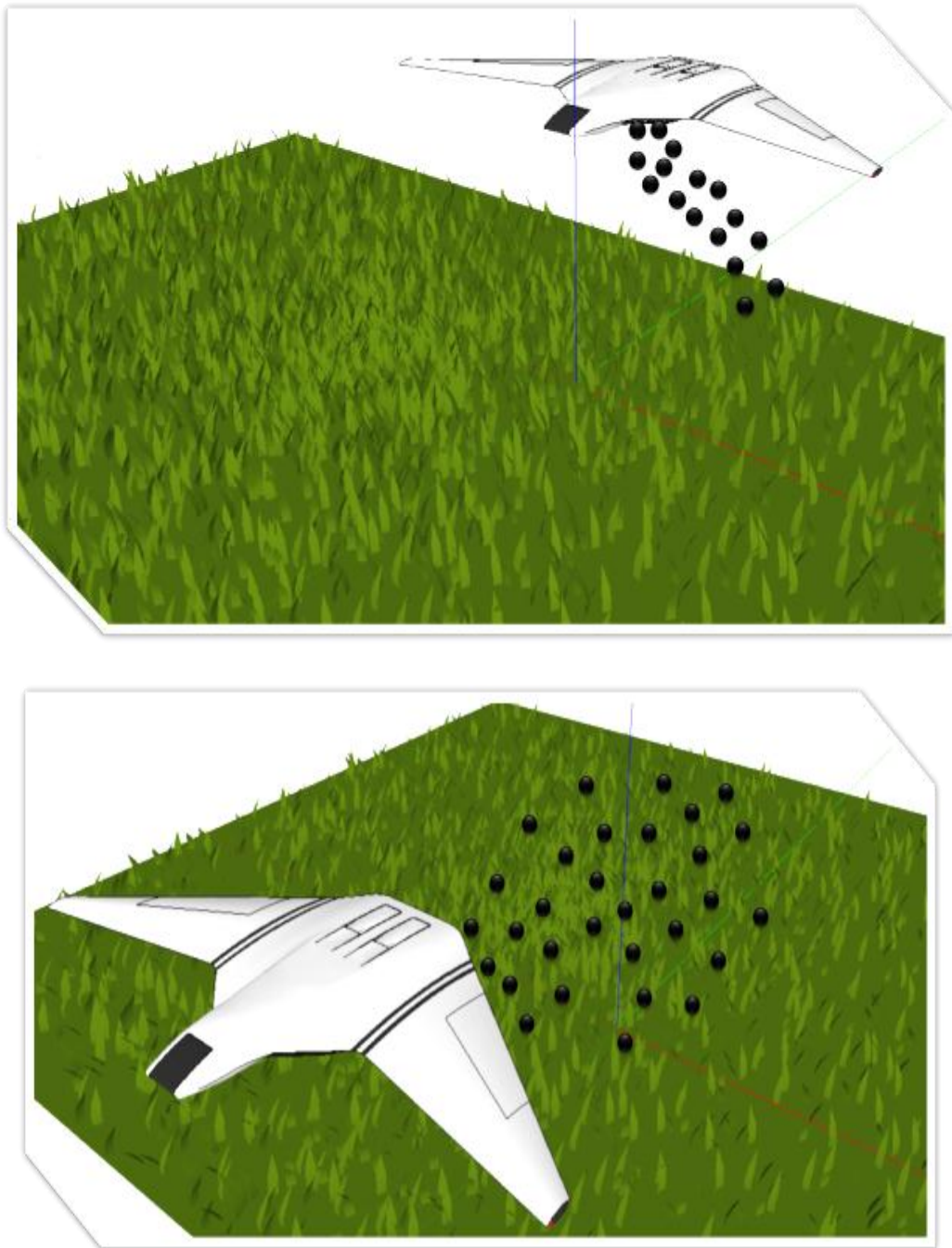


Fig. 2. Random deployment of sensor nodes from a UAV.

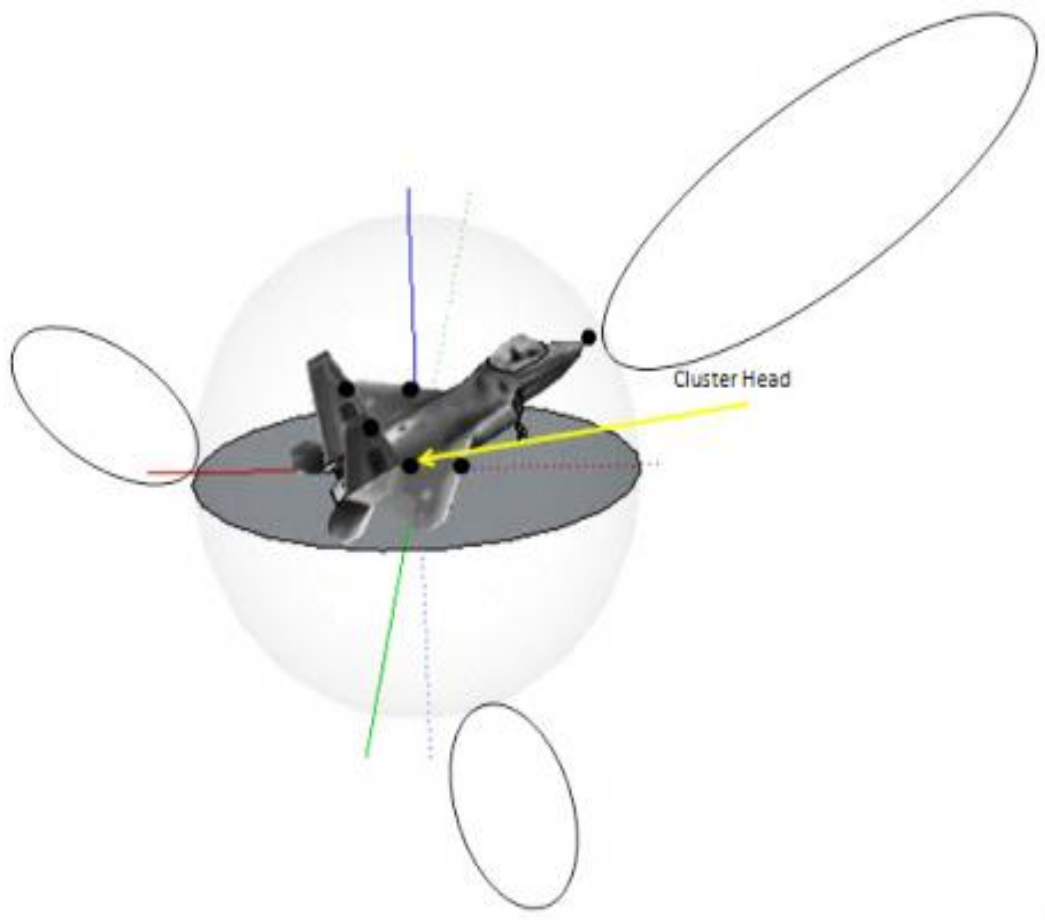


Fig. 3. F22 with randomly distributed antennas (represented by black dots).

1.5 Application of Distributed Beamforming

An application unrealistic in the past was the ability to beamform in the mobile sense. For example, a distribution of planes surveying terrain by Light Detection and Ranging (LiDAR) may benefit from sharing information to a base station far away. This application would require a directional beam to minimize energy required for transmission making collaborative beamforming desirable. This also establishes a point-to-point type architecture. Communication of this fashion is favorable over omnidirectional communication, because it limits additional spread of outside interference to the environment.

Emergency response type applications where a network is “hastily formed” will benefit best from distributed beamforming. Applications of this nature are primarily geared towards the military environment where real time visual updates are necessary in the battlefield. An example of this is shown in Fig. 4 with futuristic settings.

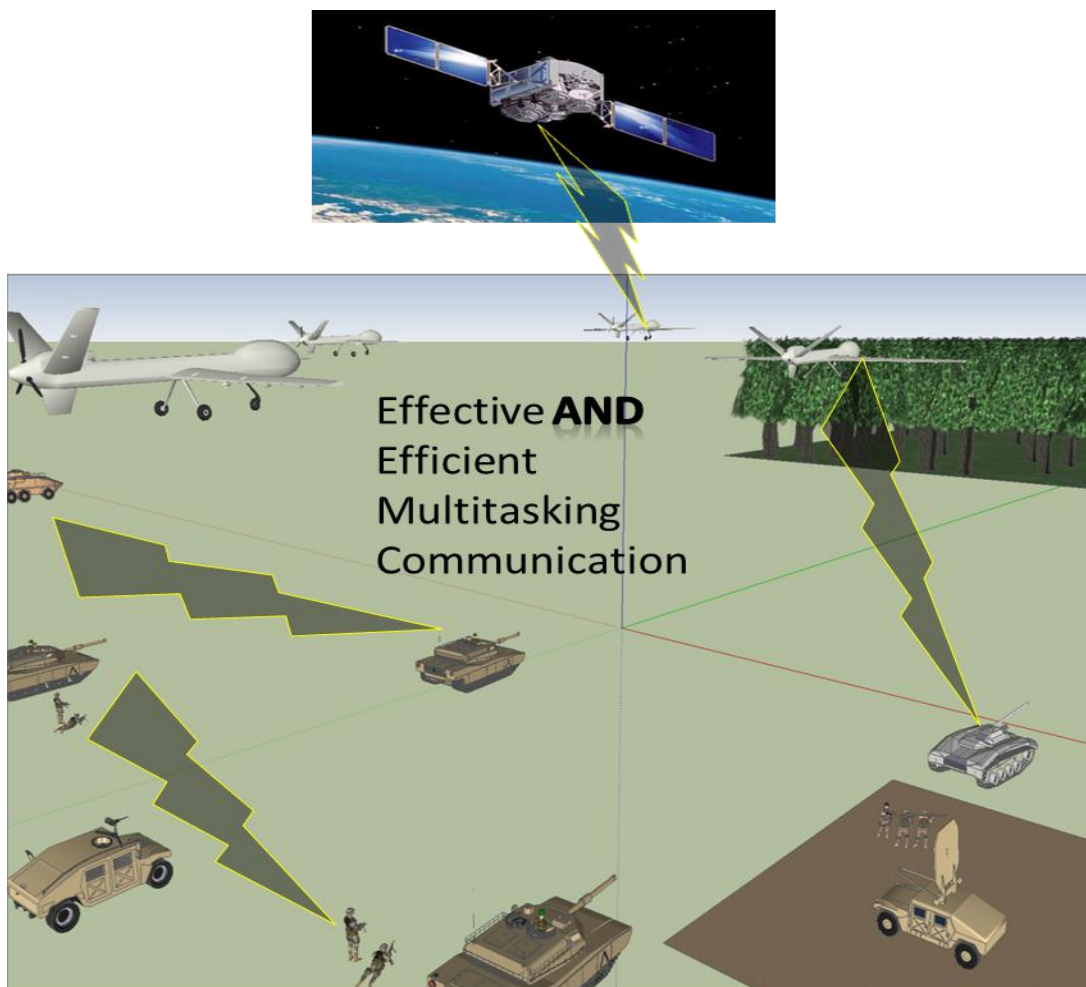


Fig. 4. Distributed beamforming in the battlefield.

1.6 Closed Loop and Open Loop Beamforming

Difficulty arises from attempting to acquire exact spatial information from a mobile antenna and attempting to estimate the location will trigger random error into the system. This leads to inaccuracy in the geometric information acquired. Since it is nearly impossible for every local oscillator to be synchronized with perfect precision. Two solutions will be investigated to cope with these impairments [9]: *closed-loop* and *open loop*.

In closed-loop each antenna receives a beacon from the destination antenna (such as a base station) and adjusts its initial phase accordingly. This is referred to as self-phasing and it is effective for systems using Time-Division Duplex (TDD). The open-loop consideration assumes the antenna ping a relative location from a nearby reference point or cluster head.

To handle phase synchronization for both types of beamforming Global Positioning Systems (GPS) can be used. This is a key reason distributed arrays are more realistic at the present, because accurate phase control is more reliable. Most importantly, this provides a reason why theory should be built up from a probabilistic sense pertaining to random arrays. It is also important to note it is now possible to effectively employ random arrays at low costs using technologies using Micro-Electro-Mechanical (MEM) systems [9]. These systems are advantageous because of their ease of use, small size and low cost from mass production.

Last of all, the advantage of collaborative beamforming whether it applies classically or distributedly is the ability to take advantage of modern Space-Division Multiplex Access (SDMA) technology. This architecture enables channeling of radio signals based upon a mobile device's location and is a MIMO (Multiple-Input-Multiple-Output) architecture. This is primarily suitable for mobile ad-hoc networks, because it sets up a one-to-one type mapping between a networks bandwidth division and identified spatial division.

1.7 Organization of this Thesis

This thesis comprises a variety of aperiodic arrays structures and a more thorough examination and emphasis is placed into determining characteristics for circular and spherical topology. Subsequent chapters of periodic geometry reside before an equivalent aperiodic structure. This provides ease in comparison as well as completeness in lieu of analysis.

Chapter II begins with simple array theory and assumptions that are used in this thesis. After a foundation of array theory is formulated an order of investigation begins with linear arrays in Chapter III, planar arrays in Chapters IV and V and volumetric arrays in Chapters VI and VII. Chapter VIII provides examples of wideband antennas which should serve well to aperiodic structures. Finally Chapter IX ends with a conclusion of random arrays.

CHAPTER II

SYSTEM MODEL AND ASSUMPTIONS

2.1 Initial Conditions

Fig. 5 shows topology of a spherically bound random array and it serves well as the basis of this thesis. This comes from the ease in simplifying to alternative geometries. In general, it is always assumed a geometry contains N elements, where $\theta \in [0, \pi]$, $\phi \in [0, 2\pi)$ and the radius A of the array is to be set by the outermost radiator in the cluster (this ability for inclusiveness is a key feature of these arrays). The location of the n th element in this array is denoted as (r_n, θ_n, ϕ_n) and the assumptions used to enable mathematical simplicity in the analysis of the random array are:

- First: The location of each antenna is chosen randomly with uniform distribution inside a topology of radius A
- Second: Each antenna is assumed to be an ideal isotropic radiator
- Third: All antenna elements transmit an equal amount of energy with equal path loss
- Fourth: No reflection or scattering of the signal exists (e.g., no multipath fading or shadowing)
- Fifth: Mutual coupling is mitigated under the assumption the antennas are separated sufficiently far away from one another
- Sixth: Adequate synchronization is available to ensure frequency offsets and phase jitter is not present

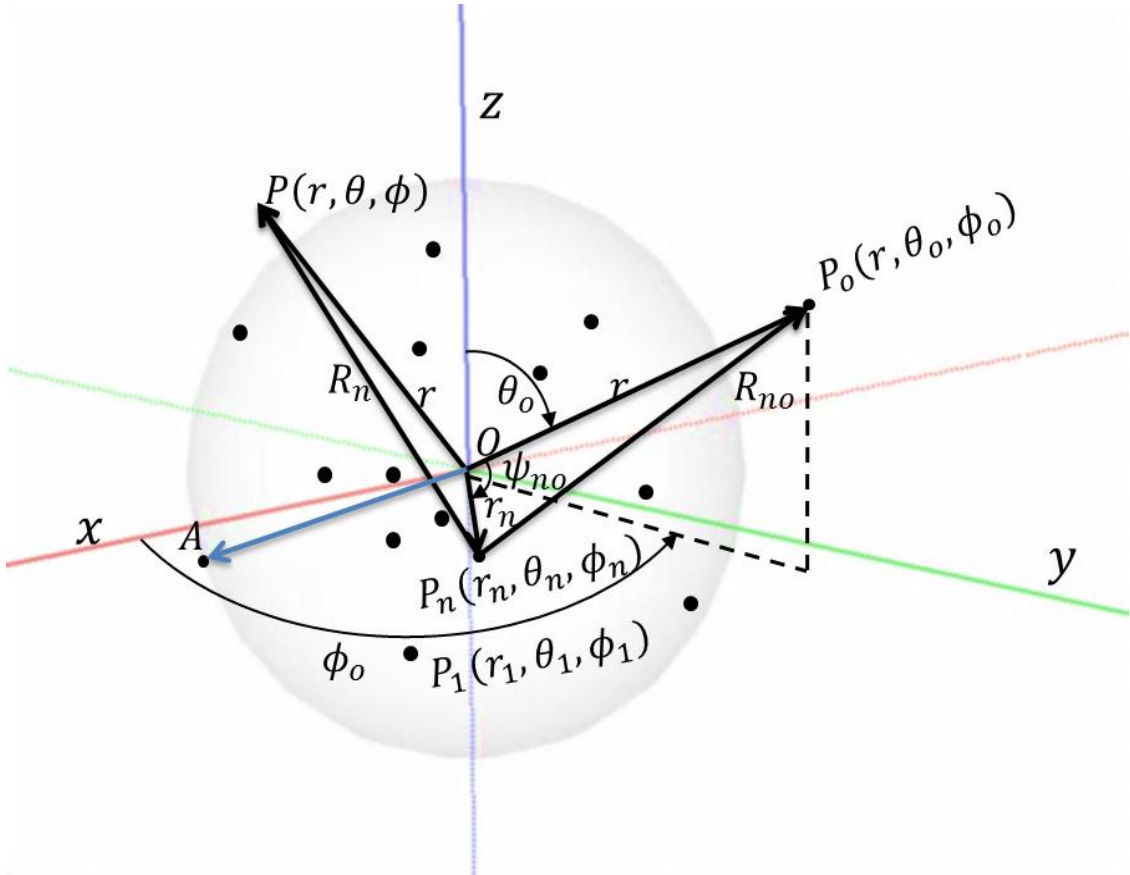


Fig. 5. Random distribution of elements in a spherical volumetric array.

2.2 Array Factor Open Loop Generalization

The array factor is derived in this section for a generalized random array of N isotropic elements with perfect phase information. It begins by examining the normalized electric field E in (0.2.1) of an array at an observation point $P(r, \theta, \phi)$ for randomly spaced elements at locations $P_n(r_n, \theta_n, \phi_n)$. In general, it is assumed a main beam of an array is scanned to a point of observation $P_o(r, \theta_o, \phi_o)$ with element distance $R_n(\theta, \phi)$ (0.2.2) giving the Euclidean distance between P_n and P ; these parameters are shown in Fig. 5 for the case of spherically bound random array geometry.

$$E(R_n, \theta, \phi) = \frac{1}{N} \sum_{n=1}^N f_{no}(R_{no}, \theta_{no}, \phi_{no}) \frac{e^{-jkR_n}}{R_n} \quad (0.2.1)$$

$$\begin{aligned} R_n(\theta, \phi | \vec{r}_n, \vec{\theta}_n, \vec{\phi}_n) &= |r - r_n| = \sqrt{(r \sin \theta \cos \phi - r_n \sin \theta_n \cos \phi_n)^2 + (r \sin \theta \sin \phi - r_n \sin \theta_n \sin \phi_n)^2 + (r \cos \theta - r_n \cos \theta_n)^2} \\ &= \sqrt{r^2 + r_n^2 - 2r r_n \sin \theta \sin \theta_n (\cos \phi \cos \phi_n + \sin \phi \sin \phi_n + \cos \theta \cos \theta_n)} \\ &= \sqrt{r^2 + r_n^2 - 2r r_n (\sin \theta \sin \theta_n \cos(\phi - \phi_n) + \cos \theta \cos \theta_n)} \quad (\text{Using Appendix C.1.d}) \\ &= r \sqrt{1 + \left(\frac{r_n}{r}\right)^2 - \frac{2r_n \cos \psi_n}{r}} \end{aligned} \quad (0.2.2)$$

In the far field $r \gg r_n$, and because of this $R_n(\theta, \phi | \vec{r}_n, \vec{\theta}_n, \vec{\phi}_n)$ can be approximated using the binomial expansion $\sqrt[3]{1+x} \approx 1 + \frac{x}{n}$ as(0.2.3).

$$R_n(\theta, \phi | \vec{r}_n, \vec{\theta}_n, \vec{\phi}_n) \approx r - r_n \cos \psi_n \quad (0.2.3)$$

If P is assumed to reside in the far field of the array, the common approximations for the magnitude $R_n \approx r$ and phase $R_n \approx r - r_n \cos \psi_n$ [65] contributions can be made by linking the direction vectors from the origin (0.2.4) and \hat{a}_m from P_n (0.2.5) to P through the direction cosine in (0.2.6).

$$\hat{a}_r = \hat{a}_x \sin \theta \cos \phi + \hat{a}_y \sin \theta \sin \phi + \hat{a}_z \cos \theta \quad (0.2.4)$$

$$\hat{a}_m = \hat{a}_x \sin \theta_n \cos \phi_n + \hat{a}_y \sin \theta_n \sin \phi_n + \hat{a}_z \cos \theta_n \quad (0.2.5)$$

$$\cos \psi_n = \hat{a}_m \cdot \hat{a}_r = \sin \theta_n \sin \theta \cos(\phi - \phi_n) + \cos \theta_n \cos \theta \quad (0.2.6)$$

The electric field in (0.2.1) reduces to (0.2.7) when the excitation coefficient $f_{no}(r_n, \theta_{no}, \phi_{no}) = I_n e^{-jk r_n \cos \psi_{no}}$ is applied to each element containing amplitude I_n and phase information $\cos \psi_{no}$.

$$E(r, \theta, \phi | \vec{r}_n, \vec{\theta}_n, \vec{\phi}_n) = \frac{1}{N} \frac{e^{-jkr}}{r} \sum_{n=1}^N I_n e^{jkr_n(\cos\psi_n - \cos\psi_{n0})} \quad (0.2.7)$$

For a uniform amplitude distribution $I_n = I_o = 1$ and the definition of the array factor $F(\theta, \phi | r_n, \theta_n, \phi_n)$ in (0.2.9) one may find the electric field to be rewritten in the form of (0.2.8).

$$E(r, \theta, \phi | \vec{r}_n, \vec{\theta}_n, \vec{\phi}_n) = F(\theta, \phi | \vec{r}_n, \vec{\theta}_n, \vec{\phi}_n) \frac{e^{-jkr}}{r} \quad (0.2.8)$$

$$F(\theta, \phi | \vec{r}_n, \vec{\theta}_n, \vec{\phi}_n) = \frac{1}{N} \sum_{n=1}^N e^{jkr_n(\cos\psi_n - \cos\psi_{n0})} \quad (0.2.9)$$

2.3 Array Factor Closed Loop Generalization

An alternative definition can be used for the initial phase of (0.2.6) such that

$$\cos(\psi_n)^+ = -\frac{r}{r_n} + \cos\psi_n = -\frac{r}{r_n} + \sin\theta_n \sin\theta \cos(\phi - \phi_n) + \cos\theta_n \cos\theta \quad (0.2.10)$$

Thus, the electric field of (0.2.7) and (0.2.8) are now rewritten as

$$E(r, \theta, \phi | \vec{r}_n, \vec{\theta}_n, \vec{\phi}_n) = \frac{1}{N} \frac{e^{-jkr}}{r} \sum_{n=1}^N I_n e^{jkr_n(\cos\psi_n - \cos(\psi_{n0})^+)} \quad (0.2.11)$$

$$E(r, \theta, \phi | \vec{r}_n, \vec{\theta}_n, \vec{\phi}_n) = F^+(\theta, \phi | \vec{r}_n, \vec{\theta}_n, \vec{\phi}_n) \frac{e^{-jkr}}{r} = F(\theta, \phi | \vec{r}_n, \vec{\theta}_n, \vec{\phi}_n) \frac{1}{r} \quad (0.2.12)$$

The observable difference between $F(\theta, \phi | \vec{r}_n, \vec{\theta}_n, \vec{\phi}_n)$ and $F^+(\theta, \phi | \vec{r}_n, \vec{\theta}_n, \vec{\phi}_n)$ is the initial phase offset e^{-jkr} . And, this means the received signal at the base station is identical for either beampattern as long as the initial phase offset is compensated for; this creates two different types of beamforming schemes (closed-loop and open loop) defined previously in Subheading 1.6.

Moreover from this point on this thesis expands strictly upon the open loop array factor (0.2.9), in order to derive characteristics of the random array.

2.4 Radiation Intensity Generalization

The radiation intensity in a given direction (0.2.14) is defined as the power radiated from the antenna per unit solid angle. This is obtained by multiplying the radiation density (0.2.13) by the square of the distance. Normalized radiation intensity is given by (0.2.15) and will be used throughout this thesis where the parameter \vec{Z} holds as a placeholder for an appropriate set of random variables. Last but not least, the factor of 2 is given in equation (0.2.13) and (0.2.14), since the \vec{E} field is assumed to represent a peak value and must be omitted for RMS values.

$$\begin{aligned} W_{rad} &= \frac{1}{2\eta} \left| \vec{E}(r, \theta, \phi | \vec{r}_n, \vec{\theta}_n, \vec{\phi}_n) \right|^2 \simeq \frac{1}{2\eta} \left[\left| E_\theta(r, \theta, \phi | \vec{r}_n, \vec{\theta}_n, \vec{\phi}_n) \right|^2 + \left| E_\phi(r, \theta, \phi | \vec{r}_n, \vec{\theta}_n, \vec{\phi}_n) \right|^2 \right] \\ &= \frac{1}{2\eta} \left[\left| \frac{2F(\theta, \phi | \vec{r}_n, \vec{\theta}_n, \vec{\phi}_n)}{r} \right|^2 \right] \text{ (For an isotropic radiator)} \end{aligned} \quad (0.2.13)$$

$$U(\theta, \phi | \vec{r}_n, \vec{\theta}_n, \vec{\phi}_n) \triangleq r^2 \frac{\vec{E}(r, \theta, \phi | \vec{r}_n, \vec{\theta}_n, \vec{\phi}_n) \vec{E}^*(r, \theta, \phi | \vec{r}_n, \vec{\theta}_n, \vec{\phi}_n)}{2\eta} = \frac{|2F(\theta, \phi | \vec{r}_n, \vec{\theta}_n, \vec{\phi}_n)|^2}{2\eta} \quad (0.2.14)$$

Where

$$\begin{aligned} \vec{E}(r, \theta, \phi | \vec{r}_n, \vec{\theta}_n, \vec{\phi}_n) &= \text{Far zone electric field intensity of the antenna} = \vec{F}(\theta, \phi | \vec{r}_n, \vec{\theta}_n, \vec{\phi}_n) \frac{e^{-jkr}}{r} \\ \vec{F}(\theta, \phi | \vec{r}_n, \vec{\theta}_n, \vec{\phi}_n) &= \left[E_\theta(\theta, \phi | \vec{r}_n, \vec{\theta}_n, \vec{\phi}_n) \hat{a}_\theta + E_\phi(\theta, \phi | \vec{r}_n, \vec{\theta}_n, \vec{\phi}_n) \hat{a}_\phi \right] F(\theta, \phi | \vec{r}_n, \vec{\theta}_n, \vec{\phi}_n) \\ E_\theta, E_\phi &= \text{Far-zone electric field of the antenna (Element Factor)}, (1 \text{ for an isotropic radiator}) \\ U(\theta, \phi | \vec{Z}) &\triangleq |F(\theta, \phi | \vec{Z})|^2 \end{aligned} \quad (0.2.15)$$

The power radiated is further defined as

$$P_{rad} = \oint_{\Omega} U d\Omega, \quad \Omega = \sin \theta d\theta d\phi \quad (0.2.16)$$

2.5 Average Radiation Intensity Generalization

When discussing an aperiodic (random) array it is interesting to find the mean or expected value of the beam pattern in order to obtain a clearer understanding of its radiative characteristics. This average radiation intensity (0.2.17) can be calculated by taking the expectation of the beam pattern (0.2.15).

$$U_{av}(\theta, \phi) \triangleq E_Z \left| U(\theta, \phi | \bar{Z}) \right| \quad (0.2.17)$$

In general, the expected value of an arbitrary function $g(X)$, with respect to the probability density function $f(x)$ is given by the inner product of $f(x)$ and $g(x)$ (0.2.18). Therefore, when equation (0.2.18) is applied to equation (0.2.17) one will have the appropriate recipe of calculating an average radiation intensity given in (0.2.19).

$$E(g(X)) = \int_{-\infty}^{\infty} g(x) f(x) dx \quad (0.2.18)$$

$$U_{av}(\theta, \phi) = E_Z \left| U(\theta, \phi | \bar{Z}) \right| = \sum_{m=1}^N \sum_{n=1}^N \int_{-\infty}^{\infty} \int_{-\infty}^{\infty} U(\theta, \phi | \bar{Z}) f(Z_n) f(Z_m) dZ_n dZ_m \quad (0.2.19)$$

2.6 Directivity

The directivity of the array factor (0.2.9) can be obtained by writing it as (0.2.20). This has a maximum directivity given by that of (0.2.21). Likewise, the directivity of a pattern independent of elevation angle can be shown by (0.2.22) and will have a maximum given by (0.2.23). Finally, since an isotropic element has a rotationally symmetric beam pattern, (0.2.23) can be reduced to that of (0.2.24) by setting the azimuthal angle $\phi_o = 0$ with no loss in generality.

$$D(\theta, \phi) = \frac{4\pi U(\theta, \phi | \bar{Z})}{P_{rad}} = \frac{4\pi U(\theta, \phi | \bar{Z})}{\oint_{\Omega} U(\theta, \phi | \bar{Z}) d\Omega} = \frac{4\pi F(\theta, \phi | \bar{Z}) F(\theta, \phi | \bar{Z})^*}{\int_0^{2\pi} \int_0^{\pi} F(\theta, \phi | \bar{Z}) F(\theta, \phi | \bar{Z})^* \sin \theta d\theta d\phi} \quad (0.2.20)$$

$$D_o = \frac{4\pi U(\theta_o, \phi_o | \bar{Z})}{P_{rad}} = \frac{4\pi U|_{\max}}{\oint_{\Omega} U(\theta, \phi | \bar{Z}) d\Omega} = \frac{4\pi U|_{\max}}{\int_0^{2\pi} \int_0^{\pi} F(\theta, \phi | \bar{Z}) F(\theta, \phi | \bar{Z})^* \sin \theta d\theta d\phi} \quad (0.2.21)$$

$$D(\phi) = \frac{4\pi U(\phi | \bar{Z})}{\oint_{\Omega} U(\phi | \bar{Z}) d\Omega} = \frac{2\pi F(\phi | \bar{Z}) F(\phi | \bar{Z})^*}{\int_0^{2\pi} F(\phi | \bar{Z}) F(\phi | \bar{Z})^* d\phi} \quad (0.2.22)$$

$$D_o = \frac{4\pi U|_{\max}}{\oint_{\Omega} U(\phi | \bar{Z}) d\Omega} = \frac{2\pi F(\phi_o | \bar{Z}) F(\phi_o | \bar{Z})^*}{\int_0^{2\pi} F(\phi | \bar{Z}) F(\phi | \bar{Z})^* d\phi} \quad (0.2.23)$$

$$D_o = \frac{4\pi U(0 | \bar{r}_n, \bar{\theta}_n, \bar{\phi}_n)_{\max}}{\oint_{\Omega} U(\phi | \bar{Z}) d\Omega} = \frac{2\pi F(0 | \bar{Z}) F(0 | \bar{Z})^*}{\int_0^{2\pi} F(0 | \bar{Z}) F(0 | \bar{Z})^* d\phi} \quad (0.2.24)$$

CHAPTER III

LINEAR ARRAYS

3.1 Periodic

A. System Development and Beampattern Definition

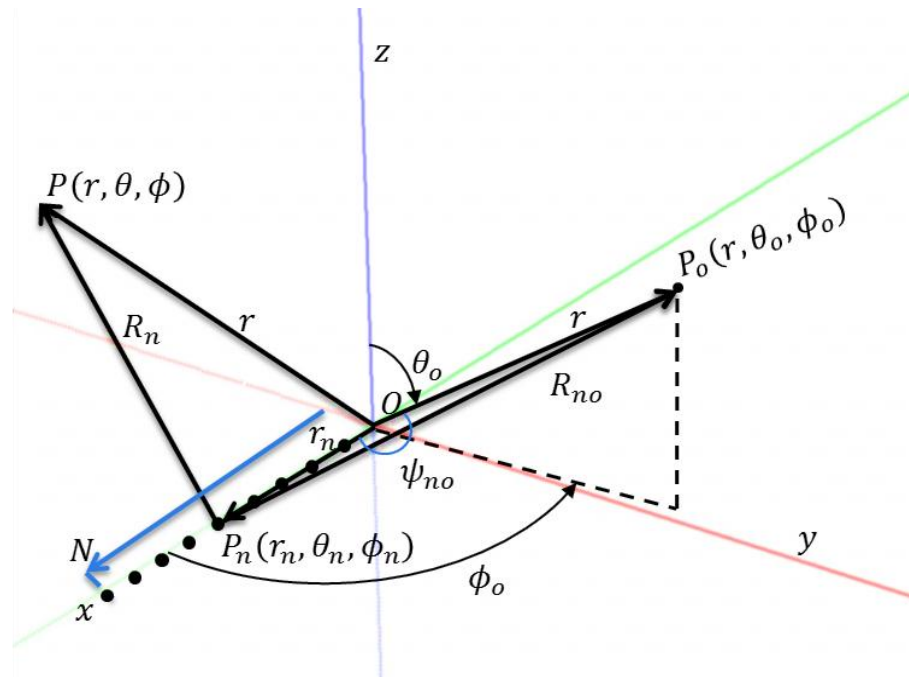


Fig. 6. Geometry of an N-element periodic linear array.

The geometry of a linear array is shown in Fig. 6. The direction cosine $\cos(\psi_n)$ of (0.2.6) is calculated as (1.1.1). This can also be shown by substituting $\theta_n = \pi/2$ and $\phi_n = 0$ into (0.2.6). The differential path length from source to the observation point is likewise specified by (1.1.2). The parameter $x_n = \frac{n}{N}d$ where d is the element spacing in terms of λ . Consequently, the array factor is rewritten as (1.1.3)

$$\cos(\psi_n) = (\hat{a}_x \cdot \hat{a}_r) = (\hat{a}_x) \cdot (\hat{a}_x \sin \theta \cos \phi + \hat{a}_y \sin \theta \sin \phi + \hat{a}_z \cos \theta) = \sin \theta \cos \phi \quad (1.1.1)$$

$$r_n \cos(\psi_n) = \vec{r}_n \cdot \hat{a}_r = (x_n \hat{a}_x) \cdot (\hat{a}_x \sin \theta \cos \phi + \hat{a}_y \sin \theta \sin \phi + \hat{a}_z \cos \theta) = x_n \sin \theta \cos \phi \quad (1.1.2)$$

$$F(\theta, \phi | \vec{x}_n) = \frac{1}{N} \sum_{n=1}^N e^{jkx_n (\sin \theta \cos \phi - \sin \theta_o \cos \phi_o)} = \frac{1}{N} \sum_{n=1}^N e^{jkx_n (\cos \psi_n - \cos \psi_o)} \quad (1.1.3)$$

Simplification can be made to (1.1.3) by the definition of Ψ in (1.1.4). This simplification is shown in (1.1.5) and (1.1.6) for a reference point taken to be at the center of the array. For small values of Ψ , the sin term is reduced to a first order approximation (C.1.24) giving (1.1.7).

$$\Psi = kx_n (\sin \theta \cos \phi - \sin \theta_o \cos \phi_o) = kx_n (\cos(\psi) - \cos(\psi_o)) \quad (1.1.4)$$

$$\begin{aligned} F(\theta, \phi | \vec{x}_n) (e^{j\Psi} - 1) &= \frac{1}{N} (-1 + e^{jN\Psi}), \\ F(\theta, \phi | \vec{x}_n) &= \frac{(-1 + e^{jN\Psi})}{(e^{j\Psi} - 1)} = e^{j\frac{(N-1)\Psi}{2}} \frac{1}{N} \left[\frac{e^{j\frac{(N-1)\Psi}{2}} - e^{-j\frac{(N-1)\Psi}{2}}}{e^{j\frac{1}{2}\Psi} - e^{-j\frac{1}{2}\Psi}} \right] \\ &= e^{j\frac{(N-1)\Psi}{2}} \frac{1}{N} \left[\frac{\sin\left(\frac{N}{2}\Psi\right)}{\sin\left(\frac{1}{2}\Psi\right)} \right] \end{aligned} \quad (1.1.5)$$

$$F(\theta, \phi | \vec{x}_n) = \frac{1}{N} \left[\frac{\sin\left(\frac{N}{2}\Psi\right)}{\sin\left(\frac{1}{2}\Psi\right)} \right] \quad (1.1.6)$$

$$F(\theta, \phi | \vec{x}_n) \approx \frac{1}{N} \left[\frac{\sin\left(\frac{N}{2}\Psi\right)}{\frac{\Psi}{2}} \right] = \text{sinc}\left(\frac{N\Psi}{2}\right) \quad (1.1.7)$$

By the definition of (0.2.15) the far field, radiation intensity is given to be

The radiation patterns of a linear periodic array are plotted for two different spacings in Fig. 7 and Fig. 8.

$$U(\theta, \phi | \vec{x}_n) = \left[\frac{1}{N} \frac{\sin\left(\frac{N}{2}\Psi\right)}{\sin\left(\frac{1}{2}\Psi\right)} \right]^2 \quad (1.1.8)$$

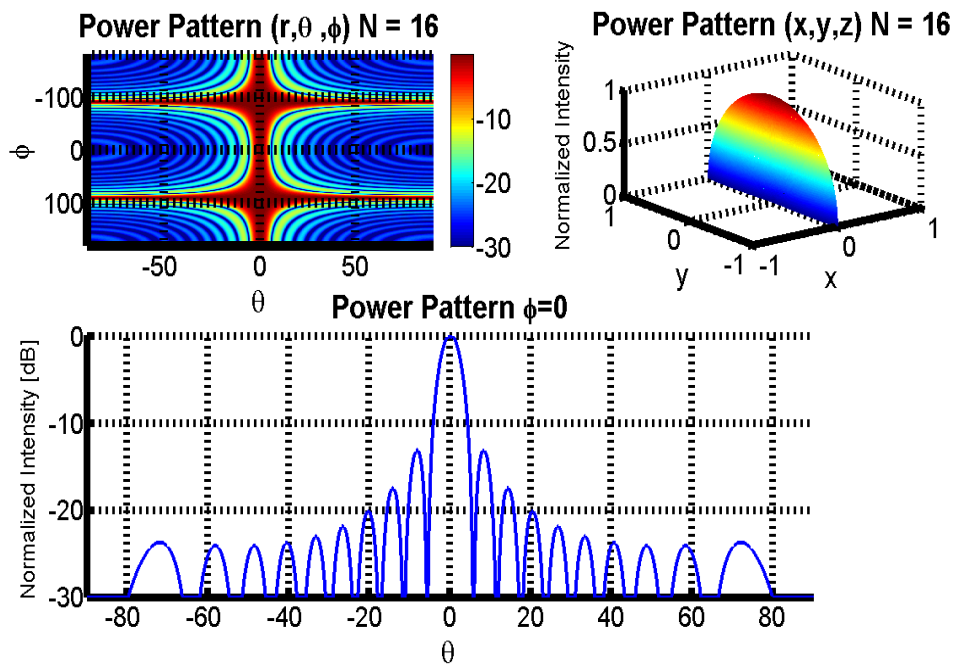


Fig. 7. Radiation intensity of 16 elements periodically spaced along the line (X-Axis) with spacing

$$d_x = 0.625 \lambda$$

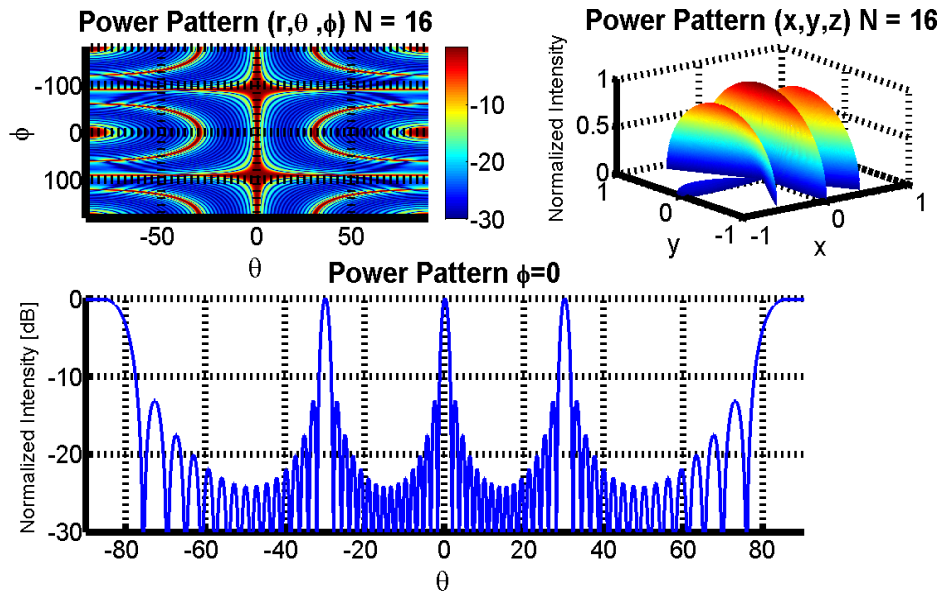


Fig. 8. Radiation intensity of 16 elements periodically spaced along the line (X-Axis) with spacing $d_x = 2 \lambda$.

3.2. Aperiodic

A. System Development and Beampattern Definition

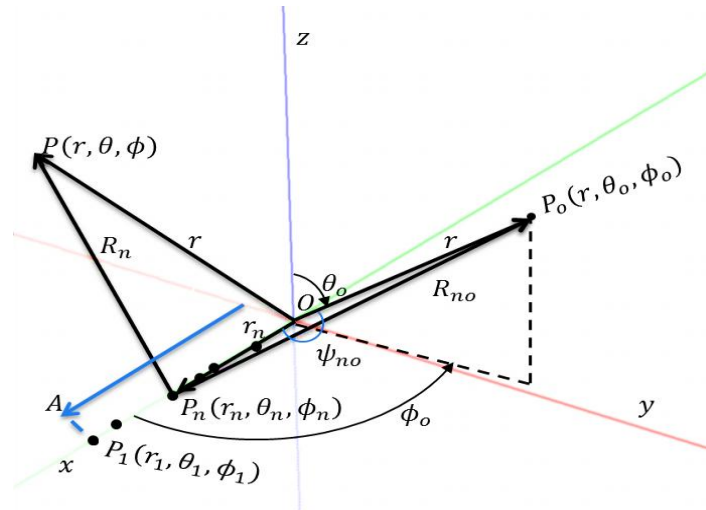


Fig. 9. Geometry of an N-element random linear array.

The geometry of a linear array is shown in Fig. 9. The array factor (1.1.9) of a random linear array (X-Axis) can be shown to be the same as (1.1.3), with the exception

x_n takes on the newly designated form of a random variable; $x_n \triangleq \frac{x_n}{A}$ normalized to the length of the array.

$$F(\theta, \phi | \vec{x}_n) = \frac{1}{N} \sum_{k=1}^N e^{j \frac{2\pi A}{\lambda} (\sin \theta \cos \phi - \sin \theta_o \cos \phi_o) x_n} = \frac{1}{N} \sum_{k=1}^N e^{j \frac{2\pi A}{\lambda} (\cos \psi_n - \cos \psi_{no}) x_n} \quad (1.1.9)$$

A simple random variable is established for those parameters that rely upon the source position given as $u_n \triangleq x_n$. It is desirable to create random variables in this nature such that the uncertainty of the source position is formulated in terms of well-known probabilistic distributions. The individual probability density functions (PDF) of the variable x_n and u_n are derived in the following manner,

$$\int_{-A}^A f_{x_n}(x) dx = 1, \quad f_{x_n}(x) = \frac{1}{2A} \text{ for } |x| \leq A \quad (1.1.10)$$

$$\int_{-A}^A f_{u_n}(u) du = 1, \quad f_{u_n}(u) = \frac{1}{2} \Big|_{A=1}, \quad -1 \leq u \leq 1 \quad (1.1.11)$$

The integration limits are set such that $A=1$ for simplicity [67]. The pattern function (1.1.9) is now rewritten in terms of a normalized radius with respect to wavelength $A = \frac{\lambda}{2}$ and the simple random variable u_n as (1.1.12). At last applying (1.1.12) to the far-field radiation intensity (0.2.15) one obtains (1.1.13) with spatial parameter $\alpha(\theta, \phi)$ (1.1.14), which provides compactness in the formulation.

$$F(\theta, \phi | \vec{x}_n) = \frac{1}{N} \sum_{n=1}^N e^{j 2\pi A (\cos \psi_n - \cos \psi_{no}) u_n} \quad (1.1.12)$$

$$U(\theta, \phi | \vec{u}) = \frac{1}{N^2} \sum_{m=1}^N \sum_{n=1}^N e^{j 2\pi A (\cos \psi_n - \cos \psi_{no}) (u_n - u_m)}$$

$$= \frac{1}{N} + \frac{1}{N^2} \sum_{m=1}^N \sum_{\substack{n=1 \\ n \neq m}}^N e^{j\alpha(\theta, \phi)(u_n - u_m)} \quad (1.1.13)$$

$$\alpha(\theta, \phi) \triangleq 2\pi A(\cos \psi_n - \cos \psi_{no}) \quad (1.1.14)$$

B. Average Properties of a Uniformly Distributed Linear Antenna Array with Perfect Phase Information

The definition of expectation (0.2.19) is used to derive the average radiation intensity (1.1.17) as follows

$$\begin{aligned} U_{av}(\theta, \phi) &= E_u \left| U(\theta, \phi | \vec{u}) \right| \\ &= \int_{-1}^1 \int_{-1}^1 \left(\frac{1}{N} + \frac{1}{N^2} \sum_{m=1}^N \sum_{\substack{n=1 \\ n \neq m}}^N e^{j\alpha(\theta, \phi)(u_n - u_m)} \right) f_{u_n}(u_n) f_{u_m}(u_m) du_n du_m \quad (1.1.15) \\ &= \int_{-1}^1 \int_{-1}^1 \left(\frac{1}{N} + \frac{1}{N^2} \sum_{m=1}^N \sum_{\substack{n=1 \\ n \neq m}}^N e^{j\alpha(\theta, \phi)(u_n - u_m)} \right) \frac{1}{2} \frac{1}{2} du_n du_m \end{aligned}$$

The average of the left side of (1.1.15) is given by (A.1.1) to be $\frac{1}{N}$. The double summation term simplifies from the identity (G.1.2) successively giving (1.1.16). The last step of the procedure is to solve the integral, and can be done using the identity (A.1.2). As a result, one obtains the average radiation intensity in its final form represented in(1.1.17).

$$E_u \left| U(\theta, \phi | \vec{u}) \right| = \frac{1}{N} + \left(1 - \frac{1}{N}\right) \left[\int_{-1}^1 \frac{1}{2} \cos(\alpha(\theta, \phi)(u_n - u_m)) du_n \int_{-1}^1 \frac{1}{2} du_m \right] \quad (1.1.16)$$

$$\begin{aligned} E_u \left| U(\theta, \phi | \vec{u}) \right| &= \frac{1}{N} + \frac{1}{4} \left(1 - \frac{1}{N}\right) \left[\int_{-1}^1 \int_{-1}^1 \cos(\alpha(\theta, \phi)(u_n - u_m)) du_n du_m \right] \\ &= \frac{1}{N} + \left(1 - \frac{1}{N}\right) \left| \text{sinc}(\alpha(\theta, \phi)) \right|^2 \end{aligned} \quad (1.1.17)$$

The power pattern of (1.1.17) is conveniently expressed as the addition of two distinct terms. The first term represents the average power level of the side lobe. It's interesting to note this term is independent of location. The second term represents the mainlobe factor, which is characterized by the oscillatory sinc function, and rapidly decreases with increasing spatial parameter $\alpha(\theta, \phi)$.

At the meridian elevation angle $\theta = \theta_o = \frac{\pi}{2}$ the radiation pattern simplifies to

$$\begin{aligned} E_u \left| U(\phi | \vec{u}) \right| &= \frac{1}{N} + \frac{1}{4} \left(1 - \frac{1}{N} \right) \left[\int_{-1}^1 \int_{-1}^1 \cos(\alpha(\phi)(u_n - u_m)) du_n du_m \right] \\ &= \frac{1}{N} + \left(1 - \frac{1}{N} \right) \left| \text{sinc}(\alpha(\phi)) \right|^2 \end{aligned} \quad (1.1.18)$$

The radiation pattern of a random linear array is plotted in Fig. 10 at the meridian angle and total pattern in Fig. 11.

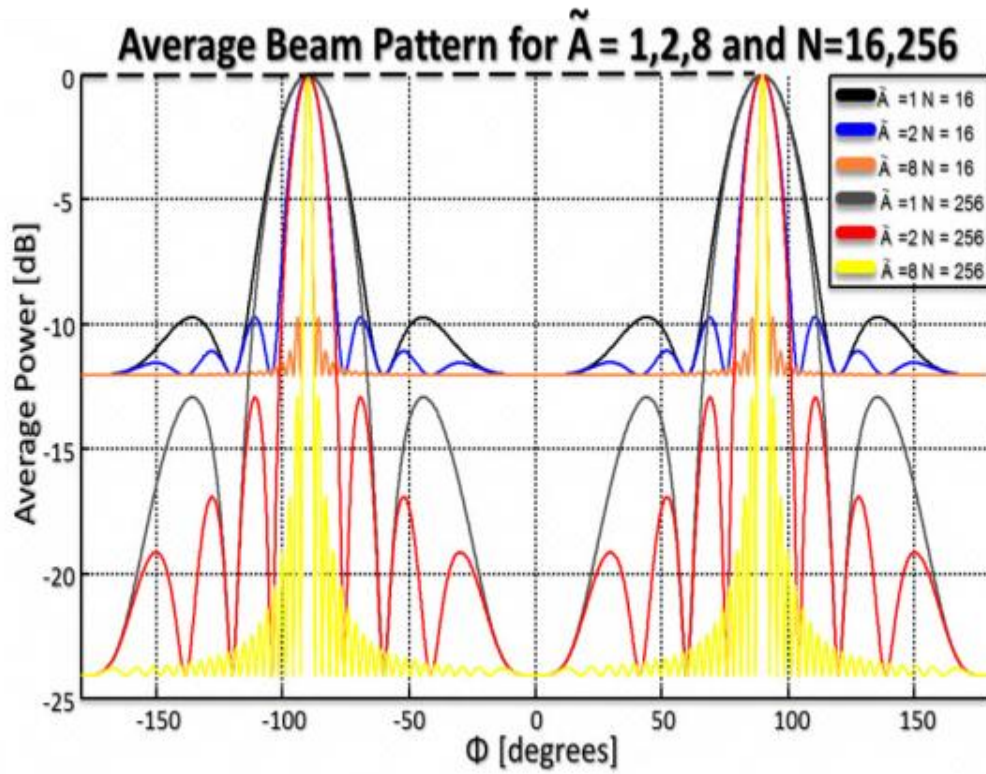


Fig. 10. Average radiation intensity at the meridian elevation angle of a random linear array (X-axis).

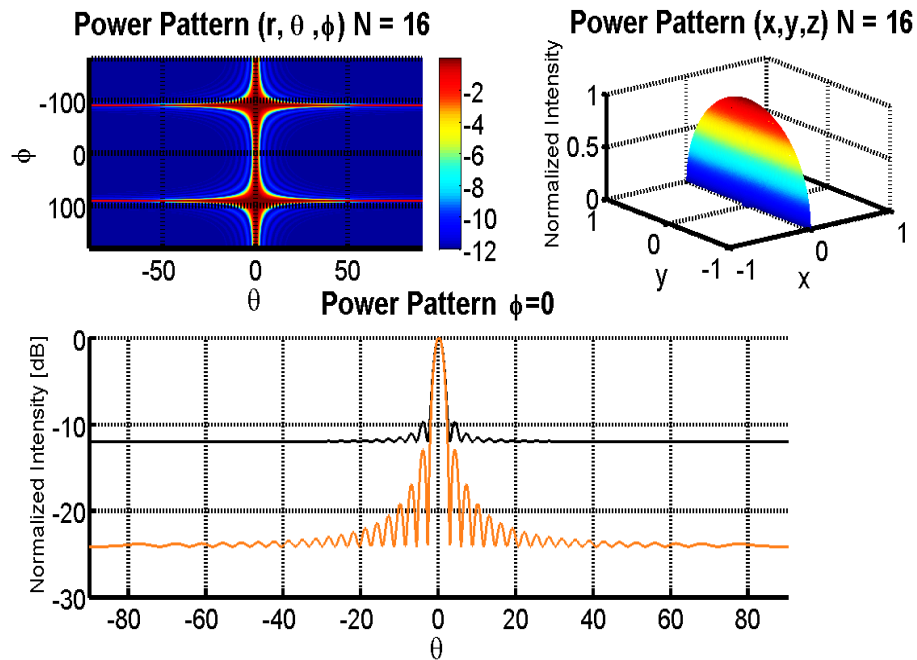


Fig. 11. Average radiation pattern of 16 and 256 elements randomly spaced along the line (X-Axis) of length $A = 10\lambda$.

C. Realization of a Uniformly Distributed Linear Antenna Array with Perfect Phase Information

The realization pattern for a random linear array is plotted in Fig. 12 with a given element distribution shown in Fig. 13.

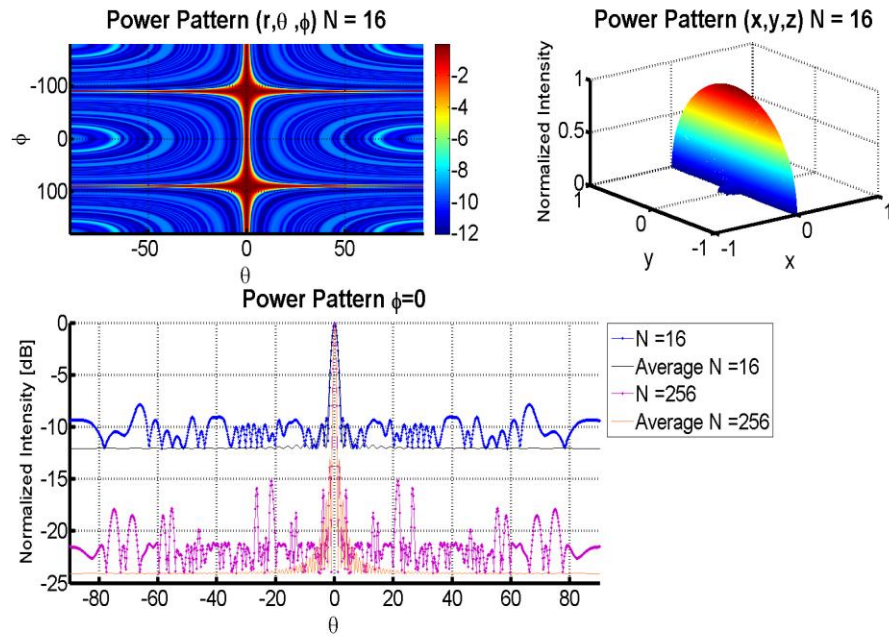


Fig. 12. Simulated and analytical results for a linear random array along the x-direction with

$A = 10$, $N = 16$ and 256 .

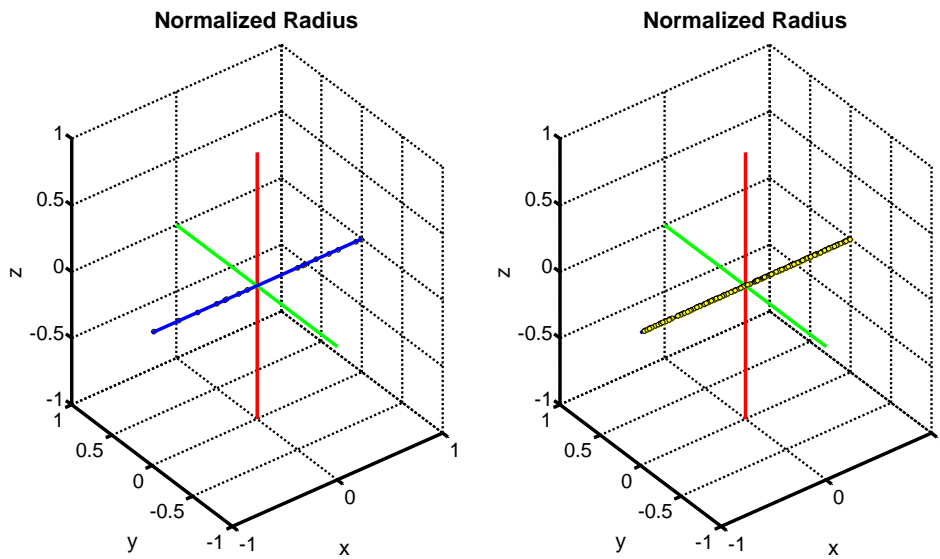


Fig. 13. 16 (left) and 256 (right) elements uniformly distributed in a normalized linear aperture along the x-axis.

CHAPTER IV

PLANAR ARRAYS

4.1 Periodic

A. System Development and Beampattern Definition

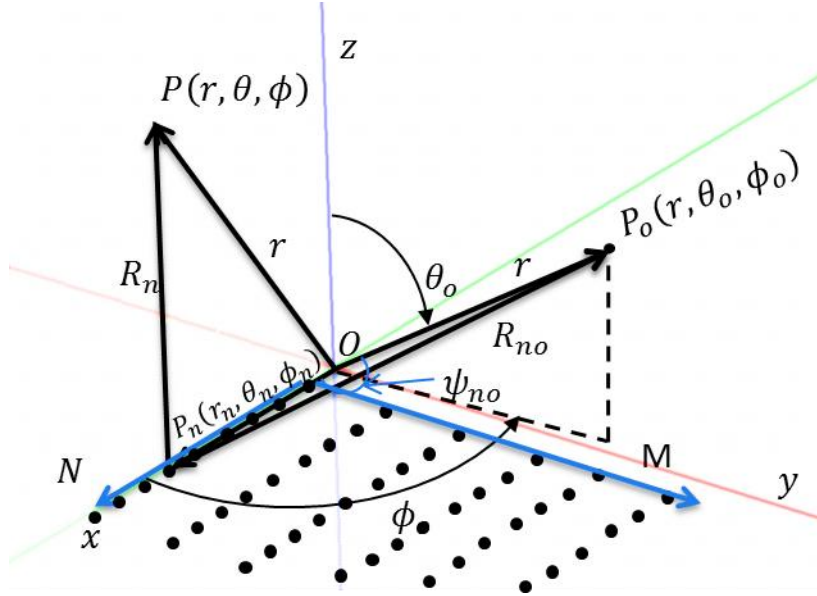


Fig. 14. Geometry of an MxN periodic planar array.

The geometry of a periodic planar array is shown in Fig. 14. The direction cosine $\cos(\psi_n)$ of (0.2.6) is calculated in (2.1.1). This can also be shown by substituting

$\theta_n = \frac{\pi}{2}$ and re-expanding the term $\cos(\phi - \phi_n)$ by the identity (C.1.4). The differential path

length from source to observation point is specified by (2.1.2) where $x_n = \frac{n}{N}d$, $y_m = \frac{m}{N}d$

and d is the element spacing in terms of λ .

$$\begin{aligned} \cos(\psi_n) &= (\hat{a}_x \cdot \hat{a}_r + \hat{a}_y \cdot \hat{a}_r) = (\hat{a}_x + \hat{a}_y) \cdot (\hat{a}_x \sin \theta \cos \phi + \hat{a}_y \sin \theta \sin \phi + \hat{a}_z \cos \theta) \\ &= \sin \theta \cos \phi + \sin \theta \sin \phi \end{aligned} \quad (2.1.1)$$

$$\begin{aligned} r_n \cos(\psi_n) &= \vec{r}_n \cdot \hat{a}_r = (x_n \hat{a}_x + y_n \hat{a}_y) \cdot (\hat{a}_x \sin \theta \cos \phi + \hat{a}_y \sin \theta \sin \phi + \hat{a}_z \cos \theta) \\ &= x_n \sin \theta \cos \phi + y_n \sin \theta \sin \phi \end{aligned} \quad (2.1.2)$$

The array factor of a planar array can be derived as an extended version of the array factor (1.1.3) of a linear array (x-direction). If M of arrays along the x-axis are placed next to one another in the y-direction a distance d apart, a square planar array is formed given in (2.1.3)

$$F(\theta, \phi | \vec{x}_n, \vec{y}_m) = \frac{1}{M} \frac{1}{N} \sum_{m=1}^M \sum_{n=1}^N e^{jkx_n (\sin \theta \cos \phi - \sin \theta_o \cos \phi_o)} e^{jky_m (\sin \theta \sin \phi - \sin \theta_o \sin \phi_o)} \quad (2.1.3)$$

Simplification can be made to (2.1.3) in the same manner used to simplify (1.1.3) with designations of Ψ_x (2.1.4) and Ψ_y (2.1.5); the respective phase progressions in the x and y directions. Nevertheless, since the phase progressions are independent for a square planar array the understanding that $\Psi_x \equiv \Psi_y \equiv \Psi$ can be presumed. So by the same approach used in (1.1.5), (1.1.6) and (1.1.7) one can show (2.1.6) and (2.1.7).

$$\Psi_x = kx_n (\sin \theta \cos \phi - \sin \theta_o \cos \phi_o) \quad (2.1.4)$$

$$\Psi_y = ky_m (\sin \theta \sin \phi - \sin \theta_o \sin \phi_o) \quad (2.1.5)$$

$$F(\theta, \phi | \vec{x}_n, \vec{y}_m) = \frac{1}{M} \frac{\sin\left(\frac{M}{2} \Psi_x\right)}{\sin\left(\frac{1}{2} \Psi_x\right)} \frac{1}{N} \frac{\sin\left(\frac{N}{2} \Psi_y\right)}{\sin\left(\frac{1}{2} \Psi_y\right)} \quad (2.1.6)$$

$$F(\theta, \phi | \vec{x}_n, \vec{y}_m) = \frac{1}{M} \text{sinc}\left(\frac{M}{2} \Psi_x\right) \frac{1}{N} \text{sinc}\left(\frac{N}{2} \Psi_y\right) \quad (2.1.7)$$

Now by the definition of (0.2.15) the far-field radiation intensity is given to be

$$U(\theta, \phi | \vec{x}_n, \vec{y}_m) = \left| \frac{1}{M} \frac{\sin\left(\frac{M}{2} \Psi_x\right)}{\sin\left(\frac{1}{2} \Psi_x\right)} \right|^2 \left| \frac{1}{N} \frac{\sin\left(\frac{N}{2} \Psi_y\right)}{\sin\left(\frac{1}{2} \Psi_y\right)} \right|^2 \quad (2.1.8)$$

When the spacing d is equal to or greater than $\frac{\lambda}{2}$, multiple main beams of equal magnitude are formed [65]. The principal maximum is referred as the *main beam* and is located in the direction of phase excitation $\Psi_x(\theta_o, \phi_o), \Psi_y(\theta_o, \phi_o)$. The remaining maxima are referred as *grating lobes*. Also the phase excitation Ψ_x and Ψ_y are independent and because of this they do not necessarily have to be phased to have the same main beam, per say in the direction $\theta = \theta_o$ and $\phi = \phi_o$. They can be adjusted so that the main beam $\Psi_x(\theta_{xo}, \phi_{xo})$ points differently than the main beam of $\Psi_y(\theta_{yo}, \phi_{yo})$. Still, for most practical purposes one main beam is typically desired. It also should be noted spacing larger than half a wavelength will provide grating lobes given by (2.1.9) and (2.1.10). If these equations are solved simultaneously a solution of (2.1.11) and (2.1.12) can be obtained.

$$\sin \theta \cos \phi + \sin \theta_o \cos \phi_o = \pm \frac{n\lambda}{d} \quad n = 0, 1, 2, \dots \quad (2.1.9)$$

$$\sin \theta \sin \phi + \sin \theta_o \sin \phi_o = \pm \frac{m\lambda}{d} \quad m = 0, 1, 2, \dots \quad (2.1.10)$$

$$\phi = \tan^{-1} \left[\frac{\sin \theta_o \sin \phi_o \pm m\lambda/d}{\sin \theta_o \cos \phi_o \pm n\lambda/d} \right] \quad (2.1.11)$$

$$\theta = \sin^{-1} \left[\frac{\sin \theta_o \cos \phi_o \pm n\lambda/d}{\cos \phi} \right] = \sin^{-1} \left[\frac{\sin \theta_o \sin \phi_o \pm m\lambda/d}{\sin \phi} \right] \quad (2.1.12)$$

The radiation pattern of a random planar array is plotted in Fig. 15 at the meridian angle and total pattern in Fig. 16.

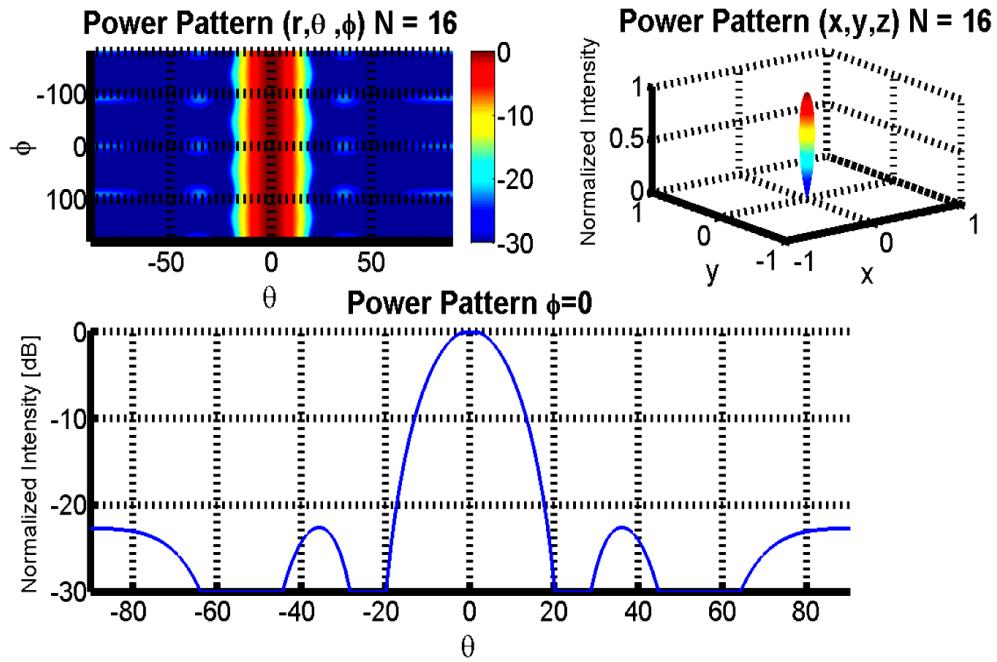


Fig. 15. Radiation pattern of 16 elements periodically spaced within a planar aperture with spacing

$$d_x=d_y=0.625 \lambda .$$

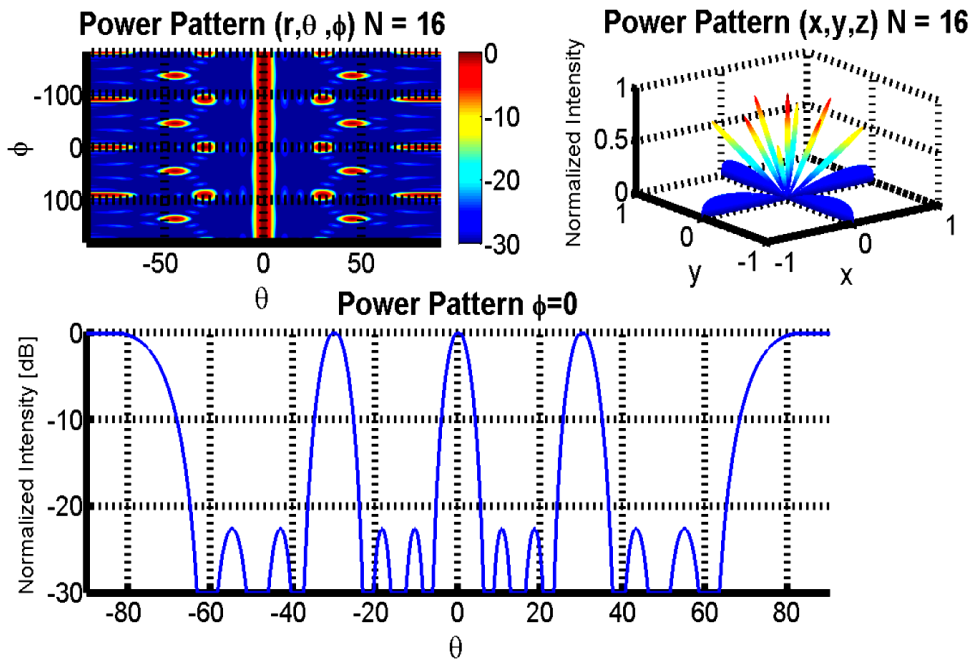


Fig. 16. Radiation pattern of 16 elements periodically spaced within a planar aperture with spacing

$$D_x=D_y=2 \lambda .$$

4.2 Aperiodic

A. System Development and Beampattern Definition

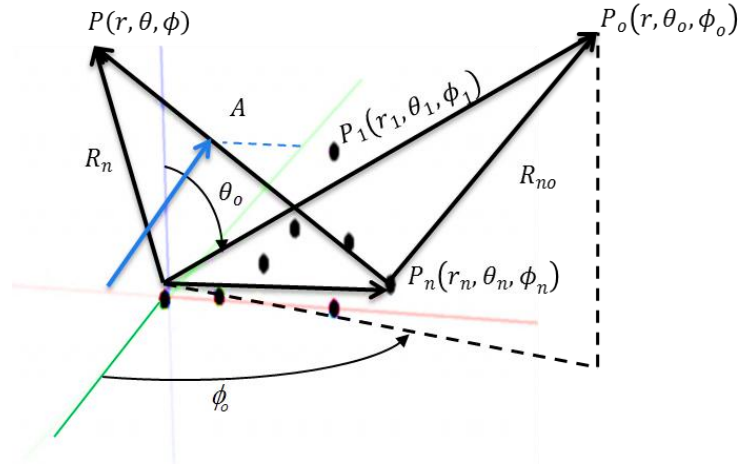


Fig. 17. Geometry of an MxN random planar array.

The geometry of a random planar array is shown in Fig. 17. The array factor of a random planar array (2.1.13) (XY-plane) can be shown to be the same as that of (2.1.3), with the exception x_n and y_n have been tailored to fit the definition of being random variables $\tilde{x}_n \triangleq \frac{x_n}{A}$ and $\tilde{y}_n \triangleq \frac{y_n}{A}$ normalized to the length of the array.

$$F(\theta, \phi | \vec{x}_n, \vec{y}_n) = \frac{1}{N} \sum_{n=1}^N e^{j \frac{2\pi A}{\lambda} \tilde{x}_n (\sin \theta \cos \phi - \sin \theta_o \cos \phi_o)} e^{j \frac{2\pi A}{\lambda} \tilde{y}_n (\sin \theta \sin \phi - \sin \theta_o \sin \phi_o)} \quad (2.1.13)$$

These simple random variables are established similar to the linear array such that $u_n \triangleq \tilde{x}_n$ and $v_n \triangleq \tilde{y}_n$. The corresponding probability density functions of x_n , and u_n will respectively still be given by (1.1.10) and (1.1.11). The P.D.F. of y_n , and v_n are given by (2.1.14) and (2.1.15).

$$\int_{-B}^B f_{y_n}(y) dy = 1, \quad f_{y_n}(y) = \frac{1}{2B} \text{ for } |B| \leq \infty \quad (2.1.14)$$

$$\int_{-B}^B f_{v_n}(v) dv = 1, \quad f_{v_n}(v) = \frac{1}{2} \Big|_{B=A=1}, \quad -1 \leq v \leq 1 \quad (2.1.15)$$

The integration limits are set such that $A=B=1$ for simplicity. A pattern function (or array factor) is now rewritten (2.1.16) in terms of the simple random variables u_n, v_n and $\tilde{A} = \frac{A}{\lambda}$; the length of the array normalized to wavelength.

$$F(\theta, \phi | \vec{u}, \vec{v}) = \frac{1}{N} \sum_{n=1}^N e^{j2\pi\tilde{A}u_n[\sin\theta\cos\phi - \sin\theta_o\cos\phi_o]} e^{j2\pi\tilde{A}v_n[\sin\theta\sin\phi - \sin\theta_o\sin\phi_o]} \quad (2.1.16)$$

At last a far-field radiation intensity (0.2.15) is derived by that of (2.1.17). The spatial parameters $\alpha(\theta, \phi)$ (also given within(1.1.13)) and $\beta(\theta, \phi)$ are given by (2.1.18) and (2.1.19) and are again provide for compactness in the formulations.

$$U(\theta, \phi | \vec{u}, \vec{v}) = \frac{1}{N} + \frac{1}{N^2} \sum_{m=1}^N \sum_{\substack{m=1 \\ m \neq n}}^N e^{j\alpha(\theta, \phi)(u_m - u_n)} e^{j\beta(\theta, \phi)(v_m - v_n)} \quad (2.1.17)$$

$$\alpha(\theta, \phi) \triangleq 2\pi A(\sin\theta\cos\phi - \sin\theta_o\cos\phi_o) \quad (2.1.18)$$

$$\beta(\theta, \phi) \triangleq 2\pi A(\sin\theta\sin(\phi) - \sin\theta_o\sin(\phi_o)) \quad (2.1.19)$$

B. Average Properties of a Uniformly Distributed Planar Antenna Array with Perfect Phase Information

The definition of expectation (0.2.19) can be applied to (4.2.9) to derive the average radiation intensity (4.2.12) as follows

$$\begin{aligned}
U_{av}(\theta, \phi) &= E_{u,v} \left| U(\theta, \phi | \vec{u}, \vec{v}) \right| \\
&= \int_{-1}^1 \int_{-1}^1 \int_{-1}^1 \int_{-1}^1 \left(\frac{1}{N} + \frac{1}{N^2} \sum_{m=1}^N \sum_{\substack{n=1 \\ n \neq m}}^N e^{j\alpha(\theta, \phi)(u_n - u_m)} e^{j\beta(\theta, \phi)(v_n - v_m)} \right) f_{u_m}(u_m) f_{u_n}(u_n) du_m du_n f_{v_m}(v_m) f_{v_n}(v_n) dv_m dv_n \\
&= \int_{-1}^1 \int_{-1}^1 \int_{-1}^1 \int_{-1}^1 \left(\frac{1}{N} + \frac{1}{N^2} \sum_{m=1}^N \sum_{\substack{n=1 \\ n \neq m}}^N e^{j\alpha(\theta, \phi)(u_n - u_m)} e^{j\beta(\theta, \phi)(v_n - v_m)} \right) \frac{1}{2} \frac{1}{2} du_m du_n \frac{1}{2} \frac{1}{2} dv_m dv_n \quad (2.1.20)
\end{aligned}$$

The average of the left side of (2.1.20) is given by (A.1.1) to be $\frac{1}{N}$. Additionally, the double summation term simplifies from the identity of (B.1.2) and in succession provides (2.1.21). The last step is to solve the integral formulation of (2.1.21) providing the average radiation intensity in its final form (2.1.22).

$$\begin{aligned}
E_v \left| U(\theta, \phi | \vec{u}, \vec{v}) \right| &= \\
\frac{1}{N} + \frac{1}{16} \left(1 - \frac{1}{N} \right) \int_{-1}^1 \int_{-1}^1 \int_{-1}^1 \int_{-1}^1 \cos(\alpha(\theta, \phi)(u_n - u_m) + \beta(\theta, \phi)(v_n - v_m)) du_m du_n dv_m dv_n & \quad (2.1.21)
\end{aligned}$$

$$U_{av}(\theta, \phi) = E_{u,v} \left| U(\theta, \phi | \vec{u}, \vec{v}) \right| = \frac{1}{N} + \left(1 - \frac{1}{N} \right) \left| \text{sinc}(\alpha(\theta, \phi)) \right|^2 \left| \text{sinc}(\beta(\theta, \phi)) \right|^2 \quad (2.1.22)$$

The average radiation intensity (2.1.22) of a random planar array is similar to that of a random linear array (1.1.17). Comparable to the linear array one finds the pattern is expressed as the addition of two distinct terms once again. However, a difference exists amongst the second term, representing the mainlobe factor. This term now describes the main beam by the multiplication of two oscillatory sinc functions. Thus, in due to multiplication of a normalized pattern taking values less than unity outside the main beam region the average pattern will rapidly decrease faster than a linear array. Or increasing either spatial parameter $\alpha(\theta, \phi)$ or $\beta(\theta, \phi)$ will contribute to the decay of the pattern whereas in the linear array only the spatial parameter $\alpha(\theta, \phi)$ contributed.

At the meridian angle $\theta = \theta_o = \frac{\pi}{2}$ (2.1.22) simplifies to (2.1.23).

$$U_{av}(\phi) = E_{u,v} \left| U(\phi | \vec{u}, \vec{v}) \right| = \frac{1}{N} + \left(1 - \frac{1}{N} \right) \left| \text{sinc}(\alpha(\phi)) \right|^2 \left| \text{sinc}(\beta(\phi)) \right|^2 \quad (2.1.23)$$

The radiation pattern of a random planar array is plotted in Fig. 18 at the meridian angle and total pattern in Fig. 19.

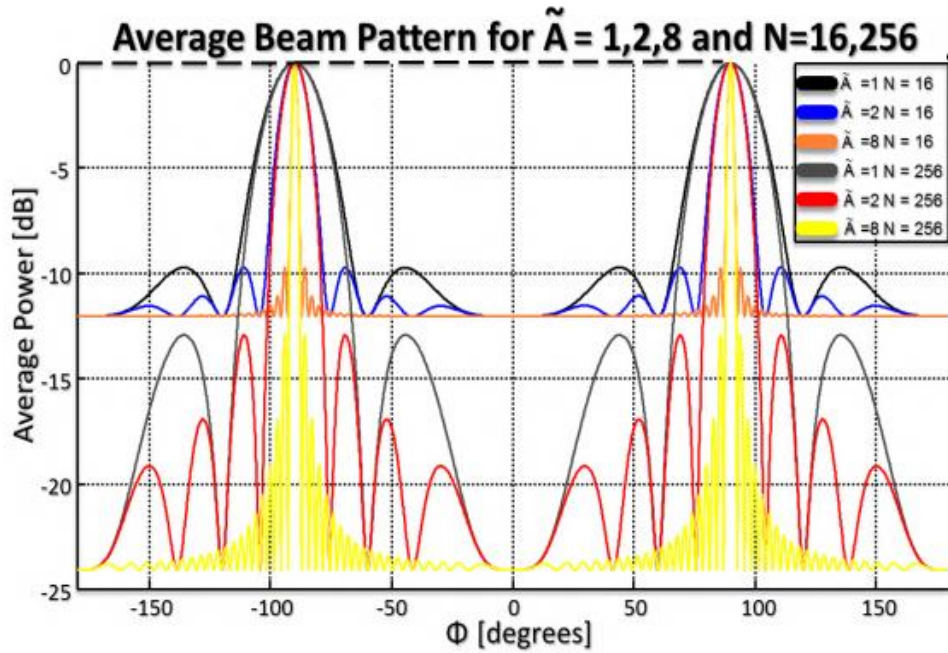


Fig. 18. Average radiation intensity at the meridian elevation angle of a random planar array (XY-Plane).

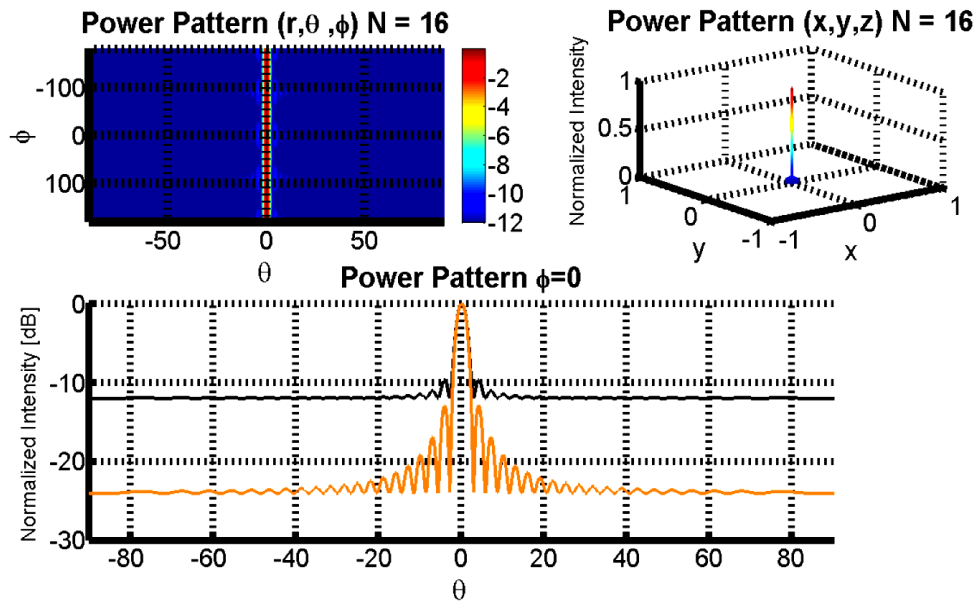


Fig. 19. Average radiation pattern of 16 and 256 elements randomly spaced within a planar aperture of $A = 10\lambda$.

C. Realization of a Uniformly Distributed Planar Antenna Array with Perfect Phase Information

The realization pattern for a random planar array is plotted in Fig. 20 with a given element distribution shown in Fig. 21.

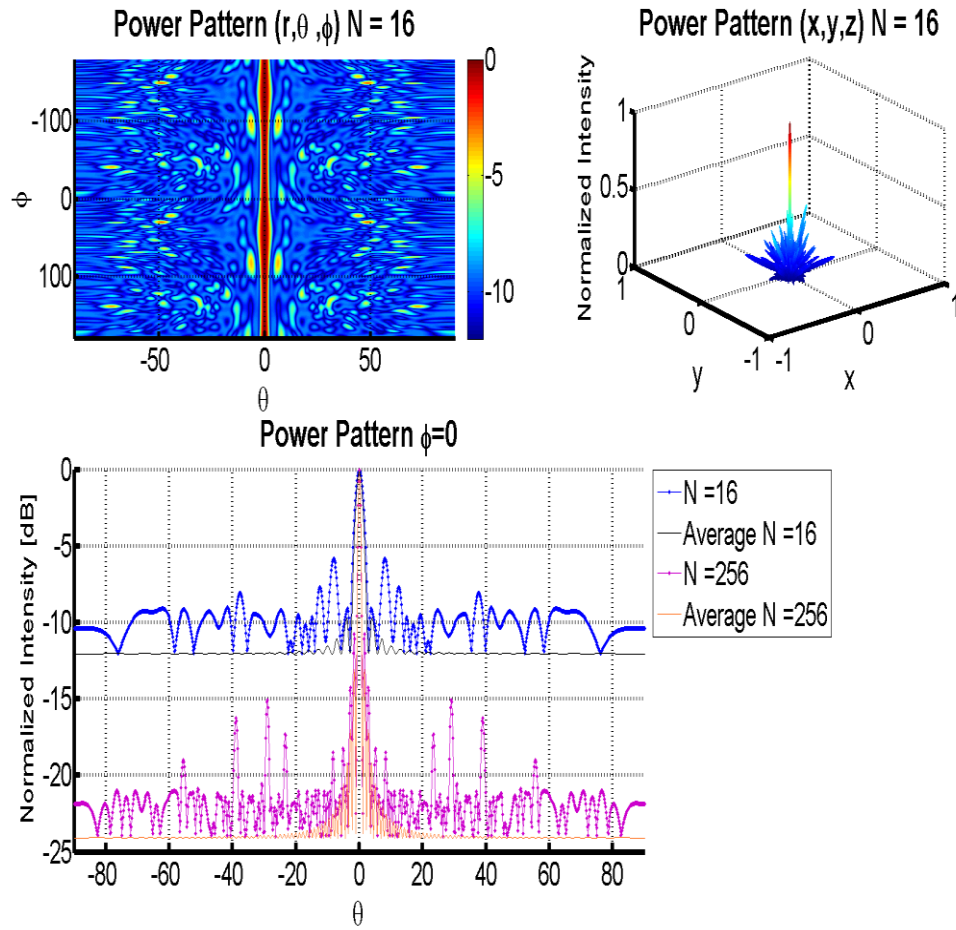


Fig. 20. Simulated and analytical results for a uniformly distributed planar random array in the

***XY-Plane* with $A = 10$, $N = 16$ and 256 .**

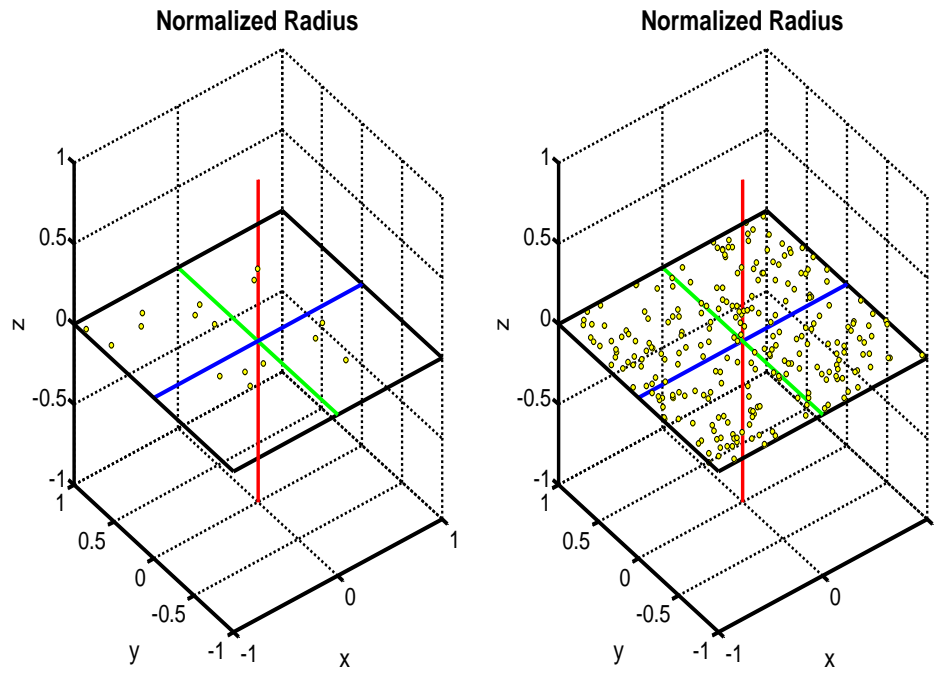


Fig. 21. 16 (left) and 256 (right) elements uniformly distributed in a normalized planar aperture in the XY-plane.

CHAPTER V

CIRCULAR ARRAYS

5.1 Periodic

A. System Development and Beampattern Definition

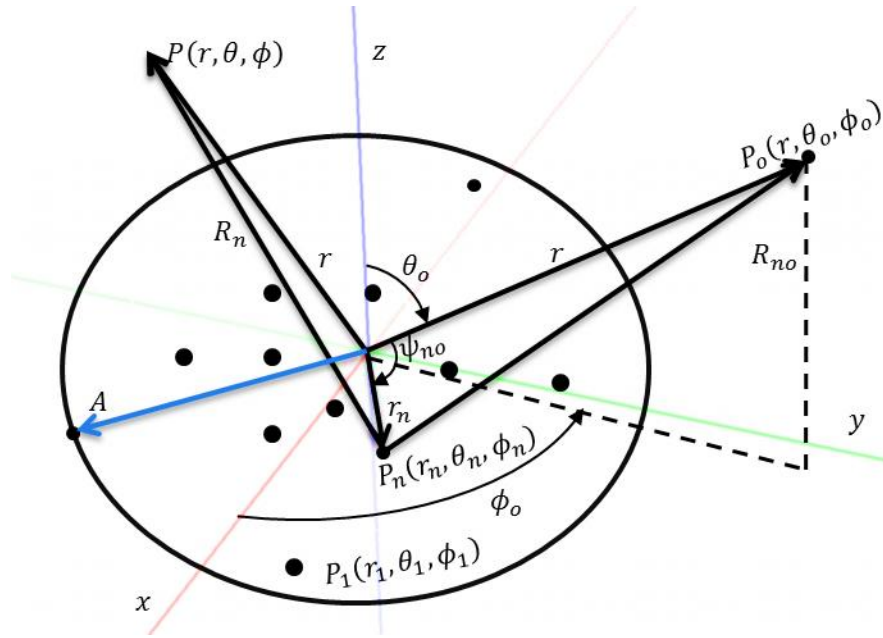


Fig. 22. Geometry of an N-element periodic circular array.

The geometry of a periodic circular array is shown in Fig. 22. The direction cosine $\cos(\psi_n)$ of (0.2.6) is calculated as (3.1.1). This could have also been shown by substituting $\theta_n = \frac{\pi}{2}$ into (0.2.6). The differential path length from source to observation point is likewise specified by (3.1.2).

$$\begin{aligned} \cos(\psi_n) &= (\hat{a}_p \cdot \hat{a}_r) = (\hat{a}_x \cos \phi_n + \hat{a}_y \sin \phi_n) \cdot (\hat{a}_x \sin \theta \cos \phi + \hat{a}_y \sin \theta \sin \phi + \hat{a}_z \cos \theta) \\ &= \sin \theta (\cos \phi \cos \phi_n + \sin \phi \sin \phi_n) = \sin \theta \cos(\phi - \phi_n) \quad (\text{Using Appendix C.1.d}) \end{aligned} \quad (3.1.1)$$

$$\begin{aligned} r_n \cos(\psi_n) &= \vec{r}_n \cdot \hat{a}_r = (\hat{a}_x \rho_n \cos \phi_n + \hat{a}_y \rho_n \sin \phi_n) \cdot (\hat{a}_x \sin \theta \cos \phi + \hat{a}_y \sin \theta \sin \phi + \hat{a}_z \cos \theta) \\ &= \rho_n \sin \theta (\cos \phi \cos \phi_n + \sin \phi \sin \phi_n) = \rho_n \sin \theta \cos(\phi - \phi_n) \end{aligned} \quad (3.1.2)$$

where

$$\phi_n = 2\pi \frac{n}{N} = \text{The angular position of the } n\text{th element} \quad (3.1.3)$$

$$\rho_n = \text{The radius of the } n\text{th circle} \quad (3.1.4)$$

The substitution of appropriate path length into the array factor of (0.2.9) gives the array factor for a circular planar array in(3.1.5).

$$F(\theta, \phi | \bar{\rho}_n, \bar{\phi}_n) = \sum_{n=1}^N e^{jk\rho_n(\sin\theta\cos(\phi-\phi_n) - \sin\theta_o\cos(\phi_o-\phi_n))} = \sum_{n=1}^N e^{jk\rho_n(\cos(\psi_n) - \cos(\psi_{no}))} \quad (3.1.5)$$

The array factor of (3.1.5) can be simplified by expanding the angular information in the exponential term with the definition of(3.1.6). This is done by means of multiplying the numerator and denominator of the exponential term by ρ_o to give (3.1.7). Thereby expanding terms reduces to (3.1.8).

$$\rho_o = \left[(\sin\theta_o\cos\phi_o - \sin\theta\cos\phi)^2 + (\sin\theta_o\sin\phi_o - \sin\theta\sin\phi)^2 \right]^{1/2} \quad (3.1.6)$$

$$kr_n(\cos\psi_n - \cos\psi_{no}) = \frac{kr_n\rho_o(\sin\theta\cos(\phi-\phi_n) - \sin\theta_o\cos(\phi_o-\phi_n))}{\sqrt{(\sin\theta\cos\phi - \sin\theta_o\cos\phi_o)^2 + (\sin\theta\sin\phi - \sin\theta_o\sin\phi_o)^2}} \quad (3.1.7)$$

$$kr_n\rho_o \left[\frac{\cos\phi_n(\sin\theta\cos\phi - \sin\theta_o\cos\phi_o) + \sin\phi_n(\sin\theta\sin\phi - \sin\theta_o\sin\phi_o)}{\sqrt{(\sin\theta\cos\phi - \sin\theta_o\cos\phi_o)^2 + (\sin\theta\sin\phi - \sin\theta_o\sin\phi_o)^2}} \right] \quad (3.1.8)$$

Reduction of (3.1.8) can be achieved by defining (3.1.9) and (3.1.10) to give (3.1.11)

where the angle δ is provided by (3.1.12) .

$$\cos\delta = \frac{\sin\theta\cos\phi - \sin\theta_o\cos\phi_o}{\sqrt{(\sin\theta\cos\phi - \sin\theta_o\cos\phi_o)^2 + (\sin\theta\sin\phi - \sin\theta_o\sin\phi_o)^2}} = \frac{A}{\sqrt{A^2 + B^2}} \quad (3.1.9)$$

where $A = \sin\theta\cos\phi - \sin\theta_o\cos\phi_o$, $B = \sin\theta\sin\phi - \sin\theta_o\sin\phi_o$

$$\sin\delta = 1 - \cos^2\delta = 1 - \frac{A^2}{A^2 + B^2} = \frac{B^2}{A^2 + B^2} \quad (3.1.10)$$

$$kr_n (\cos \psi_n - \cos \psi_{no}) = kr_n \rho_o (\cos \phi_n \cos \varphi + \sin \phi_n \sin \varphi) = kr_n \rho_o (\cos(\phi_n - \delta)) \quad (3.1.11)$$

$$\delta = \tan^{-1} \left[\frac{\sin \theta \sin \phi - \sin \theta_o \sin \phi_o}{\sin \theta \cos \phi - \sin \theta_o \cos \phi_o} \right] \quad (3.1.12)$$

The expressions above come together in terms of providing a nice compact expression (3.1.13). The periodic circular array (3.1.13) can be simplified further using the Bessel identity (D.1.7) to obtain (3.1.14). The parameter ξ_i is defined as the Kronecker delta function. Also for a circular array of one ring the radius of the ring ρ_n will be given by ρ .

$$F(\theta, \phi | \vec{\rho}_n, \vec{\phi}_n) = \sum_{n=1}^N e^{jk\rho_n \rho \cos(\delta - \phi_n)} = \sum_{n=1}^N e^{jk\rho_o \rho \cos(\phi_n - \delta)} \quad (3.1.13)$$

$$\begin{aligned} F(\theta, \phi | \vec{\rho}_n) &= \frac{1}{N} \sum_{k=-\infty}^{\infty} j^k J_k \left(2\pi\rho_o \frac{\rho}{\lambda} \right) e^{-jk\delta} \left\{ \sum_{n=1}^N e^{j2\pi \frac{n}{N} k} \right\} \\ &= \frac{1}{N} \sum_{k=-\infty}^{\infty} j^k J_k \left(2\pi\rho_o \frac{\rho}{\lambda} \right) e^{-jk\delta} N \xi_{k \bmod N} \end{aligned} \quad (3.1.14)$$

By applying the identities of (D.1.9) and (D.1.10) one should obtain (3.1.15) and (3.1.16),

$$\begin{aligned} F(\theta, \phi | \vec{\rho}_n) &= \sum_{k=-\infty}^{\infty} e^{j\left(\frac{\pi}{2} - \delta\right)kN} J_{kN} \left(2\pi\rho_o \frac{\rho}{\lambda} \right) \\ &= J_0 \left(2\pi\rho_o \frac{\rho}{\lambda} \right) + \sum_{k=1}^{\infty} J_{kN} \left(2\pi\rho_o \frac{\rho}{\lambda} \right) \left\{ e^{j\left(\frac{\pi}{2} - \delta\right)kN} + e^{j\left(\frac{\pi}{2} + \delta\right)kN} \right\} \end{aligned} \quad (3.1.15)$$

$$F(\theta, \phi | \vec{\rho}_n) = J_0 \left(2\pi\rho_o \frac{\rho}{\lambda} \right) + 2 \sum_{k=1}^{\infty} J_{kN} \left(2\pi\rho_o \frac{\rho}{\lambda} \right) \{ j^{kN} \cos(kN\delta) \} \quad (3.1.16)$$

Finally by the definition of (0.2.15) the far-field radiation intensity is given to be

$$U(\theta, \phi | \vec{\rho}_n) = \left| J_0 \left(2\pi\rho_o \frac{\rho}{\lambda} \right) + 2 \sum_{k=1}^{\infty} J_{kN} \left(2\pi\rho_o \frac{\rho}{\lambda} \right) \{ j^{kN} \cos(kN\xi) \} \right|^2 \quad (3.1.17)$$

For multiple rings the array factor of (3.1.16) is identified by (3.1.18) where $N' = N/N_R$

$$F(\theta, \phi | \vec{\rho}_n) = \sum_{n=1}^{N_R} \left[J_0 \left(2\pi \rho_o \frac{\rho_n}{\lambda} \right) + 2 \sum_{k=1}^{\infty} J_{kN'} \left(2\pi \rho_o \frac{\rho_n}{\lambda} \right) \{ J^{kN'} \cos(kN' \delta) \} \right] \quad (3.1.18)$$

The radiation pattern of a periodic circular array is plotted for different spacing in Fig. 23 and Fig. 24.

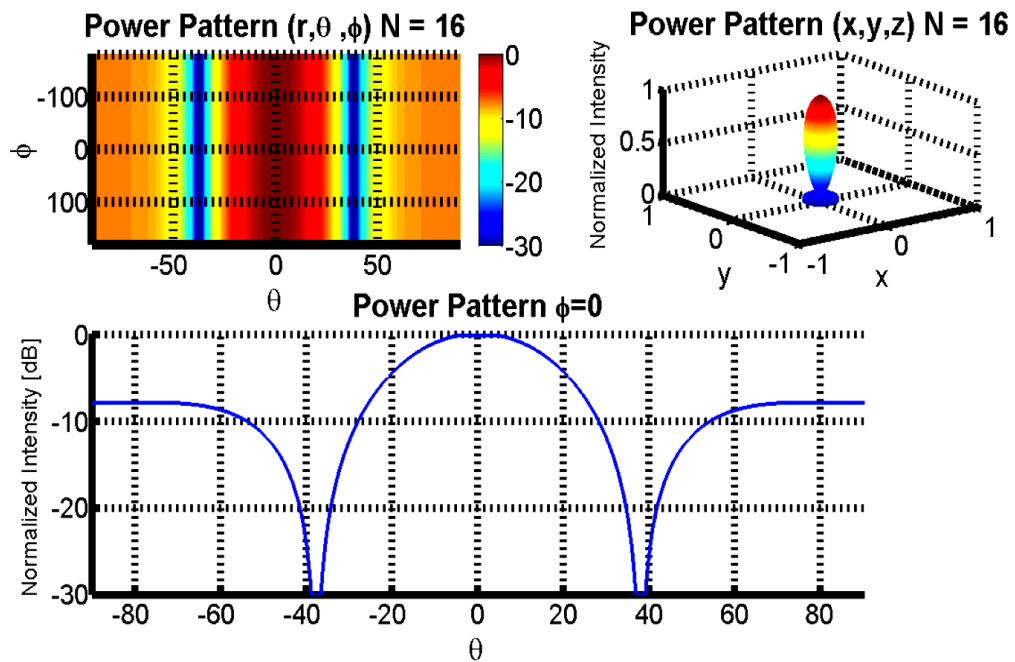


Fig. 23. Radiation pattern of 16 elements periodically spaced about one circular ring of radius

$.625 \lambda$.

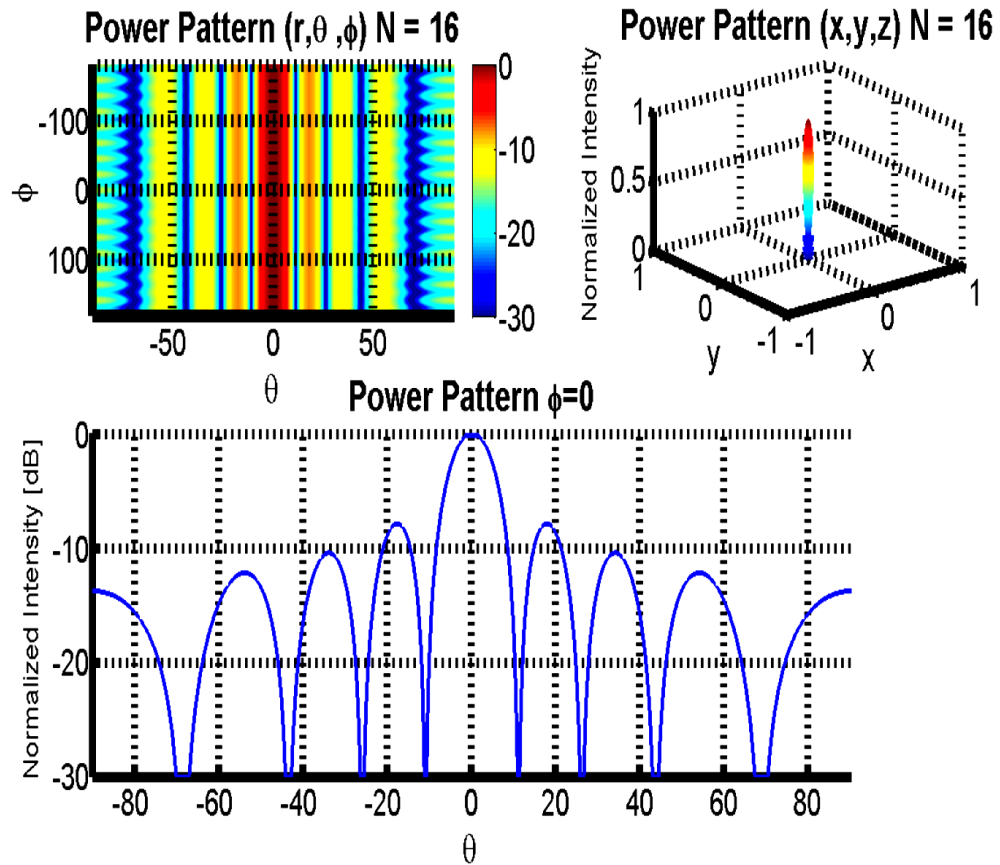


Fig. 24. Radiation pattern of 16 elements periodically spaced about one circular ring of radius 2λ .

5.2 Aperiodic

A. System Development and Beam pattern Definition

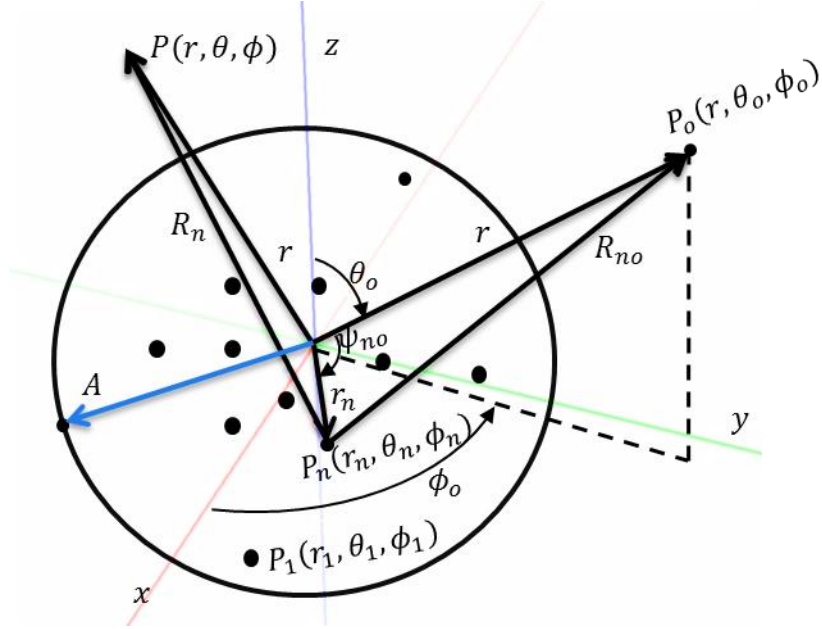


Fig. 25. Geometry of an N-element random circular array.

The geometry of a random circular array is shown in Fig. 25. The array factor of a random circular array (XY-plane) can be shown to be the same as that of either (3.1.5) or (3.1.13), with the exception ρ_n and ϕ_n are now given to be random variables in

(3.1.19) with $\rho_n \triangleq \frac{\rho_n}{A}$ and $\phi_n \triangleq \phi_n - \delta$.

$$F(\theta, \phi | \vec{\rho}_n, \vec{\phi}_n) = \frac{1}{N} \sum_{n=1}^N e^{j2\pi A \rho_n (\sin \theta \cos(\phi - \phi_n) - \sin \theta_o \cos(\phi_o - \phi_n))} = \frac{1}{N} \sum_{n=1}^N e^{j2\pi A \rho_n (\cos \psi_n - \cos \psi_{no})} \quad (3.1.19)$$

$$F(\theta, \phi | \vec{\rho}_n, \vec{\phi}_n) = \sum_{n=1}^N e^{jk \rho_n \cos \phi_n} \quad (3.1.20)$$

It is important to note (3.1.12) provides a compact expression of the array factor which can also be used for the random array. This expressions is useful because it collects the random variables ρ_n and ϕ_n into a more useful compound random variable. The compound random variable takes the form a traditional polar coordinate and the angle δ embedded is convenient, because it provides nothing more than a constant offset in the azimuth providing no added harm or randomness to the phase term.

Unlike formulating the simple random variables in linear and planar random structures a compound random variable is established such that $v_n \triangleq \{\rho_n, \phi_n\} = \rho_n \cos \phi_n, \exists |v_n| \leq 1$. The individual probability density functions (P.D.F.) of the variables ρ_n, ϕ_n are expressed in (3.1.21) and (3.1.22)

$$\int_0^A f_{\rho_n}(\rho) r dr = 1 \quad f_{\rho_n}(\rho) = \frac{2}{A^2} \text{ for } 0 \leq \rho \leq A \quad (3.1.21)$$

$$\int_0^{2\pi} f_{\phi_n}(\phi) d\phi = 1 \quad f_{\phi_n}(\phi) = \frac{1}{2\pi} \text{ for } 0 \leq \phi \leq 2\pi \quad (3.1.22)$$

The corresponding joint P.D.F. for the uniform distribution is formulated using(3.1.23). The convention $A = 1$ is used so the characteristics of the random array are referenced to the unity circle (a more insightful discussion of this can be found in [68]-[79]). The resulting P.D.F. of v_n is indicated as (3.1.24).

$$\int_0^1 \int_0^{2\pi} f_{u_n, v_n}(u, v) u du dv = 1, \quad f_{u_n, v_n}(u, v) = \frac{1}{\pi} \quad (3.1.23)$$

$$f_{v_n}(v) = \int_{-\sqrt{1-v^2}}^{\sqrt{1-v^2}} f_{u_n, v_n}(u, v) du = \int_{-\sqrt{1-v^2}}^{\sqrt{1-v^2}} \frac{1}{\pi} du = \frac{2}{\pi} \sqrt{1-v^2} \quad (3.1.24)$$

A coordinate transformation is used for converting polar to Cartesian coordinates in order to simplify the integration such that $v = \rho \sin \phi$ and $u = \rho \cos \phi$.

The pattern function (or array factor) is now rewritten (3.1.25) in terms of the compound random variable v_n and $\tilde{A} = \frac{A}{\lambda}$.

$$F(\theta, \phi | \vec{v}_n) = \sum_{n=1}^N e^{j2\pi A \rho_n v_n} \quad (3.1.25)$$

At last, a far-field radiation intensity (0.2.15) is defined as (3.1.26) given the new spatial parameter $\zeta(\theta, \phi)$ defined in (3.1.27).

$$U(\theta, \phi | \vec{v}_n) = \frac{1}{N} + \frac{1}{N^2} \sum_{m=1}^N \sum_{\substack{n=1 \\ n \neq m}}^N e^{j\zeta(\theta, \phi)(v_n - v_m)} \quad (3.1.26)$$

$$\zeta(\theta, \phi) \triangleq 2\pi A \rho_o = 2\pi A \sqrt{(\sin \theta \cos \phi - \sin \theta_o \cos \phi_o)^2 + (\sin \theta \sin \phi - \sin \theta_o \sin \phi_o)^2} \quad (3.1.27)$$

A previous analysis [9] observed the array's beampattern at the meridian elevation angle $\theta = \theta_o = \pi/2$, and arrives with an expression (3.1.28) using (C.1.4) shown below.

$$\begin{aligned} \cos(\phi_n - \phi) - \cos(\phi_n - \phi_o) &= -2 \sin\left(\frac{\phi_n - \phi + \phi_n - \phi_o}{2}\right) \sin\left(\frac{\phi_n - \phi - \phi_n + \phi_o}{2}\right) \\ &= -2 \sin\left(\phi_n - \frac{\phi + \phi_o}{2}\right) \sin\left(\frac{\phi_o - \phi}{2}\right) \end{aligned}$$

$$F(\phi | \vec{\rho}_n, \vec{\phi}_n) = \frac{1}{N} \sum_{n=1}^N e^{-j\frac{4\pi}{\lambda} r_n \sin\left(\phi_n - \frac{\phi_o + \phi}{2}\right) \sin\left(\frac{\phi_o - \phi}{2}\right)} = \frac{1}{N} \sum_{n=1}^N e^{-j4\pi A \sin\left(\frac{\phi_o - \phi}{2}\right) v_n} \quad (3.1.28)$$

$$\phi_n = \phi_n - \frac{\phi_o + \phi}{2} \quad (3.1.29)$$

A potential benefit of simplicity arises from (3.1.28) in the context of mobile array systems when it is not necessary for the array factor to be conditioned upon the

elevation angle θ . As well, since the array factor is composed of isotropic radiators a rotationally symmetric pattern exists and reduction is conceived by replacing $\phi_o = 0$. This causes no loss in generality and leads to an array factor of (3.1.30) and far-field power pattern (3.1.31). The spatial parameter $\zeta(\phi) = 4\pi A \sin(\phi/2)$ in these expressions has been used for a more compact expression.

$$F(\phi|\vec{v}) = \frac{1}{N} \sum_{n=1}^N e^{j4\pi A \sin(\frac{\phi}{2})v_n} \quad (3.1.30)$$

$$U(\phi|\vec{v}) = \frac{1}{N} + \frac{1}{N^2} \sum_{m=1}^N \sum_{\substack{n=1 \\ n \neq m}}^N e^{j\zeta(\phi)(v_n - v_m)} \quad (3.1.31)$$

B. Average Properties of a Uniformly Distributed Circular Antenna Array with Perfect Phase Information

1. Average Beampattern

Once again, the definition of expectation (0.2.19) is applied and the integral formulation of (3.1.32) is achieved.

$$\begin{aligned} U_{av}(\theta, \phi) &= E_v \left| U(\theta, \phi|\vec{v}) \right| \\ &= \int_{-1}^1 \int_{-1}^1 \left(\frac{1}{N} + \frac{1}{N^2} \sum_{m=1}^N \sum_{\substack{n=1 \\ n \neq m}}^N e^{j\zeta(\theta, \phi)(v_n - v_m)} \right) f_{v_m}(v_m) f_{v_n}(v_n) dv_m dv_n \\ &= \int_{-1}^1 \int_{-1}^1 \left(\frac{1}{N} + \frac{1}{N^2} \sum_{m=1}^N \sum_{\substack{n=1 \\ n \neq m}}^N e^{j\zeta(\theta, \phi)(v_n - v_m)} \right) \frac{2}{\pi} \sqrt{1-v_m^2} \frac{2}{\pi} \sqrt{1-v_n^2} dv_m dv_n \end{aligned} \quad (3.1.32)$$

The integration of the first term of (3.1.32) is given by (A.1.5) and once again yields an average sidelobe level of $\frac{1}{N}$ similar to the planar and linear random array. As well, the double summation term simplifies identical to the previous sections and in

succession gives(3.1.33). The last step is to solve the integral of (3.1.33) which provides the average radiation intensity in its final form (3.1.34).

$$E_v \left| U(\theta, \phi | \bar{v}) \right| = \frac{1}{N} + \left(1 - \frac{1}{N} \right) \left[\int_{-1}^1 \frac{2}{\pi} \cos(\zeta(\theta, \phi)(v_n - v_m)) \sqrt{1 - v_m^2} dv_m \int_{-1}^1 \frac{2}{\pi} \sqrt{1 - v_n^2} dv_n \right] \quad (3.1.33)$$

$$U_{av}(\theta, \phi) = E_v \left| U(\theta, \phi | \bar{v}) \right| = \frac{1}{N} + \left(1 - \frac{1}{N} \right) \left| 2 \text{jinc}(\zeta(\theta, \phi)) \right|^2 \quad (3.1.34)$$

The above result could of also been solved using the individual probability functions for ρ_n and ϕ_n . To do this one should rewrite (3.1.32) as (3.1.35).

$$\begin{aligned} U_{av}(\theta, \phi) &= E_v \left| U(\theta, \phi | \bar{v}) \right| \\ &= \int_0^{2\pi} \int_0^{2\pi} \int_0^1 \int_0^1 \left(\frac{1}{N} + \frac{1}{N^2} \sum_{\substack{m=1 \\ n \neq m}}^N \sum_{n=1}^N e^{j\zeta(\theta, \phi)(\tilde{\rho}_n \tilde{\phi}_n - \tilde{\rho}_m \tilde{\phi}_m)} \right) f_{\tilde{\rho}_m}(\tilde{\rho}_m) f_{\tilde{\rho}_n}(\tilde{\rho}_n) d\tilde{\rho}_m d\tilde{\rho}_n f_{\tilde{\phi}_m}(\tilde{\phi}_m) f_{\tilde{\phi}_n}(\tilde{\phi}_n) d\tilde{\phi}_m d\tilde{\phi}_n \\ &= \int_0^{2\pi} \int_0^{2\pi} \int_0^1 \int_0^1 \left(\frac{1}{N} + \frac{1}{N^2} \sum_{\substack{m=1 \\ n \neq m}}^N \sum_{n=1}^N e^{j\zeta(\theta, \phi)(\tilde{\rho}_n \tilde{\phi}_n - \tilde{\rho}_m \tilde{\phi}_m)} \right) 2\tilde{\rho}_n 2\tilde{\rho}_m d\tilde{\rho}_m d\tilde{\rho}_n \frac{1}{2\pi} \frac{1}{2\pi} d\tilde{\phi}_m d\tilde{\phi}_n \end{aligned} \quad (3.1.35)$$

The double summation term simplifies identical to (3.1.33) and gives

$$E_v \left| U(\theta, \phi | \bar{v}) \right| = \frac{1}{N} + \left(1 - \frac{1}{N} \right) \left[\int_0^1 \int_0^1 \int_0^{2\pi} \int_0^{2\pi} \cos(\zeta(\theta, \phi)(\tilde{\rho}_n \tilde{\phi}_n - \tilde{\rho}_m \tilde{\phi}_m)) \frac{1}{2\pi} \frac{1}{2\pi} d\tilde{\phi}_m d\tilde{\phi}_n 2\tilde{\rho}_n 2\tilde{\rho}_m d\tilde{\rho}_m d\tilde{\rho}_n \right] \quad (3.1.36)$$

Now using the Bessel identity where n=0 (3.1.36) can be written as

$$J_n(x) = \frac{1}{2\pi} \int_0^{2\pi} e^{-nj\theta + jx \sin \theta} d\theta = \frac{1}{2\pi} \int_0^{2\pi} \cos(n\theta - z \sin \theta) d\theta \quad [n \text{ is a natural number}] \quad (3.1.37)$$

$$\frac{1}{N} + \left(1 - \frac{1}{N} \right) \int_0^1 \int_0^1 J_0(\zeta(\theta, \phi) \tilde{\rho}_n) J_0(\zeta(\theta, \phi) \tilde{\rho}_m) 2\tilde{\rho}_n 2\tilde{\rho}_m d\tilde{\rho}_m d\tilde{\rho}_n \quad (3.1.38)$$

Where $J_o(t)$ is the Bessel function of the first kind of order zero. Making the substitution

$$\begin{aligned} t &= \zeta(\theta, \phi) \tilde{r} \\ dt &= \zeta(\theta, \phi) d\tilde{r} \end{aligned} \quad (3.1.39)$$

Reduces (3.1.38) to

$$\frac{2}{\zeta(\theta, \phi)^2} \frac{2}{\zeta(\theta, \phi)^2} \int_0^{\zeta(\theta, \phi)} \int_0^{\zeta(\theta, \phi)} t_n J_0(t_n) t_m J_0(t_m) dt_m dt_n \quad (3.1.40)$$

since

$$\int_0^z x J_0(x) dx = x J_1(x) \Big|_0^z = z J_1(z) \quad (3.1.41)$$

Where $J_1(z)$ is the Bessel function of order one, (3.1.40) takes the form

$$\left| \frac{2J_1 \zeta(\theta, \phi)}{\zeta(\theta, \phi)} \right|^2 \quad (3.1.42)$$

And from this it can be easily shown (3.1.38) takes the form

$$U_{av}(\theta, \phi) = \frac{1}{N} + \left(1 - \frac{1}{N}\right) \left| \frac{2J_1 \zeta(\theta, \phi)}{\zeta(\theta, \phi)} \right|^2 = |2\text{jinc}(\zeta(\theta, \phi))|^2 \quad (3.1.43)$$

The observable difference in the average radiation intensity (3.1.34) in comparison to that of a linear and planar array exists within the second term, representing the mainlobe factor characterized by an oscillatory jinc function [67] and rapidly decreases from increasing the spatial parameter $\zeta(\theta, \phi)$.

It should be noted more comprehensive analyses of the jinc function may be found in [72].

The radiation pattern of a random circular array is plotted in Fig. 27 at the meridian angle and total pattern in Fig. 26.

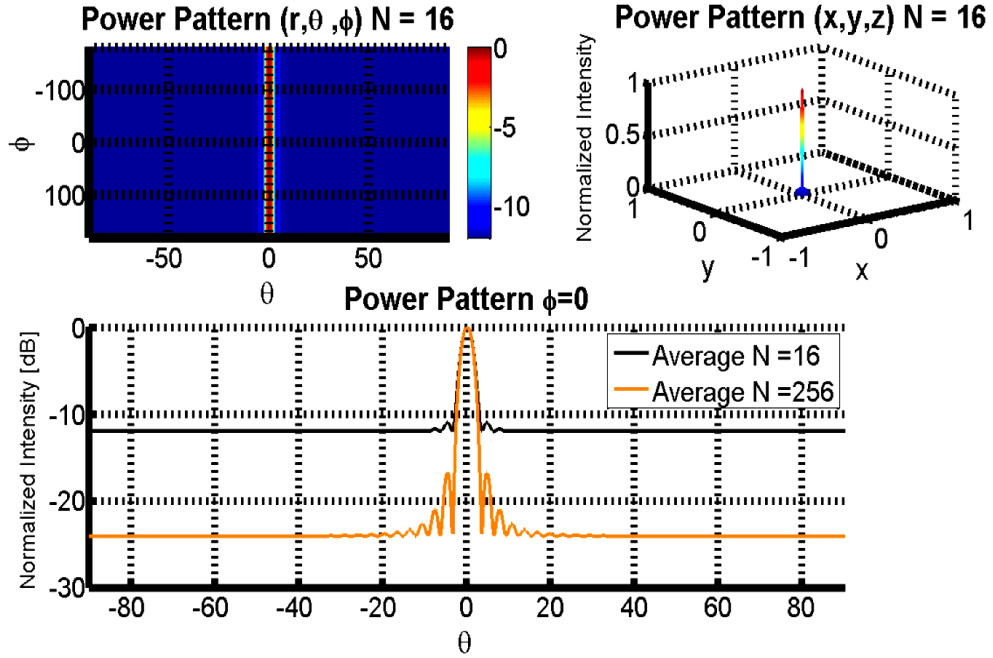


Fig. 26. Average radiation pattern of 16 and 256 elements randomly spaced (Uniformly) within a circular aperture of 10λ .

C. Average Properties of a Uniformly Distributed Circular Antenna Array with Perfect

Phase Information at the Meridian Angle $\theta = \theta_o = \frac{\pi}{2}$

1. Average Beampattern

The definition of expectation (0.2.19) may also be applied to (3.1.31) giving the average radiation intensity in (3.1.44).

$$U_{av}(\phi) = E_v \left| U(\phi|\vec{v}) \right| = \frac{1}{N} + \left(1 - \frac{1}{N} \right) \left| 2 \text{jinc}(\zeta(\phi)) \right|^2 \quad (3.1.44)$$

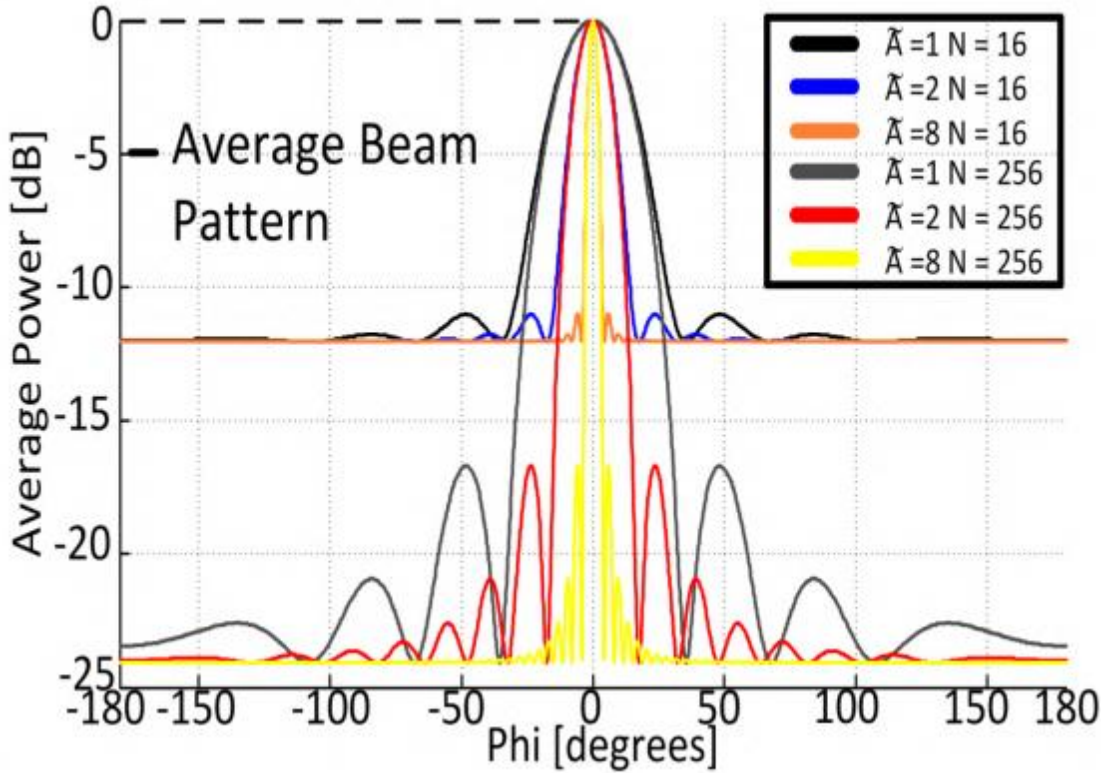


Fig. 27. Average radiation pattern of 16 and 256 elements randomly spaced (uniformly) within a circular aperture of 10λ at the meridian angle $\theta = \theta_o = \pi/2$.

2. Average Peak and Null Locations of the Sidelobes

The average power pattern is simplified to a simple analytic form (3.1.45) using the Bessel identity (D.1.8) when the argument $\zeta(\phi)$ is large. Thus, the analytic form of the first order Bessel function may be used to simplify the jinc function to that of (3.1.46) and average radiation intensity to (3.1.47).

$$J_1(\zeta(\phi)) = \sqrt{\frac{2}{\pi\zeta(\phi)}} \cos\left(\zeta(\phi) - \frac{\pi}{4} - \frac{\pi}{2}\right) = \sqrt{\frac{2}{\pi\zeta(\phi)}} \cos\left(\zeta(\phi) - \frac{3\pi}{4}\right) \quad (3.1.45)$$

$$\left|2 \frac{J_1(\zeta(\phi))}{\zeta(\phi)}\right|^2 \sim \frac{4}{\zeta(\phi)^2} \left(\frac{2}{\pi\zeta(\phi)}\right) \cos^2\left(\zeta(\phi) - \frac{3\pi}{4}\right) = \frac{8}{\pi\zeta(\phi)^3} \cos^2\left(\zeta(\phi) - \frac{3\pi}{4}\right) \quad (3.1.46)$$

$$U_{av}(\phi) \sim \frac{1}{N} + \left(1 - \frac{1}{N}\right) \frac{8}{\pi \zeta(\phi)^3} \cos^2\left(\zeta(\phi) - \frac{3\pi}{4}\right) \quad (3.1.47)$$

The expression (3.1.47) is useful for estimating null and peak sidelobe locations of an array on the condition $\zeta(\phi) = 4\pi A \sin\left(\frac{\phi}{2}\right) \gg 1$. In turn, a peak is formed when the term $\left(1 - \frac{1}{N}\right) \frac{8}{\pi \zeta(\phi)^3} \cos^2\left(\zeta(\phi) - \frac{3\pi}{4}\right)$ is greatest. Therefore, a maximum exists when the oscillatory term $\cos^2\left(\zeta(\phi) - \frac{3\pi}{4}\right) = 1$ and solving for $\zeta(\phi)$ it can be shown the nth peak average sidelobe will be given by (3.1.48).

$$\begin{aligned} \zeta(\phi_q^{peak}) &= \left(q + \frac{3}{4}\right)\pi & q = 0, 1, 2, 3, \dots \\ \zeta(\phi_q^{peak}) &= \left(q - \frac{1}{4}\right)\pi & q = 1, 2, 3, \dots \end{aligned} \quad (3.1.48)$$

As an alternative to finding the peak power, level it is possible to approximate the null positions of the sidelobes in the same manner. Zeros positions occur when the term $\cos^2\left(\zeta(\phi) - \frac{3\pi}{4}\right) = 0$ giving (3.1.49).

$$\zeta(\phi_q^{zero}) = \left(q + \frac{1}{4}\right)\pi \quad q = 1, 2, 3, \dots \quad (3.1.49)$$

The peak and null expressions in(3.1.48) and (3.1.49) can be expressed in terms of the angle $\phi_n^{zero, peak}$ to provide greater practical value and are shown in (3.1.50)and (3.1.51).

$$4\pi A \sin\left(\frac{\phi_q^{zero, peak}}{2}\right) = \left\{ \left(q + \frac{1}{4}\right)\pi, \left(q - \frac{1}{4}\right)\pi \right\}$$

$$\phi_q^{null} \sim 2 \arcsin\left(\frac{q + \frac{1}{4}}{4A}\right) \quad q = 1, 2, 3, \dots \quad (3.1.50)$$

$$\phi_q^{peak} \sim 2 \arcsin \left(\frac{q + \frac{3}{4}}{4A} \right) \quad q = 1, 2, 3, \dots \quad (3.1.51)$$

The observation of (3.1.50) and (3.1.51) shows a peak sidelobe level is less sensitive to the value of N and more sensitive to the value of A . Preferably, high peaking sidelobes can be eliminated by increasing the value of A , leaving the majority of sidelobe maxima concentrated relatively close to the mainlobe. This is also a logical statement complimenting realism such that sidelobes are nearly unworkable to remove from the mainlobe region in practice.

Lastly, it is important to note that in [9] the expression of (3.1.51) stated a peak sidelobe existed at $q-1/4$, which is unfeasible. If the former condition were to be true the main beam would be followed by a peak sidelobe and then a null position, which does not make sense. Rather the main beam should be followed by a null and then a peak which is represented by (3.1.50) and (3.1.51).

3. Average Three-dB Beamwidth

An important figure of merit used to characterize an antenna is its 3dB beamwidth and, unlike the ease of calculating the 3dB beamwidth like a deterministic antenna; it becomes a greater task to characterize in terms of the random scenario.

The alternative measure is to find the 3dB beamwidth in terms of its average power pattern and is shown in(3.1.52). In the limit $N, \rightarrow \infty$ this also reduces to (3.1.53) and by graphical means, the solution of this equation is found to be 1.616 shown in Fig. 28.

$$U_{av}(\phi^{3dB}) = \frac{1}{N} + \left(1 - \frac{1}{N}\right) \left| 2 \frac{J_1(\zeta(\phi^{3dB}))}{\zeta(\phi^{3dB})} \right|^2 = \frac{1}{2} \quad (3.1.52)$$

$$U_{av}(\phi_{av}^{3dB}) \approx \left| 2 \frac{J_1(\zeta(\phi_{av}^{3dB}))}{\zeta(\phi_{av}^{3dB})} \right|^2 = \frac{1}{2} \quad (3.1.53)$$

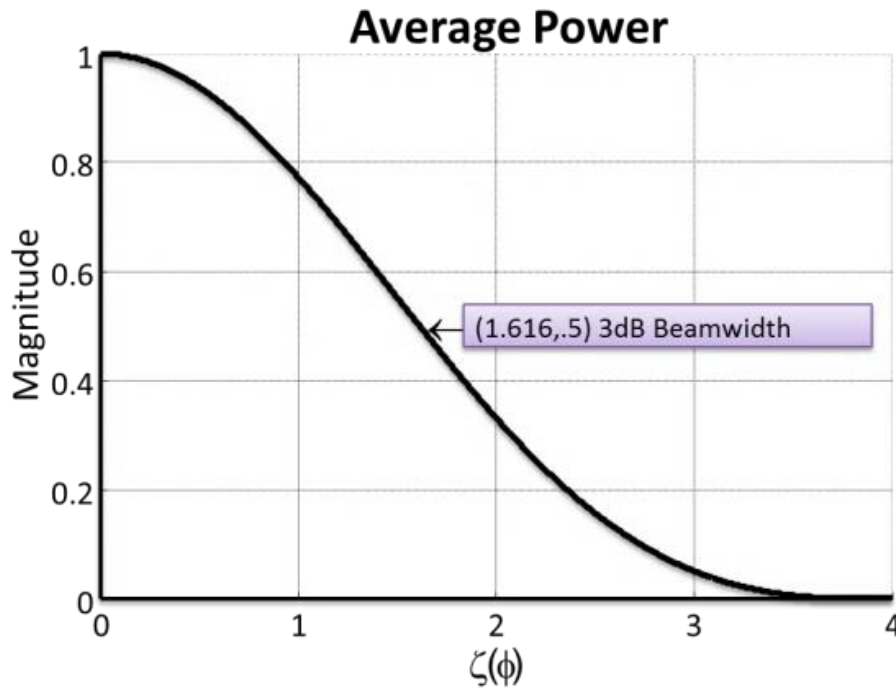


Fig. 28. Graphical solution of the three Db sidelobe.

Substituting 1.616 into $\zeta(\phi^{3dB})$ provides (3.1.54) and the solution in terms of ϕ_{av}^{3dB} results (3.1.55). For small arguments in the sin term one can use a first order approximation (C.1.24) giving (3.1.56).

$$\zeta(\phi_{av}^{3dB}) = 4\pi A \sin\left(\frac{\phi_{av}^{3dB}}{2}\right) = 1.616 \quad (3.1.54)$$

$$\phi_{av}^{3dB} = 2 \arcsin\left(\frac{.1286}{A}\right) \quad (3.1.55)$$

$$\phi_{av}^{3dB} \approx \frac{.26}{A} \quad (3.1.56)$$

The 3dB beamwidth angle is inversely proportional to the radius of the circle and asymptotically independent of N . As a result, a sparsely distributed arrangement of antennas will provide on average a narrower beam. The difficulty in this assumption arises when the far-field destination antenna has mobility, because the beam will be inversely proportional to the radius of the circle.

4. Three-dB Sidelobe Region

The region for which the average of the sidelobe beampattern falls below the threshold level of 3dB can be formulated in the following fashion similar to [9]. For large A the average sidelobe level is dominated by $1/N$, and for the condition $1/N \gg .26/A$ the 3dB sidelobe region is defined such that neither neighboring sidelobe peak in the average beampattern exceeds 3 dB. To solve this condition one should let $q \rightarrow q_o$ and solve the inequality given in (3.1.57) to give (3.1.58).

$$\frac{U_{av}(\phi_{q_o}^{peak})}{\frac{1}{N}} \sim 1 + (N-1) \frac{1}{\pi} \left[\frac{2}{\pi \left(q_o + \frac{3}{4} \right)} \right]^3 \leq 10^{\frac{3}{10}} \leq 2 \quad (3.1.57)$$

$$= \frac{2}{\pi} \left[\frac{N-1}{\pi} \right]^{\frac{1}{3}} - \frac{3}{4} \leq q_o \quad (3.1.58)$$

A more formal definition can be used to define the 3dB sidelobe region such that $S_{3dB} \triangleq \{ \phi | \phi_{q_o}^{zero} \leq |\phi| \leq \pi \}$ where the angle $\phi_{q_o}^{zero}$ is located next to the peak sidelobe; an example of the 3dB sidelobe region is shown in Fig. 29 showing a case with all sidelobes within the 3dB sidelobe region (black curve) and the alternative case where not all the

sidelobes are within the 3dB sidelobe region (green curve). A complete analysis of the 3dB Sidelobe Region, Sidelobe Peaks, Zeros, and Half Power Beamwidth Locations with $A=8$, and $N=16$ are shown in Table 1, Table 2 and Fig. 29.

Table 1. Comparison of analytic peaks vs. numerical peaks for a circular random array $\tilde{A}=5$ and $(N=32,128)$

q	(N=32, N=128) Peak($\phi_q^{peak}, U_q^{peak}$)(3.1.51),(3.1.46)	(N=32, N=128) Peak($\phi_{av}^{peak}, U_{av}^{peak}$)(3.1.44), (3.1.46)
1	(10,-13.36), (10,-16.37)	(9.5, -13.18), (9.418,-15.99)
2	(15.8,-14.54),(15.8,-19.3)	(15.25, -14.53) , (15.44,-19.23)
3	(21.61,-14.8), (21.61,-20.2)	(21.4, -14.84), (21.9,-20.27)

Table 2. Comparison of analytic peaks vs. numerical peaks for a spherical random array $\tilde{A}=5$ and $(N=32,128)$

q	N=32,N=128 Null(ϕ, U_{av})(3.1.50),(3.1.46)	N=32,N=128 Null(ϕ, U_{av})(3.1.44),(3.1.46)
1	(7.16, -15.05), (7.16, -21.07)	(7,-15.05), (7,-21.07)
2	(12.91, -15.05),(12.91, -21.07)	(12.89,-15.05), (12.89,-21.07)
3	(18.7, -15.05), (18.45, -21.07)	(18.45,-15.05), (18.3,-21.07)

The value of $q_0=0.6155$ when $N=32$ and $q_0=1.4349$ when $N=128$. So since q_0 is less than one for the case $N=32$ all the sidelobes are contained in the 3dB sidelobe region where

as in the case $N=128$ the value of q_0 is greater than 1, but less than 2. Therefore one sidelobe crosses the bounded sidelobe level.

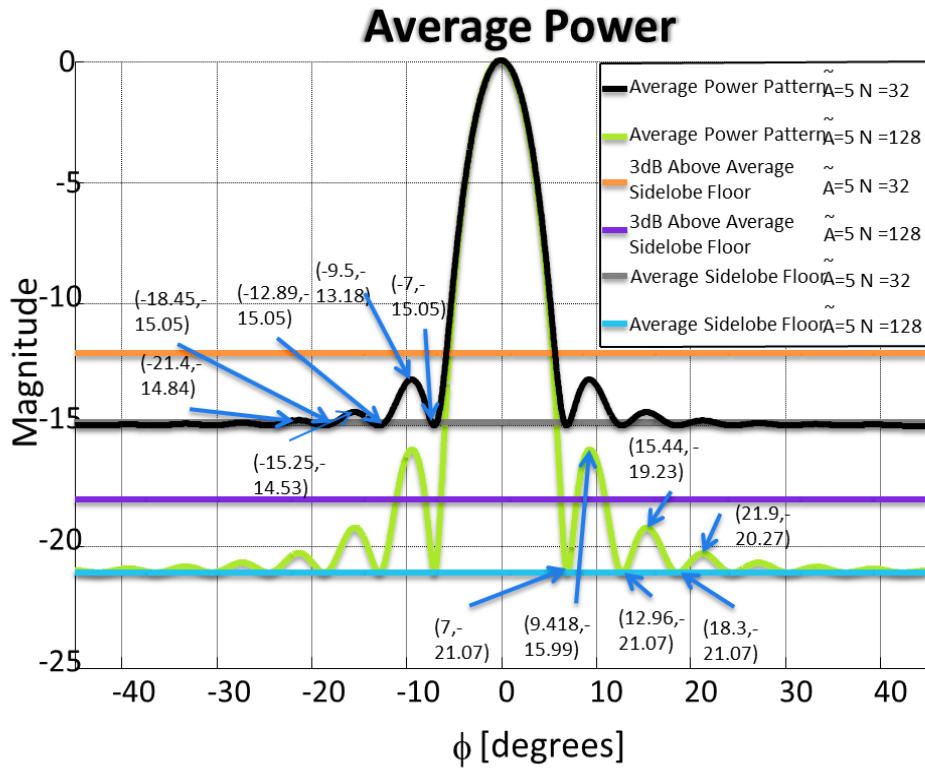


Fig. 29. 3dB sidelobe region, sidelobe peaks, zeros, and half power beamwidth locations with $A=8$, $N=16$.

Figure 30 shows a comprehensive analysis of the 3dB sidelobe and 3dB beamwidth regions in a different perspective. The main observation to be made from the Figure 30 is that the 3dB sidelobe region will be reduced as N increases unless A increases as well.

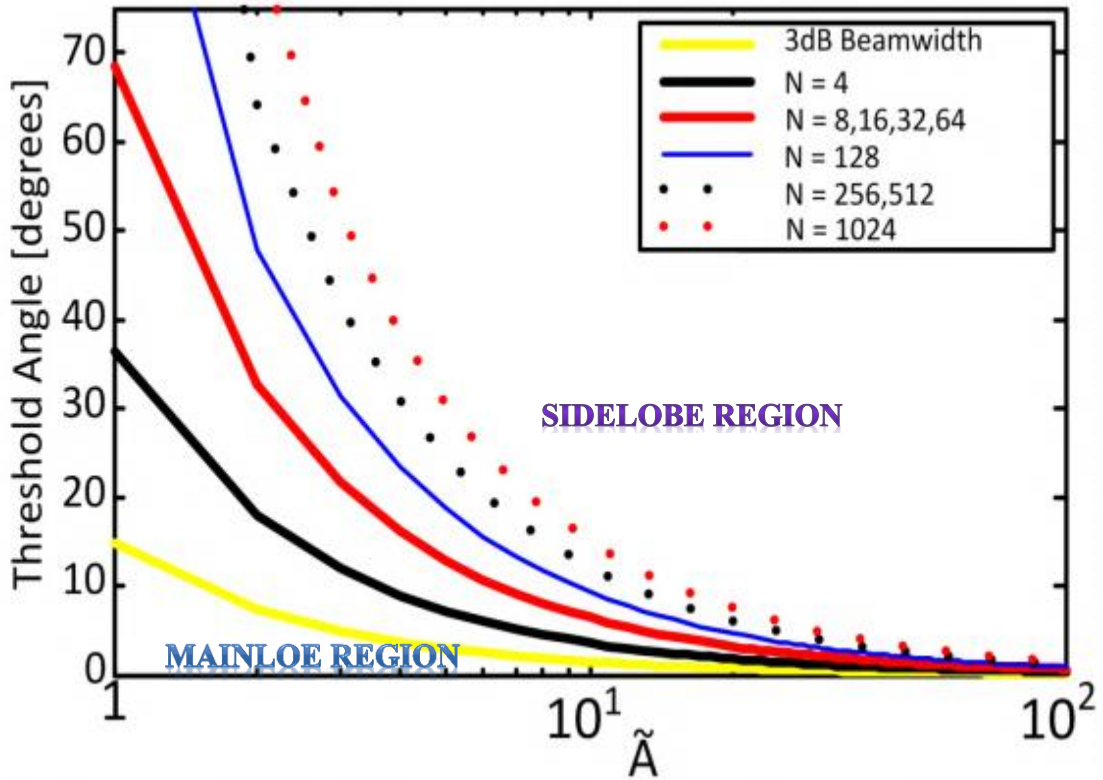


Fig. 30. Threshold angle of the three Db beamwidth and three Db sidelobe region with respect to A and N .

5. Average Directivity

The directivity(0.2.24) is found relative to a single isotropic antenna in(3.1.59).

$$D(\nu) \triangleq \frac{\int_{-\pi}^{\pi} U(0)d\phi}{\int_{-\pi}^{\pi} U(\phi)d\phi} = \frac{\int_{-\pi}^{\pi} \left(\frac{1}{N} + 1 - \frac{1}{N} \right) d\phi}{\int_{-\pi}^{\pi} U(\phi)d\phi} = \frac{2\pi}{\int_{-\pi}^{\pi} U(\phi)d\phi}$$

$$D(\nu) = \frac{2\pi}{\frac{2\pi}{N} + \frac{2\pi}{N^2} \sum_{k=1}^N \sum_{\substack{l=1 \\ l \neq k}}^N J_o(4\pi A(\nu_n - \nu_m))} = \left[\frac{1}{N} + \frac{1}{N^2} \sum_{k=1}^N \sum_{\substack{l=1 \\ l \neq k}}^N J_o(4\pi A(\nu_n - \nu_m)) \right]^{-1} \quad (3.1.59)$$

Disappointingly the direct calculation of the $E_\nu[D(\nu)]$ does not result with a

meaningful closed form solution. So as an alternative the average directivity is evaluated, using the average power pattern in(3.1.60).

$$\tilde{D}_{av} \triangleq \frac{\int_{-\pi}^{\pi} P_{av}(\phi) d\phi}{\int_{-\pi}^{\pi} P_{av}(\phi) d\phi} = \frac{2\pi}{\int_{-\pi}^{\pi} P_{av}(\phi) d\phi} = \frac{2\pi}{\frac{2\pi}{N} + \left(1 - \frac{1}{N}\right) \int_{-\pi}^{\pi} \left(2 \operatorname{jinc}\left(x \sin \frac{\phi}{2}\right)\right)^2 d\phi} \quad (3.1.60)$$

where, $x=4\pi A$

No loss in generality is sustained from(3.1.60), because Jensen's inequality states the true directivity will hold as an upper bound to the average directivity $\tilde{D}_{av} \leq D$. This means \tilde{D}_{av} is a lower bound to the true value of directivity and by the law of large numbers the denominator of $D(\nu)$ will approach its average value with high probability as N increases. Yet again this means, the inequality tightly bounds as the value of N increases to very large value. The challenging part of determining \tilde{D}_{av} is solving the integral in the denominator of(3.1.60). Useful sources for tackling this integral came from [69]-[77]. The solution to this integral is shown in (A.1.15)and is used to give(3.1.61).

$$\tilde{D}_{av} = \frac{N}{1 + (N-1) {}_2F_3\left(\frac{1}{2}, \frac{3}{2}; 1, 2, 3; -(4\pi A)^2\right)} \quad (3.1.61)$$

The expression ${}_2F_3\left(\frac{1}{2}, \frac{3}{2}; 1, 2, 3; -(4\pi A)^2\right)$ is a hypergeometric function and converges to 0 as $A \rightarrow \infty$. As a result, the gain will likely be less than N, and will approach N by means of increasing A to a very large extent. The outcome coincides well with a statement expressed earlier in this thesis which was stated in the average 3dB

sidelobe section being the main beam becomes narrower with increasing A . In view of this, it makes sense the directivity increases for larger A .

6. Lower Bounded Average Directivity

It is possible to bind the generalized hypergeometric function, and this is shown in [9] and repeated in this section for continuity. To do this one begins with the integral where the hypergeometric function emerged in(3.1.62). By substitution of variables this is rewritten as (3.1.63).

$$\int_{-\pi}^{\pi} \left(\frac{2J_1\left(x \sin \frac{\phi}{2}\right)}{x \sin \frac{\phi}{2}} \right)^2 d\phi \quad (3.1.62)$$

$$2 \int_0^{\pi} \left(\frac{2J_1\left(x \sin \frac{\phi}{2}\right)}{x \sin \frac{\phi}{2}} \right)^2 d\phi = 2 \int_0^x \left(\frac{2J_1(t)}{t} \right)^2 \frac{2}{\sqrt{x^2 - t^2}} dt \quad (3.1.63)$$

$$t = x \sin \frac{\phi}{2}, dt = \frac{x}{2} \cos \frac{\phi}{2} d\phi$$

For large arguments of t , the Bessel function is approximated using (D.1.8) giving (3.1.64).

$$\left| \frac{J_1(t)}{t} \right|^2 \sim \frac{4}{t^2} \left(\frac{2}{\pi t} \right) \cos^2 \left(t - \frac{3\pi}{4} \right) = \frac{8}{\pi t^3} \cos^2 \left(t - \frac{3\pi}{4} \right) \quad (3.1.64)$$

It is obvious this expression is bounded no greater than $\frac{8}{\pi t^3}$. However, if the argument of t is not large the Bessel function is lower bounded by $\cos^2(\zeta(\phi)t)$. Consequently, one arrives with the inequalities (3.1.65) and(3.1.66). Additionally these

inequalities may be solved for $\zeta(\phi)$ as of setting the right hand sides of (3.1.65) and (3.1.66) equal giving (3.1.67).

$$\left| 2 \frac{J_1(t)}{t} \right|^2 \leq \cos^2(\zeta(\phi)t) \quad \text{for } t \leq x_o \quad (3.1.65)$$

$$\left| 2 \frac{J_1(t)}{t} \right|^2 \leq \frac{8}{\pi t^3} \quad \text{for } t > x_o \quad (3.1.66)$$

$$\cos^2(\zeta(\phi)t) = \frac{8}{\pi t^3} \quad (3.1.67)$$

One can observe there is not enough information is given up to this point to solve the system of equations since two unknowns exist with only one equation. Consequently, a second equation is formulated from setting the left and right hand sides of (3.1.66) equal giving (3.1.68). To solve (3.1.68) a graphical approach is used shown in Fig. 31 to find the intersection of the two curves and the solution with the smallest value of t is taken to be the correct solution giving an approximate value of 2.445.

$$\left| 2 \frac{J_1(t)}{t} \right|^2 = \frac{8}{\pi t^3} \quad (3.1.68)$$

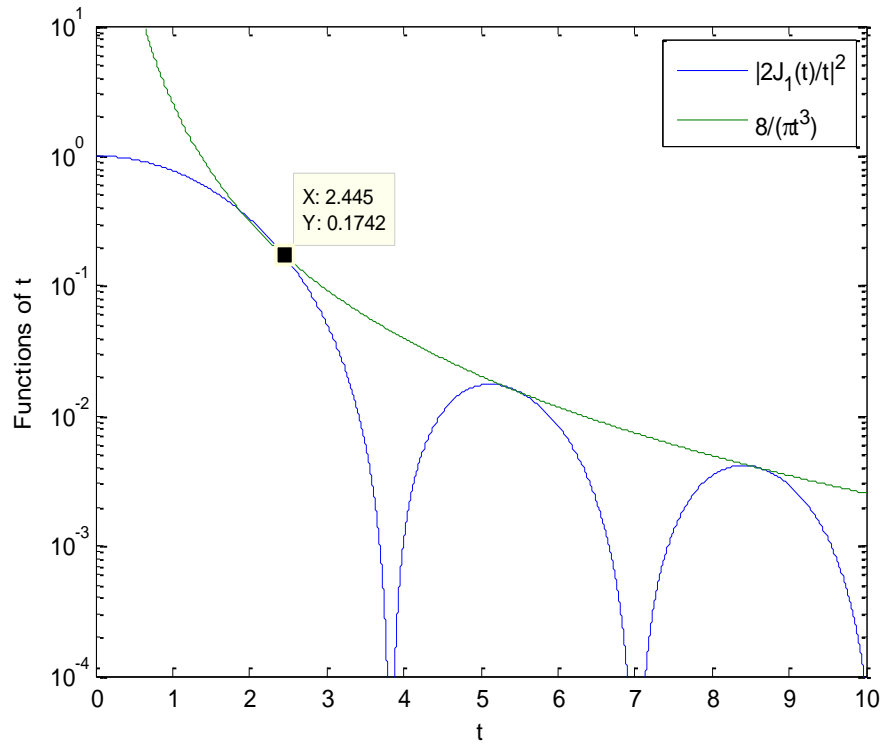


Fig. 31. Graphical solution for lower-bounding the directivity of a circular random array.

Solving for $\zeta(\phi)$ in(3.1.69), one arrives with a value of .4663. Now substituting the values of $\zeta(\phi)$ and t and respective inequalities into (3.1.63) one obtains(3.1.70). This expression may now be used to bind the hypergeometric function providing (3.1.71)and can be normalized by dividing out the 2π giving (3.1.72).

$$\zeta(\phi) = \frac{\cos^{-1}\left(\sqrt{\frac{8}{\pi t^3}}\right)}{t} = .4663 \quad (3.1.69)$$

$$2 \int_0^{x_0} \frac{\cos^2(\zeta(\phi_0)t)}{\sqrt{x^2 - t^2}} dt + \frac{16}{\pi} \int_{x_0}^x \frac{1}{t^3 \sqrt{x^2 - t^2}} dt \quad (3.1.70)$$

$$f(x) \triangleq 2 \int_0^\pi \left(\frac{2J_1\left(x \sin \frac{\phi}{2}\right)}{x \sin \frac{\phi}{2}} \right)^2 d\phi = \quad (3.1.71)$$

$$2\pi {}_2F_3\left(\frac{1}{2}, \frac{3}{2}; 1, 2, 3; (-x)^2\right) \leq 4 \int_0^{x_0} \frac{\cos^2(\alpha(\phi_0)t)}{\sqrt{x^2-t^2}} dt + \frac{32}{\pi} \int_{x_0}^x \frac{1}{t^3 \sqrt{x^2-t^2}} dt$$

$$g(x) \triangleq \frac{1}{\pi} \int_0^\pi \left(\frac{2J_1\left(x \sin \frac{\phi}{2}\right)}{x \sin \frac{\phi}{2}} \right)^2 d\phi$$

$$= {}_2F_3\left(\frac{1}{2}, \frac{3}{2}; 1, 2, 3; (-x)^2\right) \leq \frac{2}{\pi} \int_0^{x_0} \frac{\cos^2(\alpha(\phi_0)t)}{\sqrt{x^2-t^2}} dt + \frac{16}{\pi^2} \int_{x_0}^x \frac{1}{t^3 \sqrt{x^2-t^2}} dt \quad (3.1.72)$$

$$\text{where } g(x) = \frac{f(x)}{2\pi}$$

Evaluation of the first integral on the right hand side of (3.1.72) gives (3.1.73)

and the second integral gives (3.1.74).

$$\frac{2}{\pi} \int_0^{x_0} \frac{\cos^2(\zeta(\phi_0)t)}{x \sqrt{1-\frac{t^2}{x^2}}} dt = \frac{2}{\pi x} \int_0^{x_0} \left(1 + \frac{1}{2} \left(\frac{t}{x} \right)^2 + O\left(\frac{1}{x^4} \right) \right) \cos^2(\alpha(\phi_0)t) dt$$

$$= \frac{1}{\pi x} \left(x_0 + \frac{\sin(2\zeta(\phi_0)x_0)^2}{2\zeta(\phi_0)} \right) + O\left(\frac{1}{x^3} \right) \quad (3.1.73)$$

$$\frac{16}{\pi^2} \int_{x_0}^x \frac{1}{t^3 \sqrt{x^2-t^2}} dt = \frac{16}{\pi^2} \left[\frac{1}{x} \frac{\sqrt{1-\left(\frac{x_0}{x}\right)^2}}{2x_0^2} + \frac{1}{2x^3} \left\{ \ln \left(1 + \sqrt{1-\left(\frac{x_0}{x}\right)^2} \right) + \ln \left(\frac{x}{x_0} \right) \right\} \right]$$

$$= \frac{8}{\pi^2 x_0^2} \frac{1}{x} \left(1 - \left(\frac{x_0}{x} \right)^2 + O\left(\frac{1}{x^4} \right) \right) + O\left(\frac{\ln(x)}{x^3} \right)$$

$$= \frac{1}{x} \frac{8}{\pi^2 x_0^2} + O\left(\frac{\ln(x)}{x^3} \right) \quad (3.1.74)$$

Thus, applying (3.1.73) and (3.1.74) to the inequality of (3.1.72) yields (3.1.75).

$$g(x) \leq \frac{1}{\pi x} \left(x_o + \frac{\sin(2\zeta(\phi_o)x_o)^2}{2\zeta(\phi_o)} + \frac{8}{\pi x_o^2} \right) + O\left(\frac{\ln(x)}{x^3}\right) \quad (3.1.75)$$

The second term denotes big O notation and is negligible with larger orders of x. This is due since the x^3 term will grow much more quickly than the left hand side of the expression. Given these values, one is now able to calculate the coefficient $\frac{c_o}{x}$ to be

$\frac{1.1727}{x}$ where the coefficient c_o represents the term within the parenthesis of(3.1.75).

Finally, the directivity is bound to that of (3.1.76) and for large N converges to that of(3.1.77).

$$\frac{D_{av}}{N} \geq \frac{\tilde{D}_{av}}{N} \geq \frac{1}{1+(N-1)\frac{c_o}{4\pi A}} = \frac{1}{1+\left(1-\frac{1}{N}\right)\frac{c_o}{4\pi A} \frac{N}{A}} = \frac{1}{1+\left(1-\frac{1}{N}\right)\mu \frac{N}{A}} \quad (3.1.76)$$

where $\mu = .0933$

$$\frac{D_{av}}{N} \geq \frac{1}{1+\mu \frac{N}{A}} \quad (3.1.77)$$

D. Average Statistical Properties of a Uniformly Distributed Circular Antenna Array with Perfect Phase Information and Uniform Random Variable

1. Exact Statistical Development

In probability theory and statistics, a sequence or other collection of random variables is independent and identically distributed (i.i.d.) for the condition all random variables have the same probability distribution function (PDF) and are mutually independent. Accordingly, with the given definition of a (i.i.d.) one can model the associated beampattern as(3.1.78).

$$F(\phi|\vec{v}) = \frac{1}{N} \sum_{n=1}^N e^{-j4\pi A \sin(\frac{\phi}{2})} = \frac{1}{N} \sum_{n=1}^N (x_n - jy_n) = \frac{1}{N} (X - jY)$$

where

$$x_n = \cos(v_n \zeta(\phi)), \quad y_n = \sin(v_n \zeta(\phi)) \quad (3.1.78)$$

The real motivation of the transformation is to make an equation usable such that the array factor fits the form of the characteristic function method. The characteristic function is no more than taking the Fourier Transform of the distribution and in this case, it is taking the Fourier Transform of the beam pattern (3.1.79) with respect to w, v space.

$$\Phi_{x_n, y_n}(w, v) = E_{x_n, y_n} [e^{j(w x_n - v y_n)}] = E_{v_n} [e^{j(w \cos(\gamma_n \zeta(\phi)) - v \sin(\gamma_n \zeta(\phi)))}] \quad (3.1.79)$$

The function (3.1.79) is a well-behaved function for a given pair of w and v and can be calculated numerically. Taking the inverse Fourier Transform of (3.1.79) gives the joint probability density functions of X and Y and can be computed using the Fast Fourier Transform (3.1.80). The result of this may be substituted into (3.1.81) giving the complementary cumulative distribution function (CCDF) of the radiation intensity. Moreover, the result of (3.1.81) provides a probability measure in regard to when any direction ϕ exceeds the threshold power P_o .

$$f_{X,Y}(x, y) = \left(\frac{1}{2\pi}\right)^2 \int_{-\infty}^{\infty} \int_{-\infty}^{\infty} \Phi_{x_n, y_n}^N(w, v) e^{-j(wx+vy)} dw dv \quad (3.1.80)$$

$$\Pr[(\phi) > P_o] = \Pr\left[\frac{\tilde{X}^2 + \tilde{Y}^2}{N^2} > P_o\right] = \iint_{x^2 + y^2 > N^2 P_o} f_{\tilde{X}, \tilde{Y}}(x, y) dx dy \quad (3.1.81)$$

2. Approximate Statistical Development with Gaussian Distribution

As stated by [9] the exact evaluation of the CCDF is computationally demanding especially when there is need for high precision. Nevertheless, the array factor consists of a sum of N statistically (i.i.d.) random variables, and when the value of N is large according to the central limit theorem one expects the array factor, to approach a complex Gaussian distribution given in (3.1.82), except at the deterministic angle $\phi = 0$. The distributions of X and Y at the direction $\pi \geq |\phi| > 0$ will yield supporting Gaussian statistical measures given in (3.1.83)-(3.1.88).

$$F(\phi|\vec{v}) = \frac{1}{\sqrt{N}}(X - jY) \quad (3.1.82)$$

$$X = \frac{1}{\sqrt{N}} \sum_{n=1}^N \cos(v_n \zeta(\phi)), \quad Y = \frac{1}{\sqrt{N}} \sum_{n=1}^N \sin(v_n \zeta(\phi))$$

$$E[X(\phi|\vec{v})] = X(\phi) = \sum_{n=1}^N \frac{1}{\sqrt{N}} \int_{-1}^1 \frac{2}{\pi} \sqrt{1-v_n^2} \cos(v_n \zeta(\phi)) dv_n = \frac{\sqrt{N} 2J_1(\zeta(\phi))}{\zeta(\phi)} \quad (3.1.83)$$

$$E[X^2(\phi|\vec{v})] = \frac{1}{2} \left(1 + \frac{J_1(2\zeta(\phi))}{\zeta(\phi)} \right) = \frac{1}{2} \left(1 + {}_0\bar{F}_1(; 2; -\zeta(\phi)^2) \right) \quad (3.1.84)$$

$$\sigma_x^2 = \frac{1}{2} \left(1 + \frac{J_1(2\zeta(\phi))}{\zeta(\phi)} \right) - \left(\frac{2J_1(\zeta(\phi))}{\zeta(\phi)} \right)^2 \quad (3.1.85)$$

$$E_Y[Y(\phi|\vec{v})] = \sum_{n=1}^N \frac{1}{\sqrt{N}} \int_{-1}^1 \frac{2}{\pi} \sqrt{1-v_n^2} \sin(v_n \zeta(\phi)) dv_n = 0 \quad (3.1.86)$$

$$E[Y^2(\phi|\vec{v})] = \frac{1}{2} \left(1 - \frac{J_1(2\zeta(\phi))}{\zeta(\phi)} \right) \quad (3.1.87)$$

$$\sigma_y^2 = \frac{1}{2} \left(1 - \frac{J_1(2\zeta(\phi))}{\zeta(\phi)} \right) - 0 \quad (3.1.88)$$

In general, it should be noted the expected value operator of two variables is not necessarily multiplicative, i.e. $E(XY)$ is not necessarily equal to $E(X)E(Y)$. It is multiplicative for the variables X and Y though since they are orthogonal and uncorrelated. If the variables were not orthogonal the covariance and correlation matrices would be needed. More background of setting up a joint PDF of X and Y , say $j(x, y)$, is shown in(3.1.89). Nevertheless, since X and Y are independent, by definition $j(x, y) = f(x)g(y)$ where f and g are the marginal PDFs for X and Y giving(3.1.90), and is used to give (3.1.91).

$$E(XY) = \int \int x y j(x, y) dx dy \quad (3.1.89)$$

$$\begin{aligned} E(XY) &= \int \int x y f(x) g(y) dx dy = \int x f(x) \left[\int y g(y) dy \right] dx \\ &= \int x f(x) E(Y) dx = E(X)E(Y) \end{aligned} \quad (3.1.90)$$

$$f_{x,y}(x, y) = \frac{1}{2\pi\sigma_x\sigma_y} e^{\left(\frac{-(x-m_x)^2}{2\sigma_x^2} - \frac{y^2}{2\sigma_y^2} \right)} \quad (3.1.91)$$

The Complementary Cumulative Distribution Function (CCDF) of P_o using (3.1.81) is now expressed as (3.1.92)

$$\begin{aligned} \Pr[U(\phi) > U_o] &= \Pr\left[\frac{X^2 + Y^2}{N} > U_o \right] = \Pr\left[\sqrt{X^2 + Y^2} > \sqrt{NU_o} \right] \\ &= \int_{\sqrt{NP_o}}^{\infty} \int_{-\pi}^{\pi} \frac{r}{2\pi\sigma_x\sigma_y} e^{\left(\frac{-r \cos w - m_x^2}{2\sigma_x^2} - \frac{r^2 \sin^2 w}{2\sigma_y^2} \right)} dw dr \\ &= \int_{-\pi}^{\pi} \frac{1}{4\pi\sigma_x\sigma_y T_w^2} e^{V_w^2 - \frac{m_x^2}{2\sigma_x^2}} \left[\sqrt{\pi} V_w \operatorname{erfc}(W_w - V_w) + e^{-(W_w - V_w)^2} \right] dw \end{aligned} \quad (3.1.92)$$

where

$$T_w \triangleq \sqrt{\frac{\cos^2 w}{2\sigma_x^2} + \frac{\sin^2 w}{2\sigma_y^2}}, V_w \triangleq \frac{m_x \cos^2 w}{2\sigma_x^2 U_w}, W_w \triangleq \sqrt{NP_o U_w}$$

The integral of (3.1.92) simplifies when $\zeta(\phi) \gg 1$ and the terms $J_1\left(\frac{2\zeta(\phi)}{\zeta(\phi)}\right)$ and $\left|\frac{J_1\zeta(\phi)}{\zeta(\phi)}\right|^2$ embedded in the variance expressions rapidly decrease as well. Thus, in the limiting case $\sigma_x^2 \approx \sigma_y^2 \approx \frac{1}{2}$ and it is interesting to note the variances converge equally. This means the distribution will follow the Nakagami-Rice distribution and because of this a first-order Marcum-Q function of (3.1.93) is achieved.

$$\Pr[U(\phi) > U_o] = Q\left(\frac{m_x}{\sigma_x}, \frac{\sqrt{NU_o}}{\sigma_x}\right) = Q(\sqrt{2m_x}, \sqrt{2NU_o}) \quad (3.1.93)$$

Moreover, since the mean m_x approaches zero one can conclude the CCDF will have Rayleigh distribution given by

$$\Pr[U(\phi) > U_o] = e^{-NU_o} \quad (3.1.94)$$

The next set of equations show nothing new except for an alternative way of setting up (3.1.93). This is done by converting to polar coordinates with $R = \sqrt{X^2 + Y^2}$ and consequently providing (3.1.95). The term I_n is given to be the nth order modified Bessel function of the first kind and for non-negative n given as(3.1.96). In polar coordinates (3.1.93) is rewritten as (3.1.97) and like before when the $E(X)=0$ the envelope will follow a Rayleigh distribution given previously in (3.1.94).

$$f_R(r) = 2re^{-(r^2+m_x^2)} I_o(2m_x r) \quad (3.1.95)$$

$$I_n(x) = \sum_{k=0}^{\infty} \frac{1}{k!(n+k)!} \left(\frac{x}{2}\right)^{2k+n} \quad (3.1.96)$$

$$\Pr[U(\phi) > U_o] = \Pr[R > \sqrt{NU_o}] = \int_{\sqrt{NU_o}}^{\infty} f_R(r) dr = Q(\sqrt{2m_x}, \sqrt{2NU_o})$$

where

$$Q(x, y) = \int_y^{\infty} te^{-\frac{t^2+x^2}{2}} I_o(xt) dt \quad (3.1.97)$$

3. Average Statistical Beampattern Analysis within the 3dB Sidelobe Region

The simplified distribution becomes readily tractable when the mean value of the array factor is assumed zero. This value is greatly dependent upon the number of antennas present and if N increases the mean value increases. Ideally, this would be the case, but in practice, this may not necessarily hold true and because of this, the 3dB sidelobe region is re-examined.

Earlier the 3dB sidelobe region was defined to satisfy the condition(3.1.98). This term can be rewritten as (3.1.99) by adding the variance of X and Y to the Average Power patterns given in (3.1.100) and(3.1.101).

$$NU_{av}(\phi) \leq 2 \quad (3.1.98)$$

$$Var(X) + Var(Y) + |E[X]|^2 + |E[Y]|^2 \leq NU_{av}(\phi) \leq 2 \quad (3.1.99)$$

$$U_{av_x}(\phi) = E(X)^2 = 4 \left| \frac{J_1(\zeta(\phi))}{\zeta(\phi)} \right|^2 N \quad (3.1.100)$$

$$U_{av_y}(\phi) = E(Y)^2 = 0 \quad (3.1.101)$$

Given the inequalities of (3.1.99)-(3.1.101) the average power pattern is bounded to that of(3.1.102). This shows the square of the mean 3dB sidelobe region is bounded by unity when N is large. Additionally the result also shows the mean does not grow unbounded with the number of antenna N.

$$\frac{1}{2} \left(1 + \frac{J_1(2\zeta(\phi))}{\zeta(\phi)} \right) - \left[\frac{2J_1(\zeta(\phi))}{\zeta(\phi)} \right]^2 + \frac{1}{2} \left(1 - \frac{J_1(2\zeta(\phi))}{\zeta(\phi)} \right) + 4 \frac{J_1(\zeta(\phi))}{\zeta(\phi)} N \leq 2,$$

$$1 - \frac{1}{N} |E[X]|^2 + |E[X]|^2 \leq 2,$$

$$|E[X]|^2 \leq \frac{1}{\left(1 - \frac{1}{N}\right)} \quad (3.1.102)$$

4. Statistical Analysis of the Maximum Sidelobe Peak

a. Upper Bound

To prove no grating lobes exist for a random array with a large number of elements one should find a distribution of the maximum power of the sidelobes. This type of work is provided in papers from [9]and [12]and dates back to a very classic paper from Donovito [78]. Moreover, this section repeats the work by [9], [10]and [78] in terms of setting up the fundamental limit for the ideal case of a Uniform distribution.

The average representation of the number of upward crossings at a given power level is prepared under the assumption X and Y are uncorrelated zero-mean Gaussian processes with variance $\sigma_x^2 = \sigma_y^2 = \frac{1}{2}$. The terms σ_x^2 and σ_y^2 can be found, to give a useful counter of measure for determining the probability of the average number of upward crossings at a given power level say $v(a)$ [9] and [10].

The calculation of the average representation of crossings will be referred as the *outage probability* denoted by P_{out} , but first rudimentary background information of the autocovariance of a Gaussian process is explored.

In statistics, the definition of autocovariance is a real stochastic process $X(t)$ of which the covariance of the signal is compared against a time-shifted version of itself. As well, if each state of the series has a mean, $E[Xt] = \mu t$, then the autocovariance by definition is given by (3.1.103).

$$K_{xx}(t,s) = E[(X_t - \mu_t)]E[(X_s - \mu_s)] = E[X_t X_s] - \mu_t \mu_s \quad (3.1.103)$$

Thus, if one assumes the function $X(t)$ is stationary, the following conditions also hold true;

$$\begin{aligned} \mu_t &= \mu_s = \mu \quad \text{for all } t, s \\ \text{and} \\ K_{xx}(t,s) &= K_{xx}(s-t) = K_{xx}(\tau) \\ \text{where} \\ \tau &= s-t \end{aligned}$$

The variable τ is the lag time, or the amount of time by which the signal has been shifted. Thus, the autocovariance of a stationary function becomes (3.1.104) where R_{xx} represents the autocorrelation, in the signal processing sense. The autocovariance function is normalized by dividing (3.1.104) by the variance σ^2 , and it is better known the autocorrelation coefficient ρ (3.1.105), fits the range $[-1, 1]$.

$$\begin{aligned} K_{xx}(\tau) &= E\{(X(t) - \mu)(X(t+\tau) - \mu)\} \\ &= E\{X(t) \cdot (X(t+\tau))\} - \mu^2 \\ &= R_{xx}(\tau) - \mu^2 \end{aligned} \quad (3.1.104)$$

$$\rho_{xx}(\tau) = \frac{K_{xx}(\tau)}{\sigma^2} \quad (3.1.105)$$

It is important to note some texts use the terms of autocovariance and autocorrelation interchangeably.

A weaker form of stationarity commonly employed is weak-sense stationarity, wide-sense stationarity (WSS) or covariance stationarity. WSS random processes require the 1st and 2nd moments to not vary with respect to time. A continuous-time random process $X(t)$ that is WSS then has the following constraint on its mean function (3.1.106) and autocorrelation function (3.1.107).

$$E\{x(t)\} = m_x(t) = m_x(t+\tau) \forall \tau \in \mathbb{R} \quad (3.1.106)$$

$$E\{x(t_1)x(t_2)\} = R_x(t_1, t_2) = R_x(t_1+\tau, t_2+\tau) = R_x(t_1-t_2, 0) \forall \tau \in \mathbb{R} \quad (3.1.107)$$

The first property (3.1.106) implies the mean $m_x(t)$ is constant and (3.1.107) implies the correlation function depends on the difference between t_1 and t_2 . In other words, one variable should be indexed rather than two variables. This consequently, reduces the autocorrelation function with the abbreviated notation as (3.1.108). Moreover, the autocovariance function of X at two instants $u = \sin\left(\frac{\phi_1}{2}\right) = u_1$ and u_2 of the Gaussian process gives (3.1.109) can be rewritten as (3.1.110) using (C.1.16).

$$R_x(\tau) \quad (3.1.108)$$

where $\tau = t_1 - t_2$

$$K_{xx}(u_1, u_2) = E_v \left\{ \left(\cos(\nu 4\pi A u_1) \right) \left(\cos(\nu 4\pi A u_2) \right) \right\} - 0 \quad (3.1.109)$$

$$R_{xx}(u_1, u_2) = \frac{1}{2} E_v \left\{ \left(\cos(\nu 4\pi A (u_1 + u_2)) \right) \right\} + \frac{1}{2} E_v \left\{ \left(\cos(\nu 4\pi A (u_1 - u_2)) \right) \right\} \quad (3.1.110)$$

Under the assumption, a process is wide-sense stationarity (WSS) the autocorrelation function is further simplified from (3.1.110) to (3.1.111) using (3.1.108).

$$R_x(\Theta) = \frac{1}{2} E_v \left\{ \left(\cos(\nu 4\pi A \Theta) \right) \right\} \quad (3.1.111)$$

$$\Theta = u_1 - u_2$$

For a zero mean Gaussian process one should find the variance X' by differentiating (3.1.111) with respect to Θ twice, followed by setting $\Theta = 0$. Once this is completed, one should take the statistical average with respect to Υ and take the negative of the result to obtain (3.1.117).

$$\rho_x'(\Theta) = \frac{1}{2} E_v \left\{ -\nu 4\pi A \sin(\nu 4\pi A \Theta) \right\} \quad (3.1.112)$$

$$\rho_x''(\Theta) = \frac{1}{2} E_v \left\{ -(\nu 4\pi A)^2 \cos(\nu 4\pi A \Theta) \right\} \quad (3.1.113)$$

$$\rho_x''(\Theta = 0) = \frac{1}{2} E_v \left\{ -(\nu 4\pi A)^2 \right\} = 8\pi^2 A^2 E_v \left\{ -(\nu)^2 \right\} \quad (3.1.114)$$

$$E_v \left\{ -(\nu)^2 \right\} = -\frac{2}{\pi} \int_{-1}^1 \sqrt{1-v^2} v^2 dv = -\frac{1}{4} \quad (3.1.115)$$

$$\rho_x''(\Theta = 0) = \frac{1}{2} E_v \left\{ -(\nu 4\pi A)^2 \right\} = 8\pi^2 A^2 \left(-\frac{1}{4} \right) = -2\pi^2 A^2 \quad (3.1.116)$$

$$\sigma_{x'}^2 = -\rho_x''(\Theta = 0) = 2\pi^2 A^2 \quad (3.1.117)$$

In a similar manner, it can be shown that $\sigma_x^2 = \sigma_y^2$. The joint pdf of X, X', Y, Y' is given by (3.1.118) and to solve the variables one converts to polar coordinates such that $X = \Omega \cos \Theta, Y = \Omega \sin \Theta$. The derivatives of X and Y are given by (3.1.119) and (3.1.120). The magnitude squared of X and Y is given to be simply Ω^2 , but that of X' and Y' it is a little more complicated and shown in (3.1.121).

$$f_{X,Y,X',Y'}(x,y,x',y') = \frac{1}{(2\pi)^2 \sigma_x \sigma_{x'}} e^{\left(-\frac{x^2+y^2}{2\sigma_x^2} - \frac{x'^2+y'^2}{2\sigma_{x'}^2}\right)} = \frac{1}{(2\pi)^2 \pi^2 A^2} e^{\left(-\frac{(x^2+y^2)}{4\pi^2 A^2} - \frac{x'^2+y'^2}{4\pi^2 A^2}\right)} \quad (3.1.118)$$

$$X' = \frac{\partial X}{\partial \Omega \partial \Theta} = \Omega' \cos(\Theta) - \Omega \sin(\Theta) \Theta', \quad (3.1.119)$$

$$Y' = \frac{\partial Y}{\partial \Omega \partial \Theta} = \Omega' \sin(\Theta) + \Omega \cos(\Theta) \Theta' \quad (3.1.120)$$

$$\begin{aligned} (X')^2 + (Y')^2 &= \left[\begin{aligned} &(\Omega' \cos(\Theta))^2 + (\Omega' \sin(\Theta))^2 + (\Omega \sin(\Theta) \Theta')^2 + (\Omega \cos(\Theta) \Theta')^2 \\ &- (2\Omega' \Theta' \cos(\Theta) \sin(\Theta)) + (2\Omega \Theta' \cos(\Theta) \sin(\Theta)) \end{aligned} \right] \\ &= (\Omega')^2 + (\Omega \Theta')^2 \end{aligned} \quad (3.1.121)$$

The joint pdf is rewritten in polar coordinates to be that of(3.1.122). Integrating out the terms Θ, Θ' one can obtains(3.1.123).

$$f_{\Omega, \Omega', \Theta, \Theta'}(\omega, \omega', \theta, \theta') = \frac{1}{(2\pi)^2 \sigma_x^2 \sigma_{x'}^2} e^{\left(-\frac{x^2+y^2}{2\sigma_x^2} - \frac{x'^2+y'^2}{2\sigma_{x'}^2}\right)} = \frac{\omega^2}{(2\pi)^2 \sigma_x^2 \sigma_{x'}^2} e^{\left(-\frac{\omega^2}{2\sigma_x^2} - \frac{\omega'^2 + \omega^2 \theta'^2}{2\sigma_{x'}^2}\right)} \quad (3.1.122)$$

$$f_{\Omega, \Omega'}(\omega, \omega') = \frac{\omega}{\sqrt{2\pi} \sigma_x^2 \sigma_{x'}} e^{\left(-\frac{\omega^2}{2\sigma_x^2} - \frac{\omega'^2}{2\sigma_{x'}^2}\right)} \quad (3.1.123)$$

A new parameter $\nu(a)$ can be derived in(3.1.124), which by [9] represents the number of upward crossings at a giver power level a , per interval in the 3dB sidelobe region S_{3dB} . The associated average value of the number of upward crossing is given by(3.1.125).

$$\nu(a) du = du \int_0^\infty w' f_{\Omega, \Omega'}(a, \omega') d\omega' = \int_0^\infty \frac{a du w'}{\sqrt{2\pi} \sigma_x^2 \sigma_{x'}} e^{\left(-\frac{\omega^2}{2\sigma_x^2} - \frac{\omega'^2}{2\sigma_{x'}^2}\right)} = \frac{a du \sigma_{x'}}{\sqrt{2\pi} \sigma_x^2} e^{\left(-\frac{\omega^2}{2\sigma_x^2}\right)} \quad (3.1.124)$$

$$\begin{aligned} E\{\nu(a)\} &= \int_{u=\sin\left(\frac{\phi}{2}\right), \phi \in S_{3dB}} du \nu(a) = \frac{1a \sigma_{x'}}{2\sqrt{2\pi} \sigma_x^2} e^{\left(-\frac{\omega^2}{2\sigma_x^2}\right)} \int_{\phi_{q_0}}^\pi \cos\left(\frac{\phi}{2}\right) d\phi \\ &= 2\sqrt{\pi} a e^{-a^2} A \left(1 - \sin\left(\frac{\phi_{q_0}}{2}\right)\right) \end{aligned} \quad (3.1.125)$$

Lastly, since the 3dB sidelobe region is symmetric in the region $-\phi_{q_o}^{zero} \rightarrow -\pi$ one must multiply (3.1.125) by a factor of 2, providing (3.1.126).

$$E\{v(a)\} = 4\sqrt{\pi}ae^{-a^2} A \left(1 - \sin\left(\frac{\phi_{q_o}}{2}\right) \right) \quad (3.1.126)$$

The function above includes the term e^{-a^2} and decreases monotonically only when $a \geq \frac{1}{\sqrt{2}}$. So by definition the outage probability exceeding a power level of a can be given by (3.1.127).

$$P_{out} = \Pr[v(a) \geq 1] = \sum_{k=1}^{\infty} \Pr[v(a) = k] \leq \sum_{k=1}^{\infty} k \Pr[v(a) = k] = E\{v(a)\} \quad (3.1.127)$$

Equation (3.1.127) provides the upper bound for the average number of crossings exceeding a given power level a and the corresponding CCDF is given as (3.1.128)

$$\Pr[\max_{S_{3dB}} X^2 + Y^2 > NU_o] \leq 4 \left(1 - \sin\left(\frac{\phi_{q_o}}{2}\right) \right) \sqrt{\pi} A \sqrt{NU_o} e^{-NU_o}, \quad \text{for } NU_o \geq \frac{1}{2} \quad (3.1.128)$$

b. Numerical Results

By normalizing the average sidelobe level by $\left(\frac{1}{N}\right)$ and letting $U_o = NU_o$ the normalized outage probability of the maximum sidelobe peak becomes (3.1.129)

$$U_{out} \leq 4\sqrt{\pi} A \left(1 - \sin\left(\frac{\phi_{n_o}^{zero}}{2}\right) \right) \sqrt{U_o} e^{-U_o}, \quad \text{for } U_o \geq \frac{1}{2} \quad (3.1.129)$$

The above equation is simplified further by assuming A increases very large, which renders the angle $\phi_{n_o}^{zero}$ to approach zero gives (3.1.130),

$$U_{out} \leq 4\sqrt{\pi} A \sqrt{U_o} e^{-U_o}, \quad \text{for } U_o \geq \frac{1}{2} \quad (3.1.130)$$

E. Average Properties of a Gaussian Distributed Circular Antenna Array with Perfect Phase Information and Gaussian Random Variable

As a measure of comparison, the standard deviation of a uniform distribution will be evaluated such that it can be compared to the Gaussian distribution. The derivation is shown in (5.1.131)-(5.1.134). A uniform distribution has a P.D.F. defined by (3.1.135) and in terms of the mean μ and variance σ they are expressed by (5.1.136).

If the average μ is assumed zero one obtains(3.1.131), which spans in total length $2\sqrt{3}\sigma$. Moreover, if one redefines x in terms of the normalized radius of the circle i.e. $x \triangleq A$ and sets this equal to the total length $2\sqrt{3}\sigma$ (3.1.132) then it can be shown that $\sigma = A/(2\sqrt{3})$. However, in [12] the metric of comparison used was $\sigma = A/3$. The latter metric is claimed to provide 99.73% accuracy that all antennas are located within the disc of radius A such that the uniform coverage will be the same in both cases. At the present time it is unclear how this factor was obtained therefore both values of σ (3.1.133) and (3.1.134) will be used in the formulations.

$$-\sigma\sqrt{3} \leq x \leq \sigma\sqrt{3} \quad (3.1.131)$$

$$x \leq 2\sqrt{3}\sigma \quad (3.1.132)$$

$$\sigma = \frac{A}{2\sqrt{3}} \quad (3.1.133)$$

$$\sigma = \frac{A}{3} \quad (3.1.134)$$

$$\frac{1}{b-a} \quad (3.1.135)$$

$$\frac{1}{2\sigma\sqrt{3}}, -\sigma\sqrt{3} \leq x - \mu \leq \sigma\sqrt{3} \quad (3.1.136)$$

1. Average Beampattern

If $\nu_n = \tilde{\rho}_n \sin \phi_n$ is Gaussian distributed with zero mean and variance σ^2 then the pdf of ν_n is given by (3.1.137). Moreover, this type of distribution is often used to describe, approximately, any variable that tends to cluster around the mean.

$$f_\nu(\nu) = \frac{1}{\sqrt{2\pi}\sigma} e^{-\frac{\nu^2}{2\sigma^2}}, -\infty < \nu < \infty \quad (3.1.137)$$

In the case of a Gaussian distribution, the average radiation pattern can be calculated from the definition of (0.2.19) to give (3.1.138)

$$U_{av}(\theta, \phi) = \frac{1}{N} + \left(1 - \frac{1}{N}\right) \left[\left| e^{-\frac{\zeta(\theta, \phi)^2 \sigma^2}{2}} \right|^2 \right] \quad (3.1.138)$$

The average radiation intensity (3.1.138) of a circular array with Gaussian distribution still carries the trait of resounding two distinct terms. The first term represents a value of the average radiation intensity in the sidelobe region. However, the second term is not oscillatory this time around. The beampattern decays exponentially with a rate proportional the variance or spatial parameter $\zeta(\theta, \phi)^2$; in addition, the pattern contains neither nulls nor sidelobes. As the radiation intensity is free of sidelobes, it does not have the same opportunity of having high peaks in the beampattern like the previous patterns. I.e. it is not represented neither oscillatory jinc nor sinc functions.

The total radiation pattern of a random circular array with Gaussian distribution is plotted in Fig. 32. The pattern at the meridian angle is shown in Fig. 33 and Fig. 34.

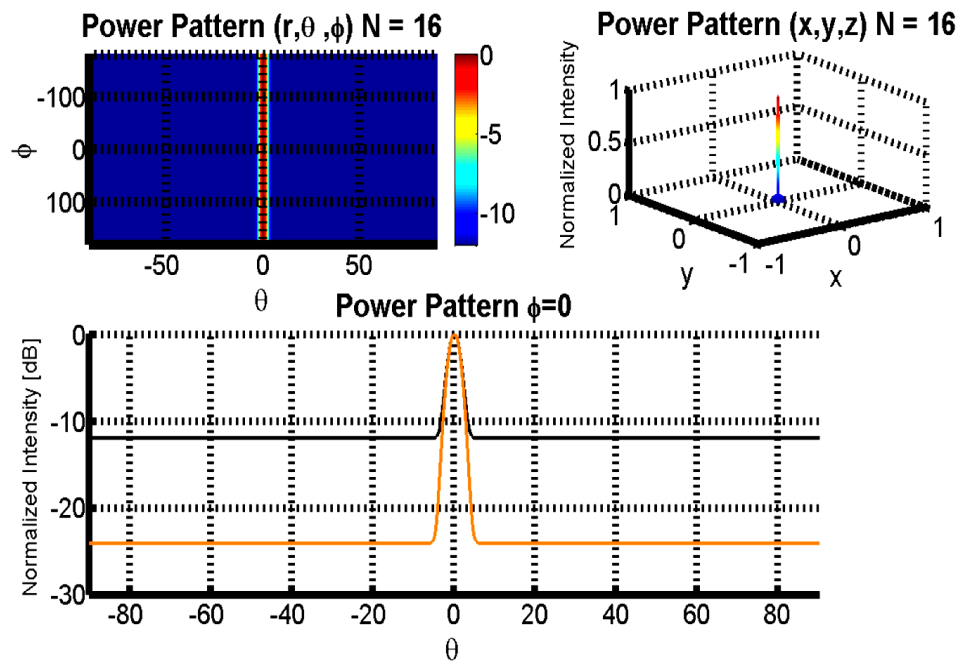


Fig. 32. Average radiation pattern of 16 elements randomly spaced within a circular aperture of 10

λ with Gaussian distribution and $\sigma = .5$.

2. Average Beampattern Simplification for $\theta = \theta_o = \frac{\pi}{2}$

At the meridian angle, $\theta = \theta_o = \frac{\pi}{2}$ the average radiation intensity can be shown to

be (3.1.139) [10].

$$U_{av}(\phi) = \frac{1}{N} + \left(1 - \frac{1}{N}\right) \left[\left| e^{-\frac{\xi(\phi)^2 \sigma^2}{2}} \right|^2 \right] \quad (3.1.139)$$

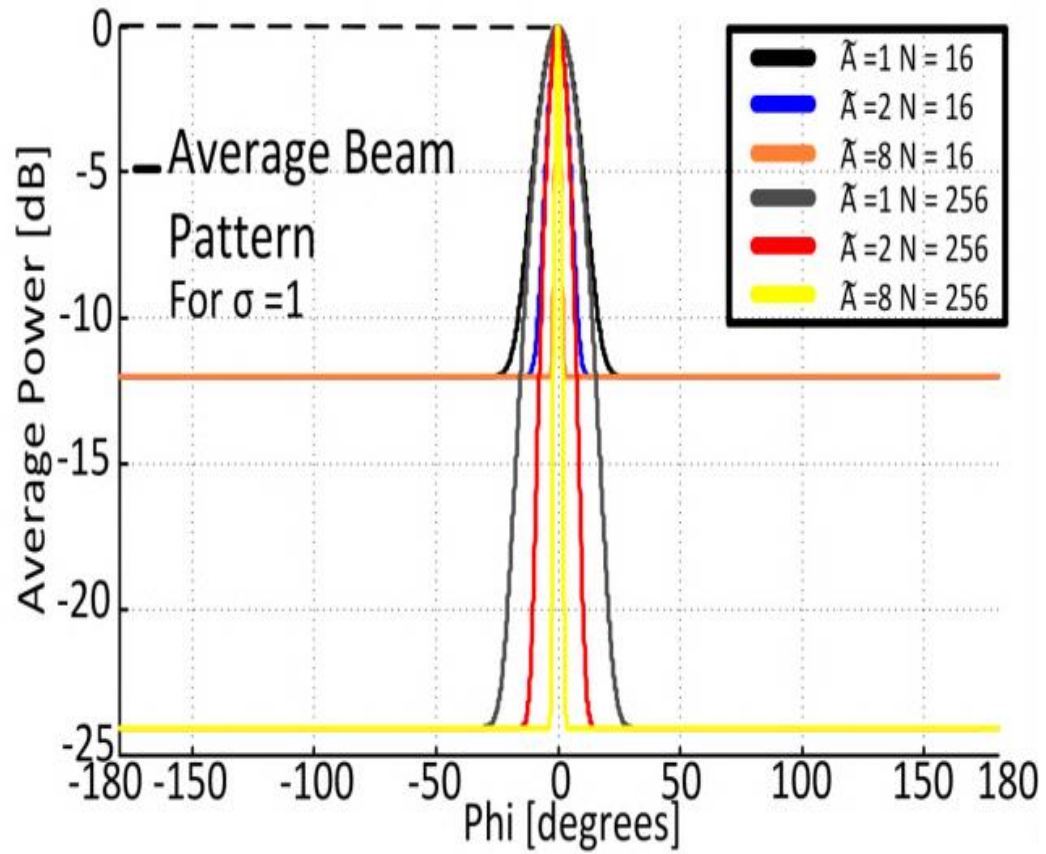


Fig. 33. Average radiation pattern of 16 and 256 elements randomly spaced within a circular aperture of 10λ with Gaussian distribution and $\sigma = 1$.

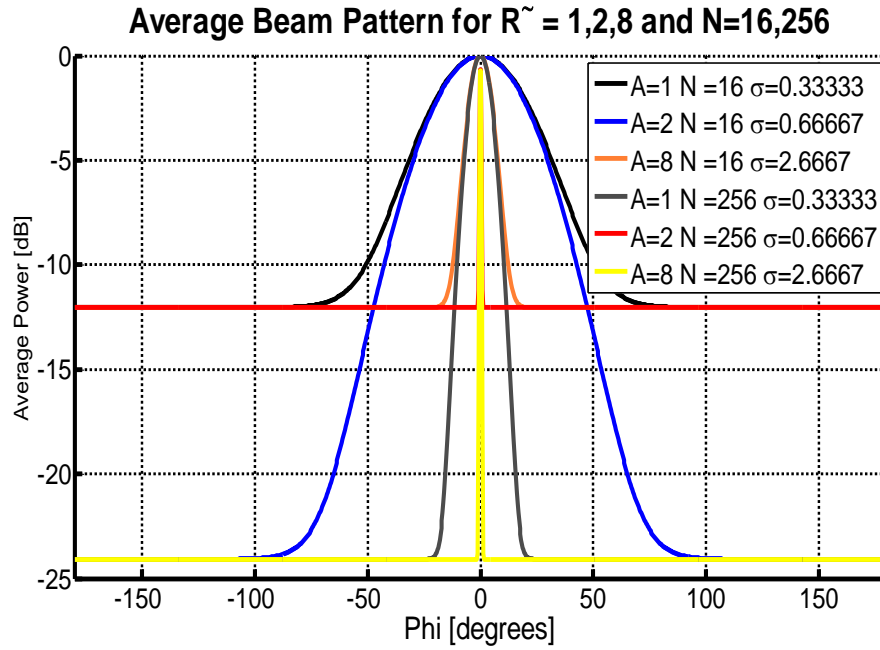


Fig. 34. Average radiation pattern of 16 and 256 elements randomly spaced within a circular

aperture of 10λ with Gaussian distribution and $\sigma = \tilde{A}|_{\lambda=1} = A/3$.

a. 3dB beamwidth

The average 3dB beamwidth for the Gaussian distribution can be calculated in the same manner used in section 5.2.C.3. Moreover, for clarity the setup is shown by (3.1.140) and reduces to (3.1.141) for large N. Solving for ϕ_{av}^{3dB} this gives (3.1.142) and since ϕ_{av}^{3dB} on average tends to be small a first order approximation may be made giving(3.1.143).

$$U_{av}(\phi_{av}^{3dB}) \frac{1}{N} + \left(1 - \frac{1}{N}\right) \left| e^{-\frac{\zeta(\phi_{av}^{3dB})^2 \sigma^2}{2}} \right|^2 = \frac{1}{2} \quad (3.1.140)$$

$$U_{av}(\phi_{av}^{3dB}) \approx \left| e^{-\frac{\zeta(\phi_{av}^{3dB})^2 \sigma^2}{2}} \right|^2 = \frac{1}{2} \quad (3.1.141)$$

$$\phi_{av}^{3dB} = 2 \sin^{-1} \left(\frac{.8326}{4\pi\sigma} \right) = 2 \sin^{-1} \left(\frac{.0663}{\sigma} \right) \quad (3.1.142)$$

$$\phi_{av}^{3dB} \approx \frac{.1326}{\sigma} \quad (3.1.143)$$

In order to compare this result to the uniform distribution one can express the 3dB azimuthal angle using (3.1.133) and (3.1.134) to give (3.1.144) and (3.1.145) respectively. The results of (3.1.144) and (3.1.145) are similar to the results of the uniform distribution, such that the 3dB azimuthal angle decreases with increasing A , however the 3dB beamwidth is seen to be larger for the same cluster area [12]. In addition the results of (3.1.144) and (3.1.145) are fairly close however, the value of σ used in [12] is seen to provide slightly better results.

$$\phi_{av}^{3dB} \approx \frac{.4}{A} \quad (3.1.144)$$

$$\phi_{av}^{3dB} \approx \frac{.46}{A} \quad (3.1.145)$$

b. 3dB Sidelobe Region

The region for which the average of the sidelobe beampattern falls below the threshold level of 3dB above $\frac{1}{N}$ and π can again be formulated in the same manner used in 5.2.C.4. The setup is shown in(3.1.146), and when solved for $\phi_{Sidelobe}$ gives(3.1.147). The result of (13) in [12] seems to be missing a factor of 2, shown inside the square root of the numerator of (3.1.147). Overall a minor mistake or typo, but for clarity the intermediate steps have been shown going from (3.1.146) to (3.1.147).

$$U_{av}(\phi_{Sidelobe}) = \frac{1}{N} + \left(1 - \frac{1}{N}\right) \left| e^{-\frac{\zeta(\phi)^2 \sigma^2}{2}} \right|^2 = \frac{2}{N} \quad (3.1.146)$$

$$\begin{aligned}
&= (N-1) \left| e^{-\frac{\zeta(\phi)^2 \sigma^2}{2}} \right|^2 = 1 \\
&= -\frac{\zeta(\phi)^2 \sigma^2}{2} = \ln \left(\frac{1}{(N-1)} \right) = -\ln(N-1) \\
&= \zeta(\phi) = 4\pi \sin \left(\frac{\phi_{\text{Sidelobe}}}{2} \right) = \sqrt{\frac{2 \ln(N-1)}{\sigma^2}} = \frac{\sqrt{2 \ln(N-1)}}{\sigma} \\
&= \phi_{\text{Sidelobe}} = 2 \sin^{-1} \left(\frac{\sqrt{2 \ln(N-1)}}{4\pi\sigma} \right) \tag{3.1.147}
\end{aligned}$$

c. Average Directivity

The directivity of the Gaussian distribution can also be found relative to a single isotropic antenna in the same manner used to calculate (3.1.59), however once again a closed form solution is unfortunately impermissible. The average directivity is calculated using the average radiation pattern of (3.1.139) providing the average directivity of (3.1.148)

$$D_{av} = \frac{\int_{-\pi}^{\pi} U_{av}(0) d\phi}{\int_{-\pi}^{\pi} U_{av}(\phi) d\phi} = \frac{2\pi}{\int_{-\pi}^{\pi} U_{av}(\phi) d\phi} = \frac{N}{1 + (N-1) {}_1F_1 \left(\frac{1}{2}; 1; -(2\pi\sigma)^2 \right)} \tag{3.1.148}$$

3. Average Statistical Properties of a Uniformly Distributed Circular Antenna Array with Perfect Phase Information and Gaussian Random Variable

a. Distribution of the Beampattern Level in the Sidelobe Region

The exact complementary cumulative distribution function (CCDF) of the beampattern level is given to be the same as (3.1.81) specified in section D. In addition, the array factor at a particular angle ϕ is given once again to be that of (3.1.82) with real part X and imaginary part Y. The underlying difference from section D exists in the

fact that Gaussian distributed P.D.F.s are used to calculate the supporting statistical measures given in (3.1.149)-(3.1.154), instead of uniform P.D.F.s used to calculate (3.1.83)-(3.1.88).

$$m_x = E[X(\phi|\vec{v})] = \sum_{n=1}^N \frac{1}{\sqrt{N}} \int_{-\infty}^{\infty} \frac{1}{\sqrt{2\pi}\sigma} e^{-\left(\frac{v_n^2}{2\sigma^2}\right)} \cos(v_n \zeta(\phi)) dv_n = \sqrt{N} e^{-\frac{\zeta(\phi)^2 \sigma^2}{2}} \quad (3.1.149)$$

$$m_y = \sum_{n=1}^N \frac{1}{2\sqrt{N}} \int_{-\infty}^{\infty} \frac{1}{\sqrt{2\pi}\sigma} e^{-\left(\frac{v_n^2}{2\sigma^2} + j(v_n \zeta(\phi))\right)} \sin(v_n \zeta(\phi)) dv_n = 0 \quad (3.1.150)$$

$$E[X^2(\phi|z)] = \sum_{n=1}^N \left[\left(\frac{1}{N} \right) \int_{-\infty}^{\infty} \frac{1}{\sqrt{2\pi}\sigma} e^{-\left(\frac{v_n^2}{2\sigma^2}\right)} \cos^2(v_n \zeta(\phi)) dv_n \right] = \frac{1}{2} (1 + e^{-2\zeta(\phi)^2 \sigma^2}) \quad (3.1.151)$$

$$E[Y^2(\phi|\vec{v})] = \frac{1}{2} (1 - e^{-2\zeta(\phi)^2 \sigma^2}) \quad (3.1.152)$$

$$\sigma_x^2 = E[X^2(\phi|\vec{v})] - E[X(\phi|\vec{v})]^2 = \frac{1}{2} (1 + e^{-2\zeta(\phi)^2 \sigma^2}) - e^{-\zeta(\phi)^2 \sigma^2} \quad (3.1.153)$$

$$\sigma_y^2 = E[Y^2(\phi|\vec{v})] - E[Y(\phi|\vec{v})]^2 = \frac{1}{2} (1 - e^{-2\zeta(\phi)^2 \sigma^2}) \quad (3.1.154)$$

The variances σ_x^2 and σ_y^2 approach a value of .5 in the limiting case just like they did in the uniform case. Hence, the beam pattern level in the sidelobe region approaches a Nakagami distribution (3.1.93). Similar to the Uniform case the mean m_x approaches zero in the sidelobe region for the Gaussian case and one may once more assume the beam pattern assumes Rayleigh distribution given by (3.1.94).

b. Distribution of the Maximum Sidelobe Peak

The probability the maximum of a sidelobe crosses a power level threshold is formulated in the same manner as it was in Subheading 5.2.D.4. The number of upward

crossings at a given level a per interval in the 3dB sidelobe region S_{3dB} is given by (3.1.155). The mean number of crossings is given by

$$v(a)du = du \int_0^\infty w' f_{\Omega, \Omega'}(a, \omega') d\omega' = \int_0^\infty \frac{a du w'}{\sqrt{2\pi\sigma_x^2\sigma_x'}} e^{\left(-\frac{\omega^2}{2\sigma_x^2} - \frac{\omega'^2}{2\sigma_x'^2}\right)} = \frac{a du \sigma_x'}{\sqrt{2\pi\sigma_x^2}} e^{\left(-\frac{\omega^2}{2\sigma_x^2}\right)} \quad (3.1.155)$$

$$E\{v(a)\} = \frac{1a\sigma_x'}{2\sqrt{2\pi\sigma_x^2}} e^{\left(-\frac{a^2}{2\sigma_x'^2}\right)} \int_{\phi_o}^\pi \cos\left(\frac{\phi}{2}\right) d\phi = 4\sqrt{\pi}\sigma_a e^{-a^2} \left(1 - \sin\left(\frac{\phi_{Sidelobe}}{2}\right)\right) \quad (3.1.156)$$

Also since the 3dB, sidelobe region is symmetric in the region $-\phi_{Sidelobe} \rightarrow -\pi$ one should multiply (3.1.156) by a factor of 2 giving (3.1.157).

$$E\{v(a)\} = 8\sqrt{\pi} \left(1 - \sin\left(\frac{\phi_{Sidelobe}}{2}\right)\right) \sigma_a e^{-a^2} \quad (3.1.157)$$

Nevertheless, the outage probability is given by (3.1.158) and for low values of ϕ_o the expression is approximated as (3.1.159).

$$\Pr\left[\max_{S_{3dB}} X^2 + Y^2 > NU_o\right] \leq 8\sqrt{\pi}\sigma\sqrt{NU_o} e^{-NU_o} \left(1 - \sin\left(\frac{\phi_{Sidelobe}}{2}\right)\right), \quad \text{for } NU_o \geq \frac{1}{2} \quad (3.1.158)$$

$$\Pr\left[\max_{S_{3dB}} X^2 + Y^2 > NU_o\right] \leq 8\sqrt{\pi}\sigma\sqrt{NU_o} e^{-NU_o}, \quad \text{for } NU_o \geq \frac{1}{2} \quad (3.1.159)$$

F. Average Properties of a Truncated Gaussian Distributed Circular Antenna Array with Perfect Phase Information and Gaussian Random Variable

1. Average Beampattern

When the Gaussian random variable $v_n = \bar{\rho}_n \sin \phi_n$ does not have infinite support it is truncated in the form of (3.1.160), which is similar to that of [12], yet this distribution is independent of the elevation angle θ . This type of distribution possibly will be more practical since it neglects antennas far away from the cluster. Typically the element

located far away will require higher power for communicating and hence, neglecting these may very well benefit the system overall in terms of energy consumption needed for transmission. However, if the cluster gets too crowded effects of mutual coupling may repeal the above assumption as too much unwanted interference negatively impacts the beam.

$$f_v(v) = \frac{1}{\sqrt{2\pi}\sigma} e^{-\frac{v^2}{2\sigma^2}}, -L < v < L \quad (3.1.160)$$

The derivation of the average beampattern is completely derived since it provides a different result from [12]. Moreover, the result, in this section, is also verified with Mathematica to determine if a mistake was possibly made in [12] and it seems plausible, therefore a full derivation is shown below.

$$\begin{aligned} U_{av}(\theta, \phi) &= E_v \left| U_{av}(\theta, \phi | \vec{v}) \right| \\ &= \int_{-\infty}^{\infty} \int_{-\infty}^{\infty} \left(\frac{1}{N} + \frac{1}{N^2} \sum_{m=1}^N \sum_{\substack{n=1 \\ n \neq m}}^N e^{j\zeta(\theta, \phi)(v_n - v_m)} \right) f_{v_n}(v_n) f_{v_m}(v_m) dv_n dv_m \quad (3.1.161) \\ &= \frac{1}{N} + \frac{1}{N^2} \left[\sum_{m=1}^N \int_{-L}^L e^{-j\zeta(\theta, \phi)v_m} \frac{1}{\sqrt{2\pi}\sigma} e^{-\frac{v_m^2}{2\sigma^2}} dv_m \sum_{\substack{n=1 \\ n \neq m}}^N \int_{-L}^L e^{j\zeta(\theta, \phi)v_n} \frac{1}{\sqrt{2\pi}\sigma} e^{-\frac{v_n^2}{2\sigma^2}} dv_n \right] \end{aligned}$$

Solving the first integral with respect to n is done by completing the square as follows.

$$\begin{aligned}
& \frac{v_n^2}{2\sigma^2} - j\zeta(\theta, \phi)v_n = 0 \\
& \text{or} \\
& v_n^2 - j\zeta(\theta, \phi)v_n 2\sigma^2 = 0 \\
& \quad \downarrow \text{(half of the middle term coef)} \\
& j\zeta(\theta, \phi)\sigma^2 \rightarrow \zeta(\theta, \phi)^2 \sigma^4 \text{ (squared)} \\
& (v_n - j\zeta(\theta, \phi)\sigma^2)^2 = \zeta(\theta, \phi)^2 \sigma^4 \\
& (v_n - j\zeta(\theta, \phi)\sigma^2)^2 \left(\frac{1}{2\sigma^2}\right) = \zeta(\theta, \phi)^2 \sigma^4 \left(\frac{1}{2\sigma^2}\right) \\
& \frac{(v_n - j\zeta(\theta, \phi)\sigma^2)^2}{2\sigma^2} - \frac{\zeta(\theta, \phi)^2 \sigma^2}{2} = 0
\end{aligned}$$

By a change of variables $x = \frac{v_n - j\zeta(\phi)\sigma^2}{\sigma}$ and $dx = \frac{dv_n}{\sigma}$ one obtains (3.1.162). Using the integral identity (A.1.16) one can obtain (3.1.163).

$$\int_{-L}^L \frac{1}{\sqrt{2\pi}\sigma} e^{-\frac{(v_n + j\zeta(\phi)\sigma^2)^2}{2\sigma^2}} dv_n = \frac{1}{\sqrt{2\pi}} \int_{\frac{-L + j\zeta(\phi)\sigma^2}{\sigma}}^{\frac{L + j\zeta(\phi)\sigma^2}{\sigma}} e^{-\frac{(x)^2}{2}} dx = \frac{1}{\sqrt{2\pi}} \int_{\frac{-L + j\zeta(\phi)\sigma^2}{\sigma}}^{\infty} e^{-\frac{(x)^2}{2}} dx - \frac{1}{\sqrt{2\pi}} \int_{\frac{L + j\zeta(\phi)\sigma^2}{\sigma}}^{\infty} e^{-\frac{(x)^2}{2}} dx \quad (3.1.162)$$

$$\int_{-L}^L \frac{1}{\sqrt{2\pi}\sigma} e^{-\frac{(v_n - j\zeta(\phi)\sigma^2)^2}{2\sigma^2}} dv_n = Q(x_1) - Q(x_2) = Q\left(\frac{-L + j\zeta(\phi)\sigma^2}{\sigma}\right) - Q\left(\frac{L + j\zeta(\phi)\sigma^2}{\sigma}\right) \quad (3.1.163)$$

It can be shown (3.1.163) can be rearranged with another identity (D.1.16) to give (3.1.164). Additionally the integral with respect to v_m is done in a similar manner also contributing the solution of (3.1.164). Moreover, the Q-function may also be rewritten in terms of error functions with the identity (D.1.17) providing (3.1.165). Therefore, multiplying the result of (3.1.165) by itself since the solution with respect v_m yields the same result as the solution to v_n ; the average radiation intensity is furnished to be that of (3.1.166).

$$\int_{-L}^L \frac{1}{\sqrt{2\pi}\sigma} e^{-\frac{(v_n - j\zeta(\theta, \phi)\sigma^2)^2}{2\sigma^2}} dv_n = 1 - Q\left(\frac{L - j\zeta(\theta, \phi)\sigma^2}{\sigma}\right) - Q\left(\frac{L + j\zeta(\theta, \phi)\sigma^2}{\sigma}\right) \quad (3.1.164)$$

$$e^{-\frac{\zeta(\theta, \phi)^2 \sigma^2}{2}} \int_{-L}^L \frac{1}{\sqrt{2\pi}\sigma} e^{-\frac{(v_n - j\zeta(\theta, \phi)\sigma^2)^2}{2\sigma^2}} dv_n = e^{-\frac{\zeta(\theta, \phi)^2 \sigma^2}{2}} \frac{1}{2} \left[\operatorname{erf}\left(\frac{L - j\zeta(\theta, \phi)\sigma^2}{\sqrt{2}\sigma}\right) + \operatorname{erf}\left(\frac{L + j\zeta(\theta, \phi)\sigma^2}{\sqrt{2}\sigma}\right) \right] \quad (3.1.165)$$

$$U_{av}(\theta, \phi) = \frac{1}{N} + \frac{1}{N^2} \left| e^{-\frac{\zeta(\theta, \phi)^2 \sigma^2}{2}} \right|^2 \left[\frac{1}{4} \sum_{m=1}^N \sum_{\substack{n=1 \\ n \neq m}}^N \left[\operatorname{erf}\left(\frac{L - j\zeta(\theta, \phi)\sigma^2}{\sqrt{2}\sigma}\right) + \operatorname{erf}\left(\frac{L + j\zeta(\theta, \phi)\sigma^2}{\sqrt{2}\sigma}\right) \right]^2 \right] \quad (3.1.166)$$

2. Average Beampattern Simplification for $\theta = \theta_o = \frac{\pi}{2}$

At the meridian angle, the average radiation intensity is given by (3.1.167) and the derivation leading to (3.1.166) is used to obtain (3.1.167) in the exact same manner. The difference between the two results lies within the spatial parameter of (3.1.167) being independent of elevation angle. Lastly, it is again restated that (3.1.167) differs from equation (9) of [12].

$$U_{av}(\phi) = \frac{1}{N} + \frac{1}{N^2} \left| e^{-\frac{\zeta(\phi)^2 \sigma^2}{2}} \right|^2 \left[\frac{1}{4} \sum_{m=1}^N \sum_{\substack{n=1 \\ n \neq m}}^N \left[\operatorname{erf}\left(\frac{L - j\zeta(\phi)\sigma^2}{\sqrt{2}\sigma}\right) + \operatorname{erf}\left(\frac{L + j\zeta(\phi)\sigma^2}{\sqrt{2}\sigma}\right) \right]^2 \right] \quad (3.1.167)$$

G. Realization of a Uniformly Distributed Circular Antenna Array with Perfect Phase Information

The realization pattern for a random circular array is plotted from a uniform distribution of elements in Fig. 35 with a given element distribution shown in Fig. 36.

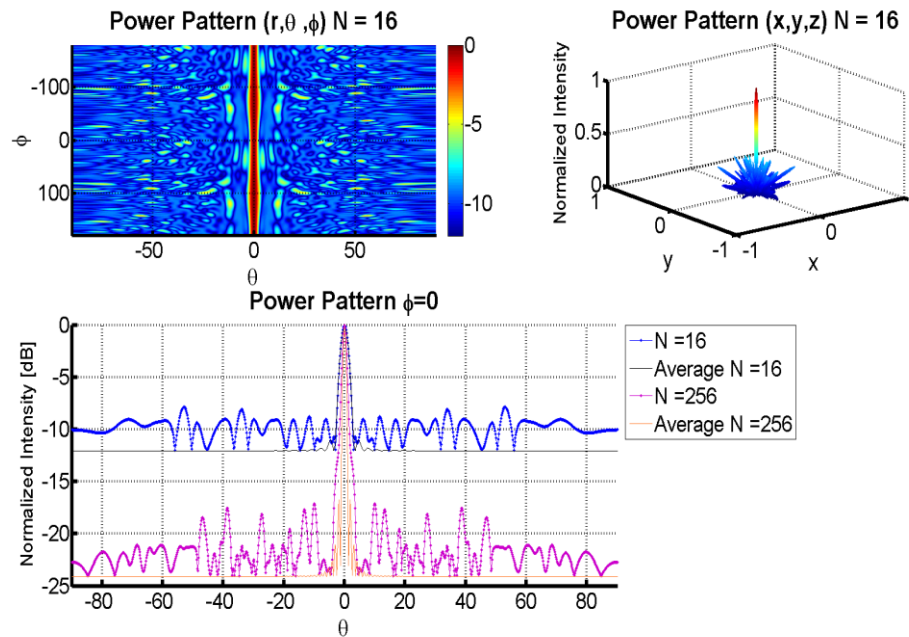


Fig. 35. Simulated and analytical radiation intensity for a circular random array (uniformly distributed) in the XY -plane with $A = 10$, $N = 16$ and 256 .

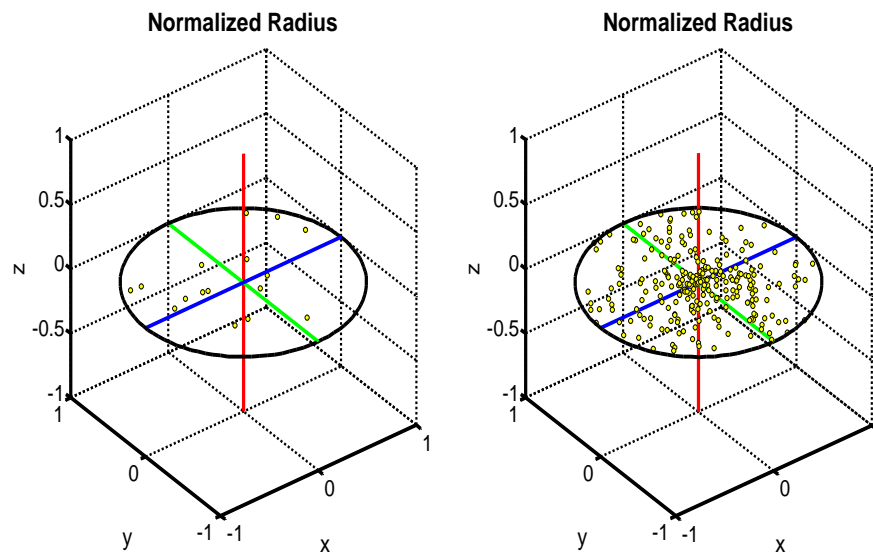


Fig. 36. 16 (left) and 256 (right) elements uniformly distributed in a normalized circular aperture along the XY -plane.

The realization pattern for a random circular array is plotted from a Gaussian distribution of elements in Fig. 37 with a given element distribution shown in Fig. 38.

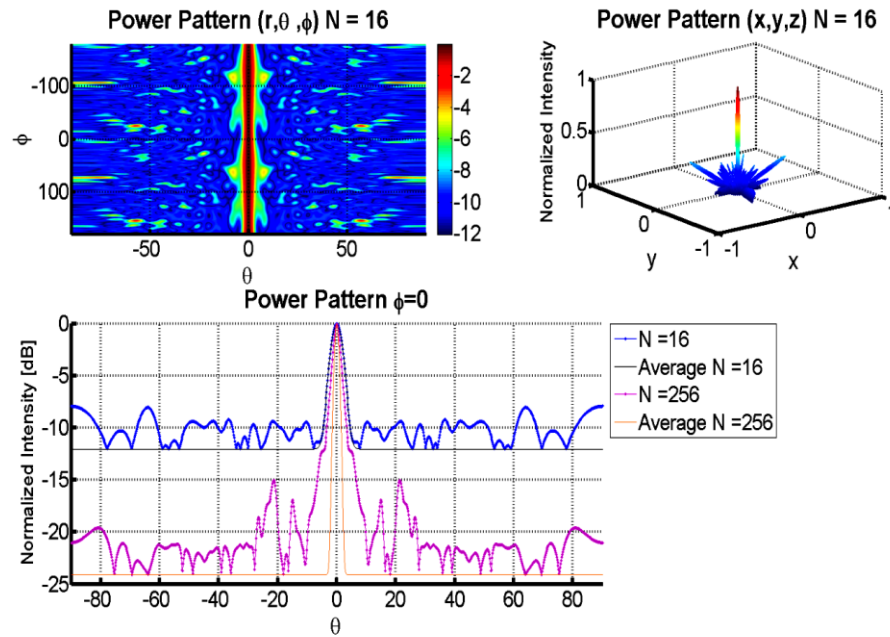


Fig. 37. Simulated and analytical radiation intensity for a circular random array (Gaussian distributed) in the XY -plane with $A = 10$, $N = 16$ and 256 .

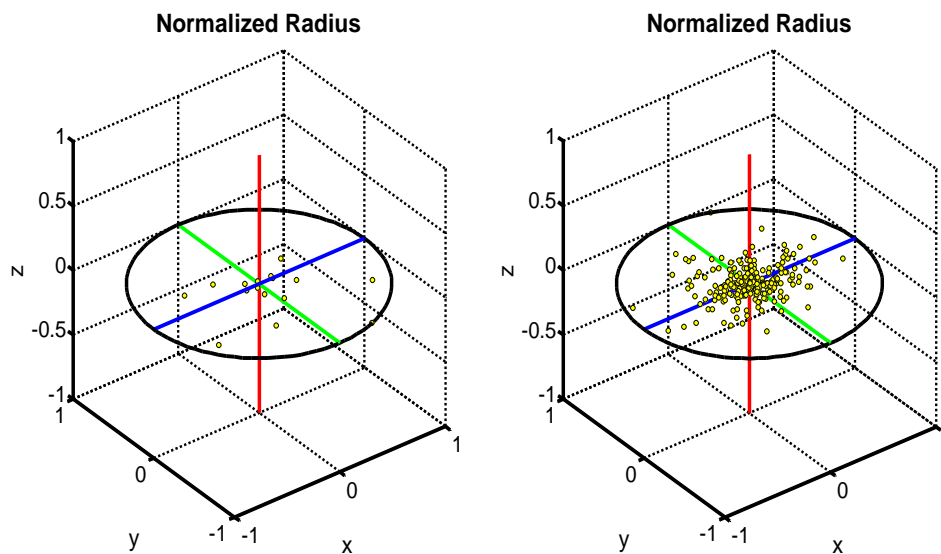


Fig. 38. 16 (left) and 256 (right) elements Gaussian distributed in a normalized circular aperture along the XY-plane.

It is interesting to notice the realization of the circular random array is rotationally symmetric in the elevation angle of Fig. 35. A similar result is seen for a planar random array in [79].

CHAPTER VI

SPHERICAL ARRAYS

6.1 Periodic

A. System Development and Beampattern Definition

Innumerable opportunity exists in assembly of element placement for a periodic spherical array, which is covered in greater depth in section H. As an alternative, this section begins with a pictorial representation of a spherical array represented in Figure 39 with each antenna placed arbitrarily, on the surface of the sphere of radius A . Moreover, unlike previous sections the analysis of a periodic spherical array will be covered in greater detail similar to [80]. The analysis is kept general showing the process for setting up any periodic array structure. In addition, the general case gives one the capability to vary parameters in any fashion desired.

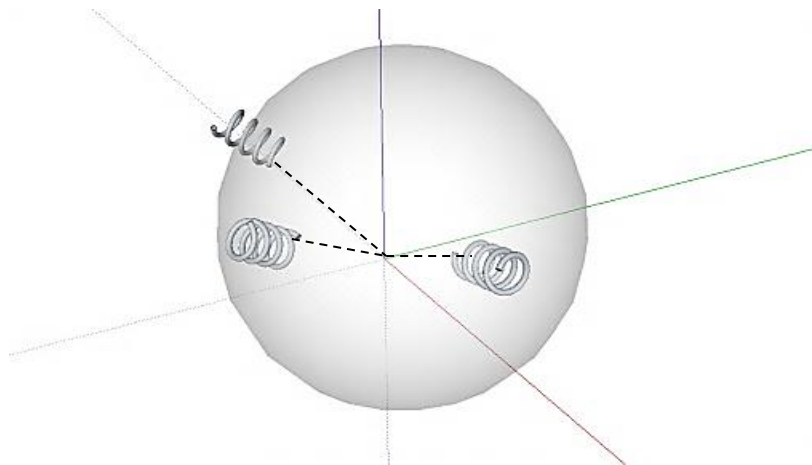


Fig. 39. Geometry of an N-element periodic spherical array of circularly polarized elements.

The field of a specific antenna originates at the observed point P' identified in Figure 40. A local coordinate system is centered at the point P' with axis x' , y' and z' ,

forming an orthogonal coordinate system. The z' axis is normal to the point P' with the x' and y' axis located coplanar to the element.

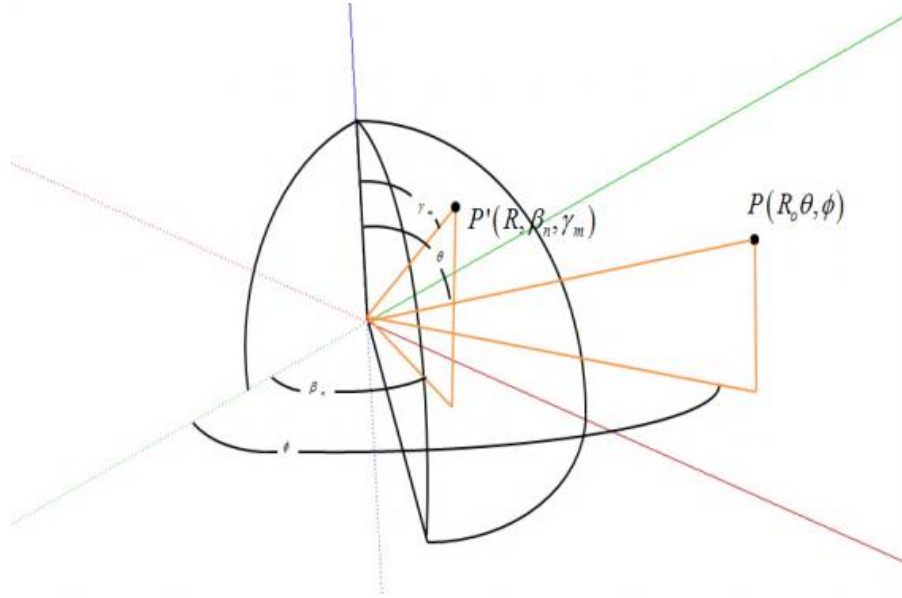


Fig. 40. Geometry of a periodic spherical array referenced to the element.

B. Element Pattern from a Point Source

The radiation pattern (4.1.1) of a single antenna is determined from the relative origin P' (location of the element) with azimuthal and conical angles β, γ measured from the true origin O . As more elements are introduced to the spherical structure in section E, the angles will be conveyed more formally as β_n, γ_m .

$$\bar{E}_{\alpha\beta} = \hat{a}_{\theta} E_{\theta'_{\alpha\beta}} + \hat{a}_{\phi} E_{\phi'_{\alpha\beta}} = \left[\hat{a}_{\theta} f_1(\theta', \phi') \frac{e^{j(\omega t - kR' - \psi_{\beta\gamma})}}{R'} + \hat{a}_{\phi} f_2(\theta', \phi') \frac{e^{j(\omega t - kR' - \psi_{\beta\gamma} - \delta)}}{R'} \right] \quad (4.1.1)$$

Where,

- $\hat{a}_{\theta'}, \hat{a}_{\phi'}$ are the unit vectors in the θ' and ϕ' directions,
- δ is the phase difference between the two components of the field,
- ω is the radian frequency of operation,
- $\psi_{\beta\gamma}$ is the phase delay introduced into the element for beam steering purpose,
- $f_1(\theta', \phi'), f_2(\theta', \phi')$ are the pattern factors of the two components of the field distribution.

Since a far field, approximation is used, the radial component a_R of the field distribution is assumed to be zero [65]. The field is also assumed elliptically polarized except for the condition $\delta = \pm\pi/2$ making the field circularly polarized.

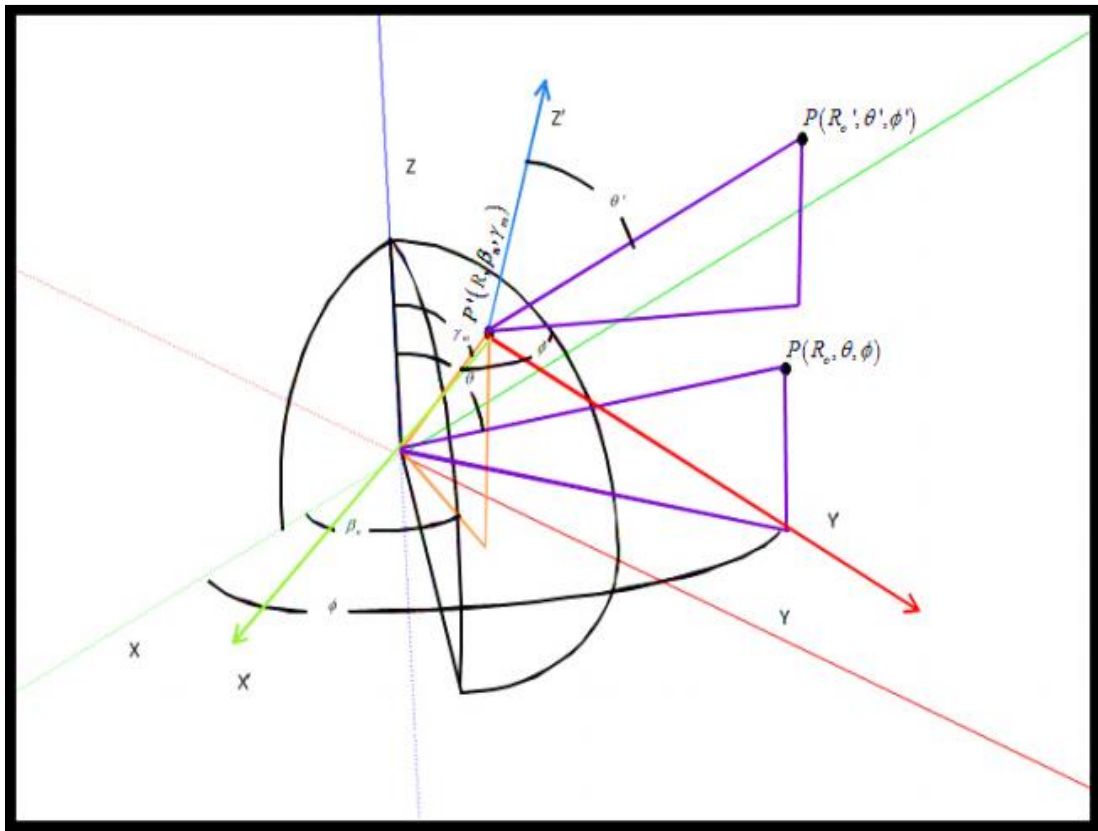


Fig. 41. Geometry of a periodic spherical array rotated about the element in order to be referenced to the origin.

Shifting the origin P' of the local coordinate system to the point O in Figure 41, (true origin) one may rewrite (4.1.1) as (4.1.2) where $\overline{OP'} = A\hat{a}_{R'}$, which is the vector originating at the origin O and ending at the surface P' . The unit vector $\hat{a}_{R'}$ is defined as the radially directed unit vector aiming to the direction P' . The direction cosine $\overline{OP'} \cdot \hat{a}_{R'}$ is thereby given in (4.1.4).

$$\overline{E}_{\alpha\beta} = [\hat{a}_{\theta'} f_1(\theta', \phi') + \hat{a}_{\phi'} f_2(\theta', \phi')] e^{j(k\overline{OP'} \cdot \hat{a}_{R'} - \psi_{P'})} \frac{e^{j(\omega t - kR_o)}}{R_o}, \quad (4.1.2)$$

$$r' \cos \psi = \overline{OP'} \cdot \hat{a}_{R'} = A\hat{a}_{R'} \cdot \hat{a}_{R'} = (A \sin \theta' \cos \phi' \hat{a}_x + A \sin \theta' \sin \phi' \hat{a}_y + A \cos \theta' \hat{a}_z) \cdot (\sin \theta \cos \phi \hat{a}_x + \sin \theta \sin \phi \hat{a}_y + \cos \theta \hat{a}_z) \quad (4.1.3)$$

$$r' \cos \psi = \overline{OP'} \cdot \hat{a}_{R'} = A(\sin \theta \sin \theta \cos(\phi - \phi') + \cos \theta \cos \theta) \quad (\text{Using Appendix C.1.4}) \quad (4.1.4)$$

C. Coordinate Transformation Relationships in Spherical Coordinates

The transformation going from primed to unprimed coordinates is obtained by using a general method of orthogonal transformation of coordinates [80]. Consequently, the angles θ' and ϕ' can be expressed where $\hat{a}_{R'}$ is the typical spherical unit vector in the radial direction defined in (4.1.7).

$$\cos \theta' = (\hat{a}_{R'} \cdot \hat{a}_z) \quad (4.1.5)$$

$$\cot \phi' = \left(\frac{\hat{a}_{R'} \cdot \hat{a}_x}{\hat{a}_{R'} \cdot \hat{a}_y} \right) \quad (4.1.6)$$

$$\hat{a}_{R'} = \sin \theta \cos \phi \hat{a}_x + \sin \theta \sin \phi \hat{a}_y + \cos \theta \hat{a}_z \quad (4.1.7)$$

The transformation between primed and unprimed unit vector coordinates are related by a rotation matrix A such that

$$\begin{bmatrix} a_x \\ a_y \\ a_z \end{bmatrix} = \tilde{A} \begin{bmatrix} a_x \\ a_y \\ a_z \end{bmatrix},$$

The rotation matrix A is determined by the product of rotation matrices shown below.

Roll, Pitch and Yaw matrices

$$\begin{bmatrix} 1 & 0 & 0 \\ 0 & \cos \alpha & \sin \alpha \\ 0 & -\sin \alpha & \cos \alpha \end{bmatrix}, \begin{bmatrix} \cos \beta & 0 & -\sin \beta \\ 0 & 1 & 0 \\ \sin \beta & 0 & \cos \beta \end{bmatrix}, \begin{bmatrix} \cos \gamma & \sin \gamma & 0 \\ -\sin \gamma & \cos \gamma & 0 \\ 0 & 0 & 1 \end{bmatrix}$$

about X axis about Y axis about Z axis

The product of these rotation matrices is followed by rotation in the following order.

- 1) about x
- 2) about z
- 3) about y

For instance if the coordinate system is rotated about the y and z axis then the matching rotation matrix is given to be the product of the pitch and yaw matrices generating primed unit vectors (4.1.8)-(4.1.10).

$$\hat{a}_{x'} = \cos \beta \cos \gamma \hat{a}_x + \cos \beta \sin \gamma \hat{a}_y - \sin \beta \hat{a}_z \quad (4.1.8)$$

$$\hat{a}_{y'} = -\sin \beta \hat{a}_x + \cos \gamma \hat{a}_y + 0 \hat{a}_z \quad (4.1.9)$$

$$\hat{a}_{z'} = \sin \beta \cos \gamma \hat{a}_x + \sin \beta \sin \gamma \hat{a}_y + \cos \beta \hat{a}_z \quad (4.1.10)$$

Substitution of unit vectors into the former equations (4.1.5) and (4.1.6) gives (4.1.11) and (4.1.12).

$$\cos \theta' = \sin \beta \sin \theta \cos(\phi - \gamma) + \cos \beta \cos \theta \quad (4.1.11)$$

$$\cot \phi' = \frac{\cos \beta \sin \theta \cos(\phi - \gamma) - \sin \beta \cos \theta}{\sin \theta \sin(\phi - \gamma)} \quad (4.1.12)$$

The angles θ' and ϕ' are found by taking the gradient of (4.1.11) and (4.1.12) where the gradient in spherical coordinates is defined in (E.3.1) giving (4.1.14) when applied to

$$(4.1.11) \text{ shown below. } \vec{\nabla}(\cos \theta') = \vec{\nabla}(\sin \beta \sin \theta \cos(\phi - \gamma) + \cos \beta \cos \theta)$$

$$\begin{aligned} \frac{1}{r} \frac{\partial \cos \theta'}{\partial \theta} \hat{a}_{\theta'} &= \frac{1}{r} \frac{\partial (\sin \beta \sin \theta \cos(\phi - \gamma) + \cos \beta \cos \theta)}{\partial \theta} \hat{a}_{\theta} \\ &+ \frac{1}{r \sin \theta} \frac{\partial (\sin \beta \sin \theta \cos(\phi - \gamma) + \cos \beta \cos \theta)}{\partial \phi} \hat{a}_{\phi} \end{aligned} \quad (4.1.13)$$

$$\hat{a}_{\theta'} = -\hat{a}_{\theta} \frac{\cos \theta \sin \beta \cos(\phi - \gamma) - \cos \beta \sin \theta}{\sin \theta'} + \hat{a}_{\phi} \frac{\sin \beta \sin(\phi - \gamma)}{\sin \theta'}. \quad (4.1.14)$$

Likewise, applying (E.3.1) to (4.1.12) gives (4.1.16).

$$\begin{aligned} \frac{1}{r \sin \theta'} \frac{\partial \cot \phi'}{\partial \phi'} \hat{a}_{\phi'} &= \frac{1}{r} \frac{\partial}{\partial \theta} \left(\frac{\cos \beta \sin \theta \cos(\phi - \gamma) - \sin \beta \cos \theta}{\sin \theta \sin(\phi - \gamma)} \right) \hat{a}_{\theta} + \\ &\frac{1}{r \sin \theta} \frac{\partial}{\partial \phi} \left(\frac{\cos \beta \sin \theta \cos(\phi - \gamma) - \sin \beta \cos \theta}{\sin \theta \sin(\phi - \gamma)} \right) \hat{a}_{\phi} \end{aligned} \quad (4.1.15)$$

$$\hat{a}_{\phi'} = -\frac{\sin \theta'}{\csc^2 \phi'} \frac{\sin \beta \sin(\phi - \gamma)}{(\sin \theta \sin(\phi - \gamma))^2} \hat{a}_{\theta} - \frac{\sin \theta'}{\csc^2 \phi'} \left[\frac{\cos \theta \sin \beta \cos(\phi - \gamma) - \sin \theta \cos \beta}{\sin^2 \theta \sin^2(\phi - \gamma)} \right] \hat{a}_{\phi} \quad (4.1.16)$$

One particular simplification is possible if $\phi' = \phi - \gamma$ and $\theta' = \theta$ giving (4.1.17)

$$\hat{a}_{\phi'} = -\frac{\sin \beta \sin(\phi - \gamma)}{\sin \theta'} \hat{a}_{\theta} - \left[\frac{\cos \theta \sin \beta \cos(\phi - \gamma) - \sin \theta \cos \beta}{\sin \theta'} \right] \hat{a}_{\phi} \quad (4.1.17)$$

The unit vectors in (4.1.14) and (4.1.17) look very similar and are shown below in (4.1.18) and (4.1.19) for easy comparison.

$$\hat{a}_{\theta'} = -\hat{a}_{\theta} \frac{\cos \theta \sin \beta \cos(\phi - \gamma) - \cos \beta \sin \theta}{\sin \theta'} + \hat{a}_{\phi} \frac{\sin \beta \sin(\phi - \gamma)}{\sin \theta'} \quad (4.1.18)$$

$$\hat{a}_{\phi'} = -\hat{a}_{\theta} \frac{\sin \beta \sin(\phi - \gamma)}{\sin \theta'} - \hat{a}_{\phi} \left[\frac{\cos \theta \sin \beta \cos(\phi - \gamma) - \sin \theta \cos \beta}{\sin \theta'} \right] \quad (4.1.19)$$

D. Field Components with Circular Polarization

Substituting $\hat{a}_{\theta'}$, $\hat{a}_{\phi'}$ components into the field distribution (4.1.2) gives (4.1.20) and(4.1.21).

$$E_{\theta\alpha\beta} = - \left[\begin{array}{l} \frac{\cos \theta \sin \beta \cos(\phi - \gamma) - \cos \beta \sin \theta}{\sin \theta'} f_1(\theta', \phi') + \\ \frac{\sin \beta \sin(\phi - \gamma)}{\sin \theta'} f_2(\theta', \phi') e^{-j\delta} \end{array} \right] e^{j(kA \cos \theta' - \psi_{\beta\gamma})} \frac{e^{j(\omega t - kR_o)}}{R_o}, \quad (4.1.20)$$

$$E_{\phi\alpha\beta} = \left[\begin{array}{l} \frac{\sin \beta \sin(\phi - \gamma)}{\sin \theta'} f_1(\theta', \phi') \\ - \frac{\cos \theta \sin \beta \cos(\phi - \gamma) - \cos \beta \sin \theta}{\sin \theta'} f_2(\theta', \phi') e^{-j\delta} \end{array} \right] e^{j(kA \cos \theta' - \psi_{\beta\gamma})} \frac{e^{j(\omega t - kR_o)}}{R_o} \quad (4.1.21)$$

In the case of circular polarization the fields produced by individual elements are given such that $f_1(\theta', \phi') = f_2(\theta', \phi') = f(\theta', \phi')$ and $\delta = \pm \frac{\pi}{2}$. Substitution of these conditions into (4.1.20) and (4.1.21) one obtains (4.1.22) and(4.1.23).

$$E_{\theta\alpha\beta} = - \left[\begin{array}{l} \frac{\cos \theta \sin \beta \cos(\phi - \gamma) - \cos \beta \sin \theta}{\sin \theta'} \\ + \frac{\sin \beta \sin(\phi - \gamma)}{\sin \theta'} e^{\mp j\frac{\pi}{2}} \end{array} \right] f(\theta', \phi') e^{j(kA \cos \theta' - \psi_{\beta\gamma})} \frac{e^{j(\omega t - kR_o)}}{R_o}, \quad (4.1.22)$$

$$E_{\phi\alpha\beta} = \left[\begin{array}{l} \frac{\sin \beta \sin(\phi - \gamma)}{\sin \theta'} \\ - \frac{\cos \theta \sin \beta \cos(\phi - \gamma) - \cos \beta \sin \theta}{\sin \theta'} e^{\mp j\frac{\pi}{2}} \end{array} \right] f(\theta', \phi') e^{j(kA \cos \theta' - \psi_{\beta\gamma})} \frac{e^{j(\omega t - kR_o)}}{R_o} \quad (4.1.23)$$

E. Total Field Components with Multiple Elements within a Spherical Array

The radiation pattern produced of a spherical array is fully achieved by means of superimposing respective field components of each element. For example, the subscripts n and m are used to represent the position of each element. Therefore, the complete pattern for θ and ϕ components are designated in (4.1.24) and(4.1.25).

$$E_{\theta\alpha\beta} = \sum_{m,n} \left[\frac{\cos \theta \sin \beta_n \cos(\phi - \gamma_m) - \cos \beta \sin \theta}{\sin \theta'} + \frac{\sin \beta_n \sin(\phi - \gamma_m)}{\sin \theta'} e^{\mp j \frac{\pi}{2}} \right] f(\theta', \phi') e^{j(kA \cos \theta' - \psi_{\beta_n \gamma_m})} \frac{e^{j(\omega t - kR_o)}}{R_o}, \quad (4.1.24)$$

$$E_{\phi\alpha\beta} = \sum_{m,n} \left[\frac{\sin \beta_n \sin(\phi - \gamma_m)}{\sin \theta'} - \frac{\cos \theta \sin \beta_n \cos(\phi - \gamma_m) - \cos \beta_n \sin \theta}{\sin \theta'} e^{\mp j \frac{\pi}{2}} \right] f(\theta', \phi') e^{j(kA \cos \theta' - \psi_{\beta_n \gamma_m})} \frac{e^{j(\omega t - kR_o)}}{R_o} \quad (4.1.25)$$

F. Special Cases

A few special cases were considered by [80] and will be repeated. When the geometry of each antenna is parallel to the z-axis (i.e. a vertical electric dipole located on the x-y plane) then (4.1.24) simplifies to (4.1.26).

$$\vec{E}_{\alpha\beta} = \sum_{m,n} \left[\hat{a}_\theta + \hat{a}_\phi e^{\mp j \frac{\pi}{2}} \right] f(\theta', \phi') e^{j(kA \cos \theta' - \psi_{\beta_n \gamma_m})} \frac{e^{j(\omega t - kR_o)}}{R_o}, \quad (4.1.26)$$

To show this simplification let $\beta = 0$ and $\theta = \theta'$. These conditions are substituted into the phi component of the electric field only; the theta component can be shown in a similar manner.

$$\begin{aligned} E_{\phi\alpha\beta} &= \sum_{m,n} \left[\frac{\sin \theta}{\sin \theta'} e^{\mp j \frac{\pi}{2}} \right] f(\theta', \phi') e^{j(kA \cos \theta' - \psi_{\beta_n \gamma_m})} \frac{e^{j(\omega t - kR_o)}}{R_o} \\ &= \sum_{m,n} \left[e^{\mp j \frac{\pi}{2}} \right] f(\theta', \phi') e^{j(kA \cos \theta' - \psi_{\beta_n \gamma_m})} \frac{e^{j(\omega t - kR_o)}}{R_o} \end{aligned} \quad (4.1.27)$$

Another special case can be shown when each element of the array is linearly polarized (i.e. radially directed dipoles) where the simplification $f_2(\theta', \phi') = 0$ is made. Thus, $f_1(\theta', \phi') = f_1(\theta')$ and the following expressions (4.1.28) and (4.1.29) are obtained for the field patterns:

$$E_{\theta\alpha\beta}(\theta, \phi) = -\frac{\cos\theta \sin\beta_n \cos(\phi - \gamma_m) - \cos\beta_n \sin\theta}{\sin\theta'} f_1(\theta') e^{j(kA \cos\theta' - \psi_{\beta_n \gamma_m})} \frac{e^{j(\omega t - kR_o)}}{R_o}, \quad (4.1.28)$$

$$E_{\phi\alpha\beta}(\theta, \phi) = \frac{\sin\beta_n \sin(\phi - \gamma_m)}{\sin\theta'} f_1(\theta') e^{j(kA \cos\theta' - \psi_{\beta_n \gamma_m})} \frac{e^{j(\omega t - kR_o)}}{R_o} \quad (4.1.29)$$

G. Far-Field Electric Field of Circularly Polarized Elements

It was previously shown that a far field field distribution at the point $P(r_o, \theta, \phi)$ is given by (4.1.30)

$$E_{\theta\alpha\beta} = \sum_{n,m} E_{nm}(\theta', \phi') e^{j(kA \cos\theta' - \psi_{nm})} \frac{e^{j(\omega t - kR_o)}}{R_o} \quad (4.1.30)$$

where

$$E_{nm}(\theta', \phi') = \hat{a}_{\theta'} f_1(\theta', \phi') + \hat{a}_{\phi'} f_2(\theta', \phi') e^{-j\delta} \quad (4.1.31)$$

Now under the judicious notion each individual element pattern is circularly polarized; one can assume an element pattern to be given by that of (4.1.32) where $\delta = \frac{\pi}{2}$

$$f_1(\theta', \phi') = f_2(\theta', \phi') = \cos\theta' e^{-j\phi'} \quad \text{for } -\frac{\pi}{2} \leq \theta' \leq \frac{\pi}{2} \quad (4.1.32)$$

The limitation of θ' between $-\pi/2 \leq \theta' \leq \pi/2$ means the individual pattern is considered a unidirectional cosine type with a given maximum at broadside. Thus,

$$E_{nm}(\theta', \phi') = (\hat{a}_{\theta'} - j\hat{a}_{\phi'}) \cos\theta' e^{-j\phi'} \quad (4.1.33)$$

(4.1.33) can also be expressed in more useful terms (θ, ϕ) in (4.1.34) and (4.1.35).

$$E_{\theta} = \left(\begin{array}{l} \hat{a}_{\theta} \left[-\frac{\cos\theta \sin\beta \cos(\phi - \gamma) - \cos\beta \sin\theta}{\sin\theta'} + j \frac{\sin\beta \sin(\phi - \gamma)}{\sin\theta'} \right] + \\ \hat{a}_{\phi} \left[\frac{\sin\beta \sin(\phi - \gamma)}{\sin\theta'} + j \frac{\cos\theta \sin\beta \cos(\phi - \gamma) - \cos\beta \sin\theta}{\sin\theta'} \right] \end{array} \right) \cos\theta' e^{-j\phi'} \quad (4.1.34)$$

$$E_\phi = \left(\begin{array}{c} \hat{a}_\theta \left[-\frac{\cos \theta \sin \beta \cos(\phi - \gamma) - \cos \beta \sin \theta}{\sin \theta'} + j \frac{\sin \beta \sin(\phi - \gamma)}{\sin \theta'} \right] + \\ -j \hat{a}_\phi \left[\frac{j \sin \beta \sin(\phi - \gamma)}{\sin \theta'} - \frac{\cos \theta \sin \beta \cos(\phi - \gamma) - \cos \beta \sin \theta}{\sin \theta'} \right] \end{array} \right) \cos \theta' e^{-j\phi'} \quad (4.1.35)$$

The phase of the unit vector a_θ is

$$-\tan(\nu_{\theta nm}) = \left(\frac{\frac{\sin \beta \sin(\phi - \gamma)}{\sin \theta'}}{\frac{\cos \theta \sin \beta \cos(\phi - \gamma) - \cos \beta \sin \theta}{\sin \theta'}} \right) = \frac{\sin \beta \sin(\phi - \gamma)}{\cos \theta \sin \beta \cos(\phi - \gamma) - \cos \beta \sin \theta} \quad (4.1.36)$$

Similarly a_ϕ is

$$-\tan(\nu_{\phi nm}) = \frac{\sin \beta \sin(\phi - \gamma)}{\cos \theta \sin \beta \cos(\phi - \gamma) - \cos \beta \sin \theta} \quad (4.1.37)$$

And it is observed that

$$-\tan(\nu_{\theta nm}) = -\tan(\nu_{\phi nm}) \equiv -\tan(\nu_{nm}) \quad (4.1.38)$$

Thus, substituting (4.1.38) into (4.1.34) one obtains (4.1.39),

$$E_\theta = (\hat{a}_\theta - j \hat{a}_\phi) \cos \theta' e^{-j(\phi' + \nu_{nm})} = -(\hat{a}_\theta - j \hat{a}_\phi) \cos \theta' e^{-j(\phi' + \nu_{nm})} \quad (4.1.39)$$

To show the expression right hand side of (4.1.39) holds let,

$$N = \frac{\cos \theta \sin \beta \cos(\phi - \gamma) - \cos \beta \sin \theta}{\sin \theta'},$$

$$D = \frac{\sin \beta \sin(\phi - \gamma)}{\sin \theta'}$$

Then

$$E_\theta = \left(\begin{array}{c} \hat{a}_\theta [-N + jD] + \\ -j \hat{a}_\phi [-N + jD] \end{array} \right) \cos \theta' e^{-j\phi'}$$

The phase term within brackets is seen to be $\tan^{-1} \frac{-D}{N}$, yet one can reorganize the field such that

$$E_\theta = - \left(\begin{array}{c} \hat{a}_\theta [N - jD]^+ \\ -j \hat{a}_\phi [N - jD] \end{array} \right) \cos \theta' e^{-j\phi'}$$

Remarkably, the phase within brackets still yields $\tan^{-1} \frac{-D}{N}$.

More simplification can be made to the field components by collecting phase terms which leads to a more compact expression. To do this one defines the angle $\xi_{nm} \triangleq \phi' + \nu_{nm}$ where ϕ' and ν_{nm} are given by (4.1.40), (4.1.41) and by applying the identity (C.1.5), one arrives at the expression given by (4.1.42)

$$\nu_{nm} = \text{arc tan} \left(\frac{-\sin \beta \sin(\phi - \gamma)}{\cos \theta \sin \beta \cos(\phi - \gamma) - \cos \beta \sin \theta} \right) \quad (4.1.40)$$

$$\phi' = \text{arctan} \left(\frac{\sin \theta \sin(\phi - \gamma)}{\cos \beta \sin \theta \cos(\phi - \gamma) - \sin \beta \cos \theta} \right) \quad (4.1.41)$$

$$\tan(\xi_{nm}) = \frac{\left[\sin(\phi - \gamma) \left(-\sin \beta (\cos \beta \sin \theta \cos(\phi - \gamma) - \sin \beta \cos \theta) + \sin \theta (\cos \theta \sin \beta \cos(\phi - \gamma) - \cos \beta \sin \theta) \right) \right]}{\left[(\cos \theta \sin \beta \cos(\phi - \gamma) - \cos \beta \sin \theta) (\cos \beta \sin \theta \cos(\phi - \gamma) - \sin \beta \cos \theta) \right] + \left[\sin \beta \sin^2(\phi - \gamma) \sin \theta \right]} \quad (4.1.42)$$

The electric field takes the form of (4.1.42) where $F(\theta, \phi)$ is the array factor defined in (4.1.43). To steer the beam with maximum radiation intensity in the direction θ_o, ϕ_o the phase excitation η_{nm} is introduced to (4.1.44) and defined in (4.1.45).

$$\vec{E}_{\alpha\beta}(\theta, \phi) = -(\hat{a}_\theta - j \hat{a}_\phi) F(\theta, \phi) \frac{e^{j(\omega t - kR_o)}}{R_o} \quad (4.1.43)$$

$$F(\theta, \phi) = \sum_{n,m} \cos \theta' e^{j(kA \cos \theta' - \psi_{nm})} e^{-j(\xi_{nm} - \eta_{nm})} \quad (4.1.44)$$

$$\eta_{nm} = \tan^{-1} \left(\frac{\left[\sin(\phi_o - \gamma) \left(\begin{array}{c} -\sin \beta (\cos \beta \sin \theta_o \cos(\phi_o - \gamma) - \sin \beta \cos \theta_o) \\ + \sin \theta_o (\cos \theta_o \sin \beta \cos(\phi_o - \gamma) - \cos \beta \sin \theta_o) \end{array} \right) \right]}{\left[\begin{array}{c} (\cos \theta_o \sin \beta \cos(\phi_o - \gamma) - \cos \beta \sin \theta_o) \\ (\cos \beta \sin \theta_o \cos(\phi_o - \gamma) - \sin \beta \cos \theta_o) \end{array} \right]} + \left[\begin{array}{c} \sin \beta \sin(\phi_o - \gamma) \\ \sin \theta_o \sin(\phi_o - \gamma) \end{array} \right] \right) \quad (4.1.45)$$

H. Element Placement

It is important for a spherical array to maintain a constant far field pattern in the course of scanning. Therefore, some sort of element distribution must be distributed across the spherical array to achieve this. Thus, as described from [80] it was found through a study of polygons the element placement is favorable at the points of icosahedrons Fig. 42. The antenna elements are to be placed equidistantly on the surface of the icosahedron and when circumscribing a sphere about the icosahedron and all elements one obtains a favorable periodic spherical array. On the contrary, the relocation of elements from the icosahedron to the spherical surface will causes symmetry to be lost, but favorable for applications of which a constant pattern must be achieved while scanning.



Fig. 42. Geometry of an icosahedron.

Studies have been done in order to determine the best placement of elements for a spherical array and it was determined from the studies of polyhedron that geometry of

an icosahedron will give desirable results. With this geometry the element placement should be followed in accord to (4.1.46) (4.1.47) where n is an integer with range [6 , 6] and m is an integer [0 , 25]. Special conditions also must be met in terms of the element placement and are given in (4.1.48) and(4.1.49). Lastly, Table 3 provides a partial analysis in terms of the element placement for positive values of n.

$$\gamma_m = 90^\circ - n15^\circ \tag{4.1.46}$$

$$\beta_{nm} = \frac{72^\circ m}{6 - |n|} \tag{4.1.47}$$

$$\beta_{0m} = \beta_{1m} \quad \text{if } n=0 \tag{4.1.48}$$

$$\beta_{6m} = 0^\circ \quad \text{if } |n|=6. \tag{4.1.49}$$

Table 3. Element placement

$N=0(\gamma, \beta)$	$N=1(\gamma, \beta)$	$N=2(\gamma, \beta)$	$N=3(\gamma, \beta)$
$(90^\circ), \left(\begin{array}{l} 14.4^\circ, 28.8^\circ, 43.2^\circ, \\ 57.6^\circ, 72.0^\circ, 86.4^\circ, \\ 100.8^\circ, 115.2^\circ, 129.6^\circ, \\ 144.0^\circ, 158.4^\circ, 172.8^\circ, \\ 187.2^\circ, 201.6^\circ, 230.4^\circ, \\ 244.8^\circ, 259.2^\circ, 273.6^\circ, \\ 288.0^\circ, 302.4^\circ, 316.8^\circ, \\ 331.2^\circ, 345.6^\circ, 360.0^\circ \end{array} \right)$	$(75^\circ), \left(\begin{array}{l} 14.4^\circ, 28.8^\circ, 43.2^\circ, \\ 57.6^\circ, 72.0^\circ, 86.4^\circ, \\ 100.8^\circ, 115.2^\circ, 129.6^\circ, \\ 144.0^\circ, 158.4^\circ, 172.8^\circ, \\ 187.2^\circ, 201.6^\circ, 230.4^\circ, \\ 244.8^\circ, 259.2^\circ, 273.6^\circ, \\ 288.0^\circ, 302.4^\circ, 316.8^\circ, \\ 331.2^\circ, 345.6^\circ, 360.0^\circ \end{array} \right)$	$(60^\circ), \left(\begin{array}{l} 18^\circ, 36^\circ, 54^\circ, \\ 72^\circ, 90^\circ, 108^\circ, \\ 126^\circ, 144^\circ, 162^\circ, \\ 180^\circ, 198^\circ, 216^\circ, \\ 234^\circ, 252^\circ, 270^\circ, \\ 288^\circ, 306^\circ, 324^\circ, \\ 342^\circ, 360^\circ \end{array} \right)$	$(45^\circ), \left(\begin{array}{l} 24^\circ, 48^\circ, 72^\circ, \\ 96^\circ, 120^\circ, 144^\circ, \\ 168^\circ, 192^\circ, 216^\circ, \\ 240^\circ, 264^\circ, 288^\circ, \\ 312^\circ, 336^\circ, 360^\circ \end{array} \right)$
$N=4(\gamma, \beta)$	$N=5(\gamma, \beta)$	$N=6(\gamma, \beta)$	
$(30^\circ), \left(\begin{array}{l} 36^\circ, 72^\circ, 108^\circ, \\ 144^\circ, 180^\circ, 216^\circ, \\ 252^\circ, 288^\circ, 324^\circ, \\ 360^\circ \end{array} \right)$	$(15^\circ), \left(\begin{array}{l} 72^\circ, 144^\circ, 216^\circ, \\ 288^\circ, 360^\circ \end{array} \right)$	$(0^\circ), (0^\circ)$	

Given the constraints of element placement (4.1.46)-(4.1.49) the array factor assumes its final form given in (4.1.50). The array is limited to have an overall maximum of 177 elements on the spherical surface with the element placement conditions.

$$F(\theta, \phi) = \sum_{n=-6}^6 \sum_{m=0}^{M(n)} \cos \theta' e^{j[ka(\cos \theta' - \psi_{nm}) - (\xi_{nm} - \eta_{nm})]} \quad (4.1.50)$$

$$\sum_{n=-6}^6 \sum_{m=0}^{M(n)} e^{j[ka(\cos \theta' - \psi_{nm})]}$$

The element placement used in (4.1.50) is not the only type of placement that can be used to model a periodic spherical array. Other types of placements can be found in [82]-[85].

I. Radiation Pattern of a Spherical Array with Element Placement Based Upon Icosahedron Geometry

The radiation pattern of a spherical array is plotted in Fig. 43 and Fig. 44 for two different element spacings. The geometry of the element spacing is shown in Fig. 45.

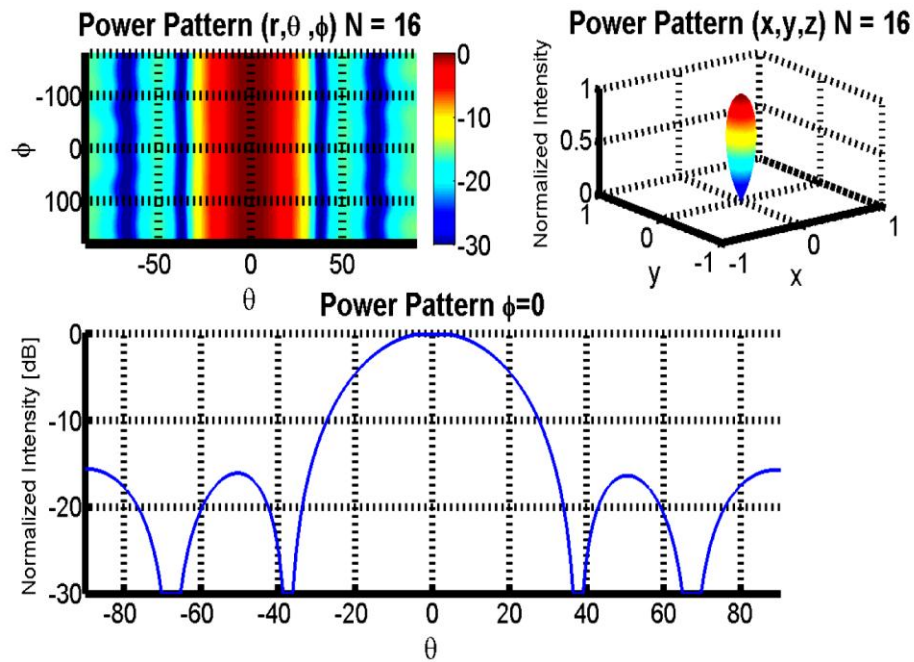


Fig. 43. Average radiation pattern of 177 elements periodically spaced about a spherical radius of $.625 \lambda$.

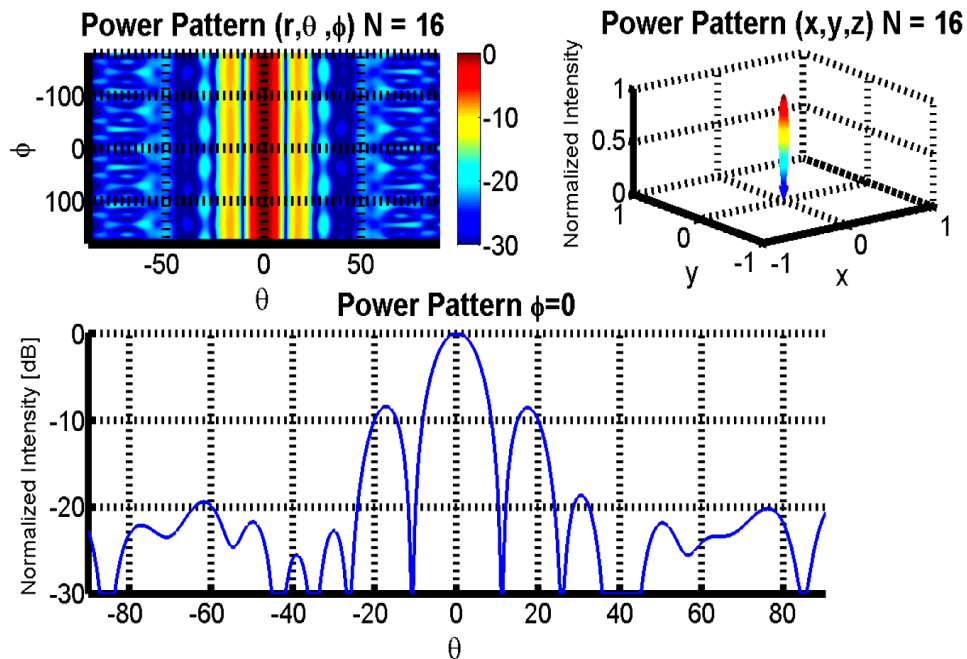


Fig. 44. Average radiation pattern of 177 elements periodically spaced about a spherical radius of 2λ .

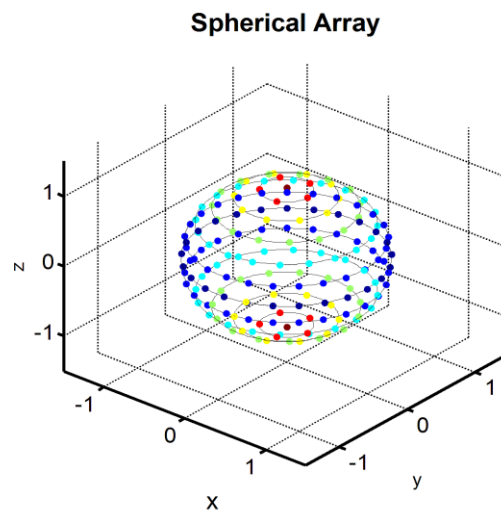


Fig. 45. 177 elements periodically spaced in a spherical geometry based upon icosahedron geometry.

6.2 Aperiodic

A. System Development and Beampattern Definition

Up to this point numerous random array geometries have been covered, however the more interesting type of random array is a 3 dimensional volumetric type. For example, a volumetric random array could model a distribution of aircraft flying freely as shown in Figure 46. Moreover, a possible way of characterizing this random distribution could be to circumscribe all the aircraft to a sphere of radius A as shown in Figure 47.

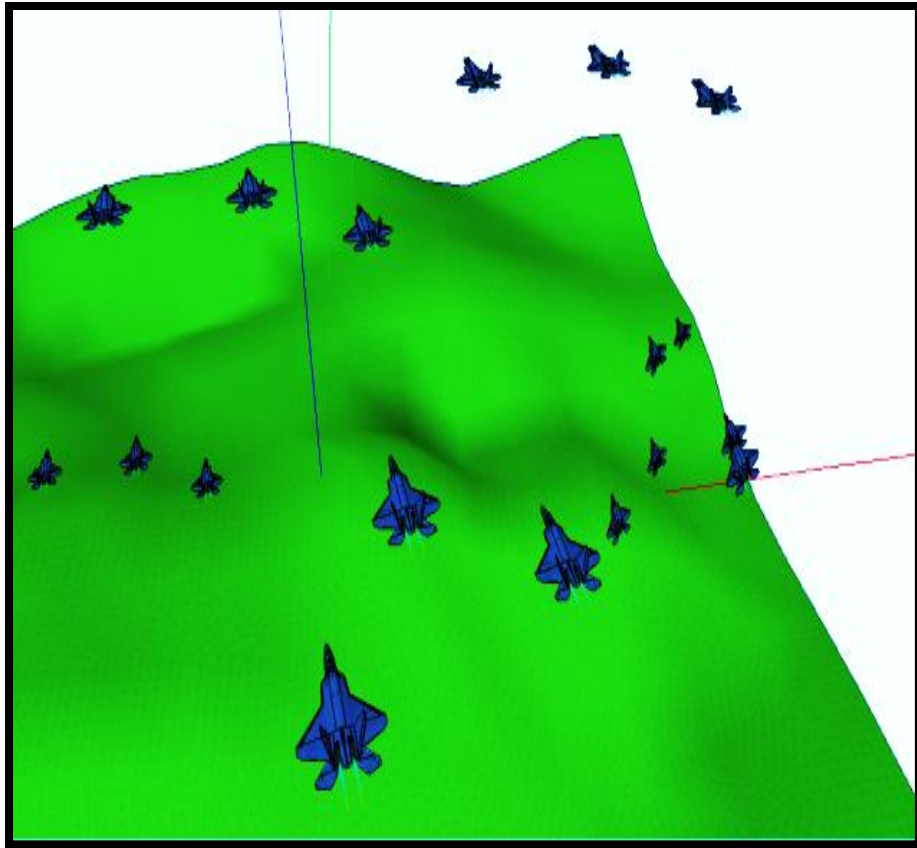


Fig. 46. Distribution of aircraft randomly distributed in three dimensional space.

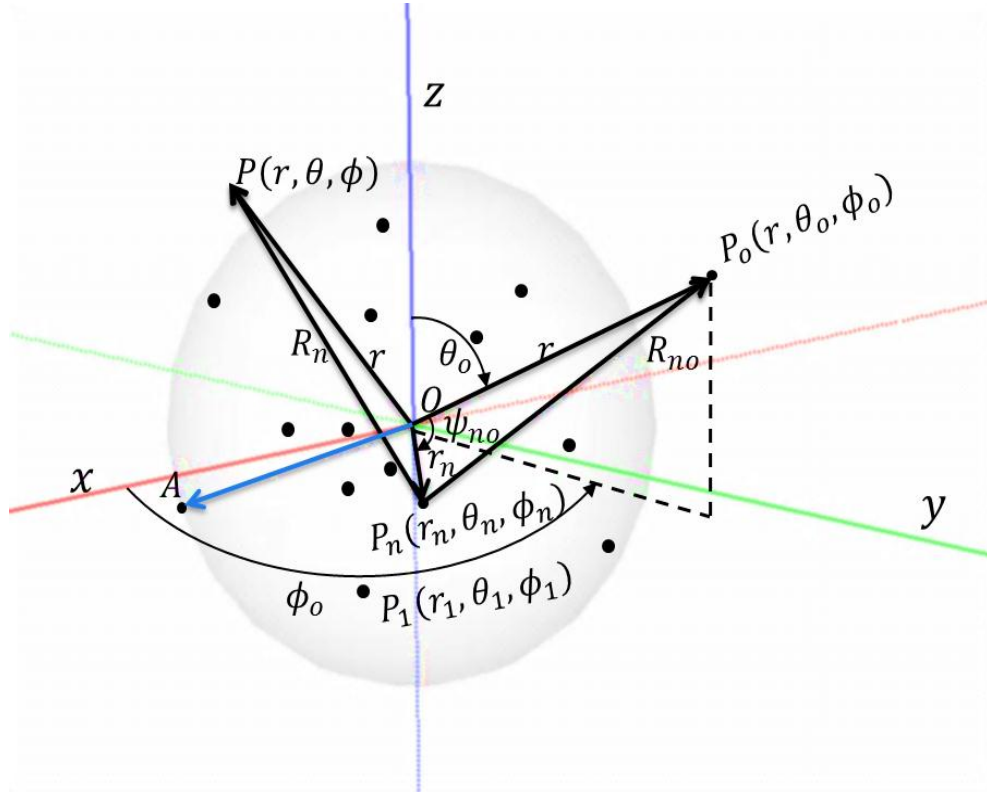


Fig. 47. Geometry of an N-element random spherical array.

The array factor of a spherical array for a distribution of isotropic elements is given in (4.1.51) and simplified to a more convenient form in (4.1.52) with spatial parameters defined in (4.1.53)-(4.1.56). Moreover a derivation going from (4.1.51) to (4.1.52) can be found in a similar manner used in section 5.1.

$$F(\theta, \phi | \vec{r}_n, \vec{\theta}_n, \vec{\phi}_n) = \sum_{n=1}^N e^{jk r_n (\sin \theta_n \sin \theta \cos(\phi_n - \phi) + \cos \theta_n \cos \theta - \sin \theta_n \sin \theta_o \cos(\phi_n - \phi_o) + \cos \theta_n \cos \theta_o)} \quad (4.1.51)$$

$$F(\theta, \phi | \vec{r}_n, \vec{\theta}_n, \vec{\phi}_n) = \sum_{n=1}^N e^{jk r_n (\rho_o \sin \theta_n \cos(\phi_n - \delta) + \cos \theta_n (\cos \theta - \cos \theta_o))} \quad (4.1.52)$$

$$\rho_o = \sqrt{(\sin \theta_o \cos \phi_o - \sin \theta \cos \phi)^2 + (\sin \theta_o \sin \phi_o - \sin \theta \sin \phi)^2} \quad (4.1.53)$$

$$\cos(\delta) = \frac{(\sin \theta_o \cos \phi_o - \sin \theta \cos \phi)}{\sqrt{(\sin \theta_o \cos \phi_o - \sin \theta \cos \phi)^2 + (\sin \theta_o \sin \phi_o - \sin \theta \sin \phi)^2}} \quad (4.1.54)$$

$$\begin{aligned}\sin(\delta) &= \sqrt{1 - \cos^2(\delta)} \\ &= \frac{(\sin \theta_o \sin \phi_o - \sin \theta \sin \phi)}{\sqrt{(\sin \theta_o \cos \phi_o - \sin \theta \cos \phi)^2 + (\sin \theta_o \sin \phi_o - \sin \theta \sin \phi)^2}}\end{aligned}\quad (4.1.55)$$

$$\delta = \tan^{-1} \left[\frac{\sin \theta \sin \phi - \sin \theta_o \sin \phi_o}{\sin \theta \cos \phi - \sin \theta_o \cos \phi_o} \right], \quad (4.1.56)$$

Since the angle δ is nothing more than a constant offset, the location angles θ_n, ϕ_n are considered uniform random variables such that $\phi_n \triangleq \phi_n - \delta, \theta_n \triangleq \theta_n$.

The final form of the array factor (6.2.7) is written using compound random variables defined as $T_n = \tilde{r}_n \cos \theta_n, -1 \leq \overline{T}_n \leq 1$ and $Y_n = \tilde{r}_n \sin \theta_n \cos(\phi_n - \delta), -1 \leq \overline{Y}_n \leq 1$. In addition, the spatial parameters $\zeta(\theta, \phi)$ and $\xi(\theta)$ are used providing a more compact expression.

$$F(\theta, \phi | \overline{Y}, \overline{T}) = \sum_{n=1}^N e^{j2\pi A(\rho_o Y_n + T_n(\cos \theta - \cos \theta_o))} = \sum_{n=1}^N e^{j\zeta(\theta, \phi)(Y_n)} e^{j\xi(\theta)(T_n)} \quad (4.1.57)$$

The P.D.F.s of ϕ_n and T_n will be the same as those given in (3.1.22) and (3.1.24). Likewise the P.D.F.s of r_n, θ_n and Y_n can be shown in a similar fashion given in (4.1.58)-(4.1.60).

$$\int_0^R f_{r_n}(r) r^2 dr = 1 \rightarrow f_{r_n}(r) = \frac{3}{R^3} \text{ for } 0 \leq r \leq R \quad (4.1.58)$$

$$\int_0^\pi f_{\theta_n}(\theta) \sin \theta d\theta = 1 \quad f_{\theta_n}(\theta) = \frac{1}{2} \text{ for } 0 \leq \theta \leq \pi \quad (4.1.59)$$

$$\begin{aligned}
& \int_0^1 \int_0^{2\pi} \int_0^\pi f_{Y_n, T_n, w}(Y, T, w) r^2 dr \sin \theta d\theta d\phi = 1 \\
& f_{Y_n, T_n, w}(Y, T_n, w) = \frac{3}{4\pi} \\
& f_{Y_n, T_n}(Y, T_n) = \int_{-\sqrt{1-Y^2-T^2}}^{\sqrt{1-Y^2-T^2}} f_{Y_n, v, w}(Y, T_n, w) dw = \frac{3}{4\pi} \int_{-\sqrt{1-T^2-Y^2}}^{\sqrt{1-T^2-Y^2}} dw \\
& f_{Y_n}(Y) = \frac{3}{4\pi} \int_{-\sqrt{1-Y^2}}^{\sqrt{1-Y^2}} 2\sqrt{1-Y^2-T^2} dT = \frac{3}{4\pi} \pi(1-Y^2) = \frac{3(1-Y^2)}{4} \quad (4.1.60) \\
& -1 \leq \bar{Y} \leq 1
\end{aligned}$$

A coordinate transformation converting spherical to Cartesian coordinates was used to simplify the integration such that $Y = r \sin \theta \cos \phi$, $T = r \cos \theta$ and $w = r \sin \theta \sin \phi$.

The far-field radiation intensity of (0.2.15) is now defined as (4.1.61) with spatial parameters $\zeta(\theta, \phi)$ given by (3.1.27) and $\xi(\theta)$ by (4.1.62).

$$U(\theta, \phi | \bar{Y}, \bar{T}) = \frac{1}{N} + \frac{1}{N^2} \sum_{m=1}^N \sum_{\substack{n=1 \\ n \neq m}}^N e^{j\zeta(\theta, \phi)(Y_n - Y_m)} e^{j\xi(\theta)(T_n - T_m)} \quad (4.1.61)$$

$$\xi(\theta) \triangleq 2\pi A(\cos \theta - \cos \theta_o) \quad (4.1.62)$$

Also for comparison purposes [9] the arrays beampattern will be observed at the meridian angle $\theta = \theta_o = \pi/2$, and compared to that of the circular random array. At this particular elevation angle the analysis is simplified in the same manner used in section 5.1 to give the array factor (4.1.63) and radiation intensity(4.1.64). The terms (4.1.63) and (3.1.30) both contain the same spatial parameter at the meridian angle, yet are embedded with different types of random variable. The random variables v_n serves as a compound random variable in polar coordinates whereas Y_n serves as a compound random variable in spherical coordinates.

$$F(\phi|\bar{\Upsilon}) = \frac{1}{N} \sum_{n=1}^N e^{-j\zeta(\phi)\Upsilon_n} \quad (4.1.63)$$

$$U(\phi|\bar{\Upsilon}) = \frac{1}{N} + \frac{1}{N^2} \sum_{n=1}^N \sum_{\substack{m=1 \\ n \neq m}}^N e^{j\zeta(\phi)(\Upsilon_n - \Upsilon_m)} \quad (4.1.64)$$

B. Average Properties of a Uniformly Distributed Spherical Antenna Array with Perfect Phase Information

1. Average Beampattern

When the definition of expectation (0.2.19) is applied to (4.1.57) the average radiation intensity can be rewritten as (4.1.65)

$$U_{av}(\theta, \phi) = E_{\Upsilon_n, \Upsilon_m} \left| U(\theta, \phi|\bar{\Upsilon}, \bar{\Upsilon}) \right| \\ = \int_{-1}^1 \int_{-1}^1 \int_{-1}^1 \int_{-1}^1 \left(\frac{1}{N} + \frac{1}{N^2} \sum_{\substack{n=1 \\ n \neq m}}^N \sum_{\substack{m=1 \\ n \neq m}}^N e^{j\zeta(\theta, \phi)(\Upsilon_n - \Upsilon_m)} e^{j\xi(\theta)(\Upsilon_n - \Upsilon_m)} \frac{3}{4}(1 - \Upsilon_n^2) \frac{3}{4}(1 - \Upsilon_m^2) d\Upsilon_n d\Upsilon_m \right) \\ \left(\frac{2}{\pi} \sqrt{1 - \Upsilon_n^2} \frac{2}{\pi} \sqrt{1 - \Upsilon_m^2} d\Upsilon_n d\Upsilon_m \right) \quad (4.1.65)$$

The average of the first term is once again $\frac{1}{N}$ like in the previous chapters of planar geometry. In addition, the double summation term reduces to an analytic form in the same manner as the previous sections giving (4.1.66). Finally the solution of the integrals and (A.1.25) together yield the average radiation intensity given by (4.1.67).

$$E_{\Upsilon_n, \Upsilon_m} \left| \left(\theta, \phi|\bar{\Upsilon}, \bar{\Upsilon} \right) \right| = \frac{1}{N} + \frac{9}{4\pi^2} \int_{-1}^1 \int_{-1}^1 \int_{-1}^1 \int_{-1}^1 \left(\left(1 - \frac{1}{N} \right) \cos \left(\zeta(\theta, \phi)(\Upsilon_n - \Upsilon_m) + \xi(\theta)(\Upsilon_n - \Upsilon_m) \right) (1 - \Upsilon_n^2) d\Upsilon_n \right) \\ \left((1 - \Upsilon_m^2) d\Upsilon_m \sqrt{1 - \Upsilon_n^2} \sqrt{1 - \Upsilon_m^2} d\Upsilon_n d\Upsilon_m \right) \quad (4.1.66)$$

$$E_{\Upsilon_n, \Upsilon_m} \left| \left(\theta, \phi|\bar{\Upsilon}, \bar{\Upsilon} \right) \right| = \frac{1}{N} + \left(1 - \frac{1}{N} \right) \left| 3\text{tinc}(\zeta(\theta, \phi)) \right|^2 \left| 2\text{jinc}(\xi(\theta)) \right|^2 \quad (4.1.67)$$

The solution to the average radiation intensity (4.1.67) of a spherical random array is similar to that of a circular array with the exception a sinc function $3\text{sinc}(\zeta(\theta, \phi))$ has been multiplied by the familiar jinc function with an alternative spatial parameter $\xi(\theta)$ or $\text{jinc}(2\xi(\theta))$. This means the spherical array is collected with circular symmetry in the elevation angle or surface area and coupled with spherical symmetry or volume elsewhere. Moreover, the second term now represents the mainlobe factor characterized by two independent oscillatory functions, comprised of sinc and jinc functions and causes the beam to rapidly attenuate as either spatial parameter $\zeta(\theta, \phi)$ or $\xi(\theta)$ increase.

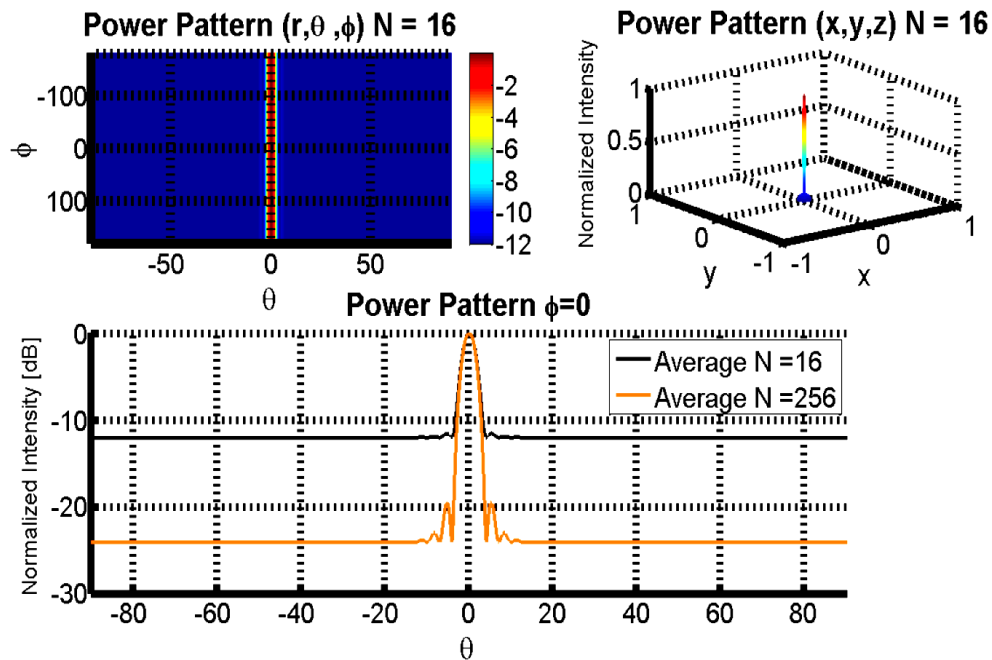


Fig. 48. Average radiation pattern of 16 and 256 elements randomly spaced (Uniformly) within a spherical aperture of 10λ .

C. Average Beampattern Simplification with $\theta = \theta_o = \pi/2$

1. Average Beampattern

At the meridian angle the radiation pattern can be shown to be (4.1.68) and the result matches closely once again to the circular random array solution (3.1.44). The mainlobe is represented by a jinc function for the circular array and a tinc function for the spherical array. The spatial parameter $\zeta(\phi)$ or argument of the oscillatory functions is identical for both types of arrays.

$$E_r |U(\phi|\bar{Y})| = \frac{1}{N} + \left(1 - \frac{1}{N}\right) |3\text{tinc}(\zeta(\phi))|^2 \quad (4.1.68)$$

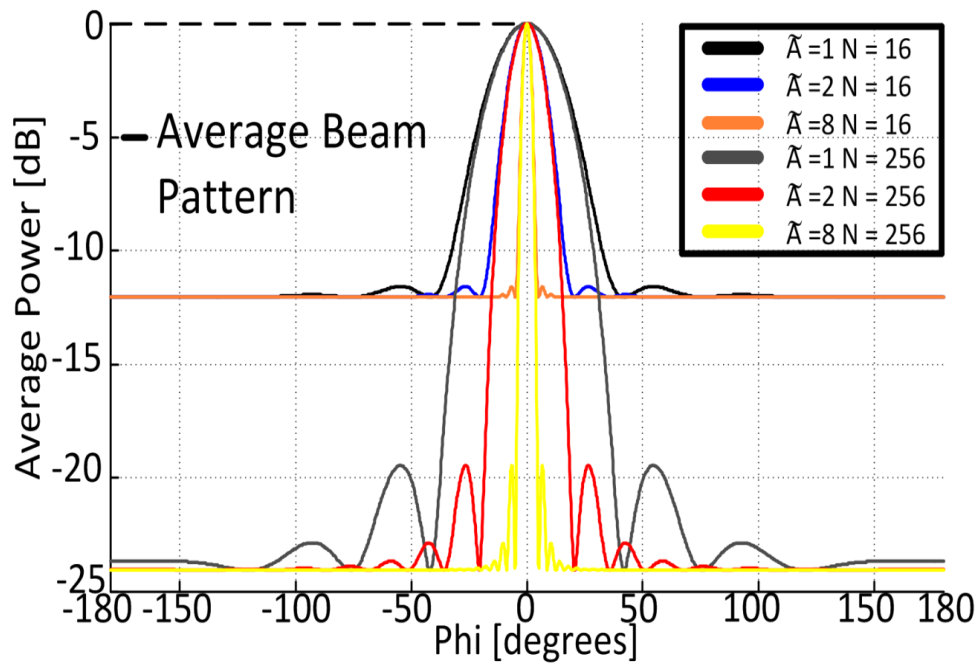


Fig. 49. Average radiation pattern of 16 elements randomly spaced (uniformly) within a spherical aperture of 10λ with $\theta = \theta_o = \pi/2$.

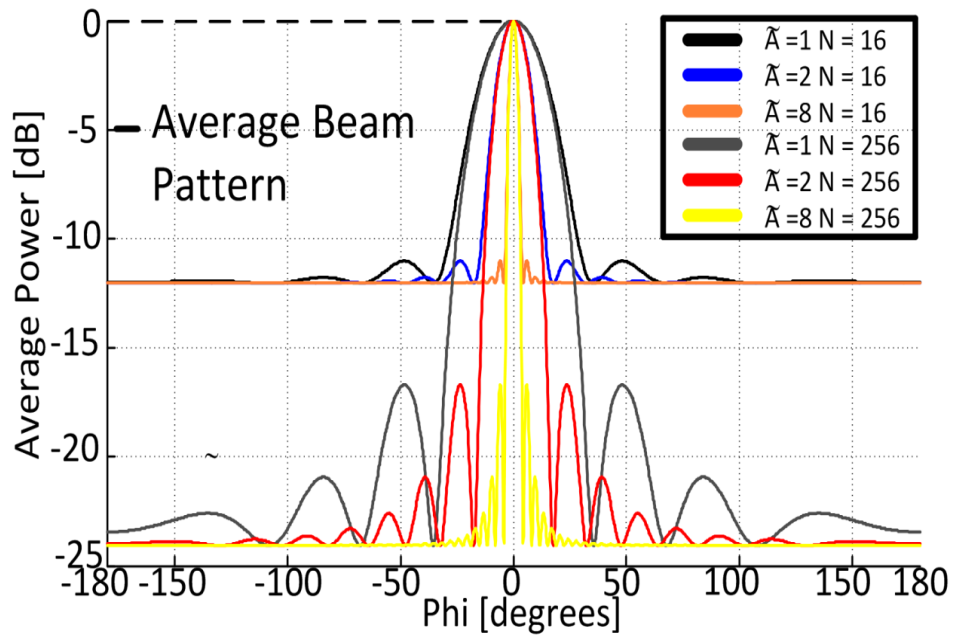


Fig. 50. Average radiation pattern of 16 elements randomly spaced (uniformly) within a circular aperture of 10λ with $\theta = \theta_o = \pi/2$.

The average power pattern for a spherical random array Figure 49 compared to the average of a two dimensional circular random array Figure 50 [1] is seen to have significantly lower sidelobes. This makes sense as the size of the aperture A has increased and allows for the larger spread of the elements.

Furthermore, since the power pattern is conditioned on ϕ it is worth noting that the pattern [1] is an average of bounded independent and identically distributed (i.i.d.) complex random variables, and by the weak law of large numbers the power pattern converges to ensemble average in probability as $N \rightarrow \infty$.

2. Average Peak and Null Locations of the Sidelobes

The following sections 2-6 can be derived in the same manner used to give the results given in the circular array Subheading 5.2.C.(2-6). For that reason, the analysis will be skipped and only the final results will be shown.

The average peak and null expressions in terms of the azimuthal angle ϕ_n for the average far away beampattern (4.1.69) given are given in (4.1.73) and (4.1.74).

$$U_{av}^{FarAway}(\phi) = \frac{1}{N} + \left(1 - \frac{1}{N}\right) \frac{9}{\zeta(\phi)^4} \cos^2(\zeta(\phi)) \quad (4.1.69)$$

$$\zeta(\phi_q^{peak}) = q\pi \quad q = 2, 3, 4, \dots \quad (4.1.70)$$

$$\zeta(\phi_q^{peak}) = (q+1)\pi \quad q = 1, 2, 3, 4, \dots \quad (4.1.71)$$

$$\zeta(\phi_q^{null}) = \left(q + \frac{1}{2}\right)\pi \quad q = 1, 2, 3, \dots \quad (4.1.72)$$

$$\phi_q^{null} \sim 2 \arcsin\left(\frac{q + \frac{1}{2}}{4A}\right) \quad q = 1, 2, 3, \dots \quad (4.1.73)$$

$$\phi_q^{peak} \sim 2 \arcsin\left(\frac{q}{4\tilde{A}}\right) \quad q = 2, 3, 4, \dots \quad (4.1.74)$$

$$\phi_q^{peak} \sim 2 \arcsin\left(\frac{q+1}{4\tilde{A}}\right) \quad q = 1, 2, 3, \dots \quad (4.1.75)$$

Note the indices of (4.1.74) begin at 2 since a null (4.1.73) will follow a main beam preceded by a peak.

Observation of (4.1.73) and (4.1.74) show the peak sidelobe level is less sensitive to the value of N given in the average sidelobe level of the beampattern and more sensitive to the value of A . Thus, by increasing the value of A it is more likely that high

peaking sidelobes will be eliminated, leaving the majority of the sidelobe peaks concentrated relatively around the mainlobe.

3. Average Three-dB Beamwidth

The average 3dB beamwidth (4.1.76) for large N was solved by graphical means yielding a value of 1.815, similar to a result given by [59]. Moreover, substituting this result into $\zeta(\phi_{av}^{3dB})$ results with (4.1.77) ; for small arguments in the sin, term reduces to (4.1.78).

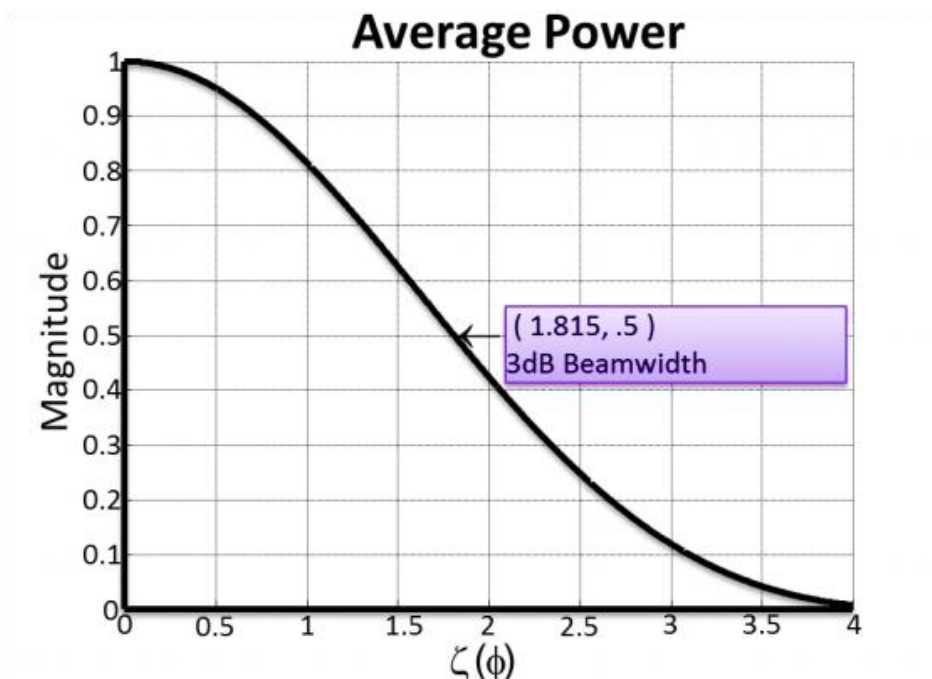


Fig. 51. Average 3dB beamwidth of a spherical random array.

$$U_{av}(\phi_{av}^{3dB}) = \left| 3 \frac{j_1(\zeta(\phi_{av}^{3dB}))}{\zeta(\phi_{av}^{3dB})} \right|^2 = \frac{1}{2} \quad (4.1.76)$$

$$\phi_{av}^{3dB} = 2 \arcsin\left(\frac{.1444}{A}\right) \quad (4.1.77)$$

$$\phi_{av}^{3dB} \approx \frac{.2888}{A} \quad (4.1.78)$$

The 3dB beamwidth angle of (4.1.78) like the circular random array is inversely proportional to the radius of the sphere and asymptotically independent of N. However, for a spherical random array typically one would assume the antennas are more mobile than that of a circular random array; since the narrowness of the beam is inversely proportional to the radius of the sphere one may need to account for a broader fluctuating beam.

4. Three-dB Sidelobe Region

The region for which the average of the sidelobe beampattern falls below 3dB in the range $S_{3dB} \triangleq \{\phi | \phi_{q_o}^{zero} \leq |\phi| \leq \pi\}$ is provided by (4.1.79).

$$\begin{aligned} \frac{U_{av}(\phi_{q_o}^{peak})}{\frac{1}{N}} &\sim 1 + (N-1) \left[\frac{9}{((q_o+1)\pi)^4} \right] \leq 10^{\frac{3}{10}} \leq 2 \\ &= \frac{(9(N-1))^{1/4}}{\pi} \quad -1 \leq q_o \end{aligned} \quad (4.1.79)$$

The angle $\phi_{q_o}^{zero}$ is located next to the peak sidelobe; an example of the 3dB sidelobe region is shown in Fig. 52 showing one case with all sidelobes within the 3dB sidelobe region versus an alternative case where not all sidelobes are within the 3dB sidelobe region.

Fig. 53 shows a comprehensive analysis of the 3dB sidelobe and 3dB beamwidth regions in a different perspective. The main observation to be made from the figure is that the 3dB sidelobe region will be reduced as N increases unless A is increased as well. It is also interesting to notice the 3dB sidelobe region is faintly affected by increasing the number of nodes for the spherical case in comparison to the circular array Fig. 54.

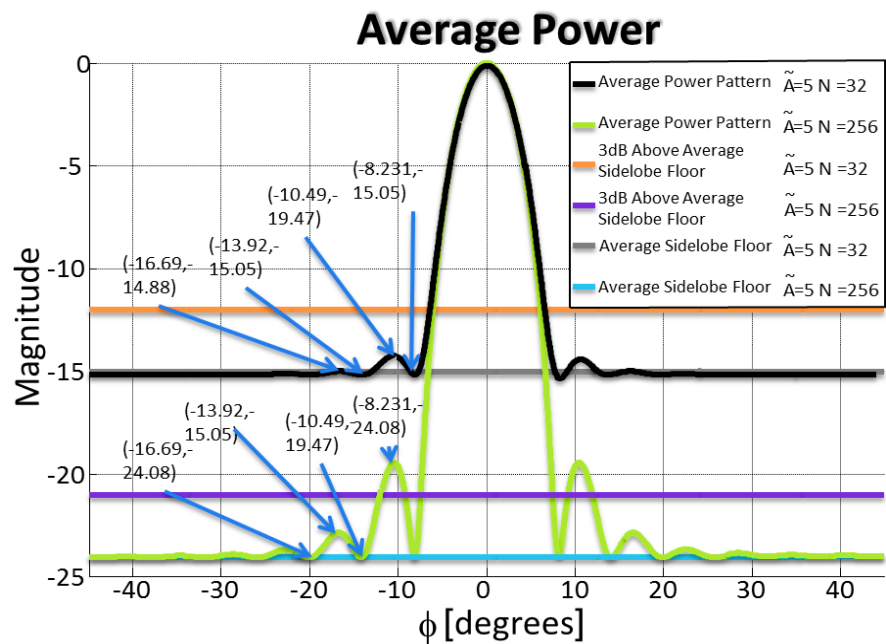


Fig. 52. 3 dB sidelobe region, and null and peak positions of a spherically bound random array.

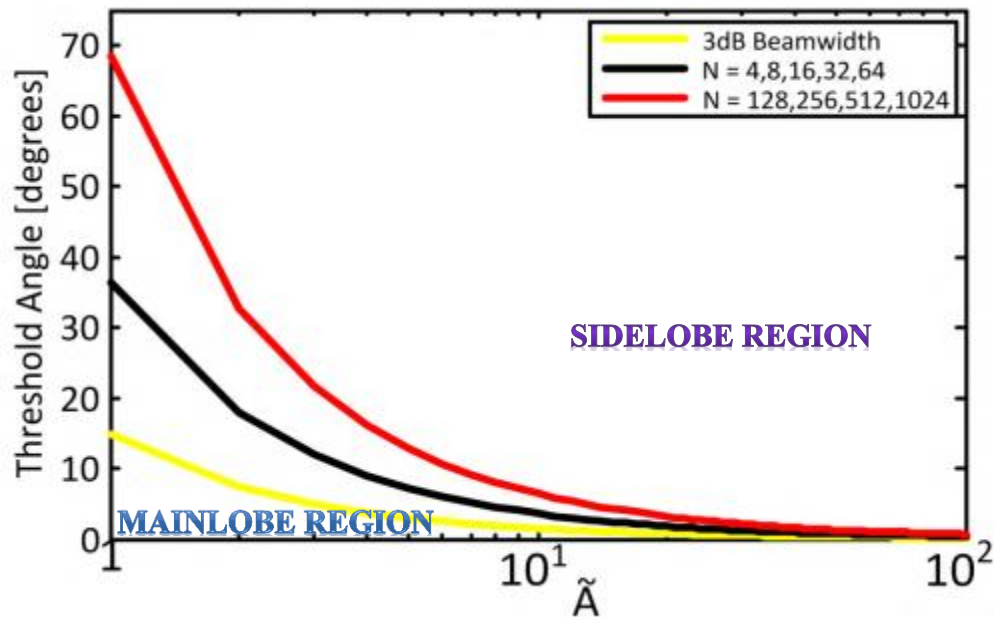


Fig. 53. Spherical random array threshold angle of the three Db beamwidth and three Db sidelobe region with respect to \tilde{A} and N.

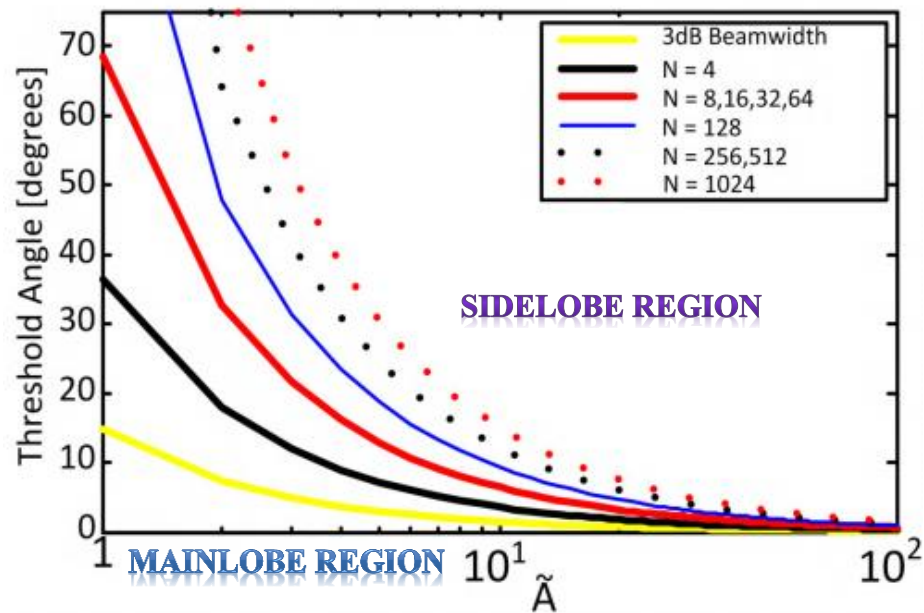


Fig. 54. Circular random array threshold angle of the three Db beamwidth and three Db sidelobe region with respect to \tilde{A} and N.

5. Average Directivity

The true directivity of a spherical array is given by the same expression given in (3.1.59) composed with the alternative random variable Υ shown in (4.1.80)

The average directivity (4.1.81) is found by extensive mathematical manipulation as it entails the integral of a sinc-squared function and is shown in (A.1.26). Hence, the average directivity is found in (4.1.81) where

$\left\{ {}_6F_2\left(\frac{1}{2}; 3, \frac{7}{2}; -(4\pi A)^2\right), {}_1F_2\left(\frac{1}{2}; 4, \frac{7}{2}; -(4\pi A)^2\right) \right\}$ are hypergeometric functions and converge to 0 as $A \rightarrow \infty$. It is likely the gain will be less than N , but approached when A is increased. This result coincides with a previous statement made in this paper; that the main beam come to be narrower with increasing A , and reinforces the result as to why the directivity increases. A comparison of the directivity for a circular and spherical random array is shown in Fig. 55

$$D(\Upsilon) \triangleq \frac{\int_{-\pi}^{\pi} U(0) d\phi}{\int_{-\pi}^{\pi} U(\phi) d\phi} = \frac{2\pi}{\frac{2\pi}{N} + \frac{2\pi}{N^2} \sum_{m=1}^N \sum_{\substack{n=1 \\ n \neq m}}^N J_0(4\pi A(\Upsilon_n - \Upsilon_m))} = \left[\frac{1}{N} + \frac{1}{N^2} \sum_{k=1}^N \sum_{\substack{l=1 \\ l \neq k}}^N J_0(4\pi A(\Upsilon_n - \Upsilon_m)) \right]^{-1} \quad (4.1.80)$$

$$\begin{aligned} \tilde{D}_{av} &\triangleq \frac{\int_{-\pi}^{\pi} U_{av}(0) d\phi}{\int_{-\pi}^{\pi} U_{av}(\phi) d\phi} = \frac{2\pi}{\frac{2\pi}{N} + \left(1 - \frac{1}{N}\right) \int_{-\pi}^{\pi} \left(3 \operatorname{tinc}\left(x \sin \frac{\phi}{2}\right)\right)^2 d\phi} \\ &= \frac{N}{1 + (N-1) \frac{2}{5} \left[\begin{array}{c} {}_6F_2\left(\frac{1}{2}; 3, \frac{7}{2}; -(4\pi A)^2\right) \\ - {}_1F_2\left(\frac{1}{2}; 4, \frac{7}{2}; -(4\pi A)^2\right) \end{array} \right]} \end{aligned} \quad (4.1.81)$$

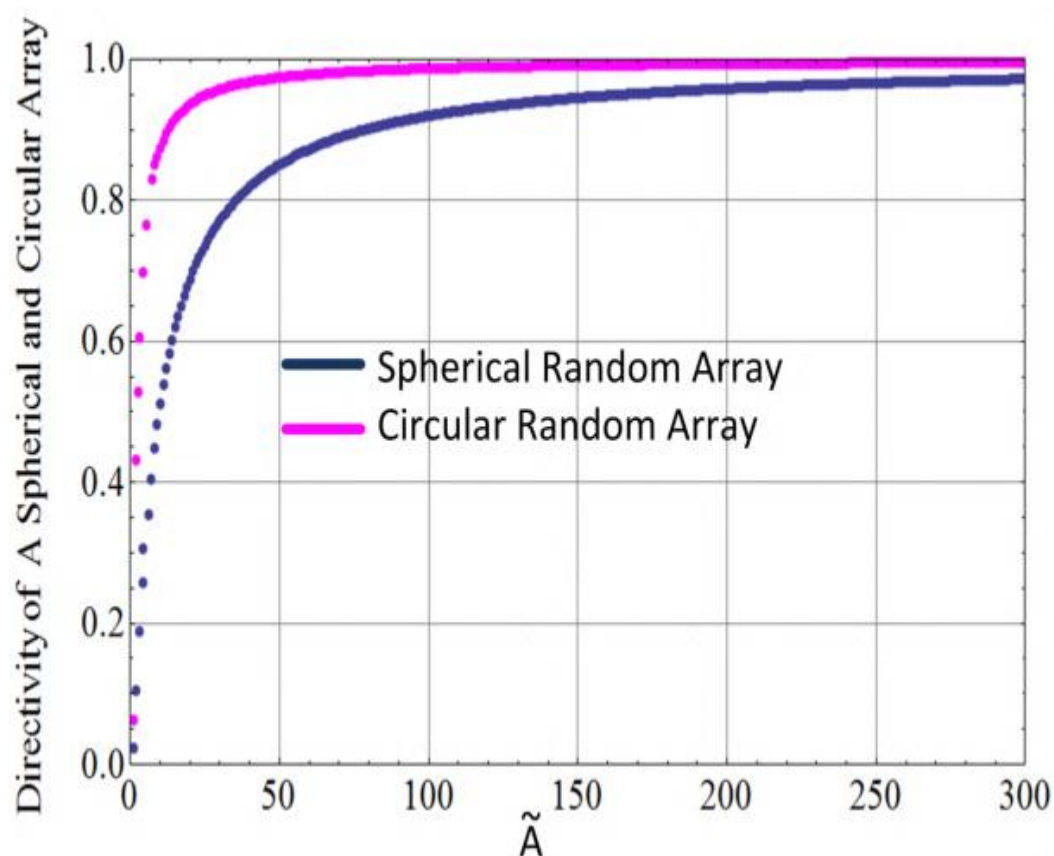


Fig. 55. Comparison of the average directivity of a random circular and spherical array for $N=16$.

The only downfall encountered thus far of the spherical random array is the elements need be sparser than a circular random array to approach an average directivity of magnitude N .

D. Average Statistical Properties of a Uniformly Distributed Spherical Antenna Array with Perfect Phase Information and Uniform Random Variable

1. Statistical Development

The exact complementary cumulative distribution function (CCDF) of the beam pattern level is given to be the same as (3.1.81) specified in section 5.2.D. In

addition, the array factor at a particular angle ϕ is given again to be that of (3.1.82) with an interchange of random variable $\nu \rightarrow \Upsilon$. The underlying difference from section 5.D exists in the fact that a compound random variable in spherical coordinates is used to calculate the statistical measures given in (4.1.82)-(4.1.87), differing from those in (3.1.83)-(3.1.88).

$$E[X(\phi|\bar{\Upsilon})] = \frac{3\sqrt{N}j_1(\zeta(\phi))}{\zeta(\phi)} \quad (4.1.82)$$

$$E[X^2(\phi|\bar{\Upsilon})] = \frac{1}{2} \left(1 + \frac{3}{2} \frac{j_1\zeta(\phi)}{\zeta(\phi)} \right) \quad (4.1.83)$$

$$E[Y^2(\phi|\bar{\Upsilon})] = \frac{1}{2} \left(1 - \frac{3}{2} \frac{j_1\zeta(\phi)}{\zeta(\phi)} \right) \quad (4.1.84)$$

$$E[Y(\phi|\bar{\Upsilon})] = 0 \quad (4.1.85)$$

$$\sigma_x^2 = \frac{1}{2} \left(1 + \frac{3}{2} \frac{j_1\zeta(\phi)}{\zeta(\phi)} \right) - \left(3 \frac{j_1\zeta(\phi)}{\zeta(\phi)} \right)^2 N \quad (4.1.86)$$

$$\sigma_y^2 = \frac{1}{2} \left(1 - \frac{3}{2} \frac{j_1\zeta(\phi)}{\zeta(\phi)} \right) - 0 \quad (4.1.87)$$

The variances σ_x^2 and σ_y^2 approach a value of .5 in the limiting case for a spherical array just as they did in the circular array. Hence, the beampattern level in the sidelobe region approaches a Nakagami distribution given by (3.1.93). Also, since the mean m_x of a spherical random array will approach zero in the sidelobe region one may once more assume the beampattern assumes Rayleigh distribution also previously given by (3.1.94).

2. Average Statistical Beampattern Analysis within the 3dB Sidelobe Region

The 3dB sidelobe region is defined to satisfy the condition (3.1.98) and can be rewritten as (4.1.88) by adding the variance of X and Y to the Average Power patterns. It follows that the 3dB sidelobe region, is bounded by unity when N is large (4.1.91). Thus, like the circular random array this means the mean does not grow unbounded with the number of nodes N.

$$\text{Var}(X) + \text{Var}(Y) + |E\{X\}|^2 \leq 2 \quad (4.1.88)$$

$$\frac{1}{2} \left(1 + \frac{3}{2} \frac{J_1(2\zeta(\phi))}{\zeta(\phi)} \right) - \left(3 \frac{J_1(\zeta(\phi))}{\zeta(\phi)} \right)^2 + \frac{1}{2} \left(1 - \frac{3}{2} \frac{J_1(2\zeta(\phi))}{\zeta(\phi)} \right) + N \left(3 \frac{J_1(\zeta(\phi))}{\zeta(\phi)} \right)^2 \quad (4.1.89)$$

$$1 - \frac{1}{N} |E\{X\}|^2 + |E\{X\}|^2 \leq 2 \quad (4.1.90)$$

$$|E\{X\}|^2 \leq \frac{1}{\left(1 - \frac{1}{N}\right)} \quad (4.1.91)$$

3. Statistical Analysis of the Maximum Sidelobe Peak

The average representation of the number of upward crossings at a given power level from the spherical random array can be set up in the same fashion as that in 5.2.3D.3.a. Moreover, under the assumption the process is wide-sense stationary (WSS) the autocorrelation function is given as (4.1.92). Moreover, the variance of X' is found by differentiating (4.1.92) with respect to Θ twice. Then setting $\Theta = 0$ followed by taking the statistical average with respect to Υ one obtains (4.1.93). Finally, the variance σ_x^2 is given as (4.1.94).

$$R_x(\Theta) = \frac{1}{2} E_r \left\{ \left(\cos(\Upsilon 4\pi \tilde{A} \Theta) \right) \right\} \quad (4.1.92)$$

$$\Theta = u_1 - u_2$$

$$\rho_x^*(\Theta = 0) = \frac{1}{2} E_r \left\{ -(\Upsilon 4\pi \tilde{A})^2 \right\} = 8\pi^2 \tilde{A}^2 \left(-\frac{1}{4} \right) = -\frac{8}{5} \pi^2 \tilde{A}^2 \quad (4.1.93)$$

$$\sigma_x^2 = -\rho_x^*(\nu = 0) = \frac{8}{5} \pi^2 \tilde{A}^2 \quad (4.1.94)$$

In a similar manner it can be shown that $\sigma_x^2 = \sigma_{y'}^2$ and the joint pdf of X, X', Y, Y' is given by (4.1.95). Integrating out Θ, Θ' of the joint P.D.F. gives (4.1.96) and from this the number of positive upward crossings of the process ω at a given power level a per interval du can be derived as (4.1.97). Finally, the mean number of upward crossings for the interval S_{3dB} is given by (4.1.97) and since the 3dB, sidelobe region is symmetric in the region $-\phi_{qo}^{zero} \rightarrow -\pi$ the total, mean number of upward crossings is given by (4.1.99)

$$f_{X,Y,X',Y'}(x, y, x', y') = \frac{1}{(2\pi)^2 \sigma_x \sigma_{x'}} e^{\left(-\frac{x^2+y^2}{2\sigma_x^2} - \frac{x'^2+y'^2}{2\sigma_{x'}^2} \right)} = \frac{1}{(2\pi)^2 \pi^2 \tilde{A}^2} e^{\left(-(x^2+y^2) - \frac{x'^2+y'^2}{4\pi^2 \tilde{A}^2} \right)} \quad (4.1.95)$$

$$f_{\Omega,\Omega'}(\omega, \omega') = \frac{\omega}{\sqrt{2\pi} \sigma_x^2 \sigma_{x'}} e^{\left(-\frac{\omega^2}{2\sigma_x^2} - \frac{\omega'^2}{2\sigma_{x'}^2} \right)} = \frac{\sqrt{5}\omega}{2\pi^{3/2} \tilde{A}} e^{\left(-\omega^2 - \frac{5\omega'^2}{16\pi^2 \tilde{A}^2} \right)} \quad (4.1.96)$$

$$v(a) du = du \int_0^\infty w' f_{\Omega,\Omega'}(a, \omega') d\omega' = \frac{4adue^{-a^2} \sqrt{\pi} \tilde{A}}{\sqrt{5}} \quad (4.1.97)$$

$$E\{v(a)\} = \frac{2ae^{-a^2} \sqrt{\pi} \tilde{A}}{\sqrt{5}} \int_{\phi_{n_o}^{zero}}^\pi \cos\left(\frac{\phi}{2}\right) d\phi = \frac{2}{\sqrt{5}} \left(1 - \sin\left(\frac{\phi_{n_o}^{zero}}{2}\right) \right) \sqrt{\pi} \tilde{A} e^{-a^2} \quad (4.1.98)$$

$$E\{v(a)\} = \frac{4}{\sqrt{5}} \left(1 - \sin\left(\frac{\phi_{n_o}^{zero}}{2}\right) \right) \sqrt{\pi} \tilde{A} e^{-a^2} \quad (4.1.99)$$

Like it stated in the circular array section (4.1.99) decreases monotonically for $a \geq \frac{1}{\sqrt{2}}$. Thus, the outage probability at least one peak is to exceed a given power level a is (4.1.100).

$$\Pr\left[\max_{S_{3dB}}, X^2 + Y^2 > P_o\right] \leq E\{v(a)\} = \frac{4}{\sqrt{5}} \left(1 - \sin\left(\frac{\phi_n^{zero}}{2}\right)\right) \sqrt{\pi} A \sqrt{NP_o} e^{-NP_o}, NP_o \geq \frac{1}{2} \quad (4.1.100)$$

E. Average Properties of a Gaussian Distributed Spherical Antenna Array with Perfect Phase Information and Gaussian Random Variable

1. Average Beampattern

If the compound random variables $\Upsilon_n = \tilde{r}_n \sin \theta_n \sin \phi_n, T_n = \tilde{r}_n \cos \theta_n$ are Gaussian distributed with zero mean and variance σ^2 then the P.D.F. (4.1.101) can be used, which is the bivariate normal distribution. This distribution is often used to describe, at least approximately, any variable that tends to cluster around the mean.

$$f_{\Upsilon_n, T_n}(\tilde{\Upsilon}, \tilde{T}) = \frac{1}{2\pi\sigma_v\sigma_w} e^{-\frac{\tilde{\Upsilon}^2}{2\sigma_v^2}} e^{-\frac{\tilde{T}^2}{2\sigma_w^2}}, -\infty < \tilde{\Upsilon} < \infty, -\infty < \tilde{T} < \infty \quad (4.1.101)$$

In the case of a Bivariate Gaussian distribution, the average radiation pattern can be calculated from the definition of (0.2.19) to give (4.1.102).

$$U_{av}(\theta, \phi) = \frac{1}{N} + \left(1 - \frac{1}{N}\right) \left[\left| e^{-\frac{\zeta(\theta, \phi)^2 \sigma^2}{2}} \right|^2 \left| e^{-\frac{\zeta(\theta)^2 \sigma^2}{2}} \right|^2 \right] \quad (4.1.102)$$

The average radiation intensity (4.1.102) of a spherical array with Gaussian distribution gives a similar result to that of a circular random array(3.1.138). However, the main lobe is now composed of the multiplication of two exponentially decaying functions instead of one exponentially decaying function given in(3.1.138). In addition,

the first exponential embedded with the spatial parameter $\zeta(\theta, \phi)$ is indeed the solution to the Gaussian distributed circular random array and it makes sense the spherical array would contain this term since the geometry of a sphere contains circular and spherical symmetry. Therefore, the addition of the second main beam parameter composed of surface area symmetry of the spatial parameter $\xi(\theta)$ coupled with the main beams second term of volume symmetry is enough to abundantly represent spherical symmetry.

Moreover, like always, the first term of the average radiation intensity describes the average sidelobe region and the second term is not oscillatory this time around. The beam pattern decays exponentially with a rate proportional to the multiplication of the exponentials embedded with the variance and spatial parameter $\zeta(\theta, \phi)^2$ and $\xi(\theta)^2$. Thus, the pattern contains neither nulls nor sidelobes and the sidelobe region will be reached at a faster rate from the multiplication of the exponentials.

The total radiation pattern of a random spherical array with Gaussian distribution is shown in Fig. 56 and plotted in Fig. 57 and Fig. 58 at the meridian angle with differing standard deviations.

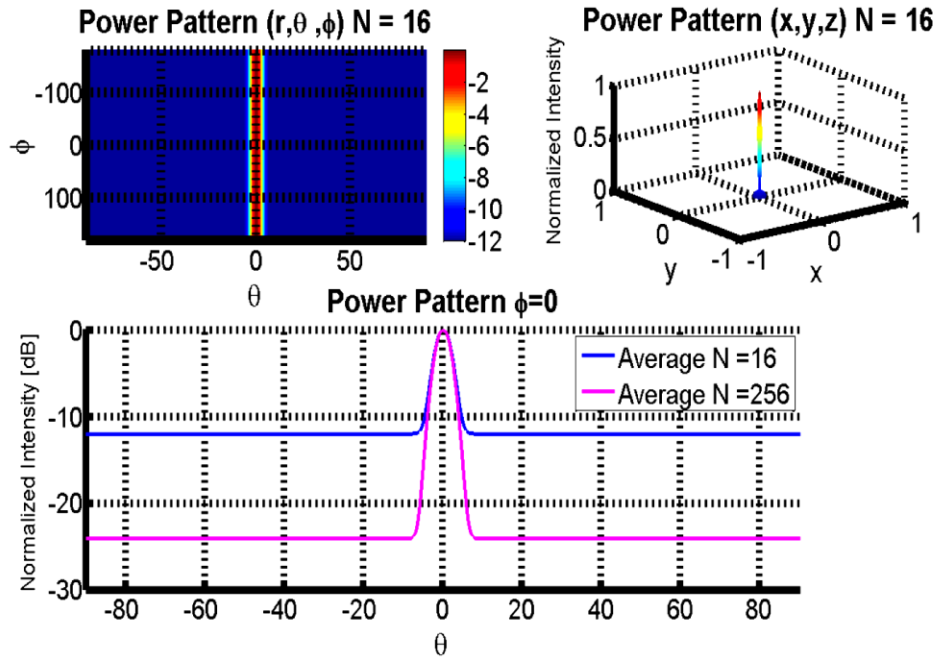


Fig. 56. Average radiation pattern of 16 elements randomly spaced (Gaussian distributed) within a spherical aperture of 10λ and $\sigma = .5$.

2. Average Beampattern Simplification for $\theta = \theta_o = \pi/2$

At the meridian angle, $\theta = \theta_o = \pi/2$ the average beampattern is given by (4.1.103) and provides an interesting result. The average beampattern at the meridian angle is given to be the same as the average radiation intensity of the circular random array given in (3.1.139).

$$U_{av}(\phi) = \frac{1}{N} + \left(1 - \frac{1}{N}\right) \left[\left| e^{-\frac{\zeta(\phi)^2 \sigma^2}{2}} \right|^2 \right] \quad (4.1.103)$$

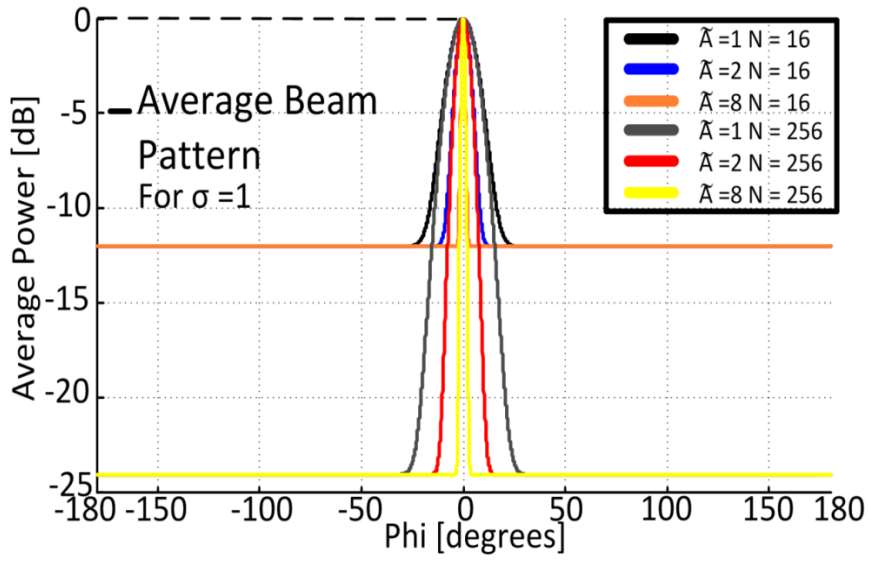


Fig. 57. Average radiation pattern of 16 and 256 elements randomly spaced within a spherical aperture of 10λ with Gaussian distribution and $\sigma = 1$ (Same as Fig. 33).

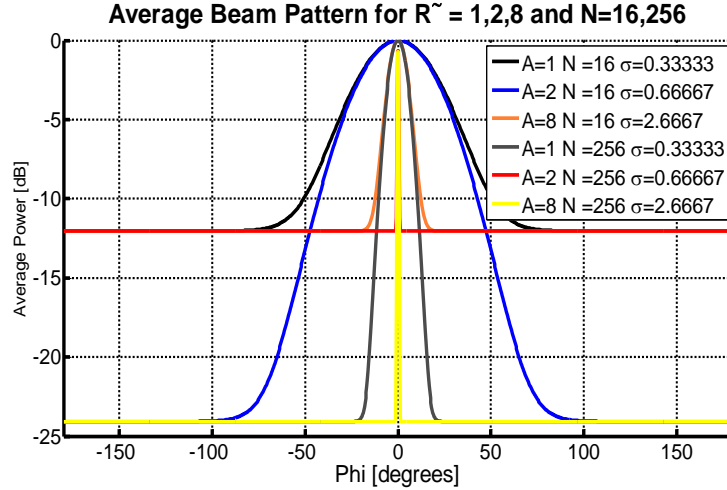


Fig. 58. Average radiation pattern of 16 and 256 elements randomly spaced within a spherical aperture of 10λ with Gaussian distribution and $\sigma = \tilde{A}|_{\lambda=1} = A/3$.

a. 3dB Beamwidth, 3dB Sidelobe Region, and Average Directivity

Since the Random Circular (3.1.139) and Spherical (4.1.103) array share the same average radiation intensity at the meridian angle the characteristics of 3dB beamwidth, 3dB sidelobe Region and Average Directivity will be given by those derived in the circular array Chapter Subheading 2.E.2.(a-c). Given this conclusion the results of 3dB beamwidth are given by (3.1.144) and (3.1.145), 3dB sidelobe by (3.1.147) and average directivity (3.1.148).

b. Average Statistical Properties of a Uniformly Distributed Spherical Antenna Array with Perfect Phase Information and Gaussian Random Variable

Properties of the exact complementary cumulative distribution function (CCDF) in lieu of the beampattern level of a spherical random array at the meridian angle convey identical results towards the circular random array section 5.2.G. As a consequence the CCDF is given by(3.1.81), array factor by (3.1.82) and supporting statistical measures (3.1.149)-(3.1.154). Furthermore, since the variances σ_x^2 and σ_y^2 approach equals values of .5 in the limiting case; the beampattern level (in the sidelobe region) is modeled by a Nakagami-Rice distribution presented in (3.1.93). Since the mean m_x (3.1.149) approaches zero in the sidelobe region one also can assume the beampattern undertakes a Rayleigh distribution shown in (3.1.94). Lastly the mean number of crossings of a sidelobe for a given power threshold in the 3dB sidelobe region S_{3dB} is provided by (3.1.157).

F. Average Properties of a Truncated Gaussian Distributed Spherical Antenna Array with Perfect Phase Information and Gaussian Random Variable

1. Average Beampattern

When the Gaussian random variables $\Upsilon_n = \tilde{r}_n \sin \theta_n \sin \phi_n, T_n = \tilde{r}_n \cos \theta_n$ do not have infinite support, they are truncated in the form of (4.1.104). This type of distribution is similar to that used in the circular random array section 5.2.F.1 and [12] and might be more practical since antennas far away from the cluster are neglected. By the removal of antennas located far away it may perhaps lower the overall power consumption needed for communication to the destination point. This conclusion is drawn from the fact that antennas located far-away from the cluster typically require higher power for transmission. However, if the cluster gets too crowded effects of mutual coupling may repeal the assumption a truncated distribution gives further desirable results as too much unwanted interference negatively impacts the beam.

$$f_{\Upsilon_n, T_n}(\bar{\Upsilon}, \bar{T}) = \frac{1}{2\pi\sigma_\Upsilon\sigma_T} e^{-\frac{\bar{\Upsilon}^2}{2\sigma_\Upsilon^2}} e^{-\frac{\bar{T}^2}{2\sigma_T^2}}, -L < \bar{\Upsilon} < L, -L < \bar{T} < L \quad (4.1.104)$$

The joint density function given by (4.1.104)

$$U_{av}(\theta, \phi) = \frac{1}{N} + \frac{1}{N^2} \left| e^{-\frac{\zeta(\theta, \phi)^2 \sigma^2}{2}} \right| \left| e^{-\frac{\xi(\theta)^2 \sigma^2}{2}} \right| \left[\frac{1}{16} \sum_{m=1}^N \sum_{\substack{n=1 \\ n \neq m}}^N \left[\operatorname{erf} \left(\frac{L - j\xi(\theta) \sigma^2}{\sqrt{2}\sigma} \right) + \operatorname{erf} \left(\frac{L + j\xi(\theta) \sigma^2}{\sqrt{2}\sigma} \right) \right]^2 \right] \left[\operatorname{erf} \left(\frac{L - j\zeta(\theta, \phi) \sigma^2}{\sqrt{2}\sigma} \right) + \operatorname{erf} \left(\frac{L + j\zeta(\theta, \phi) \sigma^2}{\sqrt{2}\sigma} \right) \right]^2 \quad (4.1.105)$$

2. Average Beampattern Simplification for $\theta = \theta_o = \pi/2$

At the meridian elevation angle $\theta = \theta_o = \pi/2$ (4.1.105) simplifies to (4.1.106).

$$U_{av}(\phi) = \frac{1}{N} + \frac{1}{N^2} \left| e^{-\frac{\zeta(\phi)^2 \sigma^2}{2}} \left[\frac{1}{4} \sum_{m=1}^N \sum_{\substack{n=1 \\ n \neq m}}^N \left[\operatorname{erf} \left(\frac{L - j\zeta(\phi)\sigma^2}{\sqrt{2}\sigma} \right) + \operatorname{erf} \left(\frac{L + j\zeta(\phi)\sigma^2}{\sqrt{2}\sigma} \right) \right] \right]^2 \right| \quad (4.1.106)$$

G. Realization of a Uniformly Distributed Spherical Antenna Array with Perfect Phase Information

The realization pattern for a random spherical array is plotted from a uniform distribution of elements in Fig. 59 with a given element distribution shown in Fig. 60.

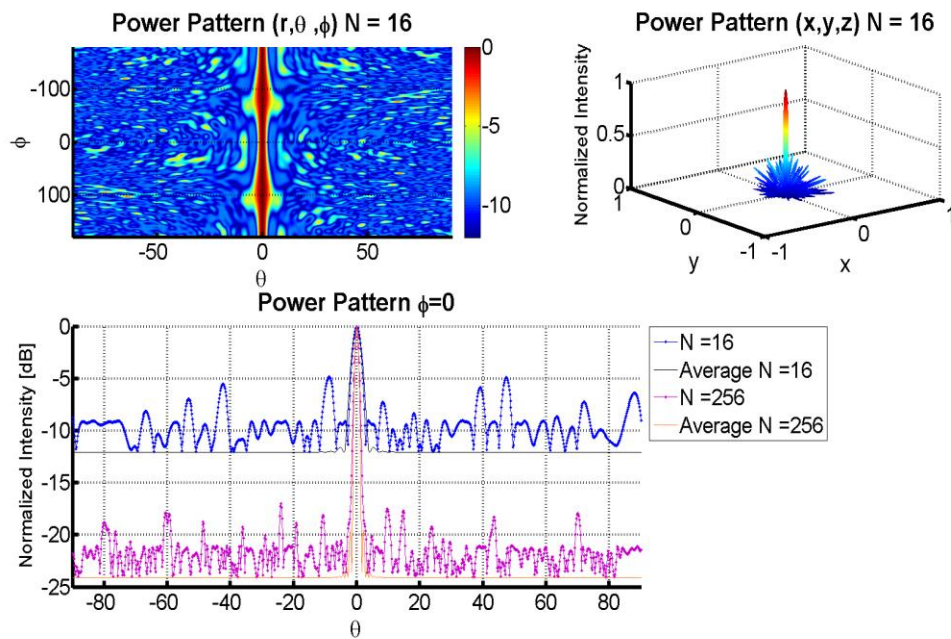


Fig. 59. Radiation pattern of a random spherical array with 16 and 256 elements uniformly distributed in a spherical radius 10λ .

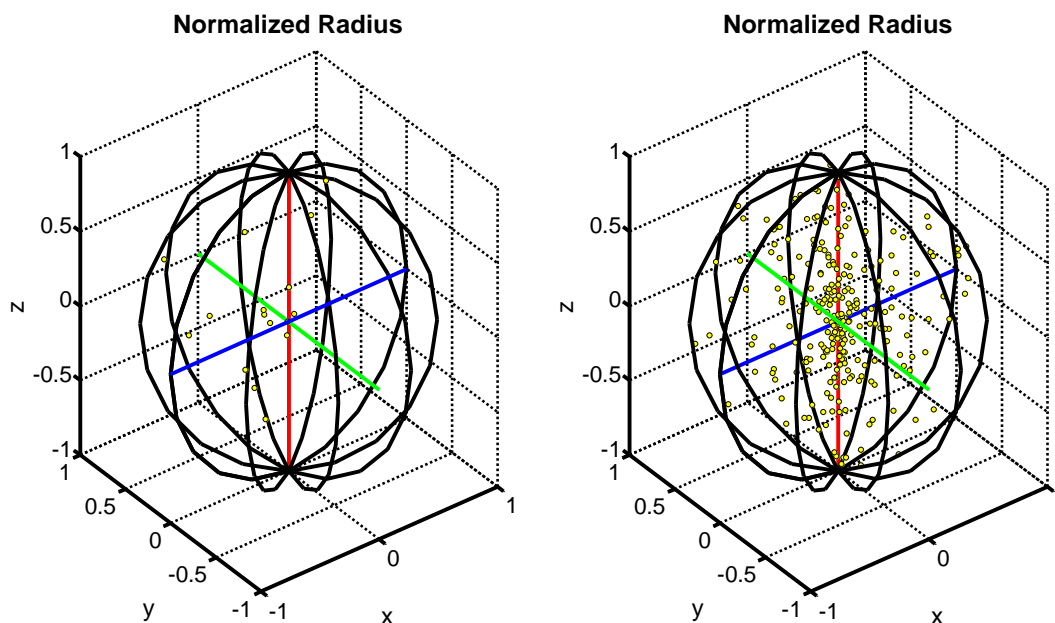


Fig. 60. 16 and 256 elements uniformly distributed in a normalized spherical aperture.

The realization pattern for a random circular array is plotted from a Gaussian distribution of elements in Fig. 61 with a given element distribution shown in Fig. 62.

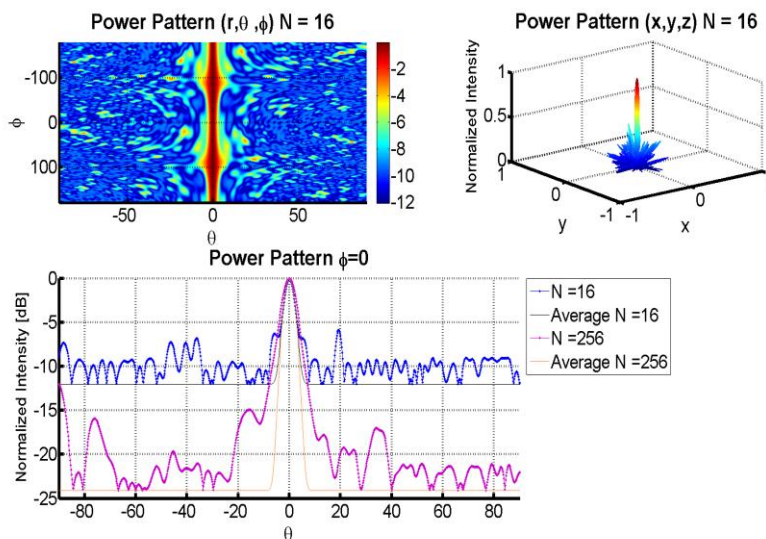


Fig. 61. Radiation pattern of a random spherical array with 16 and 256 elements Gaussian distributed in a spherical radius 10λ .

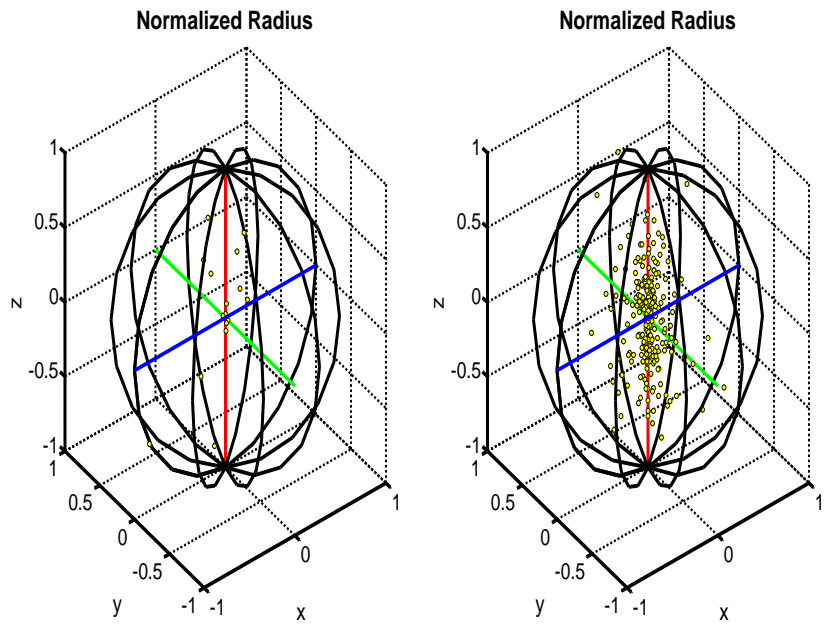


Fig. 62. 16 and 256 elements Gaussian distributed in a normalized spherical aperture.

CHAPTER VII

ADDITIONAL VOLUMETRIC ARRAYS

7.1 Aperiodic

A. Cubic Array

1. System Development and Beampattern Definition

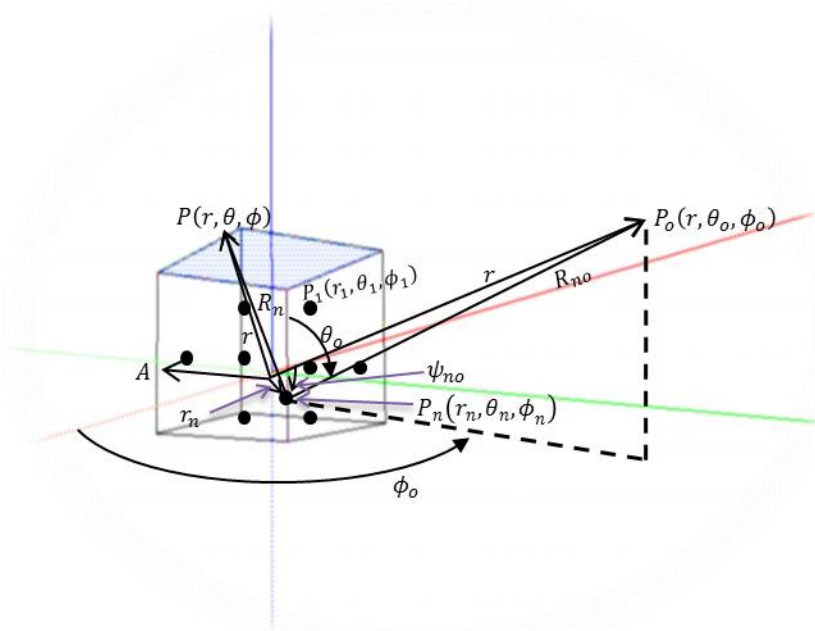


Fig. 63. Geometry of an N-element random cubical array.

The geometry of a random cubical array is shown in Fig. 63. The differential path length from source to observation point for a cubical array is calculated as (5.1.1).

$$\begin{aligned} r_n \cos(\psi_n) &= \vec{r}_n \cdot \hat{a}_r = \left((x_n \hat{a}_x + y_n \hat{a}_y + z_n \hat{a}_z) \cdot (\hat{a}_x \sin \theta \cos \phi + \hat{a}_y \sin \theta \sin \phi + \hat{a}_z \cos \theta) \right) \\ &= x_n \sin \theta \cos \phi + y_n \sin \theta \sin \phi + z_n \cos \theta \end{aligned} \quad (5.1.1)$$

The array factor of a random cubical array is similar to that of (2.1.13) with the exception the random variable $\chi_n = \tilde{z}_n \triangleq \frac{z_n}{A}$ is added taking into account the randomness of the height of the element. In addition the P.D.F.s of x_n , u_n , y_n and v_n will be the same as those given in (1.1.10), (1.1.11), (2.1.14) and (2.1.15). The new P.D.F. for z_n and χ_n is derived in a similar fashion and shown in (5.1.2) and (5.1.3).

$$\int_{-C}^C f_{z_n}(z) dz = 1, \quad f_{z_n}(z) = \frac{1}{2C} \text{ for } |z| \leq C \quad (5.1.2)$$

$$\int_{-1}^1 f_{\chi_n}(\chi) d\chi = 1, \quad f_{\chi_n}(\chi) = \frac{1}{2} \Big|_{C=B=A=1}, \quad -1 \leq \chi \leq 1 \quad (5.1.3)$$

Once more like in the planar and linear case the integration limits have been set such that $A=B=C=1$ for simplicity. The pattern function for a unit cube is now rewritten as (5.1.4).

$$F(\theta, \phi | \vec{u}, \vec{v}, \vec{\chi}) = \frac{1}{N} \sum_{n=1}^N e^{j2\pi \tilde{A} u_n [\sin \theta \cos(\phi) - \sin \theta_o \cos(\phi_o)]} e^{j2\pi \tilde{A} v_n [\sin \theta \sin(\phi) - \sin \theta_o \sin(\phi_o)]} e^{j2\pi \tilde{A} \chi_n [\cos \theta - \cos \theta_o]} \quad (5.1.4)$$

At last the far-field radiation intensity (0.2.15) is defined as (5.1.5) where the spatial parameters $\alpha(\theta, \phi)$, $\beta(\theta, \phi)$ and $\chi(\theta)$ were previously defined in (1.1.14), (2.1.19) and (4.1.62) are repeated in (5.1.6)-(5.1.8).

$$U(\theta, \phi | \vec{u}, \vec{v}, \vec{\chi}) = \frac{1}{N} + \frac{1}{N^2} \sum_{m=1}^N \sum_{n=1}^N e^{j\alpha(\theta, \phi)(u_n - u_m)} e^{j\beta(\theta, \phi)(v_n - v_m)} e^{j\xi(\theta)(\chi_n - \chi_m)} \quad (5.1.5)$$

$$\alpha(\theta, \phi) \triangleq 2\pi \tilde{A} (\sin \theta \cos(\phi) - \sin \theta_o \cos(\phi_o)) \quad (5.1.6)$$

$$\beta(\theta, \phi) \triangleq 2\pi \tilde{A} (\sin \theta \sin \phi - \sin \theta_o \sin \phi_o) \quad (5.1.7)$$

$$\xi(\theta) \triangleq 2\pi \tilde{A} (\cos \theta - \cos \theta_o) \quad (5.1.8)$$

2. Average Properties of a Uniformly Distributed Cubic Antenna Array with Perfect Phase Information

a. Average Beampattern

All over again the definition of expectation (0.2.19) is applied to (5.1.5) giving a means of deriving the average radiation intensity from the setup of (5.1.9)

$$P(\theta, \phi) = E_{u,v,\chi} \left| P(\phi | \vec{u}, \vec{v}, \vec{\chi}) \right| = \frac{1}{N} + \frac{1}{N^2} \sum_{m=1}^N \sum_{\substack{n=1 \\ n \neq m}}^N \int_{-1}^1 \int_{-1}^1 e^{j\alpha(\theta, \phi)(u_n - u_m)} \frac{1}{2} \frac{1}{2} du_n du_m \int_{-1}^1 \int_{-1}^1 e^{j\beta(\theta, \phi)(v_n - v_m)} \frac{1}{2} \frac{1}{2} dv_n dv_m \int_{-1}^1 \int_{-1}^1 e^{j\xi(\theta)(\chi_n - \chi_m)} \frac{1}{2} \frac{1}{2} d\chi_n d\chi_m \quad (5.1.9)$$

The integration of the first term of (5.1.9) is given by (A.1.1) and once more yields the value $\frac{1}{N}$. The double summation term still simplifies to an analytic expression and the solution to the integration is given by (5.1.9). This provides the average radiation intensity in its final form (5.1.10).

$$P(\theta, \phi) = E_{u,v,\chi} \left| P(\phi | \vec{u}, \vec{v}, \vec{\chi}) \right| = \frac{1}{N} + \left(1 - \frac{1}{N}\right) \left| \text{sinc}(\alpha(\theta, \phi)) \right|^2 \left| \text{sinc}(\beta(\theta, \phi)) \right|^2 \left| \text{sinc}(\xi(\theta)) \right|^2 \quad (5.1.10)$$

The average radiation intensity (5.1.10) of a cubic random array is similar to that of a linear (1.1.17) and planar array (2.1.22). The difference exists from the multiplication of an added sinc function to the mainlobe term embedded with the spatial parameter $\xi(\theta)$. This parameter is developed from taking into account the elevation of the array. Last of all the mainlobe factor is now comprised with three independent oscillatory sinc functions, which rapidly attenuate the beam as the spatial parameters $\alpha(\theta, \phi)$, $\beta(\theta, \phi)$ or $\xi(\theta)$ increase. Therefore, the cubical array will benefit from its

counterpart linear and planar arrays since the main beam outside of the main beam region will attenuate at a faster. This makes sense, because the aperture size of a cubical array has increased allowing for greater spread between the elements. Moreover, as it was seen in the circular and spherical arrays the 3dB point of the mainlobe falls off inversely proportional to the aperture size, and aids to increased directivity.

The total radiation pattern of a random cubic array is plotted in Fig. 64 and at the meridian elevation angle in Fig. 65.

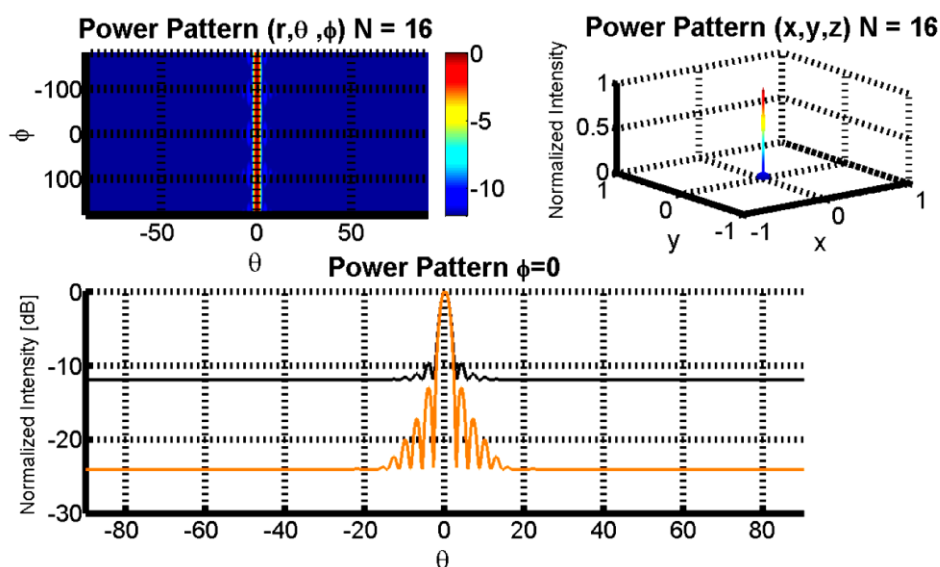


Fig. 64. Average radiation pattern of 16 and 256 elements randomly spaced (uniformly) within a cubical aperture of 10λ .

b. Average Beampattern Simplification for $\theta = \theta_o = \frac{\pi}{2}$

At the meridian angle $\theta = \theta_o = \frac{\pi}{2}$ the average radiation pattern is simplified to that of (5.1.11) and provides an interesting result, such that the average beampattern at the

meridian angle is given to be exactly the same as the average radiation intensity of a planar random array at its meridian angle given by (2.1.23) also shown in (5.1.11)

$$P(\theta, \phi) = E_{u,v} |P(\phi | \vec{u}, \vec{v})| = \frac{1}{N} + \left(1 - \frac{1}{N}\right) |\text{sinc}(\alpha(\phi))|^2 |\text{sinc}(\beta(\phi))|^2 \quad (5.1.11)$$

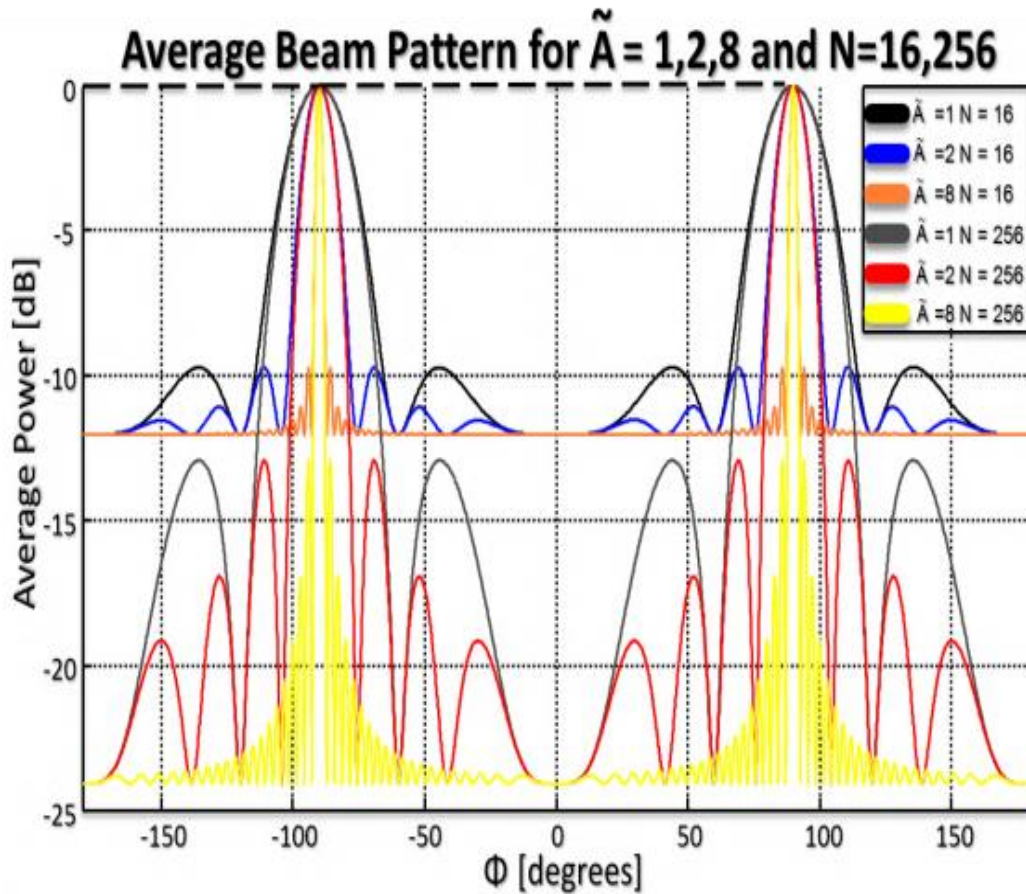


Fig. 65. Average radiation intensity at the meridian elevation angle of a random cubic array.

3. Realization of a Uniformly Distributed Cubical Antenna Array with Perfect Phase Information

The realization pattern for a random cubic array is plotted in Fig. 66 with a given element distribution shown in Fig. 67.

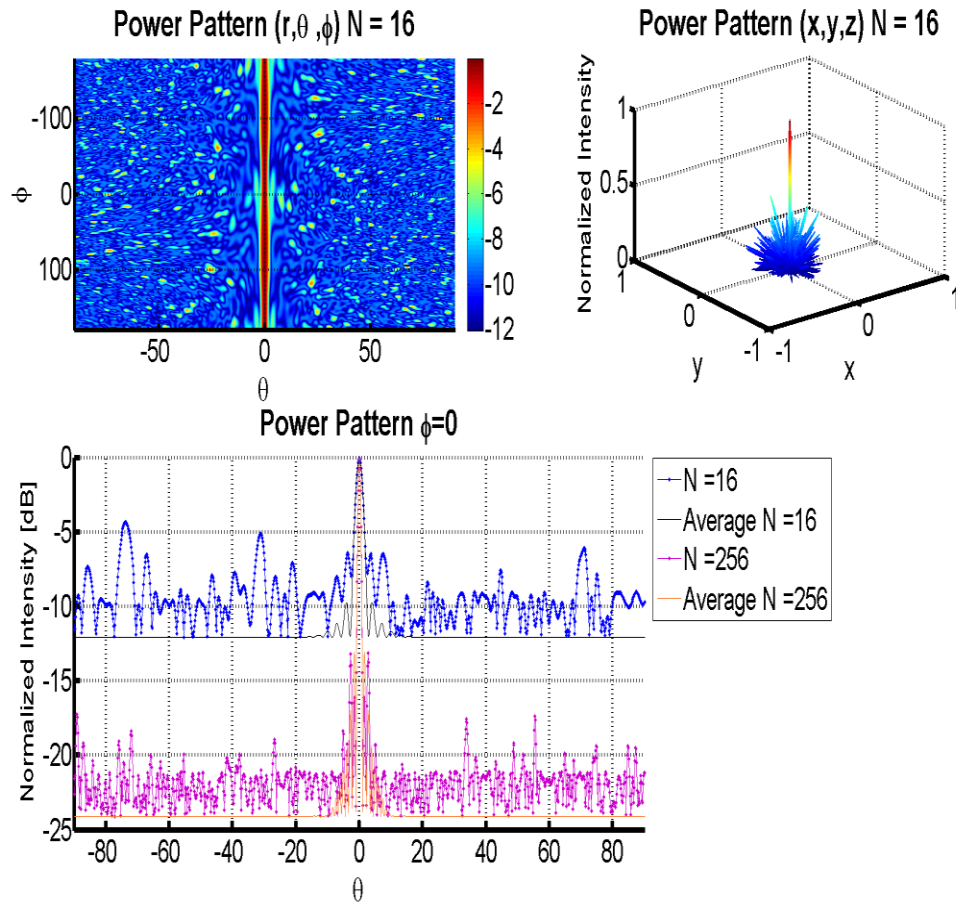


Fig. 66. Radiation pattern of a random cubical array with 16 and 256 elements uniformly distributed in a radius of 10λ .

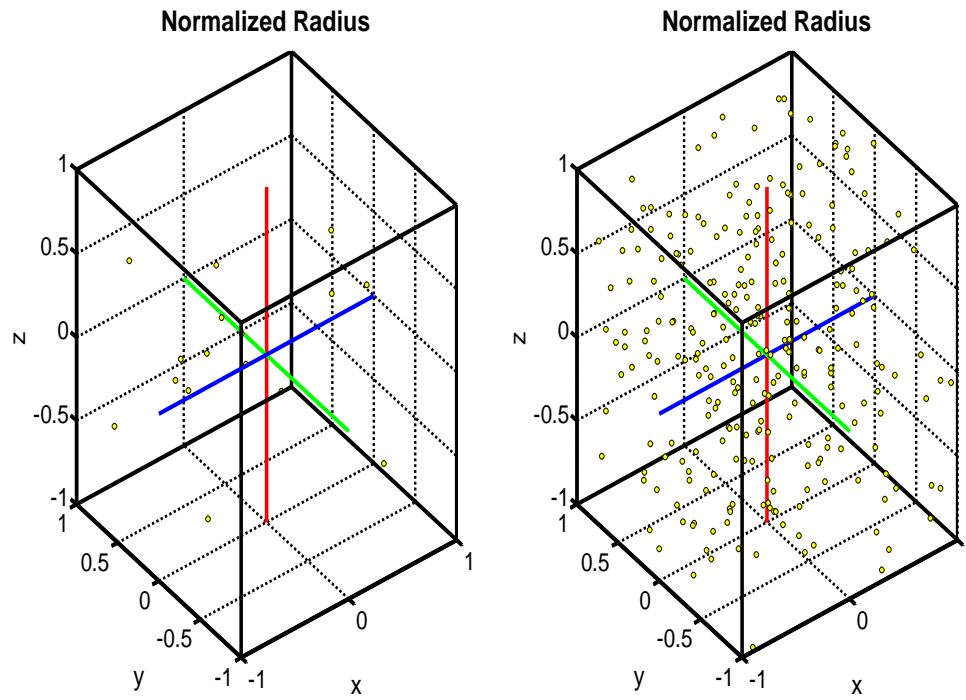


Fig. 67. 16 and 256 elements uniformly distributed in a normalized cubical aperture.

B. Cylindrical Array

1. System Development and Beampattern Definition

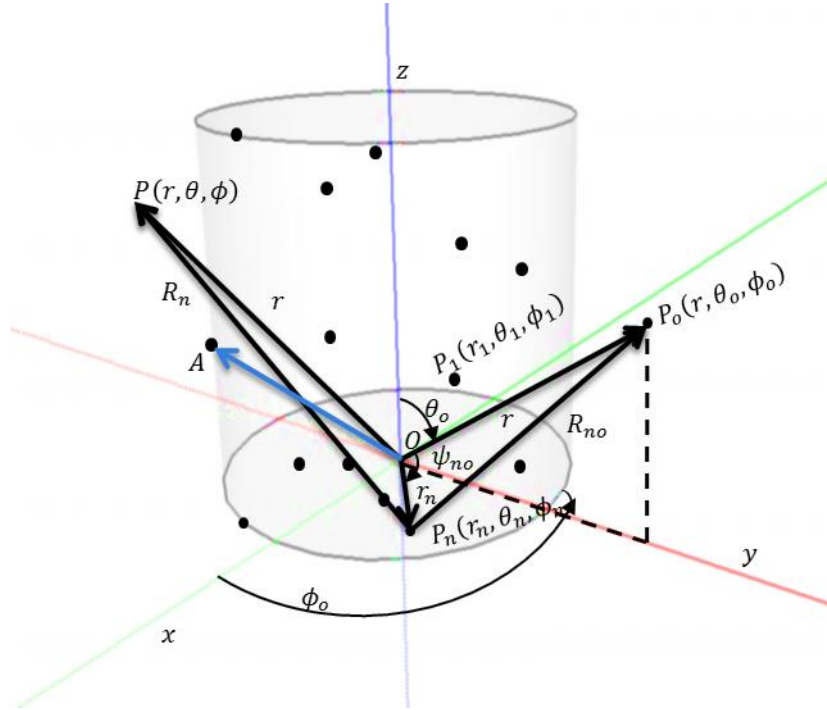


Fig. 68 Geometry of an N-element random cylindrical array.

The geometry of a random cylindrical array is shown in Fig. 68. The differential path length from source to observation point for a cylindrical array is calculated as (5.1.12).

$$\begin{aligned} r_n \cos(\psi_n) &= \vec{r}_n \cdot \hat{a}_r = \left((\rho_n \cos \phi_n \hat{a}_x + \rho_n \sin \phi_n \hat{a}_y + z_n \hat{a}_z) \cdot (\hat{a}_x \sin \theta \cos \phi + \hat{a}_y \sin \theta \sin \phi + \hat{a}_z \cos \theta) \right) \\ &= \rho_n \sin \theta (\cos(\phi - \phi_n)) + z_n \cos \theta \end{aligned} \quad (5.1.12)$$

The array factor of a random cylindrical array is similar to that of (3.1.19) with the exception the random variable $\chi_n = \tilde{z}_n \triangleq \frac{z_n}{A}$ is added taking into account the randomness of the height of the element. In addition the P.D.F.s of ρ_n , ϕ_n , ν_n , z_n and

χ_n will be the same as those given in (3.1.21), (3.1.22), (3.1.24) , (5.1.2) and (5.1.3). No new P.D.F.s need to be re-derived.

The array factor of a random cylindrical array is similar to that of (5.2.1) with the exception the random variable $\chi_n = \tilde{z}_n \triangleq \frac{z_n}{A}$ is added taking into account the height of the element. The corresponding array factor is thus, given in (5.1.13) and ultimately the far-field radiation intensity (0.2.15) is defined as (5.1.14)

$$F(\theta, \phi | \vec{v}_n, \vec{\chi}_n) = \sum_{n=1}^N e^{j(v_n \zeta(\theta, \phi) + \chi_n \xi(\theta))} \quad (5.1.13)$$

$$U(\theta, \phi | \vec{v}, \vec{\chi}) = \frac{1}{N} + \frac{1}{N^2} \sum_{m=1}^N \sum_{\substack{n=1 \\ n \neq m}}^N e^{j((v_n - v_m) \zeta(\theta, \phi) + (\chi_n - \chi_m) \xi(\theta))} \quad (5.1.14)$$

2. Average Properties of a Uniformly Distributed Cylindrical Antenna Array with Perfect Phase Information

a. Average Beampattern

Applying the definition of expectation (0.2.19) to (5.1.14) one can derive the average radiation intensity (5.1.15) in the same fashion used for the previous geometries.

$$U_{av}(\theta, \phi) = E_{v, \chi} |U(\theta, \phi | \vec{v}, \vec{\chi})| = \frac{1}{N} + \left(1 - \frac{1}{N}\right) |2\text{jinc}(\zeta(\theta, \phi))|^2 |\text{sinc}(\xi(\theta))|^2 \quad (5.1.15)$$

At the meridian angle the radiation pattern (5.1.15) reduces to being the same pattern a random circular array contains (3.1.44) at its meridian angle and the result of (3.1.44) is shown in (5.1.16).

$$E_v |U(\phi | \vec{v})| = \frac{1}{N} + \left(1 - \frac{1}{N}\right) |2\text{jinc}(\zeta(\phi))|^2 \quad (5.1.16)$$

The total radiation pattern of a random cylindrical array is plotted in Fig. 69 and at the meridian elevation angle in Fig. 70.

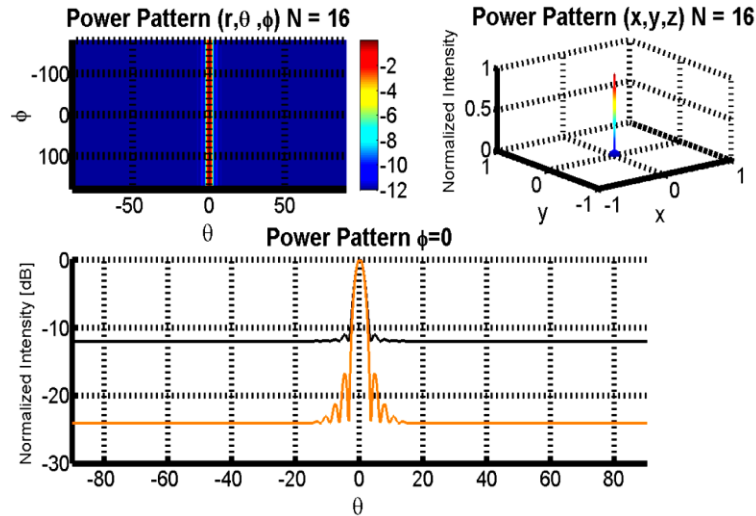


Fig. 69. Average radiation pattern of 16 elements randomly spaced (uniformly) within a cylindrical aperture of 10λ .

b. Average Beampattern Simplification for $\theta = \theta_o = \pi/2$

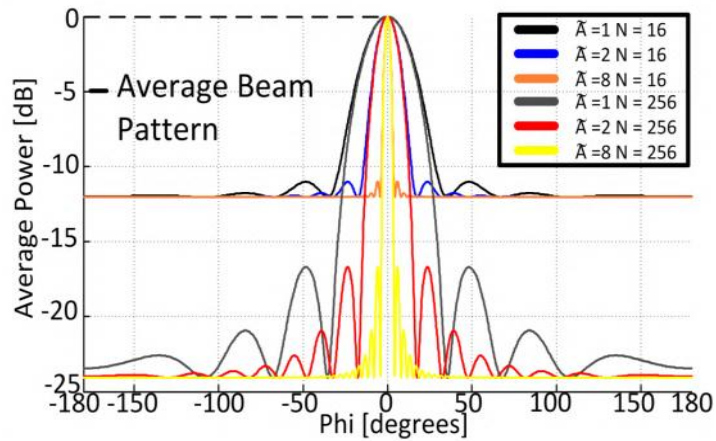


Fig. 70. Average radiation pattern of 16 and 256 elements randomly spaced (uniformly) within a cylindrical aperture of 10λ at the meridian elevation angle $\theta = \theta_o = \pi/2$.

3. Realization of a Uniformly Distributed Cylindrical Antenna Array with Perfect Phase Information

The realization pattern for a random cylindrical array is plotted in Fig. 71 with a given element distribution shown in Fig. 72.

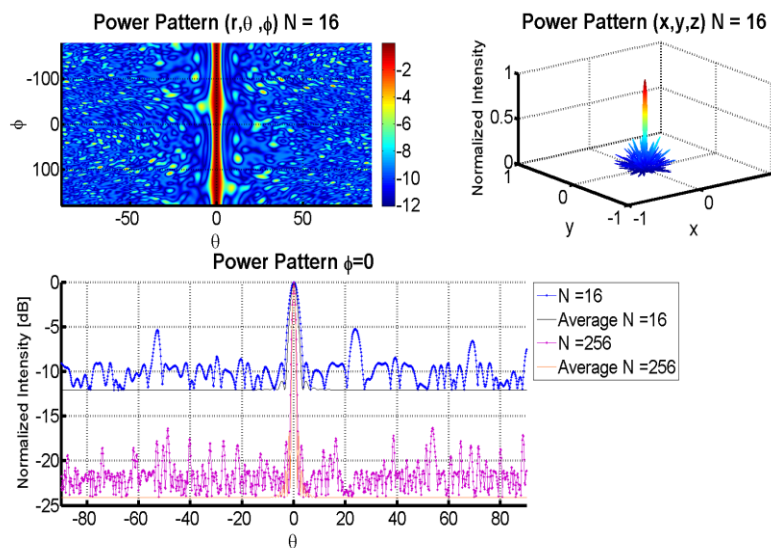


Fig. 71. Radiation pattern of a random cylindrical array with 16 and 256 elements uniformly distributed in a radius of 10λ .

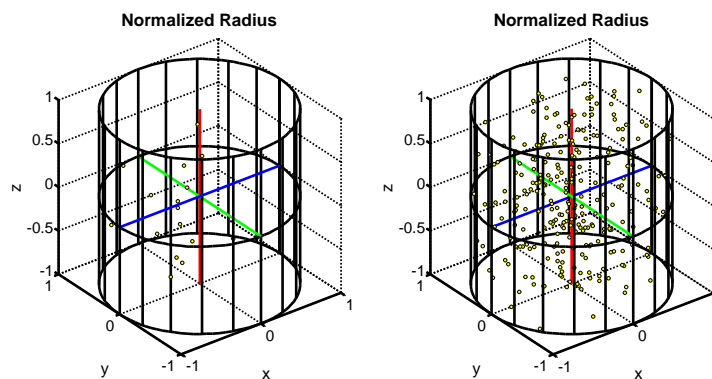


Fig. 72. 16 and 256 elements uniformly distributed in a normalized cylindrical aperture.

CHAPTER VIII

ONGOING AND FUTURE WORK

One direction of future work deals with the synthesis problem, which is nothing more than finding a realizable function J so the pattern function f is close to the desired pattern function f_d . This type of work was studied by [81], but in a probabilistic fashion. Moreover, general optimization theory is formulated on the premise that all parameters are adjusted according to unlimited accuracy; however, no practical antenna can be built with absolute precision. Imperfections are limited due to physical reality of random errors from non-perfect conductors, finite bandwidth requirements, interference from other sources and many more causes leading to difficulty. Therefore, Lo and Richards investigated the possibility of achieving pattern optimization in a probabilistic sense and found that a pattern function may be approximated closely to a desired pattern only by means of exciting high currents in a finite region. Disadvantageously these high currents lead to large Ohmic losses therefore asking for too much precision will actually lead to more harm than good. However, a metric of optimization was found possible in the probabilistic sense and will be explored in the future.

8.1 Flying Antenna's

Gathering true experimental results from a random array is very difficult in practice and to cope with this challenge a disc shaped flyer is currently under construction as shown in Fig. 73.

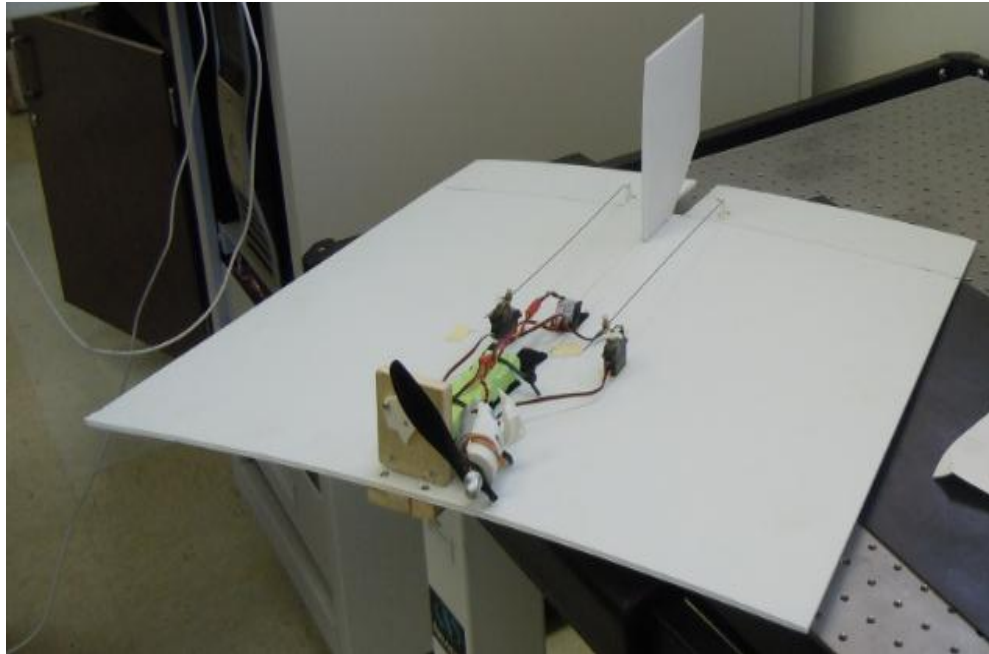


Fig. 73. Box shaped flyer.

8.2 Wideband Antenna's

For many years, applications have required broad bandwidth communication links with antennas that must operate over a frequency range of several octaves. Consequently, antenna structures with multi-octave capability are useful for modern communications systems. This section focuses on two types of wideband antennas for the application of random arrays: spiral and biconical.

Also modern communication systems require coverage in the 900 MHz frequency range and evolving networks typically require coverage at 1700-2200 MHz. Moreover, additional coverage is often required for Terrestrial Trunked Radio (TETRA) frequency (around 400 MHz), wireless LAN and wireless local loop (2500 MHz, 3500MHz and 5500 MHz). Therefore, to satisfy all these frequencies it is necessary for antennas to provide effective coverage from 400 MHz to 6 GHz [86].

In some applications, this can be accomplished by a series of individual antennas each assigned to a portion of the band. For a more discrete appearance the array is beneficial to use very large broadband radiators. Multi-functionality is also another appealing feature of many modern systems. Broadband antennas can be incorporated with multi-band capability of which may be fixed for use in multiple applications.

In general, the bandwidth is a measure of how much the frequency can be varied while still obtaining an acceptable voltage standing wave ratio VSWR (2:1 or less). This figure of merit is a standard for minimizing unwanted losses and corresponds to a 9.5dB (or 10%) return loss.

The two methods for computing the bandwidth of an antenna are shown in (6.1.1) and (6.1.2) where F_U is the upper frequency limit, F_L is the lower frequency limit and F_C is the cutoff frequency.

$$B = \left(\frac{F_U - F_L}{F_C} \right) (100) \quad (6.1.1)$$

$$B = \frac{F_U}{F_L} \quad (6.1.2)$$

The spiral antenna has long been used in defense applications for direction finding systems and general threat detection [86]. Fig. 74. Characteristics of a cavity backed and conical spiral antenna [87] shows a typical cavity backed spiral and conical spiral antenna, their radiation pattern and characteristics.

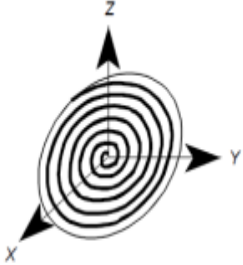

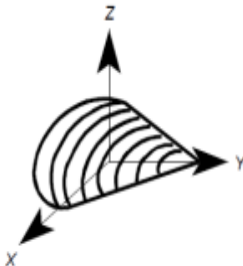

Antenna Type	Radiation Pattern	Characteristics
CAVITY BACKED SPIRAL (Flat Helix) 	<i>Elevation & Azimuth</i> 	Polarization: Circular <i>Left hand as shown</i> Typical Half-Power Beamwidth: 60 deg x 90 deg Typical Gain: 2-4 dB Bandwidth: 160% or 9:1 Frequency Limit: Lower: 500 MHz Upper: 18 GHz
CONICAL SPIRAL 	<i>Elevation & Azimuth</i> 	Polarization: Circular <i>Left hand as shown</i> Typical Half-Power Beamwidth: 60 deg x 60 deg Typical Gain: 5-8 dB Bandwidth: 120% or 4:1 Frequency Limit: Lower: 50 MHz Upper: 18 GHz

Fig. 74. Characteristics of a cavity backed and conical spiral antenna [87].

Depending upon the size or type of spiral selected, coverage can be provided across the bands between 50 MHz and 18 GHz. Consequently, this type of antenna is useful for covering the spectrum between 400 MHz to 6 GHz for most commercial applications and a good fit for random array type applications.

A biconical antenna produces a linearly polarized signal, exhibits extremely low azimuth ripple, and operates over a large frequency range usually in the region of two octaves [86]. Normally the bandwidth depends upon the extent to how much transition is made towards a cone to a cylinder and its miniaturization. Commonly these antennas

can be tailored to very small size and are attractive for wideband applications where a central deployment would be the most effective means for antennas with this kind of radiation pattern. For example, a product capable of covering all the frequency bands from 800 MHz to 2.2 GHz can be packaged in a structure of 32 mm diameter by 225 mm long.[86] Fig. 75 shows a typical biconical and biconical with polarizer antenna, their radiation pattern and characteristics.

The downfall to this type of radiator is an omnidirectional pattern is given in the azimuth direction. However, this can be overcome in an array type application by fixing the array factors radiation pattern of one that is directional. Furthermore, for applications such as UAV or other aerial applications it may be more useful to modify the biconical antenna to a planar bowtie antenna.

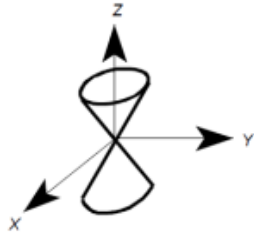

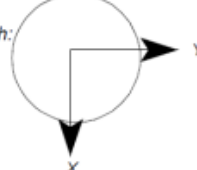
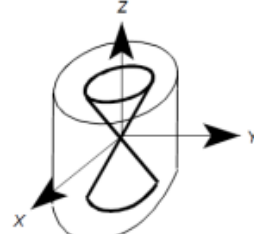

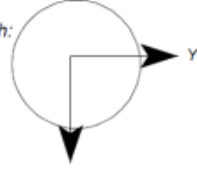
Antenna Type	Radiation Pattern	Characteristics
<p data-bbox="358 310 477 331">BICONICAL</p> 	<p data-bbox="688 323 773 344">Elevation:</p>  <p data-bbox="688 470 773 491">Azimuth:</p> 	<p data-bbox="1040 323 1208 365">Polarization: Linear, Vertical as shown</p> <p data-bbox="1040 386 1321 428">Typical Half-Power Beamwidth: 20-100 deg x 360 deg</p> <p data-bbox="1040 449 1224 470">Typical Gain: 0-4 dB</p> <p data-bbox="1040 491 1256 512">Bandwidth: 120% or 4:1</p> <p data-bbox="1040 533 1192 575">Frequency Limit: Lower: 500 MHz Upper: 40 GHz</p>
<p data-bbox="358 680 623 701">BICONICAL W/POLARIZER</p> 	<p data-bbox="688 672 773 693">Elevation:</p>  <p data-bbox="688 819 773 840">Azimuth:</p> 	<p data-bbox="1040 672 1321 714">Polarization: Circular, Direction depends on polarization</p> <p data-bbox="1040 735 1321 777">Typical Half-Power Beamwidth: 20-100 deg x 360 deg</p> <p data-bbox="1040 798 1256 819">Typical Gain: -3 to 1 dB</p> <p data-bbox="1040 840 1256 861">Bandwidth: 100% or 3:1</p> <p data-bbox="1040 882 1192 924">Frequency Limit: Lower: 2 GHz Upper: 18 GHz</p>

Fig. 75. Characteristics of a biconical and biconical w/polarizer antenna [87].

CHAPTER IX

CONCLUSION

There is an increasing demand for new frequency bands to be added to modern communications networks and because of this larger, bandwidths are desired. As these new frequency bands become available for commercial, it is more important for one to design the antenna system such that it covers all of the additional frequencies. This is important to design the antenna platform with sufficient bandwidth, so that it is capable of maintaining its performance over a fixed frequency range, but additional room for multi-functionality in modern communications. Specifically in the mobile sense this design criteria becomes very suitable for a variety of up-to-the-minute applications.

This paper has analyzed the performance of aperiodic arrays and has added a significant contribution to the literature. It has provided a comparison of the periodic array counterpart for easy comparison illustration as well. Also it has been shown under ideal conditions the directivity of aperiodic array are capable of achieving values of order N with nice narrow beams, as long as the antenna are located sparsely enough. In addition, it has been shown a volumetric array being spherical will on average produce lower sidelobes than its two-dimensional circular counterpart does. Lastly, a number of open issues remain, such that beamforming from a destination in rapid motion creates challenges causing channel suffering and severe multipath fading. Consequently, algorithms ought to be developed for frequency offset correction as well as methods for initial phase or location estimation.

Overall Circular and spherical random arrays were first looked at by Panicali and

Lo In the early 70's. They believed "no particular element arrangement on the circle or sphere of a random array could result in mathematical simplicity, thereby leading to a closed form solution except for the special case of very small element spacing's where some approximate solution could be found." Mathematical simplicity actually does exist for the circular and spherical random array. This simplicity was used to formulate simple closed form solutions. The newly derived theory makes understanding random arrays simple. Last of all the derivations of a random array are shown such that the topic traces back to its origins very easily.

REFERENCES

- [1] I. Kocaman, "Distributed beamforming in a swarm UAV network," M.S. thesis, Dept. Elect. Eng., Naval Postgraduate School, Monterey, CA, 2008.
- [2] Y. Loke, "Sensor synchronization, geolocation and wireless communication in a shipboard opportunistic array," M.S. thesis, Dept. Elect. Eng., Naval Postgraduate School, Monterey, CA, 2006.
- [3] C. M. Chan, "Distributed beamforming in man portable communication networks," M.S. thesis, Dept. Elect. Eng., Naval Postgraduate School, Monterey, CA, 2007.
- [4] E. C. Yeo, "Wirelessly networked opportunistic digital phased array: System analysis and development of a 2.4 GHZ Demonstrator," M.S. thesis, Dept. Elect. Eng., Naval Postgraduate School, Monterey, CA, 2006.
- [5] W. F. Young, "Measurements of randomly placed wireless transmitters used as an array for receivers located within the array volume with application to emergency responders," *IEEE Trans. Antennas Propag. Mag.*, vol. 57, no. 1, pp. 241-247, Jan. 2009.
- [6] K. Buchanan and G. Huff, "A comparison of geometrically bound random arrays in Euclidean space," *IEEE Antennas and Propag. Society Int. Symp.*, Spokane, WA, 2011,
- [7] H. Ochiai, "On the effects of phase estimation errors on collaborative beamforming in wireless ad hoc networks," *Proc. of Acoustics, Speech, and Signal Proc.*, vol. 53, no. 11, pp. 4110 – 4124, Nov. 2005.

- [8] H. Ochiai, "Variable-rate two-phase collaborative communication protocols for wireless networks," *IEEE Transactions on Information Theory*, vol. 52, no. 9, pp. 4299, Sept. 2006.
- [9] H. Ochiai, "Collaborative beamforming for distributed wireless ad hoc sensor networks," *IEEE Transactions on Signal Processing*, vol. 53, no. 11, pp. 4110, Nov. 2005.
- [10] M. F. A. Ahmed and S. A. Vorobyov, "Performance characteristics of collaborative beamforming for wireless sensor networks with Gaussian distributed sensor nodes," *Proc. of Acoustics Speech and Signal Proc.*, pp. 3249-3252, Mar. 2008.
- [11] M. F. A. Ahmed and S. A. Vorobyov, "Beampattern random behavior in wireless sensor networks with Gaussian distributed sensor nodes," in *Canadian Conference on Electrical and Computer Engineering*, Niagara Falls, ON, 2008, pp. 257-260.
- [12] M. F. A. Ahmed and S. A. Vorobyov, "Collaborative beamforming for wireless sensor networks with Gaussian distributed sensor nodes," *IEEE Transactions on Wireless Communications*, vol. 8, no. 2, pp. 638-643, Feb. 2009.
- [13] M. F. A. Ahmed and S. A. Vorobyov, "Node selection for sidelobe control in collaborative beamforming for wireless sensor networks," *Signal Processing Advances in Wireless Comm.*, Perugia, 2009, pp. 519-523.

- [14] M. F. A. Ahmed and S. A. Vorobyov, "Sidelobe control in collaborative beamforming via node selection," *IEEE Trans. on Signal Proc.*, vol. 58, no. 12, pp. 6168-6180, Dec. 2010.
- [15] J. T. Bernhard, "Wideband random phased arrays: theory and design," in *Wideband and Multi-band Antennas and Arrays, 2005. IEE* (Ref. No. 2005/11059), pp. 89-93, Sept. 2005
- [16] K. C. Kerby and J. T. Bernhard, "Sidelobe level and wideband behavior of arrays of random subarrays," *IEEE Antennas and Propag.*, vol. 54, no. 8, pp. 2253, Aug. 2006.
- [17] K. C. Kerby and J. T. Bernhard, "Correction to sidelobe level and wideband behavior of arrays of random subarrays," *IEEE Antennas and Propag*, vol. 55, no. 1, pp. 250, Jan. 2007.
- [18] Z. Huseyin-Arslan and M. D. Benedetto, *Ultra Wideband Wireless Communication*. London, UK: Wiley, (2005).
- [19] M. Lanne, "Wideband Array Antenna System Development," in *Phased Array Systems and Technology Int. Symp.*, pp. 789, Oct. 2010.
- [20] W. Liu, *Wideband Beamforming Concepts and Techniques*. London, UK: Wiley, 2010.
- [21] B. Svensson and Y. Jensen, "Verification of a large broadband electronically scanned array aperture," in *Proc. of the Fourth European Conf. in Antennas and Propag.*, Spain, pp. 1-3, Apr. 2010.

- [22] S. W. Ellingson, "Beamforming and interference canceling with very large wideband arrays," *IEEE Antennas and Propagation*, vol. 51, pp. 1338-1346, Jun. 2003.
- [23] P. Saengudomlert and V. W. S. Chan, "Hybrid optical and electronic signal processing for ultra-wideband RF antenna arrays," in *IEEE Int. Conf. in Communications*, 2005, pp. 2063-2069.
- [24] L. C. Godara, "Application of antenna arrays to mobile communications. II. Beam-forming and direction-of-arrival considerations," *Proc. of the IEEE*, vol. 85, no. 8, pp. 1195, Apr. 1997.
- [25] L. C. Godara, "Applications of antenna arrays to mobile communications. I. Performance improvement, feasibility, and system considerations," *Proc. of the IEEE*, vol. 85, no 7, pp. 1031, Jul. 1997.
- [26] M. Andreassen, "Linear arrays with variable interelement spacings," *IEEE Antennas and Propag.*, vol. 10, no.2, pp. 137, Mar. 1962.
- [27] F. Anderson, "Ultra-wideband beamforming in sparse arrays," *IEEE Proc. Microw. Antennas and Propag.*, vol. 153, no.4, pp. 342, Aug. 1991.
- [28] Y. Lo, "A spacing weighted antenna array," in *IRE International Convention Record*, Urbana, IL., 1962, pp. 191-195.
- [29] Y. Lo, "Sidelobe level in nonuniformly spaced antenna arrays," *IEEE Antennas and Propag.*, vol. 11, no. 4, pp. 511, 1963.
- [30] Y. Lo, "A probabilistic approach to the design of large antenna arrays," *IEEE Antennas and Propagation*, vol. 11, no. 1, pp. 95-96, 1963.

- [31] Y. Lo, "A mathematical theory of antenna arrays with randomly spaced elements," *IEEE Antennas and Propag.*, vol. 12, pp. 257-268, 1964.
- [32] V. Agrawal and L. Yuen, "Mutual coupling in phased arrays of randomly spaced antennas," *IEEE Antennas and Propag.*, vol. 20, no. 3, pp. 288-295, 1972.
- [33] V. D. Agrawal and Y. T. Lo, "Distribution of sidelobe level in random arrays," *Proc. of the IEEE*, vol. 57, no. 10, pp. 1764-1765, Oct. 1969.
- [34] A. Maffett, "Array factors with nonuniform spacing parameter," *IRE Antennas and Propag.*, vol. 10, no. 2, pp. 131-136, Mar. 1962.
- [35] D. King, R. Packard, and R. Thomas, "Unequally-spaced, broad-band antenna arrays," *IEEE Trans. Antennas Propag.*, vol. 8, no. 4, pp. 380-384, Jul. 1960.
- [36] G. Swenson, Jr. and Y. Lo, "The University of Illinois radio telescope," *Trans. Antennas and Propag.*, vol. 9, no. 1, pp. 9-16, Jan. 1961.
- [37] Y. Lo and R. Simcoe, "An experiment on antenna arrays with randomly spaced elements," *IEEE Trans. Antennas Propag.*, vol. 15, pp. 231-235, 1967.
- [38] K. C. Kerby and J. T. Bernhard, "Wideband periodic array of random subarrays," in *IEEE Antennas and Propag. Society Int. Symp.*, vol.1, 2006, pp. 555-558.
- [39] J. T. Bernhard, "Development of wideband random phased arrays composed of modified canted sector antennas," in *Wireless Communications and Applied Comp. Electromagnetics Int. Conf*, pp. 229-232, 2005.

- [40] M. C. Viganò, G. Toso, P. Angeletti, I. E. Lager, A. Yarovoy, D. Caratelli, "Sparse antenna array for earth-coverage satellite applications," in *Proc. of the Fourth European Conf. on Antennas and Propag.*, 2010.
- [41] M.C. Viganò, G. Caille, G. Toso, C. Mangenot, I.E. Lager, "Sparse planar array synthesis technique for satellite applications," in *Antennas and Propagation Society Int. Symp.*, Toronto, ON, 2010, pp. 1-4.
- [42] P. Steinmann; J. M. R. Weaver, "Nanometer-scale gaps between metallic electrodes fabricated using a statistical alignment technique," *Applied Phys. Letters*, vol.86, no.6, pp.63104-63104, Feb. 2005.
- [43] M. Rattan, M. Patterh, B.S. Sohi (2008, Jan.), *Antenna Array Optimization Using Evolutionary Approaches* [Online]. Available: <http://redshift.vif.com>
- [44] G.H. Huff; T.L. Roach;, "Stripline-based spiral antennas with integrated feed structure, impedance transformer, and Dyson-style balun," in *Antennas and Propag. Int. Symp.*, Honolulu, HI, 2007, pp. 2698-2701.
- [45] J. Dyson, "The equiangular spiral antenna," in *Proc. of Antenna Applications Symp.*, Monticello, IL, vol. ECM, October 1955, pp. 1 – 12.
- [46] Kaiser, J.A.: 'The Archimedean two-wire spiral antenna', *IRE Transactions on Antennas and Propagation*, vol. 8, pp. 312–323, May 1960.
- [47] P. E. Mayes, "Frequency-independent antennas and broad-band derivatives thereof," *Proc. of the IEEE*, vol. 80, pp. 103 – 112, January 1992.

- [48] R. Gunnarsson, T. Martin, A. Ouacha, "Wide-band circular antenna arrays consisting of bicone, semi bicone or bowtie elements," in *APMC Microw. Conf.*, Yokohama, 2006, pp.2074-2077.
- [49] H. Wheeler, "The radiation resistance of an antenna in an Infinite Array or Waveguide," *Proc. of the IRE*, vol.36, no.4, pp. 478- 487, Apr. 1948.
- [50] H. Wheeler, "Simple relations derived from a phased-array antenna made of an infinite current sheet," *Trans. Antennas and Propag.*, vol.13, no.4, pp. 506- 514, 1965.
- [51] D. Pozar, "General relations for a phased array of printed antennas derived from infinite current sheets," *Trans. Antennas and Propag.*, vol.33, no.5, pp. 498- 504, May 1985.
- [52] J. A. Kasemodel, C. Chen, J. L. Volakis, "Low-cost, planar and wideband phased array with integrated balun and matching network for wide-angle scanning," in *Antennas and Propag. Society Int. Symp.* Toronto, ON, 2010, pp.1-4.
- [53] Y. Chen, S. Yang, Z. Nie, "The role of ground plane plays in wideband phased array antenna," in *IEEE Int. Conference Ultra-Wideband (ICUWB)*, Nanjing, China , 2010, pp.1-4.
- [54] L. M. Hilliard, et al., "Lightweight linear broadband antennas enabling small UAV wing systems and space flight nanosat concept," in *Proc. IEEE Int. Geoscience and Remote Sensing Symposium*, Anchorage , AK., 2004, pp. 3577-3580 vol.5.

- [55] Y. Bar-Ness and A. Haimovich, "Synthesis of random antenna array patterns with prescribed nulls," *Trans. Antennas and Propag.*, vol. 32, no. 12, pp. 1298-1307, 1984.
- [56] A. Trucco and F. Repetto, "A stochastic approach to optimizing the aperture and the number of elements of an aperiodic array," in *OCEANS Prospects for the 21st Century*, Fort Lauderdale, FL, 1996, pp. 1510-1515.
- [57] C. Wai, "Distributed beamforming in wireless sensor networks" M.S. thesis, Dept. Elect. Eng., Naval Postgraduate School, Monterey, CA, 2004.
- [58] A. Panicali and L. Yuen, "A probabilistic approach to large circular and spherical arrays," *Trans. Antennas and Propag.*, vol. 17, no.4, pp. 514-522, Jul. 1969.
- [59] T. A. Dzekov and R. S. Berkowitz, "Parameters of a spherical random antenna array," *Electronics Letters*, vol. 14, pp. 495-496, 1978.
- [60] D. Yavuz, "Frequency Response and Bandwidth of a Spherical Random Array," *Electronics Letters*, vol. 15, pp. 314-315, 1979.
- [61] D. Yavuz, "Frequency and Focal Region Properties of Random Sparse Arrays," *Trans. Antennas and Propag.*, vol. 32, pp. 456-465, 1984.
- [62] A. Fereidountabar, "Wide-bandformer with integrated antennas," *Trans. on Communications, WSEAS*, vol. 8, no. 2, Feb. 2009.
- [63] M. Hussain, A. S. Al-Zayed, "Aperture-sparsity analysis of ultrawideband two-dimensional focused array," *Trans. Antennas and Propag.*, vol. 56, no.7, pp.1908-1918, July 2008

- [64] P. K. Weber, "Optimization of random sparse 2-D transducer arrays for 3-D electronic beam steering and focusing," in *IEEE Ultrasonics Symp.*, vol. 3, no. 3, pp. 1503-1506, Nov. 1994.
- [65] C. A. Balanis, *Antenna Theory: Analysis and Design 3 ed.* New York: John Wiley & Sons, Inc., 2005.
- [66] B. I. Raju and C. S. Hall, "Space-filling, aperiodic array ultrasonic therapy transducers," in *Ultrasonics Symposium, 2008. IUS 2008. IEEE, 2008*, pp. 463-466.
- [67] R. E. Blahut, *Theory of Remote Image Formation.* New York: Cambridge University Press, 2004.
- [68] L. C. Andrews, *Special Functions for Engineers and Applied Mathematicians.* New York: MacMilan, 1986.
- [69] Y. L. Luke, *The Special Functions and Their Approximations vol. 1.* New York: Academic Press, 1969.
- [70] W. N. Bailey, *Generalized Hypergeometric Series.* New York: Stechert-Hafner Service Agency, 1964.
- [71] I. S. Gradshteyn, *Table of Integrals Series and Products vol. 7.* New York: Academic Press, 2007.
- [72] Q. Cao, "Generalized Jinc functions and their application to focusing and diffraction of circular apertures," *Opt. Soc. Am. A*, vol. 20, 2003.
- [73] G. N. Watson, *A Treatise on the Theory of Bessel Functions.* London: Cambridge University Press, 1922.

- [74] Wolfram. (2007). Generalized Cases for Powers of Spherical Bessel. Available: <http://functions.wolfram.com/Bessel-TypeFunctions/SphericalBesselJ/26/02/20/>
- [75] I. S. Eduardo, I. Guendelman, G. Cantatore, and K. Zioutas, "Photon production from the scattering of axions out of a solenoidal magnetic field," *Journal of Cosmology and Astroparticle Physics*, vol. 1, pp. 1-19, 2010.
- [76] J. N. Newman and W. Frank, "An integral containing the square of a bessel function," *American Mathematical Society*, vol. 17, pp. 64-70, 1963.
- [77] C. W. Qiu, "On the integral identities consisting of two spherical bessel functions," *Trans. Antennas and Propag*, vol. 55, pp. 240-244, 2007.
- [78] M. Donvito and S. Kassam, "Characterization of the random array peak sidelobe," *Trans. Antennas and Propag.*, vol. 27, pp. 379-385, 1979.
- [79] D. L. Jaggard, A. Jaggard, and O. Manuar, "Fractal Random Arrays," NSF/AMP, Summer Undergraduate Research.
- [80] D. L. Sengupta, "Azimuth and elevation direction finder study," Fort Monmouth United States Army Electronics Command 1965.
- [81] W. Richards and L. Yuen, "Antenna pattern synthesis based on optimization in a probabilistic sense," *IEEE Transactions on Antennas*, vol. 23, pp. 165-172, 1975.
- [82] B. Tomasic, "Spherical arrays - design considerations," in. Applied Electromagnetics and Communications, 2005. ICECom 2005. *18th International Conference on*, 2005, pp. 1-8.

- [83] L. Marantis, "Comparison of various spherical antenna array element distributions," in *3rd European Conference on, Antennas and Propagation*, 2009. EuCAP 2009. 2009, pp. 2980-2984.
- [84] G. D. Ouderkirk, "Geodesic dome phased array radars," in *Radar Conference*, IEEE, 2007, pp. 431-436.
- [85] R. Goossens, "Phase-mode processing for spherical antenna arrays with a finite number of antenna elements and including mutual coupling," *IEEE Transactions on Antennas and Propagation*, vol. 57, pp. 3783-3790, 2009.
- [86] C. Walker (2007, Jan.), the Use of Broadband Antenna Technology in Modern Communication Systems [Online]. Available: <http://digital-transmissions.co.uk/2007-01defencebroadband.html>
- [87] Granite Island Group, Radiation patterns [Online]. Available: <http://www.tscm.com/radiapat.pdf>, Feb. 2011.

APPENDIX A

INTEGRAL IDENTITIES

$$\int_{x_1}^{x_2} dx = x_2 - x_1 \quad (\text{A.1.1})$$

$$\int_{-1}^1 \int_{-1}^1 \cos(\alpha(x_n - x_m)) dx_n dx_m = \left| \frac{2 \sin \alpha}{\alpha} \right|^2 = |2 \text{sinc}(\alpha)|^2 \quad (\text{A.1.2})$$

$$\int_{-1}^1 \int_{-1}^1 \sin \alpha x_n \sin \alpha x_m dx_n dx_m = 0 \quad (\text{A.1.3})$$

$$\int_{-1}^1 \int_{-1}^1 \int_{-1}^1 \int_{-1}^1 (\cos(\alpha(x_n - x_m) + \beta(\theta, \phi)(x_n - x_m))) dx_n dx_m dx_n dx_m = \left| 2 \frac{\sin \alpha}{\alpha} \right|^2 \left| 2 \frac{\sin \beta}{\beta} \right|^2 = |2 \text{sinc} \alpha|^2 |2 \text{sinc} \beta|^2 \quad (\text{A.1.4})$$

$$\frac{2}{\pi} \int_{-1}^1 \sqrt{1-x_n^2} dx_n = 1 \quad (\text{A.1.5})$$

$$J_\nu(z) = \frac{\left(\frac{z}{2}\right)^\nu}{\Gamma\left(\nu + \frac{1}{2}\right)\Gamma\left(\frac{1}{2}\right)} \int_{-1}^1 (1-t^2)^{\nu-1/2} \cos(zt) dt \quad \text{Re } \nu > -\frac{1}{2} \quad (\text{Table of Integrals and Series 912\#8}) \quad (\text{A.1.6})$$

$$\frac{2}{\pi} \int_{-1}^1 (1-x^2)^{1/2} \cos(xt) dx = \frac{2J_1(x)}{x} = 2 \text{jinc}(x) \quad (\text{A.1.7})$$

$$\int_{-\pi}^{\pi} e^{-j(n\tau - \tau \sin \tau)} d\tau = 2\pi J_n \quad (\text{A.1.8})$$

$$J_{2n}(x) = \frac{2}{\pi} \int_0^{\pi/2} \cos(x \sin \phi) \cos(2n\phi) d\phi \quad (\text{A.1.9})$$

$$\int_{-\pi}^{\pi} e^{-j4\pi A \sin\left(\frac{\phi}{2}\right)(x_n - x_m)} d\phi = 2\pi J_0(4\pi A(x_n - x_m)) \quad (\text{Using A.1.8}) \quad (\text{A.1.10})$$

$$\Gamma(x) = \int_0^{\infty} x^{x-1} e^{-z} dz \quad (\text{A.1.11})$$

$$\frac{1}{2} \beta(x, y) = \frac{\Gamma(x)\Gamma(y)}{2\Gamma(x+y)} = \int_0^{\pi/2} \cos^{2x-1}(\theta) \sin^{2y-1}(\theta) d\theta \quad (\text{A.1.12})$$

$$\int_0^\pi \left(\sin \frac{\phi}{2}\right)^{2m} d\phi = \int_{-\pi}^0 \left(\sin \frac{\phi}{2}\right)^{2m} d\phi = \frac{\sqrt{\pi}\Gamma\left(m+\frac{1}{2}\right)}{\Gamma(m+1)} \quad (\text{A.1.13})$$

$$\int_{-\pi}^\pi \sin^{2m}(\theta)d\theta = \frac{4\sqrt{\pi}\Gamma\left(m+\frac{1}{2}\right)}{2\Gamma(m+1)} = \frac{2\sqrt{\pi}\Gamma\left(m+\frac{1}{2}\right)}{\Gamma(m+1)} \quad (\text{A.1.14})$$

$$\begin{aligned} \int_{-\pi}^\pi \left(2\text{jinc}\left(x \sin \frac{\phi}{2}\right)\right)^2 d\phi &= \sum_{m=0}^\infty 2^3 \frac{\Gamma\left(m+\frac{1}{2}\right)\Gamma\left(m+\frac{3}{2}\right)}{\Gamma(m+3)\Gamma(m+2)\Gamma(m+1)} \frac{(-1x^2)^m}{m!} \\ &= \sum_{m=0}^\infty 8 \frac{\pi}{4} \frac{\left(\frac{1}{2}\right)^{(m)} \left(\frac{3}{2}\right)^{(m)}}{(1)^{(m)} (2)^{(m)} (3)^{(m)}} \frac{(-1x^2)^m}{m!} = 2\pi {}_2F_3\left(\frac{1}{2}, \frac{3}{2}; 1, 2, 3; -(x^2)\right) \end{aligned} \quad (\text{A.1.15})$$

$$\int_x^\infty \frac{1}{\sqrt{2\pi}} e^{-\frac{x^2}{2}} = Q(x) \quad (\text{A.1.16})$$

$$\int_{-\infty}^\infty e^{j\alpha z} \frac{1}{\sqrt{2\pi\sigma}} e^{-\frac{z^2}{2\sigma^2}} dz = e^{-\frac{\alpha^2\sigma^2}{2}} \quad (\text{A.1.17})$$

$$\int_{-\pi}^\pi \left| e^{-\left(8\pi^2 \sin^2\left(\frac{\phi}{2}\right)\right)\sigma^2} \right|^2 d\phi = 2\pi {}_1F_1\left(\frac{1}{2}; 1; -(2\pi\sigma)^2\right) \quad (\text{A.1.18})$$

$$\int_{-L}^L e^{-j\alpha x} \frac{1}{\sqrt{2\pi\sigma}} e^{-\frac{x^2}{2\sigma^2}} dx = e^{-\frac{\alpha^2\sigma^2}{2}} \left[\text{erf}\left(\frac{L-j\alpha\sigma^2}{\sqrt{2}\sigma}\right) + \text{erf}\left(\frac{L+j\alpha\sigma^2}{\sqrt{2}\sigma}\right) \right] \quad (\text{A.1.19})$$

$$\frac{2}{\pi} \int_{-1}^1 \sqrt{1-x^2} \sin(x\alpha) dx = 0 \quad (\text{A.1.20})$$

$$\frac{2}{\pi} \int_{-1}^1 \left(\sqrt{1-x^2}\right) \cos^2(x\alpha) dx = \frac{1}{2} \left(1 + \frac{J_1(2\alpha(\phi))}{\alpha(\phi)} \right) \quad (\text{A.1.21})$$

$$\frac{2}{\pi} \int_{-1}^1 \sqrt{1-x^2} \sin^2(x\alpha) dx = \frac{1}{2} \left(1 - \frac{J_1(2\alpha)}{\alpha} \right) \quad (\text{A.1.22})$$

$$-\frac{2}{\pi} \int_{-1}^1 \sqrt{1-z^2} z^2 dz = -\frac{1}{4} \quad (\text{A.1.23})$$

$$\int_{\left(\frac{-\phi_k}{2}\right)}^{\left(\frac{\phi_k}{2}\right)} 2 \operatorname{jinc}\left(4\pi A \sin\left(\frac{\phi - \delta\phi_k}{2}\right)\right) \frac{1}{2\phi_k} d\delta\phi_k = \quad (\text{A.1.24})$$

$$\frac{1}{2}\left(1 - \frac{\phi}{\phi_k}\right) {}_1F_2\left(\frac{1}{2}; \frac{3}{2}, 2; -(\pi A(\phi - \phi_k))^2\right) + \frac{1}{2}\left(1 + \frac{\phi}{\phi_k}\right) {}_1F_2\left(\frac{1}{2}; \frac{3}{2}, 2; -(\pi A(\phi + \phi_k))^2\right)$$

$$\int_{-1}^1 (1-t^2) \cos(xt) dt = \frac{2^{3/2} \sqrt{\pi} J_{3/2}(x)}{x^{3/2}} = 3 \frac{J_1(x)}{x} = 3 \operatorname{tinc}(x) \quad (\text{A.1.25})$$

$$\int_{-\pi}^{\pi} \left(\frac{J_1(z)}{z}\right)^2 d\phi = \frac{2\pi}{45} \left[-6 {}_1F_2\left(\frac{1}{2}; 3, \frac{7}{2}; -(4\pi \tilde{R})^2\right) + {}_1F_2\left(\frac{1}{2}; 4, \frac{7}{2}; -(4\pi \tilde{R})^2\right) \right] \quad (\text{A.1.26})$$

$$\frac{3}{4} \int_{-1}^1 (1-x^2) \cos^2(x\alpha) dx = \frac{1}{2} \left(1 + \frac{3}{2} \frac{J_1(2\alpha)}{\alpha} \right) \quad (\text{A.1.27})$$

$$\frac{J_{3/2}(2x)}{(x)^{3/2}} = \frac{1}{\sqrt{\pi}} \int_{-1}^1 (1-t^2) \cos(2xt) dt \quad (\text{A.1.28})$$

$$\int_{-1}^1 (1-x^2) \sin^2(x\alpha) dx = \frac{1}{2} \left(1 - \frac{3}{2} \frac{J_1(2\alpha)}{\alpha} \right) \quad (\text{A.1.29})$$

$$-\frac{3}{4} \int_{-1}^1 (1-v^2) v^2 dv = -\frac{3}{4} \int_{-\pi/2}^{\pi/2} \cos^3(u) \sin^2(u) du = -\frac{1}{5} \quad (\text{A.1.30})$$

$$\begin{aligned} \frac{1}{64} \int_{-1}^1 \int_{-1}^1 \int_{-1}^1 \int_{-1}^1 \int_{-1}^1 \int_{-1}^1 \cos(\alpha(x_n - x_m) + \beta(y_n - y_m) + \chi(z_n - z_m)) dx_n dx_m dy_n dy_m dz_n dz_m \\ = |\operatorname{sinc}(x)|^2 |\operatorname{sinc}(y)|^2 |\operatorname{sinc}(z)|^2 \end{aligned} \quad (\text{A.1.31})$$

APPENDIX B

SUMMATION IDENTITIES

$$\sum_{m=1}^N \sum_{\substack{n=1 \\ n \neq m}}^N e^{j\alpha(x_n - x_m)} = N(N-1) \cos(\alpha(x_n - x_m)) \quad (\text{B.1.1})$$

$$\sum_{m=1}^N \sum_{\substack{n=1 \\ n \neq m}}^N e^{j\alpha(x_n - x_m)} e^{j\beta(y_n - y_m)} = N(N-1) \cos(\alpha(x_n - x_m) + \beta(y_n - y_m)) \quad (\text{B.1.2})$$

$$\sum_{m=1}^N \sum_{\substack{n=1 \\ n \neq m}}^N e^{j\alpha(x_n - x_m)} e^{j\beta(y_n - y_m)} e^{j\chi(z_n - z_m)} = N(N-1) \cos(\alpha(x_n - x_m) + \beta(y_n - y_m) + \chi(z_n - z_m)) \quad (\text{B.1.3})$$

APPENDIX C

TRIGONOMETRIC IDENTITIES

1. Sum or difference:

$$\sin(x + y) = \sin x \cos y + \cos x \sin y \quad (\text{C.1.1})$$

$$\sin(x - y) = \sin x \cos y - \cos x \sin y \quad (\text{C.1.2})$$

$$\cos(x + y) = \cos x \cos y - \sin x \sin y \quad (\text{C.1.3})$$

$$\cos(x - y) = \cos x \cos y + \sin x \sin y \quad (\text{C.1.4})$$

$$\tan(x + y) = \frac{\tan x + \tan y}{1 - \tan x \tan y} \quad (\text{C.1.5})$$

$$\tan(x - y) = \frac{\tan x - \tan y}{1 + \tan x \tan y} \quad (\text{C.1.6})$$

$$\sin^2 x + \cos^2 x = 1 \quad (\text{C.1.7})$$

$$\tan^2 x - \sec^2 x = -1 \quad (\text{C.1.8})$$

$$\cot^2 x - \csc^2 x = 1 \quad (\text{C.1.9})$$

2. Sum or difference into products

$$\sin x + \sin y = 2 \sin \frac{1}{2}(x + y) \cos \frac{1}{2}(x - y) \quad (\text{C.1.10})$$

$$\sin x - \sin y = 2 \cos \frac{1}{2}(x + y) \sin \frac{1}{2}(x - y) \quad (\text{C.1.11})$$

$$\cos x + \cos y = 2 \cos \frac{1}{2}(x + y) \cos \frac{1}{2}(x - y) \quad (\text{C.1.12})$$

$$\cos x - \cos y = -2 \cos \frac{1}{2}(x + y) \sin \frac{1}{2}(x - y) \quad (\text{C.1.13})$$

3. Products into sum or difference:

$$2 \sin x \cos y = \sin(x+y) + \sin(x-y) \quad (\text{C.1.14})$$

$$2 \cos x \sin y = \sin(x+y) - \sin(x-y) \quad (\text{C.1.15})$$

$$2 \cos x \cos y = \cos(x+y) + \cos(x-y) \quad (\text{C.1.16})$$

$$2 \sin x \sin y = -\cos(x+y) + \cos(x-y) \quad (\text{C.1.17})$$

4. Double and half angles

$$\sin 2x = 2 \sin x \cos x \quad (\text{C.1.18})$$

$$\cos 2x = \cos^2 x - \sin^2 x = 2 \cos^2 x - 1 = 1 - 2 \sin^2 x \quad (\text{C.1.19})$$

$$\tan 2x = \frac{2 \tan x}{1 - \tan^2 x} \quad (\text{C.1.20})$$

$$\sin \frac{1}{2}x = \pm \sqrt{\frac{1 - \cos x}{2}} \quad \text{or} \quad 2 \sin^2 x \quad \text{or} \quad 1 - \cos 2x \quad (\text{C.1.21})$$

$$\cos \frac{1}{2}x = \pm \sqrt{\frac{1 + \cos x}{2}} \quad \text{or} \quad 2 \cos^2 x \quad \text{or} \quad 1 + \cos 2x \quad (\text{C.1.22})$$

$$\tan \frac{1}{2}x = \pm \sqrt{\frac{1 - \cos x}{1 + \cos x}} = \frac{\sin x}{1 + \cos x} = \frac{1 - \cos x}{\sin x} \quad (\text{C.1.23})$$

5. Series

$$\sin x = \frac{e^{jx} - e^{-jx}}{2j} = x - \frac{x^3}{3!} + \frac{x^5}{5!} - \frac{x^7}{7!} + \dots \quad (\text{C.1.24})$$

$$\cos x = \frac{e^{jx} + e^{-jx}}{2} = 1 - \frac{x^2}{2!} + \frac{x^4}{4!} - \frac{x^6}{6!} + \dots \quad (\text{C.1.25})$$

$$\tan x = \frac{e^{jx} - e^{-jx}}{j(e^{jx} + e^{-jx})} = x + \frac{x^3}{3!} + \frac{2x^5}{15} + \frac{17x^7}{315} + \dots \quad (\text{C.1.26})$$

APPENDIX D

SPECIAL FUNCTIONS

$$(2m)! = (2m-1)!!m!2^m = \frac{\Gamma\left(m + \frac{1}{2}\right)m!2^{2m}}{\sqrt{\pi}} \quad (\text{D.1.1})$$

$$(2m-1)!! = \frac{\Gamma\left(m + \frac{1}{2}\right)2^m}{\sqrt{\pi}} \quad (\text{D.1.2})$$

$$(2m+2) = \frac{(2m+2)!\sqrt{\pi}}{2^{2m+1}m!\Gamma\left(m + \frac{3}{2}\right)} \quad (\text{D.1.3})$$

$$\Gamma(m+2) = (m+1)m! \quad (\text{D.1.4})$$

$$x^{(n)} = \frac{\Gamma(x+n)}{\Gamma(x)} \quad (\text{D.1.5})$$

$$\beta(x, y) = \frac{\Gamma(x)\Gamma(y)}{\Gamma(x+y)} \quad (\text{D.1.6})$$

$$e^{jx \cos \theta} = \sum_{n=-\infty}^{\infty} j^n J_n(x) e^{jn\theta} \quad (\text{D.1.7})$$

$$J_p(\alpha(\phi)) \approx \sqrt{\frac{2}{\pi\alpha(\phi)}} \cos\left(\alpha(\phi) - \frac{\pi}{4} - \frac{p\pi}{2}\right) \quad (\text{D.1.8})$$

$$J_{-n}(x) = (-1)^n J_n(x) \quad (\text{D.1.9})$$

$$\left\{ e^{j\left(\frac{\pi}{2}-\xi\right)IN} + e^{j\left(\frac{\pi}{2}+\xi\right)IN} \right\} = j^{IN} \left\{ e^{jIN\xi} + e^{-jIN\xi} \right\} = 2j^{IN} \cos(IN\xi) \quad (\text{D.1.10})$$

$$J_1^2(z) = \sum_{m=0}^{\infty} \frac{(-1)^m (2m+2)! \left(\frac{z}{2}\right)^{2m+2}}{m!(m+2)!((m+1)!)^2} \quad (\text{Frank and Newman Source}) \quad (\text{D.1.11})$$

$$\frac{J_1(2x)}{x} = \frac{2}{\pi} \int_{-1}^1 (1-t^2)^{1/2} \cos(2xt) dt \quad (\text{D.1.12})$$

$$\frac{J_1(2\alpha)}{\alpha} = {}_0\bar{F}_1(;2;-\alpha^2) \quad (\text{D.1.13})$$

$$J_n(z) = \sum_{k=0}^{\infty} \left(\frac{\left(\frac{z}{2}\right)^{2k+1}}{\Gamma(n+1)(n+k)!} \right) = \sum_{k=0}^{\infty} \left(\frac{\frac{z}{2}}{\Gamma(n+1)} {}_0F_1\left(n+1; \frac{-z^2}{4}\right) \right) \quad (\text{D.1.14})$$

$$\frac{J_1(2x)}{x} = \frac{1}{\Gamma(2)} {}_0F_1(2; -x^2) \quad (\text{D.1.15})$$

$$Q(-x) = 1 - Q(x) \quad (\text{D.1.16})$$

$$Q(x) = \frac{1}{2} - \frac{1}{2} \operatorname{erf}\left(\frac{x}{\sqrt{2}}\right) \quad (\text{D.1.17})$$

$$j_\nu(z)^2 = \frac{\sqrt{\pi}}{2} G_{1,3}^1 \left(z, \frac{1}{2} \middle| \nu, -\frac{1}{2}, -\nu-1 \right) \quad (\text{D.1.18})$$

$$G_{p,q}^{m,n} \left(x, r \middle| \nu, -\frac{1}{2}, -\nu-1 \right) = \frac{1}{2\pi j} \int_l \frac{\prod_{j=1}^m [\Gamma(b_j + s)] \prod_{j=1}^n [\Gamma(1 - a_j - s)]}{\prod_{j=n+1}^p [\Gamma(a_j + s)] \prod_{j=m+1}^q [\Gamma(1 - b_j - s)]} z^{-s/r} ds \quad (\text{D.1.19})$$

$$\frac{j_1(z)^2}{z^2} = \frac{(1+z^2 - \cos(2z) + z^2 \cos(2z) - 2z \sin(2z))}{2z^6} \quad (\text{D.1.20})$$

$$J_{3/2}(\alpha) = \sqrt{\frac{2\alpha}{\pi}} j_1(\alpha) \quad (\text{D.1.21})$$

$$j_0(x) = \frac{\sin x}{x} \quad (\text{D.1.22})$$

$$j_1(x) = \frac{\sin x}{x^2} - \frac{\cos x}{x} \quad (\text{D.1.23})$$

$$j_2(x) = \left(\frac{3}{x^3} - \frac{1}{x} \right) \sin x - \frac{3}{x^2} \cos x \quad (\text{D.1.24})$$

$${}_0\bar{F}_1(b; z) = \sum_{k=0}^{\infty} \frac{(z)^k}{\Gamma(k+b)(b)^k k!} \quad (\text{D.1.25})$$

APPENDIX E

VECTOR IDENTITIES

E.1 Rectangular Coordinates

$$\bar{\nabla}\psi = \hat{a}_x \frac{\partial\psi}{\partial x} + \hat{a}_y \frac{\partial\psi}{\partial y} + \hat{a}_z \frac{\partial\psi}{\partial z} \quad (\text{E.1.1})$$

$$\bar{\nabla} \cdot \bar{A} = \frac{\partial A_x}{\partial x} + \frac{\partial A_y}{\partial y} + \frac{\partial A_z}{\partial z} \quad (\text{E.1.2})$$

$$\bar{\nabla} \times \bar{A} = \hat{a}_x \left(\frac{\partial A_z}{\partial y} - \frac{\partial A_y}{\partial z} \right) + \hat{a}_y \left(\frac{\partial A_x}{\partial z} - \frac{\partial A_z}{\partial x} \right) + \hat{a}_z \left(\frac{\partial A_y}{\partial x} - \frac{\partial A_x}{\partial y} \right) \quad (\text{E.1.3})$$

E.2 Cylindrical Coordinates

$$\bar{\nabla}\psi = \hat{a}_\rho \frac{\partial\psi}{\partial\rho} + \hat{a}_\phi \frac{1}{\rho} \frac{\partial\psi}{\partial\phi} + \hat{a}_z \frac{\partial\psi}{\partial z} \quad (\text{E.2.1})$$

$$\bar{\nabla} \cdot \bar{A} = \frac{1}{\rho} \frac{\partial}{\partial\rho} (\rho A_\rho) + \frac{1}{\rho} \frac{\partial A_\phi}{\partial\phi} + \frac{\partial A_z}{\partial z} \quad (\text{E.2.2})$$

$$\bar{\nabla} \times \bar{A} = \hat{a}_\rho \left(\frac{1}{\rho} \frac{\partial A_z}{\partial\phi} - \frac{\partial A_\phi}{\partial z} \right) + \hat{a}_\phi \left(\frac{\partial A_\rho}{\partial z} - \frac{\partial A_z}{\partial\rho} \right) + \hat{a}_z \left(\frac{1}{\rho} \frac{\partial(\rho A_\phi)}{\partial\rho} - \frac{1}{\rho} \frac{\partial A_\rho}{\partial\phi} \right) \quad (\text{E.2.3})$$

E.3 Spherical Coordinates

$$\bar{\nabla}\psi = \hat{a}_r \frac{\partial\psi}{\partial r} + \hat{a}_\theta \frac{1}{r} \frac{\partial\psi}{\partial\theta} + \hat{a}_\phi \frac{1}{r \sin\theta} \frac{\partial\psi}{\partial\phi} \quad (\text{E.3.1})$$

$$\bar{\nabla} \cdot \bar{A} = \frac{1}{r^2} \frac{\partial}{\partial r} (r^2 A_r) + \frac{1}{r \sin\theta} \frac{\partial}{\partial\theta} (A_\theta \sin\theta) + \frac{1}{r \sin\theta} \frac{\partial A_\phi}{\partial\phi} \quad (\text{E.3.2})$$

$$\bar{\nabla} \times \bar{A} = \frac{\hat{a}_r}{r \sin\theta} \left(\frac{\partial}{\partial\theta} (A_\phi \sin\theta) - \frac{\partial A_\phi}{\partial\phi} \right) + \frac{\hat{a}_\theta}{r} \left(\frac{1}{\sin\theta} \frac{\partial A_r}{\partial\phi} - \frac{\partial}{\partial r} (r A_\phi) \right) + \frac{\hat{a}_\phi}{r} \left(\frac{\partial(r A_\theta)}{\partial r} - \frac{\partial A_r}{\partial\theta} \right) \quad (\text{E.3.3})$$

APPENDIX F

PROOF OF SELECT INTEGRALS

F.1

$$\frac{1}{N} \int_{-1}^1 \int_{-1}^1 \frac{1}{2} \frac{1}{2} dx_n dx_m = \frac{1}{N} \quad (\text{Using A.1.1}) \quad (\text{F.1.1})$$

F.2

$$\int_{-1}^1 \int_{-1}^1 \cos(\alpha(x_n - x_m)) dx_n dx_m = |2\text{sinc}(\alpha)|^2 \quad (\text{A.1.2 Proof Below}) \quad (\text{F.1.2})$$

Using the identity (C.1.4) the integral of (F.1.2) reduces to

$$\int_{-1}^1 \int_{-1}^1 \cos \alpha x_n \cos \alpha x_m du_n du_m - \int_{-1}^1 \int_{-1}^1 \sin \alpha x_n \sin \alpha x_m du_n du_m$$

The integral of the cosine terms gives

$$\int_{-1}^1 \cos \alpha x_n dx_n \int_{-1}^1 \cos \alpha x_m dx_m = \left| \frac{2 \sin \alpha}{\alpha} \right|^2$$

The integral of the sine terms evaluate to zero.

$$\int_{-1}^1 \sin \alpha x_n dx_n \int_{-1}^1 \sin \alpha x_m dx_m = \int_{-1}^1 \sin \alpha x_n \left. \frac{-\cos \alpha x_m}{\alpha} \right|_{x_m=-1}^{x_m=1} = \int_{-1}^1 \sin \alpha x_n \left(\frac{-\cos \alpha}{\alpha} + \frac{\cos \alpha}{\alpha} \right) dx_n = 0$$

Thus,

$$\int_{-1}^1 \int_{-1}^1 \cos(\alpha(x_n - x_m)) dx_n dx_m = \left| \frac{2 \sin \alpha}{\alpha} \right|^2 = |2\text{sinc}(\alpha)|^2$$

F.3

$$\int_{-1}^1 \int_{-1}^1 \int_{-1}^1 \int_{-1}^1 (\cos(\alpha(x_n - x_m) + \beta(y_n - y_m))) dx_n dx_m dy_n dy_m = |2\text{sinc} \alpha|^2 |2\text{sinc} \beta|^2 \quad (\text{F.1.3})$$

Using the identities (C.1.1) -(C.1.4) the L.H.S. can be reduced as follows,

$$\begin{aligned} & \cos(\alpha(x_n - x_m) + \beta(y_n - y_m)) \\ &= \cos(\alpha(x_n - x_m)) \cos(\beta(y_n - y_m)) - \sin(\alpha(x_n - x_m)) \sin(\beta(y_n - y_m)) \end{aligned}$$

where

$$\cos(\alpha(x_n - x_m)) = \cos(\alpha x_n)\cos(\alpha x_m) - \sin(\alpha y_n)\sin(\alpha y_m)$$

$$\cos(\beta(y_n - y_m)) = \cos(\beta y_n)\cos(\beta y_m) - \sin(\beta y_n)\sin(\beta y_m)$$

$$\sin(\alpha(x_n - x_m)) = \sin(\alpha x_n)\cos(\alpha x_m) - \cos(\alpha x_n)\sin(\alpha x_m)$$

$$\sin(\beta(y_n - y_m)) = \sin(\beta y_n)\cos(\beta y_m) - \cos(\beta y_n)\sin(\beta y_m)$$

As shown in H.2 all integrals including a sin term evaluate to zero thus, the integral reduces to

$$\int_{-1}^1 \int_{-1}^1 \int_{-1}^1 \int_{-1}^1 (\cos(\alpha x_n)\cos(\alpha x_m)\cos(\beta y_n)\cos(\beta y_m)) dx_n dx_m dy_n dy_m$$

And by Appendix A.2

$$\int_{-1}^1 \int_{-1}^1 \int_{-1}^1 \int_{-1}^1 (\cos(\alpha(x_n - x_m) + \beta(y_n - y_m))) dx_n dx_m dy_n dy_m = |2\text{sinc}\alpha|^2 |2\text{sinc}\beta|^2$$

F.4

$$\left(\frac{1}{N}\right) \int_{-1}^1 \frac{2}{\pi} \sqrt{1-x_n^2} dx_n \int_{-1}^1 \frac{2}{\pi} \sqrt{1-x_m^2} dx_m = \frac{1}{N} \quad (\text{F.1.4})$$

By a change of variables the integral on the left hand side reduces as follows,

$$x_n = \sin u \quad dx_n = \cos u du$$

$$\int_{-1}^1 \sqrt{1-x_n^2} dx_n = \int_{-\frac{\pi}{2}}^{\frac{\pi}{2}} (1 - \sin^2 u)^{\frac{1}{2}} \cos u du$$

Using the identity (C.1.19) by solving for $\cos^2 u$ one obtains

$$= \int_{-\frac{\pi}{2}}^{\frac{\pi}{2}} \left(\frac{1}{2} + \frac{\cos(2u)}{2} \right) du$$

$$= \frac{u}{2} + \left(\frac{1}{2}\right) \left(\frac{1}{2}\right) \sin(2u) \Bigg|_{u=-\frac{\pi}{2}}^{u=\frac{\pi}{2}}$$

Now using the identity (C.1.18) this simplifies to

$$= \frac{u}{2} + \left(\frac{1}{2}\right) \cos u \sin u \Big|_{u=-\frac{\pi}{2}}^{u=\frac{\pi}{2}}$$

$$= \frac{\pi}{2}$$

Thus,

$$\left(\frac{1}{N}\right) \int_{-1}^1 \frac{2}{\pi} \sqrt{1-x_n^2} dx_n \int_{-1}^1 \frac{2}{\pi} \sqrt{1-x_m^2} dx_m = \frac{1}{N}$$

F. 5

$$\frac{1}{N} + \left(1 - \frac{1}{N}\right) \left[\int_{-1}^1 \int_{-1}^1 \frac{2}{\pi} \sqrt{1-x_m^2} \frac{2}{\pi} \sqrt{1-x_n^2} dx_n dx_m \right] = \frac{1}{N} + \left(1 - \frac{1}{N}\right) |2\text{jinc}(\alpha)|^2 \quad (\text{F.1.5})$$

To solve the integral identity (A.1.6) is used,

$$J_\nu(x) = \frac{\left(\frac{x}{2}\right)^\nu}{\Gamma\left(\nu + \frac{1}{2}\right) \Gamma\left(\frac{1}{2}\right)^{-1}} \int_0^1 (1-t^2)^{\nu-1/2} \cos(xt) dt \quad \text{Re } \nu > -\frac{1}{2} \text{ (Table of Integrals and Series 912\#8)}$$

With

$$\nu=1 \Rightarrow \Gamma\left(\frac{3}{2}\right) = \frac{\sqrt{\pi}}{2} \text{ and } \Gamma\left(\frac{1}{2}\right) = \sqrt{\pi}$$

or

$$J_1(x) = \left(\frac{x}{2}\right) \frac{2}{\pi} \int_{-1}^1 (1-t^2)^{1/2} \cos(xt) dt$$

Thus,

$$\frac{2J_1(x)}{x} = \frac{2}{\pi} \int_{-1}^1 (1-t^2)^{1/2} \cos(xt) dt$$

Sub-sequentially applying the given identity will reduce the integration as

$$\begin{aligned}
& \frac{1}{N} + \left(1 - \frac{1}{N}\right) \left[\int_{-1}^1 \frac{2}{\pi} \sqrt{1-x_m^2} \left\{ \frac{2}{\alpha} J_1(\alpha) \cos(\alpha x_m) \right\} dx_m \right] \\
&= \frac{1}{N} + \left(1 - \frac{1}{N}\right) \left\{ \frac{2}{\alpha} J_1(\alpha) \right\} \left[\int_{-1}^1 \frac{2}{\pi} \sqrt{1-x_m^2} \cos(\alpha x_m) dx_m \right] \\
&= \frac{1}{N} + \left(1 - \frac{1}{N}\right) \left| \frac{2}{\alpha} J_1(\alpha) \right|^2 \\
&= \frac{1}{N} + \left(1 - \frac{1}{N}\right) |2\text{jinc}(\alpha)|^2
\end{aligned}$$

F. 6

$$\int_{-\pi}^{\pi} \left(\frac{1}{N} + \frac{1}{N^2} \sum_{\substack{m=1 \\ n \neq m}}^N \sum_{n=1}^N e^{-j \sin \frac{\phi}{2} (x_n - x_m)} \right) d\phi = \frac{2\pi}{N^2} \sum_{\substack{m=1 \\ n \neq m}}^N \sum_{n=1}^N J_o(x_n - x_m) \quad (\text{F.1.6})$$

$$\int_{-\pi}^{\pi} \left(\frac{1}{N} + \frac{1}{N^2} \sum_{\substack{m=1 \\ n \neq m}}^N \sum_{n=1}^N e^{-j \sin \frac{\phi}{2} (x_n - x_m)} \right) d\phi = \frac{2\pi}{N} + \frac{1}{N^2} \sum_{\substack{m=1 \\ n \neq m}}^N \sum_{n=1}^N \int_{-\pi}^0 e^{-j \sin \frac{\phi}{2} (x_n - x_m)} d\phi + \frac{1}{N^2} \sum_{\substack{m=1 \\ n \neq m}}^N \sum_{n=1}^N \int_0^{\pi} e^{-j \sin \frac{\phi}{2} (x_n - x_m)} d\phi$$

Now for the integral on the left $-u = \frac{\phi}{2}$, $-du = \frac{1}{2} d\phi$, $-2du = d\phi$

and for the integral on the right side let $u = \frac{\phi}{2}$, $du = \frac{1}{2} d\phi$, $2du = d\phi$

$$\begin{aligned}
& \frac{2\pi}{N} + \frac{-2}{N^2} \sum_{\substack{m=1 \\ n \neq m}}^N \sum_{n=1}^N \int_{\frac{\pi}{2}}^0 e^{-j \sin u (x_n - x_m)} du + \frac{2}{N^2} \sum_{\substack{m=1 \\ n \neq m}}^N \sum_{n=1}^N \int_0^{\frac{\pi}{2}} e^{-j \sin u (x_n - x_m)} du \\
&= \frac{2\pi}{N} + \frac{2}{N^2} \sum_{\substack{m=1 \\ n \neq m}}^N \sum_{n=1}^N \int_0^{\frac{\pi}{2}} \cos(\sin u (x_n - x_m)) du
\end{aligned}$$

Now using the identity (A.1.9) with $x=1$ and $n=0$ one obtains

$$\int_{-\pi}^{\pi} \left(\frac{1}{N} + \frac{1}{N^2} \sum_{\substack{m=1 \\ n \neq m}}^N \sum_{n=1}^N e^{-j \sin \frac{\phi}{2} (x_n - x_m)} \right) d\phi = \frac{2\pi}{N^2} \sum_{\substack{m=1 \\ n \neq m}}^N \sum_{n=1}^N J_o(x_n - x_m)$$

F. 7

$$\int_{-\pi}^{\pi} \left(2 \operatorname{jinc} \left(x \sin \frac{\phi}{2} \right) \right)^2 d\phi = \int_{-\pi}^{\pi} \left(\frac{2 J_1 \left(x \sin \frac{\phi}{2} \right)}{x \sin \frac{\phi}{2}} \right)^2 d\phi = 2\pi {}_2F_3 \left(\frac{1}{2}, \frac{3}{2}; 1, 2, 3; -(x)^2 \right) \quad (\text{F.1.7})$$

this is an even function so integrate only half

$$= 8 \int_0^{\pi} \left(\frac{J_1 \left(x \sin \frac{\phi}{2} \right)}{x \sin \frac{\phi}{2}} \right)^2 d\phi$$

From Newman and Frank the bessel function squared can be expressed as

$$J_1^2(z) = \sum_{m=0}^{\infty} \frac{(-1)^m (2m+2)! \left(\frac{z}{2}\right)^{2m+2}}{m!(m+2)!((m+1)!)^2}$$

Now letting

$$\text{let } z = x \sin \left(\frac{\phi}{2} \right)$$

$$\begin{aligned} 8 \int_0^{\pi} \left(\frac{J_1(z)}{z} \right)^2 d\phi &= 8 \sum_{m=0}^{\infty} \frac{(-1)^m (2m+2)! \left(\frac{z}{2}\right)^{2m+2}}{m!(m+2)!((m+1)!)^2} d\phi \\ &= 8 \int_0^{\pi} \sum_{m=0}^{\infty} \frac{(-1)^m (2m+2)! (z)^{2m}}{m!(m+2)!((m+1)!)^2 (2)^{2m+2}} d\phi \end{aligned}$$

plugging back z and swap the summation and integral terms

$$\begin{aligned} &= 8 \sum_{m=0}^{\infty} \int_0^{\pi} \frac{(-1)^m (2m+2)! (z)^{2m}}{m!(m+2)!((m+1)!)^2 (2)^{2m+2}} d\phi \\ &= 8 \sum_{m=0}^{\infty} \frac{(-1)^m (2m+2)!}{m!(m+2)!((m+1)!)^2 (2)^{2m+2}} \int_0^{\pi} \left(x \sin \left(\frac{\phi}{2} \right) \right)^{2m} d\phi \\ &= 8 \sum_{m=0}^{\infty} \frac{(-1)^m x^{2m} (2m+2)(2m+1)(2m)!}{m!(m+2)!(m+1)^2 m! (2)^{2m+2}} \int_0^{\pi} \left(\sin \left(\frac{\phi}{2} \right) \right)^{2m} d\phi \end{aligned}$$

$$\begin{aligned}
&= 8 \sum_{m=0}^{\infty} \frac{(-1x^2)^m 2(m+1)(2m+1)(2m)!}{m!(m+2)!(m+1)^2 m!^2 (2)^{2m+2}} \int_0^{\pi} \left(\sin\left(\frac{\phi}{2}\right) \right)^{2m} d\phi \\
&= 8 \sum_{m=0}^{\infty} \frac{(-1x^2)^m (2m+1)(2m)!}{m!(m+2)!(m+1)m!^2 (2)^{2m+1}} \int_0^{\pi} \left(\sin\left(\frac{\phi}{2}\right) \right)^{2m} d\phi
\end{aligned}$$

Using the identity (D.1.1)

Then

$$\begin{aligned}
&= 8 \sum_{m=0}^{\infty} \frac{(-1x^2)^m (2m+1)(2m-1)!! m! 2^m}{m!(m+2)!(m+1)m!^2 (2)^{2m+1}} \int_0^{\pi} \left(\sin\left(\frac{\phi}{2}\right) \right)^{2m} d\phi \\
&= 8 \sum_{m=0}^{\infty} \frac{(2m+1)(2m-1)!!}{(m+2)!(m+1)(2)^{m+1} m!} \frac{(-1x^2)^m}{m!} \int_0^{\pi} \left(\sin\left(\frac{\phi}{2}\right) \right)^{2m} d\phi
\end{aligned}$$

Now using the identity (D.1.1) again and substituting

$$\begin{aligned}
&= 8 \sum_{m=0}^{\infty} \frac{(2m+1)\Gamma\left(m+\frac{1}{2}\right)2^m}{(m+2)!m!(m+1)(2)^{m+1}\sqrt{\pi}} \frac{(-1x^2)^m}{m!} \int_0^{\pi} \left(\sin\left(\frac{\phi}{2}\right) \right)^{2m} d\phi \\
&= 8 \sum_{m=0}^{\infty} \frac{\Gamma\left(m+\frac{1}{2}\right)}{\Gamma(m+3)\Gamma(m+1)} \frac{(-1x^2)^m}{m!} \frac{(2m+1)}{(2m+2)\sqrt{\pi}} \int_0^{\pi} \left(\sin\left(\frac{\phi}{2}\right) \right)^{2m} d\phi
\end{aligned}$$

Where

$$(2m+2) = \frac{(2m+2)!\sqrt{\pi}}{2^{2m+1} m! \Gamma\left(m+\frac{3}{2}\right)}$$

Then

$$\begin{aligned}
&= 8 \sum_{m=0}^{\infty} \frac{\Gamma\left(m+\frac{1}{2}\right)}{\Gamma(m+3)\Gamma(m+1)} \frac{(-1x^2)^m}{m!} \frac{(2m+1)2^{2m+1} m! \Gamma\left(m+\frac{3}{2}\right)}{(2m+2)!\sqrt{\pi}\sqrt{\pi}} \int_0^{\pi} \left(\sin\left(\frac{\phi}{2}\right) \right)^{2m} d\phi \\
&= 8 \sum_{m=0}^{\infty} \frac{\Gamma\left(m+\frac{1}{2}\right)\Gamma\left(m+\frac{3}{2}\right)}{\Gamma(m+3)\Gamma(m+1)} \frac{(-1x^2)^m}{m!} \frac{(2m+1)2^{2m+1} m!}{(2m+2)!\pi} \int_0^{\pi} \left(\sin\left(\frac{\phi}{2}\right) \right)^{2m} d\phi
\end{aligned}$$

Where

$$\Gamma(m+2) = (m+1)m!$$

$$= 8 \sum_{m=0}^{\infty} \frac{\Gamma\left(m+\frac{1}{2}\right)\Gamma\left(m+\frac{3}{2}\right)}{\Gamma(m+3)\Gamma(m+1)} \frac{(-1x^2)^m}{m!} \frac{(2m+1)2^{2m+1}m!}{2(2m+1)(2m)!(m+1)\pi} \int_0^{\pi} \left(\sin\left(\frac{\phi}{2}\right)\right)^{2m} d\phi$$

substituting

$$(2m)! = \frac{\Gamma\left(m+\frac{1}{2}\right)m!2^{2m}}{\sqrt{\pi}}$$

and canceling

$$\begin{aligned} &= 8 \sum_{m=0}^{\infty} \frac{\Gamma\left(m+\frac{1}{2}\right)\Gamma\left(m+\frac{3}{2}\right)}{\Gamma(m+3)\Gamma(m+1)} \frac{(-1x^2)^m}{m!} \frac{1}{(m+1)m!} \frac{m!\sqrt{\pi}}{\Gamma\left(m+\frac{1}{2}\right)\pi} \int_0^{\pi} \left(\sin\left(\frac{\phi}{2}\right)\right)^{2m} d\phi \\ &= 8 \sum_{m=0}^{\infty} \frac{\Gamma\left(m+\frac{1}{2}\right)\Gamma\left(m+\frac{3}{2}\right)}{\Gamma(m+3)\Gamma(m+1)\Gamma(m+2)} \frac{(-1x^2)^m}{m!} \frac{m!}{\Gamma\left(m+\frac{1}{2}\right)\sqrt{\pi}} \int_0^{\pi} \left(\sin\left(\frac{\phi}{2}\right)\right)^{2m} d\phi \\ &= 8 \sum_{m=0}^{\infty} \frac{\Gamma\left(m+\frac{1}{2}\right)\Gamma\left(m+\frac{3}{2}\right)}{\Gamma(m+3)\Gamma(m+1)\Gamma(m+2)} \frac{(-1x^2)^m}{m!} \frac{\Gamma(m+1)}{\Gamma\left(m+\frac{1}{2}\right)\sqrt{\pi}} \int_0^{\pi} \left(\sin\left(\frac{\phi}{2}\right)\right)^{2m} d\phi \end{aligned}$$

The integral $\int_0^{\pi} \left(\sin\left(\frac{\phi}{2}\right)\right)^{2m} d\phi = \frac{\sqrt{\pi}\Gamma\left(m+\frac{1}{2}\right)}{\Gamma(m+1)}$

To show this the definition of the gamma function is observed as

$$\Gamma(z) = \int_0^{\infty} x^{z-1} e^{-x} dx$$

Using u-substitution

$$\text{Let } u^2 = x \quad dx = 2udu$$

$$\Gamma(z) = \int_0^{\infty} u^{2z-2} e^{-u^2} 2udu$$

$$\Gamma(z) = 2 \int_0^{\infty} u^{2z-1} e^{-u^2} du \quad [1]$$

Taking the product of two gamma functions

$$\begin{aligned} \Gamma(x)\Gamma(y) &= 2 \int_0^{\infty} u^{2x-1} e^{-u^2} du \cdot 2 \int_0^{\infty} v^{2y-1} e^{-v^2} dv \\ &= 4 \int_0^{\infty} \int_0^{\infty} e^{-(u^2+v^2)} u^{2x-1} v^{2y-1} dudv \quad [2] \end{aligned}$$

Using a change of variables

$$u = r \cos(\theta) \quad v = r \sin(\theta)$$

$$u^2 + v^2 = r^2 \quad dudv = r dr d\theta$$

$$\begin{aligned} \Gamma(x)\Gamma(y) &= 4 \int_0^{\pi/2} \int_0^{\infty} e^{-r^2} r^{2x-1} \cos^{2x-1}(\theta) r^{2y-1} \sin^{2y-1}(\theta) r dr d\theta \\ &= 4 \int_0^{\infty} e^{-r^2} r^{2(x+y)-1} dr \int_0^{\pi/2} \cos^{2x-1}(\theta) \sin^{2y-1}(\theta) d\theta \end{aligned}$$

Using [1] from above this can be written as

$$= 2\Gamma(x+y) \int_0^{\pi/2} \cos^{2x-1}(\theta) \sin^{2y-1}(\theta) d\theta$$

This can be written as

$$\frac{\Gamma(x)\Gamma(y)}{2\Gamma(x+y)} = \int_0^{\pi/2} \cos^{2x-1}(\theta) \sin^{2y-1}(\theta) d\theta$$

$$\text{Let } x = \frac{1}{2} \text{ and } y = m + \frac{1}{2}$$

$$\frac{\Gamma\left(\frac{1}{2}\right)\Gamma\left(m+\frac{1}{2}\right)}{2\Gamma\left(\frac{1}{2}+m+\frac{1}{2}\right)} = \int_0^{\pi/2} \cos^0(\theta) \sin^{2m}(\theta) d\theta$$

$$\frac{\sqrt{\pi}\Gamma\left(m+\frac{1}{2}\right)}{2\Gamma(m+1)} = \int_0^{\pi/2} \sin^{2m}(\theta) d\theta$$

$\sin^{2m}(\theta)$ is symmetric about the line $\theta = \frac{\pi}{2}$ therefore:

$$\int_{\pi/2}^{\pi} \sin^{2m}(\theta) d\theta = \int_0^{\pi/2} \sin^{2m}(\theta) d\theta = \frac{\sqrt{\pi}\Gamma\left(m+\frac{1}{2}\right)}{2\Gamma(m+1)}$$

Therefore

$$\int_0^{\pi} \sin^{2m}(\theta) d\theta = \frac{2\sqrt{\pi}\Gamma\left(m+\frac{1}{2}\right)}{2\Gamma(m+1)} = \frac{\sqrt{\pi}\Gamma\left(m+\frac{1}{2}\right)}{\Gamma(m+1)}$$

Since $\sin^{2m}(\theta)$ is also symmetric with respect to the y-axis

$$\int_{-\pi}^0 \sin^{2m}(\theta) d\theta = \int_0^{\pi} \sin^{2m}(\theta) d\theta = \frac{\sqrt{\pi}\Gamma\left(m+\frac{1}{2}\right)}{\Gamma(m+1)}$$

Therefore

$$\int_0^{\pi} \sin^{2m}(\theta) d\theta = \frac{2\sqrt{\pi}\Gamma\left(m+\frac{1}{2}\right)}{2\Gamma(m+1)} = \frac{\sqrt{\pi}\Gamma\left(m+\frac{1}{2}\right)}{\Gamma(m+1)}$$

$$\int_0^{\pi} \sin^{2m}(\theta) d\theta = \frac{\sqrt{\pi}\Gamma\left(m+\frac{1}{2}\right)}{\Gamma(m+1)}$$

Since $\sin^{2m}(\theta)$ is also symmetric with respect to the y-axis

$$\int_{-\pi}^0 \sin^{2m}(\theta) d\theta = \int_0^{\pi} \sin^{2m}(\theta) d\theta = \frac{\sqrt{\pi}\Gamma\left(m+\frac{1}{2}\right)}{\Gamma(m+1)}$$

Therefore

$$\int_{-\pi}^{\pi} \sin^{2m}(\theta) d\theta = \frac{4\sqrt{\pi}\Gamma\left(m + \frac{1}{2}\right)}{2\Gamma(m+1)} = \frac{2\sqrt{\pi}\Gamma\left(m + \frac{1}{2}\right)}{\Gamma(m+1)}$$

And substituting into our earlier expression we arrive at the following

$$\begin{aligned} \int_{-\pi}^{\pi} \left(\frac{2J_1\left(x \sin \frac{\phi}{2}\right)}{x \sin \frac{\phi}{2}} \right)^2 d\phi &= \sum_{m=0}^{\infty} 8 \frac{\Gamma\left(m + \frac{1}{2}\right)\Gamma\left(m + \frac{3}{2}\right)}{\Gamma(m+3)\Gamma(m+2)\Gamma(m+1)} \frac{(-1x^2)^m}{m!} \frac{\Gamma(m+1)}{\Gamma\left(m + \frac{1}{2}\right)\sqrt{\pi}} \frac{\sqrt{\pi}\Gamma\left(m + \frac{1}{2}\right)}{\Gamma(m+1)} \\ &= \sum_{m=0}^{\infty} 2^3 \frac{\Gamma\left(m + \frac{1}{2}\right)\Gamma\left(m + \frac{3}{2}\right)}{\Gamma(m+3)\Gamma(m+2)\Gamma(m+1)} \frac{(-1x^2)^m}{m!} \end{aligned}$$

The above can be rewritten as a ${}_2F_3$ hypergeometric formula.

To do this the pochhammer symbol will be used or more formally rising factorial $x^{(n)}$

where $x^{(n)}$ is related to the gamma function as

$$x^{(n)} = \frac{\Gamma(x+n)}{\Gamma(x)}$$

Thus

$$\left(\frac{1}{2}\right)^{(m)} = \frac{\Gamma\left(m + \frac{1}{2}\right)}{\Gamma\left(\frac{1}{2}\right)} = \frac{\Gamma\left(m + \frac{1}{2}\right)}{\sqrt{\pi}}$$

$$\left(\frac{3}{2}\right)^{(m)} = \frac{\Gamma\left(m + \frac{3}{2}\right)}{\Gamma\left(\frac{3}{2}\right)} = \frac{2\Gamma\left(m + \frac{3}{2}\right)}{\sqrt{\pi}}$$

$$(1)^{(m)} = \frac{\Gamma(m+1)}{\Gamma(1)} = \frac{\Gamma(m+1)}{1}$$

$$(2)^{(m)} = \frac{\Gamma(m+2)}{\Gamma(2)} = \frac{\Gamma(m+2)}{1}$$

$$(3)^{(m)} = \frac{\Gamma(m+3)}{\Gamma(3)} = \frac{\Gamma(m+3)}{2}$$

And

$$\frac{\left(\frac{1}{2}\right)^{(m)} \left(\frac{3}{2}\right)^{(m)}}{(1)^{(m)} (2)^{(m)} (3)^{(m)}} = \frac{4}{\pi} \frac{\Gamma\left(m + \frac{1}{2}\right) \Gamma\left(m + \frac{3}{2}\right)}{\Gamma(m+1) \Gamma(m+2) \Gamma(m+3)}$$

Making use of the above we can rewrite our expression as

$$\begin{aligned} \sum_{m=0}^{\infty} 2^3 \frac{\Gamma\left(m + \frac{1}{2}\right) \Gamma\left(m + \frac{3}{2}\right)}{\Gamma(m+3) \Gamma(m+2) \Gamma(m+1)} \frac{(-1x^2)^m}{m!} &= \sum_{m=0}^{\infty} 8 \frac{\pi}{4} \frac{\left(\frac{1}{2}\right)^{(m)} \left(\frac{3}{2}\right)^{(m)}}{(1)^{(m)} (2)^{(m)} (3)^{(m)}} \frac{(-1x^2)^m}{m!} \\ &= 2\pi {}_2F_3\left(\frac{1}{2}, \frac{3}{2}; 1, 2, 3; -(x)^2\right) \end{aligned}$$

$$2\pi {}_2F_3\left(\frac{1}{2}, \frac{3}{2}; 1, 2, 3; -(x)^2\right)$$

F. 8

$$\int_{-1}^1 \int_{-1}^1 \left(\frac{1}{N} + \frac{1}{N^2} \sum_{m=1}^N \sum_{\substack{n=1 \\ n \neq k}}^N e^{-j\alpha(x_n - x_m)} \right) \frac{1}{\sqrt{2\pi\sigma}} e^{\frac{-x_n^2}{2\sigma^2}} \frac{1}{\sqrt{2\pi\sigma}} e^{\frac{-x_m^2}{2\sigma^2}} dx_n dx_m = \frac{1}{N} + \left(1 - \frac{1}{N}\right) \left[\left| e^{\frac{-\alpha^2 \sigma^2}{2}} \right|^2 \right] \quad (\text{F.1.8})$$

It can be seen that the solution to one of the integrals will be solved in the same manner as the other.

Solving the first integral with respect to n is done by completing the square as follows.

$$\begin{aligned} \frac{x_n^2}{2\sigma^2} + j\alpha x_n &= 0 \\ \text{or} \\ x_n^2 + j\alpha x_n 2\sigma^2 &= 0 \\ \downarrow (\text{half of the middle terms coef}) \\ j\alpha\sigma^2 &\rightarrow -\alpha^2\sigma^4 \\ (x_n + j\alpha\sigma^2)^2 &= -\alpha^2\sigma^4 \\ \left[-(x_n + j\alpha\sigma^2)^2 - \alpha^2\sigma^4 \right] &* \left(\frac{1}{2\sigma^2} \right) = 0 * \left(\frac{1}{2\sigma^2} \right) \\ \frac{-(x_n + j\alpha\sigma^2)^2}{2\sigma^2} - \frac{\alpha^2\sigma^2}{2} &= 0 \end{aligned}$$

Then

$$x = x_n + j\alpha\sigma^2$$

$$\frac{dx}{dx_n} = 1$$

and

$$\int_{-\infty}^{\infty} \frac{1}{\sqrt{2\pi\sigma}} e^{-\frac{(x_n + j\alpha\sigma^2)^2}{2\sigma^2}} dx_n = \frac{1}{\sqrt{2\pi\sigma}} \int_{-\infty}^{\infty} e^{-\frac{(x)^2}{2\sigma^2}} dx = 1$$

The above is regarded as the Q function and is equal to 1 thus

$$\int_{-1}^1 \int_{-1}^1 \left(\frac{1}{N} + \frac{1}{N^2} \sum_{m=1}^N \sum_{\substack{n=1 \\ n \neq k}}^N e^{-j\alpha(x_n - x_m)} \right) \frac{1}{\sqrt{2\pi\sigma}} e^{-\frac{x_n^2}{2\sigma^2}} \frac{1}{\sqrt{2\pi\sigma}} e^{-\frac{x_m^2}{2\sigma^2}} dx_n dx_m = \frac{1}{N} + \left(1 - \frac{1}{N}\right) \left[e^{-\frac{\alpha^2\sigma^2}{2}} \right]^2$$

F.9

Since the function $\frac{2}{\pi} \sqrt{1-x_n^2}$ is even then the integral $\sum_{n=1}^N \frac{1}{\sqrt{N}} \int_{-1}^1 \frac{2}{\pi} \sqrt{1-x_n^2} \sin(x_n \alpha(\phi)) dx_n = 0$

evaluates to zero, because the sin function is odd, such that an even function times an odd function = odd function.

A more formal proof is shown below.

Theorem. Let the real function f be Riemann-integrable on $[-a, a]$.

If f is an

$$\text{even function, then } \int_{-a}^a f(x) dx = 2 \int_0^a f(x) dx,$$

$$\text{odd function, then } \int_{-a}^a f(x) dx = 0$$

Since the definite integral is additive with respect to the interval of integration, one has

$$I = \int_{-a}^a f(x) dx = \int_{-a}^0 f(t) dt + \int_0^a f(x) dx$$

Making the substitution $t = -x$, $dt = -dx$ and swapping the limits of integration one gets

$$I = \int_{-a}^a f(x) dx = \int_0^a f(-x) dx + \int_0^a f(x) dx$$

Now using the definitions of even (+) and odd (-) function yields

$$I = \int_0^a f(\pm x) dx + \int_0^a f(x) dx = \pm \int_0^a f(x) dx + \int_0^a f(x) dx \quad (\text{F.1.9})$$

this settles the equations of the theorem.

F. 10

$$\sum_{n=1}^N \left[\left(\frac{2}{N\pi} \right) \int_{-1}^1 (\sqrt{1-x_n^2}) \sin^2(x_n \alpha) dx_n \right] \frac{1}{2} \left(1 - \frac{J_1(2\alpha)}{\alpha} \right)$$

Using the identity

$$\sin^2(x) = \frac{1}{2} - \frac{\cos(2x)}{2}$$

Then

The rest of the procedure is similar H.5 giving

$$E[Y^2(\phi|z)] = \frac{1}{2} \left(1 - \frac{J_1(2\alpha(\phi))}{\alpha(\phi)} \right) \quad (\text{F.1.10})$$

F. 11

$$-\frac{2}{\pi} \int_{-1}^1 \sqrt{1-x^2} x^2 dx = -\frac{1}{4} \quad (\text{F.1.11})$$

With a change of variables

$$x = \sin(u)$$

$$dx = \cos(u)$$

The integral becomes

$$-\frac{2}{\pi} \int_{-\frac{\pi}{2}}^{\frac{\pi}{2}} \cos^2(u) \sin^2(u) du$$

Now applying (A.1.12)

$$-\frac{2}{\pi} \int_0^{\frac{\pi}{2}} \cos^2(u) \sin^2(u) du = -\frac{2}{\pi} \frac{\Gamma\left(\frac{3}{2}\right)\Gamma\left(\frac{3}{2}\right)}{2\Gamma(3)} = -\frac{1}{8}$$

Now by another change of variables

$$\begin{aligned}
 u &= -v \\
 &= \frac{2}{\pi} \int_0^{-\frac{\pi}{2}} \cos^2(-v) \sin^2(-v) dv = \frac{\Gamma\left(\frac{3}{2}\right)\Gamma\left(\frac{3}{2}\right)}{2\Gamma(3)} \\
 &= -\frac{2}{\pi} \int_{-\frac{\pi}{2}}^0 \cos^2(-v) \sin^2(-v) dv = -\frac{2}{\pi} \frac{\Gamma\left(\frac{3}{2}\right)\Gamma\left(\frac{3}{2}\right)}{2\Gamma(3)} = -\frac{1}{8}
 \end{aligned}$$

And thus,

$$-\frac{2}{\pi} \int_{-\frac{\pi}{2}}^{\frac{\pi}{2}} \cos^2(u) \sin^2(u) du = -\frac{1}{4}$$

F. 12

$$\begin{aligned}
 &\left(\frac{1}{N}\right) \int_{-1}^1 \frac{3(1-x_n^2)}{4} dx_n \int_{-1}^1 \frac{3(1-x_m^2)}{4} dx_m \\
 &\frac{3}{4} \int_{-1}^1 (1-x_n^2) dx_n = \left(x_n - \frac{x_n^3}{3}\right) \Bigg|_{x_n=-1}^{x_n=1} = \frac{3}{4} \frac{4}{3} = 1
 \end{aligned} \tag{F.1.12}$$

F. 13

$$\begin{aligned}
& \frac{1}{N} + \frac{9}{16N^2} \left(1 - \frac{1}{N}\right) \left[\int_{-1}^1 \cos(\alpha(x_n - x_m)) (1 - x_n^2) dx_n \int_{-1}^1 (1 - x_m^2) dx_m \right] \\
&= \frac{1}{N} + \left(1 - \frac{1}{N}\right) \left| 3 \frac{j_1 \alpha(\phi)}{\alpha(\phi)} \right|^2 = \frac{1}{N} + \left(1 - \frac{1}{N}\right) |3 \text{tinc}(\alpha(\phi))|^2
\end{aligned} \tag{F.1.13}$$

Using the identity (A.1.6)

$$\nu = \left(\frac{3}{2}\right) \Rightarrow \Gamma(2) = 1, \quad \Gamma\left(\frac{1}{2}\right) = \sqrt{\pi}$$

Or

$$J_{\frac{3}{2}}(z) = \left(\frac{z}{2}\right)^{\frac{3}{2}} \frac{1}{\sqrt{\pi}} \int_{-1}^1 (1-t^2) \cos(zt) dt$$

Thus,

$$\frac{2^{\frac{3}{2}} \sqrt{\pi} J_{\frac{3}{2}}(z)}{z^{\frac{3}{2}}} = \int_{-1}^1 (1-t^2) \cos(zt) dt$$

Sub-sequentially applying the given integral the

$$\begin{aligned}
& \frac{1}{N} + \frac{9}{16N^2} \left(1 - \frac{1}{N}\right) \left[\int_{-1}^1 \int_{-1}^1 \cos(\alpha(x_n - x_m)) (1 - x_n^2) dx_n (1 - x_m^2) dx_m \right] \\
&= \frac{1}{N} + \frac{9}{16} \left(1 - \frac{1}{N}\right) \left[\int_{-1}^1 (1 - x_m^2) \frac{2^{\frac{3}{2}} \sqrt{\pi} J_{\frac{3}{2}}(\alpha)}{\alpha^{\frac{3}{2}}} \cos(\alpha x_m) dx_m \right] \\
&= \frac{1}{N} + \frac{9}{16} \left(1 - \frac{1}{N}\right) \frac{2^{\frac{3}{2}} \sqrt{\pi} J_{\frac{3}{2}}(\alpha)}{\alpha^{\frac{3}{2}}} \left[\int_{-1}^1 (1 - x_m^2) \cos(\alpha x_m) dx_m \right] \\
&= \frac{1}{N} + \frac{9}{16} \left(1 - \frac{1}{N}\right) \left| \frac{2}{\alpha} \sqrt{\frac{2\pi}{\alpha}} J_{\frac{3}{2}}(\alpha) \right|^2 \\
&= \frac{1}{N} + \frac{9}{4} \left(1 - \frac{1}{N}\right) \left| \frac{\sqrt{2\pi} J_{\frac{3}{2}}(\alpha)}{\alpha^{\frac{3}{2}}} \right|^2
\end{aligned}$$

Using (D.1.21) this can be rewritten in terms of spherical Bessel functions as

$$\begin{aligned} & \frac{1}{N} + \frac{9}{16N^2} \left(1 - \frac{1}{N}\right) \left[\int_{-1}^1 \int_{-1}^1 \cos(\alpha(x_n - x_m)) (1 - x_n^2) dx_n (1 - x_m^2) dx_m \right] \\ &= \frac{1}{N} + \left(1 - \frac{1}{N}\right) \left| 3 \frac{j_1(\alpha(\phi))}{\alpha(\phi)} \right|^2 = \frac{1}{N} + \left(1 - \frac{1}{N}\right) |3 \text{tinc}(\alpha(\phi))|^2 \end{aligned}$$

F.14

$$\int_{-\pi}^{\pi} (3 \text{tinc}(x))^2 d\phi = 9 \int_{-\pi}^{\pi} \left(\frac{j_1(x)}{x} \right)^2 d\phi = 2\pi \left\{ \frac{4}{5} \left[{}_1F_2 \left(\frac{1}{2}; 4, \frac{7}{2}; -\left(4\pi \tilde{R}\right)^2 \right) - 6 {}_1F_2 \left(\frac{1}{2}; 3, \frac{7}{2}; -\left(4\pi \tilde{R}\right)^2 \right) \right] \right\} \quad (\text{F.1.14})$$

This is an even function and the integral reduces to,

$$18 \int_0^{\pi} \left(\frac{j_1(x)}{x} \right)^2 d\phi$$

Subsequently applying the identity (D.1.18) to the spherical Bessel function squared

$$j_1(x)^2 = \frac{\sqrt{\pi}}{2} G_{1, 3}^{1, 1} \left(z, \frac{1}{2} \middle| \begin{matrix} 0 \\ 1 & -1/2 & -2 \end{matrix} \right)$$

where $G_{1, 3}^{1, 1} \left(z, \frac{1}{2} \middle| \begin{matrix} 0 \\ 1 & -1/2 & -2 \end{matrix} \right) = \frac{\sqrt{\pi}}{2} \frac{1}{2\pi j} \int_1 \left\{ \frac{\prod_{j=1}^1 [\Gamma(b_j + s)] \prod_{j=1}^1 [\Gamma(1 - a_j - s)]}{\prod_{j=2}^1 [\Gamma(a_j + s)] \prod_{j=2}^3 [\Gamma(1 - b_j - s)]} \right\} z^{-2s} ds$

To evaluate the above one begins by evaluating the sum of products confined within the curly braces starting $j=1$ to obtain

$$\frac{\Gamma(1+s)\Gamma(1-s)}{1}$$

For $j=2$

$$\frac{1}{\Gamma\left(\frac{3}{2} - s\right)}$$

And lastly for $j=3$

$$\frac{1}{\Gamma(3-s)}$$

Substituting the result into the expression gives

$$\begin{aligned} \frac{j_1(x)^2}{x^2} &= \frac{1}{4\sqrt{\pi}j} \int_l \left\{ \frac{\prod_{j=1}^1 [\Gamma(b_j + s)] \prod_{j=1}^1 [\Gamma(1 - a_j - s)]}{\prod_{j=2}^1 [\Gamma(a_j + s)] \prod_{j=2}^3 [\Gamma(1 - b_j - s)]} \right\} z^{-2s-2} ds \\ &= \frac{1}{4\sqrt{\pi}j} \int_l \left\{ \frac{\Gamma(1+s)\Gamma(1-s)}{\Gamma\left(\frac{3}{2}-s\right)\Gamma(3-s)} \right\} z^{-2s-2} ds \end{aligned}$$

Now integrating along the contour of this integral gives

$$\frac{j_1(x)^2}{x^2} = \frac{(1+x^2 - \cos(2x) + z^2 \cos(2x) - 2z \sin(2x))}{2x^6}$$

Now letting $x = 4\pi A \sin\left(\frac{\phi}{2}\right)$ gives

$$\frac{j_1\left(4\pi \tilde{R} \sin\left(\frac{\phi}{2}\right)\right)^2}{\left(4\pi \tilde{R} \sin\left(\frac{\phi}{2}\right)\right)^2} = \frac{\left(1 + \left(4\pi \tilde{R} \sin\left(\frac{\phi}{2}\right)\right)^2 - \cos\left(8\pi \tilde{R} \sin\left(\frac{\phi}{2}\right)\right) + \left(4\pi \tilde{R} \sin\left(\frac{\phi}{2}\right)\right)^2 \cos\left(8\pi \tilde{R} \sin\left(\frac{\phi}{2}\right)\right)\right)}{2^{13} \pi^6 \tilde{R}^6 \sin^6\left(\frac{\phi}{2}\right)}$$

And the above expression is simplified as

$$\frac{j_1\left(4\pi \tilde{R} \sin\left(\frac{\phi}{2}\right)\right)^2}{\left(4\pi \tilde{R} \sin\left(\frac{\phi}{2}\right)\right)^2} = \frac{\left(-4\pi \tilde{R} \sin\left(\frac{\phi}{2}\right) \cos\left[4\pi \tilde{R} \sin\left(\frac{\phi}{2}\right)\right] + \sin\left[4\pi \tilde{R} \sin\left(\frac{\phi}{2}\right)\right]\right)^2}{2^{12} \pi^6 \tilde{R}^6 \sin^6\left(\frac{\phi}{2}\right)}$$

Now applying the integral gives

$$\begin{aligned}
18 \int_0^\pi \left(\frac{j_1(x)}{x} \right)^2 d\phi &= \int_0^\pi \frac{\left(-4\pi \tilde{R} \sin\left(\frac{\phi}{2}\right) \cos \left[4\pi \tilde{R} \sin\left(\frac{\phi}{2}\right) \right] + \sin \left[4\pi \tilde{R} \sin\left(\frac{\phi}{2}\right) \right] \right)^2}{2^{12} \pi^6 \tilde{R}^6 \sin^6\left(\frac{\phi}{2}\right)} d\phi \\
&= 2\pi \left\{ \frac{2}{5} \left[{}_1F_2\left(\frac{1}{2}; 4, \frac{7}{2}; -\left(4\pi \tilde{R}\right)^2\right) - 6 {}_1F_2\left(\frac{1}{2}; 3, \frac{7}{2}; -\left(4\pi \tilde{R}\right)^2\right) \right] \right\}
\end{aligned}$$

F.15

$$\int_{-\pi}^{\pi} \left| e^{-\left(8\pi^2 \sin^2\left(\frac{\phi}{2}\right)\right)\sigma^2} \right|^2 d\phi = 2\pi {}_1F_1\left(\frac{1}{2}; 1; -(2\pi\sigma)^2\right)$$

$$\int_{-\pi}^{\pi} \left| e^{-\left(8\pi^2 \sin^2\left(\frac{\phi}{2}\right)\right)\sigma^2} \right|^2 d\phi = \int_{-\pi}^{\pi} e^{-\left(16\pi^2 \sin^2\left(\frac{\phi}{2}\right)\right)\sigma^2} = \int_{-\pi}^{\pi} e^{-\left(4\pi\sigma \sin\left(\frac{\phi}{2}\right)\right)^2}$$

Now letting

$$c = (4\pi\sigma)^2$$

And making a change of variables, $u = \sin\left(\frac{\phi}{2}\right)$ $\frac{du}{d\phi} = \frac{1}{2} \cos\left(\frac{\phi}{2}\right)$ the integral becomes

$$\int_{-\pi}^{\pi} \left| e^{-\frac{\alpha(\phi)^2 \sigma^2}{2}} \right|^2 d\phi = \int_{-1}^1 e^{-cu^2} \frac{2}{\cos\left(\frac{\phi}{2}\right)} du = \int_{-1}^1 e^{-cu^2} \frac{2}{\sqrt{1-\sin^2\left(\frac{\phi}{2}\right)}} du = \int_{-1}^1 e^{-cu^2} \frac{2}{\sqrt{1-u^2}} du$$

Now again changing the variables such that $x = u^2$, $\frac{dx}{du} = 2u$ the integral is again rewritten

as

$$\int_{-\pi}^{\pi} \left| e^{-\frac{\alpha(\phi)^2 \sigma^2}{2}} \right|^2 d\phi = \int_{-1}^1 e^{-cx} \frac{2}{\sqrt{1-x}} \frac{1}{2\sqrt{x}} dx$$

And since the integral is an even function

$$\int_{-\pi}^{\pi} \left| e^{-\frac{\alpha(\phi)^2 \sigma^2}{2}} \right|^2 d\phi = 2 \int_0^1 e^{-cx} (1-x)^{-1/2} (x)^{-1/2} dx$$

and now using the integral identity

$$\int_0^1 e^{-cx} (1-x)^{b-a-1} (x)^{a-1} dx = \frac{\Gamma(b-a)\Gamma(a)}{\Gamma(b)} {}_1F_1(a; b; c)$$

$$\int_{-\pi}^{\pi} \left| e^{-\frac{\alpha(\phi)^2 \sigma^2}{2}} \right|^2 d\phi = 2 \frac{\Gamma\left(1-\frac{1}{2}\right)\Gamma\left(\frac{1}{2}\right)}{\Gamma(1)} {}_1F_1\left(\frac{1}{2}; 1; -(2\pi\sigma)^2\right) = 2\pi {}_1F_1\left(\frac{1}{2}; 1; -(2\pi\sigma)^2\right) \quad (\text{F.1.15})$$

APPENDIX G

SUMMATION PROOF

$$\sum_{m=1}^N \sum_{\substack{n=1 \\ n \neq m}}^N e^{j\alpha(x_n - x_m)} = N(N-1)\cos(\alpha(x_n - x_m))$$

Observing the magnitude of $e^{j\alpha(x_n - x_m)}$ is 1 and making use of the summation identity shown below the above result can be obtained.

$$\sum_{i=m}^n 1 = n - m + 1$$

Applying the identity to the above double summation is a bit tricky in the sense one of the summation terms is restricted to the condition l does not equal k . The above formula may however, still be applied if done correctly. As an example an analysis of the derivation will be shown by letting $N=4$.

For $n=1, m=2$ we would have $e^{j\alpha(x_1 - x_2)}$

For $n=2, m=1$ we would have $e^{j\alpha(x_2 - x_1)} = e^{-j\alpha(x_1 - x_2)}$

Symmetry is observed to exist in formulation above. For the case $(n=1, m=2) + (n=2, m=1)$ thus this can be written as

$$2\cos(\alpha(x_n - x_m)) = 2\cos(\alpha(x_m - x_n)) \quad (\text{G.1.1})$$

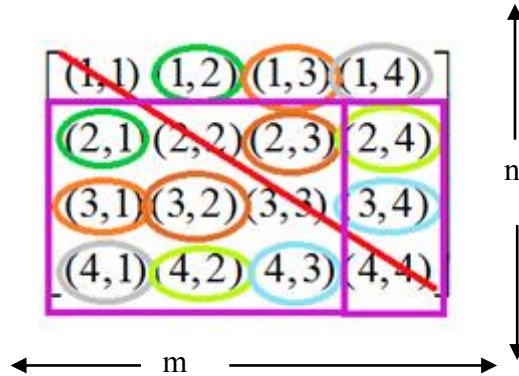
Since $\cos(x)$ is an even function

The generalization above satisfies the phase of the double summation term. However, the summation identity has yet to be applied. The amplitude of the double summation term is considered such that all possibilities are likely (relaxing the condition $n \neq m$) which gives

$$\sum_{m=1}^N \sum_{n=2}^N 1 = (N-1+1)(N-2+1) = N(N-1)$$

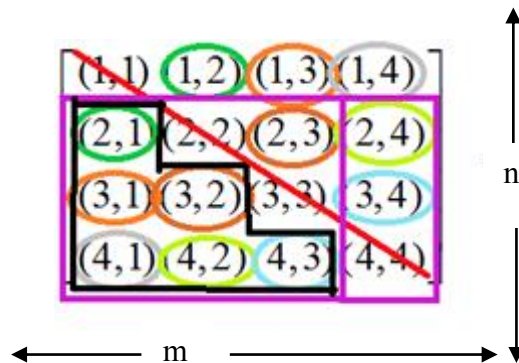
When the constraint $m \neq n$ is applied, it can be shown this result is divided by 2. To show this is true a pictorial analysis is demonstrated for the case $N=4$.

$$\sum_{k=1}^4 \sum_{l=2}^4 1 = (4-1+1)(4-2+1) = 4(3-1) = 12$$



The red diagonal line cross out the numbers where $m=n$. The rest of the numbers are color-coded showing symmetry within the matrix. The purple rectangle shows an arbitrarily picked area containing the $N(N-1) = 12$ terms (for $N=4$). This would be the result from the analytic expression shown above when the condition $m \neq n$ is relaxed.

Now considering the phase factor or the result from (G.1.1) one notices only those numbers shown within the black staircase survive.



Re-examining the figure above one can observe the black staircase is half the area of the purple rectangle and the reasoning behind the factor of 1/2. Hence, the summation identity is specified as

$$\sum_{m=1}^N \sum_{\substack{n=1 \\ n \neq m}}^N e^{j\alpha(x_n - x_m)} = N(N-1) \cos(\alpha(x_n - x_m)) \quad (\text{G.1.2})$$

The results of (G.1.3) and (G.1.4) can be derived in the same fashion used to derive (G.1.2).

$$\sum_{m=1}^N \sum_{\substack{n=1 \\ n \neq m}}^N e^{j\alpha(x_n - x_m)} e^{j\beta(y_n - y_m)} = N(N-1) \cos(\alpha(x_n - x_m) + \beta(y_n - y_m)) \quad (\text{G.1.3})$$

$$\sum_{m=1}^N \sum_{\substack{n=1 \\ n \neq m}}^N e^{j\alpha(x_n - x_m)} e^{j\beta(y_n - y_m)} e^{j\chi(z_n - z_m)} = N(N-1) \cos(\alpha(x_n - x_m) + \beta(y_n - y_m) + \chi(z_n - z_m)) \quad (\text{G.1.4})$$

VITA

Kristopher Ryan Buchanan received a bachelor's degree in electrical and computer engineering in 2009 (Magana Cum Laude), from the University of Nevada Las Vegas, Las Vegas, NV. He entered the Electrical Engineering program at Texas A&M University in College Station, TX in January 2010 and received his Master of Science degree in May 2011. From Nov. 2003 to the present he has been a member of the Army National Guard and currently holds the rank of 2nd LT. From 2007-2008, he was an intern at National Security Technologies (NSTec) a subcontractor for the Department of Energy. From 2008-2009 he was part of the electromagnetics research group at the University of Nevada Las Vegas and is now a part of the electromagnetics research group at the Texas A&M University. He currently participates in summer internships (2009-present) at the Army Research Laboratory, Adelphi, MD. His research interests include collaborative beamforming, antenna theory, nanotechnology and electromagnetics.

Mr. Buchanan is a member of Tau Beta Pi, Eta Kappa Nu and Phi Kappa Phi honor societies. He may be reached at 3128 TAMU, 214 Zachry Bldg., College Station, TX, 77843. His email is kris.buchanan@hotmail.com. His advisor is Dr. Gregory Huff, who is an associate professor in the Zachary Engineering Bldg.